The Cellular Localisation and Role of S100P in the Motility and Invasion of Trophoblasts

Tara Louise Lancaster

Doctor of Philosophy

Aston University

March 2020

The Cellular Localisation and Role of S100P in the Motility and Invasion of Trophoblasts

Tara Lancaster

Doctor of Philosophy

2020

Thesis Summary

The S100 family of proteins are calcium-binding proteins expressed in a wide variety of tissues that participate in both intracellular and extracellular activities. One family member, S100P, has gained attention primarily in the context of promotion of carcinogenesis. Containing no enzymatic activity of its own, it interacts with multiple target proteins to regulate motility and invasion of cancer cells. Little is known about the role of S100P in trophoblast cells of the placenta, but our initial work has shown that it plays a crucial role in regulating both cellular motility and invasion. In this work, we sought to first establish the cellular localisation of S100P using different fractionation analysis. We first demonstrated the strictly cytoplasmic and membrane-associated localisation of S100P in different trophoblast cells including JEG-3, BeWo and HTR8, as well as cancer cells, regardless of the levels of S100P or any other changes such as excess calcium, addition of a non-ionic detergent, or the use of nuclear export inhibitors (Leptomycin B). Interestingly, tagging S100P with the fluorescent marker YFP led to a relocalisation of S100P from the cytoplasm/membrane fractions to nuclear fractions, suggesting the fusion protein had differential properties and cellular localisation. Further cellular compartmentalisation allowed us to determine that some of the S100P pools were also found in the plasma membrane fraction in both trophoblasts and in cancer cells. S100P was detectable at the extracellular surface using plasma membrane purification and biotinylation experiments. Analysis of the S100P structure suggests the presence of possible membrane-interacting residues. The C-terminal polybasic domain, in combination with potentially lipid-modified residues, may promote the association of S100P with negatively-charged membrane structures. Blockade of extracellular S100P through use of an S100P antibody or with cromolyn, a molecule shown to interact with helix 4 of S100P, results in decreases in both migration and invasion of choriocarcinoma cell line JEG-3, EVT-like HTR8/SVneo cells and EVT cells isolated from first trimester placenta, but did not lead to any changes in the formation of focal adhesions. This is in contrast to changes in total cellular levels of S100P in JEG-3 and HTR8 cells where a decrease in paxillin-containing focal adhesions can be seen. These studies therefore show that different pools of S100P, either intracellular or membrane-associated, promote trophoblast motility and invasion through two independent pathways. Further analysis in order to fully characterise the S100P interactome demonstrated the presence of S100P in high molecular weight complexes in trophoblast cells, and mass spectrometry analysis presented a number of proteins with increased abundance in S100P-expressing cells, although characterisation of specific S100P interactors remains to be fully explored.

Key words: trophoblast, focal adhesions, subcellular fractionation, extracellular, membrane

Acknowledgements

I would like to take this opportunity to thank those who have supported me during the course of my studies. Firstly, I would like to express my sincere gratitude to Dr Stephane Gross, my supervisor, for all of his invaluable help, advice, knowledge and general support throughout this process. My sincere thanks also to Professor Andrew Devitt and Ivana Milic - your advice and hard work regarding mass spectrometry experiments has helped to add a new dimension to this thesis. I'd like to extend a thank you to Charlie Clarke-Bland from ARCHA for her expertise in microscopy.

I'm thankful to a number of colleagues, whose enthusiasm for their research has motivated me in my own endeavours. To Maral, who has been there through both the ups and downs in the lab - especially trying to culture primary cells on weekends! Thank you for all the conversations and experiences we shared. I'd also like to thank Aiman for her wonderful friendship over the past four years. Your chemistry knowledge has been invaluable, and of course you've made me laugh more times than I can count! I will forever miss going hunting for free pens at Fresher's Fair with you. A big thanks also to members of Lab 331, both past and present, for their friendship, support and technical advice throughout this process.

I am incredibly grateful to my family for their love and support, and for listening me go on and on about my PhD! Thank you all for believing in me.

Lastly, I am incredibly thankful to Alex, my fiancé. You've spent ages listening to me talk about my research, and have encouraged me to aim higher than I ever thought I could. You have supported me through it all, and I will forever be grateful for your love and patience.

Table of Contents

List of Abbreviations

6-ACA - 6-aminocaproic acid

ACS - Acute coronary syndrome

AIIt - Annexin A2-S100A10 heterotetramer

ANOVA - Analysis of variance

APS - Ammonium Persulfate

BN-PAGE - Blue native polyacrylamide gel electrophoresis

BSA - Bovine Serum Albumin

Ca^{2+} - calcium

CacyBP/SIP - Calcyclin-binding protein/Siah-1-interacting protein

CB - Cytoskeleton Buffer

CBBG250 - Coomassie Brilliant Blue G250

CCC - Cytotrophoblast cell column

Cdc-42 - Cell division control protein 42 homolog

CHIP - C-terminus of Hsc70-interacting protein

CO_2 - Carbon dioxide

cRAGE - Cleaved RAGE

CRM1 - Chromosomal maintenance 1

CTB - Cytotrophoblast

CTS - Cytotrophoblastic shell

Cu^{2+} - Copper ions

DMEM - Dulbecco's Modified Eagle Medium

DMSO - Dimethyl Sulfoxide

DTT - Dithiothreitol

E-cadherin - Epithelial cadherin

ECL - Enhanced Chemiluminescence

ECM - Extracellular matrix

EDTA - Ethylenediaminetetraacetic acid

EGF - Epidermal growth factor

EGTA - Ethylene glycol-bis(β-aminoethyl ether)-N,N,N′,N′-tetraacetic acid

ELISA - Enzyme-linked immunosorbent assay

EMT - Epithelial-to-Mesenchymal Transition

esRAGE - Endogenous secretory RAGE

ERK - Extracellular-regulated kinase

EVT - Extravillous trophoblast

F-actin - Filamentous actin

FAK - Focal adhesion kinase

FBS - Foetal Bovine Serum

FGF-1 - Fibroblast Growth Factor 1

FITC - Fluorescein isothiocyanate

FN - Fibronectin

G - Gram

g - G force (or relative centrifugal force)

$G\gamma_2$ - G protein gamma 2

GFP - Green fluorescent protein

GPCRs - G protein-coupled receptors

HaCaT - Human keratinocyte cell line

HDAC2 - Histone Deacetylase 2

HEK-293H - Human embryonic kidney cells

HEPES - 4-(2-hydroxyethyl)-1-piperazineethanesulfonic acid

HGF - Human growth factor

HRP - Horseradish Peroxidase

HSA - Human serum albumin

IF - Immunofluorescence

IFN-β - Interferon beta

IKKα - Inhibitor of nuclear factor kappa-B kinase subunit alpha

IκBα - NF-Kappa-B Inhibitor Alpha

IL-11 - Interleukin 11

IUGR - Intrauterine growth restriction

K_d - Dissociation constant

LMB - Leptomycin B

µ - Micro

m - milli

M - Molar

MAPK - Mitogen-activated protein kinase

MEK - Mitogen-activated protein kinase kinase

MEM - Minimum Essential Media

Mg^{2+} - Magnesium ions

MMPs - matrix metalloproteinases

MODA- Membrane Optimal Docking Area

MS - Mass spectrometry

MTS - Tetrazolium inner salt (3-(4,5-Dimethylthiazol-2-yl)-5-(3-carboxymethoxyphenyl)-2-(4-sulfophenyl)-2*H*-tetrazolium)

n - Nano

N-cadherin - Neural cadherin

N-ERMAD - N-terminal ERM association domain

NES - Nuclear Export Signal

NFκB - Nuclear factor kappa-light-chain-enhancer of activated B cells

NLS - Nuclear localisation sequence

NMIIA - Non-muscle myosin IIA

NO - Nitric oxide

NP-40 - Nonidet P40

NS - Not significant

O_2 - Oxygen

PAGE - Polyacrylamide gel electrophoresis

PAK - p21-activated kinase

PBS - Phosphate-Buffered Saline

PFA - Paraformaldehyde

PI3K - Phosphoinositide 3-kinase

$PI(4,5)P_2$ - phosphatidylinositol 4,5-bisphosphate

PKB - Protein kinase B

PTM - Post-translational modification

PVDF - Polyvinylidene fluoride

RAGE - Receptor for Advanced Glycation Endproducts

ROCKs - Rho-associated protein kinases

RT-PCR - Real-time Polymerase Chain Reaction

S100PBP - S100P Binding Protein

SD - Standard Deviation

SDS - Sodium Dodecyl Sulfate

SDS-PAGE - Sodium Dodecyl Sulfate Polyacrylamide Gel Electrophoresis

SEM - Standard Error of the Mean

siRNA - Small interfering RNA

STB - Syncytiotrophoblast

TBS - Tris-Buffered Saline

TEMED - Tetramethylethylenediamine

TG - Thapsigargin

TLR4 - Toll-like receptor 4

tPA - Tissue plasminogen activator

TRE - Tetracycline Response Element

v/v - Volume per volume

vCTB - Villous cytotrophoblast

w/v - Weight per volume

WB - Western Blot

WT - Wild-type

YFP - Yellow fluorescent protein

Zn^{2+} - Zinc ions

List of Figures

List of Tables

Chapter 1:

Introduction

Chapter 1: Introduction

Contents

1.1. S100 Proteins

1.1.1. S100 protein family

The S100 family consists of at least 25 different members with a high degree of structural similarity and tissue specific expression and distribution (Figure 1.1.1). They are characterised by EF-hand domains at both the N-terminal and C-terminal regions, separated by a hinge region, which are highly conserved among members of this family. The EF-hands present within S100 proteins, otherwise known as helix-loop-helix domains, have the role of binding calcium, an intracellular second messenger that is required to regulate a number of different cellular processes, including cellular proliferation, motility and protein phosphorylation (Donato, 2001). Members of the S100 family are not known to contain any intrinsic enzymatic activity, and instead modulate the activities of their binding partners (Yammani 2012).

The presence of the S100 protein family was first discovered in brain tissue by J.W Moore, with this member of the S100 family later being named S100B (Moore 1965). All members of the S100 family are small 10-12kDa proteins that have a role in the regulation of both intracellular and extracellular processes in a variety of tissues and cell types. For example, S100A1 is present in high concentrations within cardiac muscle, and has been shown to regulate titin-actin interactions (Duarte-Costa *et al.* 2014). Purified S100A1 has been shown to prevent the assembly of brain microtubule proteins, subsequently affecting cellular migration (Donato, 1988). S100B is localised to glial cells in the brain, and has been documented to be involved in several processes, including but not limited to apoptosis, differentiation and cell migration (Donato *et al.* 2009).

Each EF-hand present within the S100 proteins have differing affinities for calcium ions. The C-terminal canonical EF-hand, spanning around 12 amino acids, demonstrates a high calcium binding affinity ranging between 10 and 50μM, compared to the N-terminal pseudo EF-hand, spanning 14 amino acids, which has a much weaker calcium binding affinity of between 200 and 500μM for each of the different S100 proteins (Donato, Rosario 1986). These EF-hand regions display a high level of conservation between different members of the S100 family, signifying their importance in S100 protein functionality. Binding of calcium ions to the loop regions of S100 proteins results in structural changes, generally within helices 3 and 4 (Gross *et al.* 2014). Calcium-induced conformational changes consequently lead to exposure of a number of hydrophobic residues present within the C-terminal helices of this family, which in turn allows for S100 protein target binding (Becker *et al.* 1992). In many cases, target protein binding leads to the activation of said target protein. Since each S100 monomer has a hydrophobic cleft, which allows the binding of two target proteins that can either be identical or

heterogeneous (Donato, 2001). Only minor changes occur in the N-terminal EF hand structure upon binding of calcium ions (Capozzi *et al.* 2006).

The multifunctionality and diversity of S100 proteins can perhaps be attributed to several features. This includes their ability to be localised to a variety of cellular compartments, in addition to their ability to bind a range of metal ions, primarily Ca^{2+}, but also including Zn^{2+}, Mg^{2+} and Cu^{2+} (Gilston *et al.* 2016). A combination of these features leads to S100 proteins being able to interact with a wide variety of target proteins (Heizmann, Claus W. 2002). Most family members can bind 4 calcium ions per dimer formed, even though each member may have varying affinities for calcium ions (Zimmer *et al.* 2003). For example, S100B has a moderate affinity for calcium ions (K_D = 2-20μM), and a high affinity for zinc ions (K_D = 0.1-1μM) (Leclerc *et al.* 2009). Interestingly, one member of the S100 protein family, S100A10, contains mutations in its EF-hand regions, rendering it unable to bind calcium ions (Réty *et al.* 1999). Gribenko and Makhatadze (1998) demonstrate that binding of magnesium ions to the N-terminal EF hand of S100P causes the calcium-binding affinity of the C-terminal EF hand to increase. Zinc ions in particular have been shown to influence oligomerisation state of S100 proteins *in vitro* (Moroz *et al.* 2009). The extracellular space contains a significantly higher concentration of calcium ions than the intracellular environment, suggesting the promotion of certain calcium-binding S100 proteins into higher order oligomeric states (Heizmann, Claus W. 2002). The effects of oligomeric S100 proteins and their capacity for target protein interaction has yet to be fully explored.

S100 protein family members also exhibit differences in their dimerisation capabilities. Some family members can form both hetero- and homodimers, whereas others can only form one or the other. For example, S100A8 and A9 heterodimers have been shown to be released from monocytes and neutrophils in order to modulate the inflammatory response (Pruenster *et al.* 2016). Spratt *et al.* (2019) showed that S100A1 and S100B heterodimers are preferentially formed over their respective homodimers. One member of the S100 family, calbindin-D9k (S100G), cannot form dimers, most likely due to the amphiphilicity of helix 4 in comparison to other S100 proteins (Potts *et al.* 1996).

Given the wide variety of roles S100 proteins play in both intracellular and extracellular processes, it is unsurprising that they can be found in a multitude of cell types and subcellular localisations.

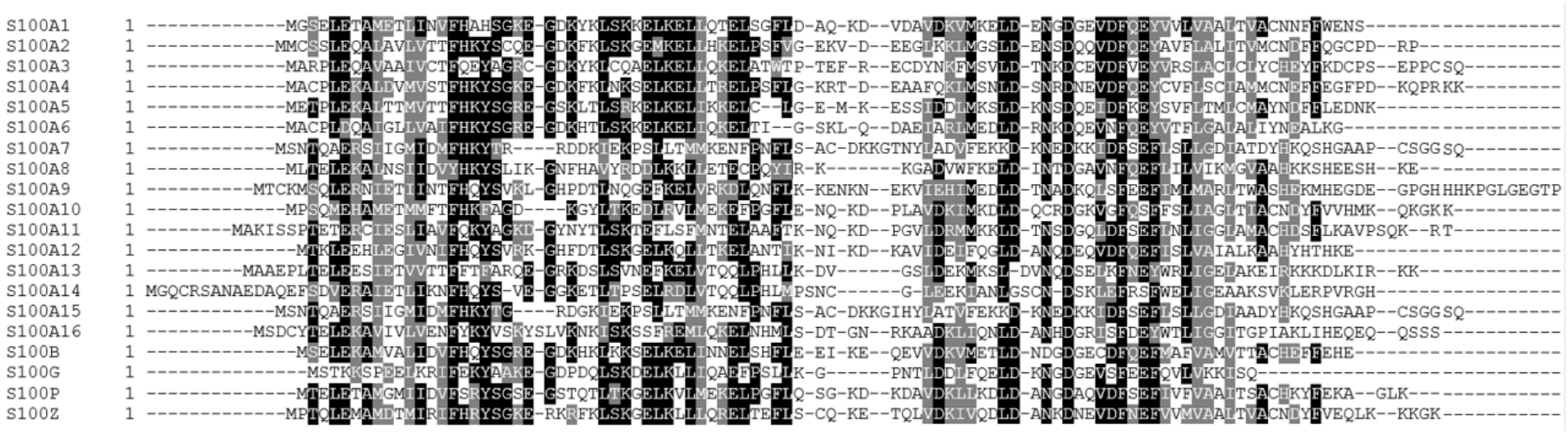

Figure 1.1.1: Comparison of S100 family protein sequences

Multiple alignment of S100 protein sequences using CLUSTALW software. Protein accession numbers used for alignment are as follows: S100A1, P23297; S100A2, P29034; S100A3, P33764; S100A4, P26447; S100A5, P33763; S100A6, P60703; S100A7, P31151; S100A8, P05109; S100A9, P06702; S100A10, P60903; S100A11, P31949; S100A12, P80511; S100A13, Q99584; S100A14, Q9HCY8; S100A15, Q86SG5; S100A16, Q96FQ6; S100B, P04271; S100G, P29377; S100P, P25815; S100Z, Q8WXG8. Alignment output from CLUSTALW was shaded using BOXSHADE, in which conserved residues in each member of the S100 family are highlighted in black, and similar residues are highlighted in grey. Adapted from Gross *et al.* (2014)

1.1.1.1 Extracellular S100 proteins

Extracellular actions of several S100 proteins have been reported by multiple groups. Their reported effects are wide, ranging from stimulating secretion of nitric oxide (NO) by neurons and astrocytes to propagation of inflammation (Donato, Rosario 2003). Below, the various modes of extracellular S100 protein activity, either by secretion or through binding to cell surface receptors, is discussed.

1.1.1.1.1 S100 protein secretion

Secretion of several S100 proteins have been investigated. S100 proteins lack a signal peptide for their secretion, suggesting that their secretion through canonical pathways does not take place. Whether S100 proteins are actively or passively secreted from cells is still under debate (Bresnick *et al.* 2015). Secretion of S100B through canonical pathways have been ruled out, as its mRNA does not encode an N-terminal secretion signal. However, S100B has been detected in the extracellular fluid of the brain, in addition to conditioned media from glioma cells (Barger *et al.* 1992).

Prior investigations concerning the S100A8/A9 heterodimer have posited that active S100A8/A9 secretion in neutrophils occurs through a novel pathway (Rammes *et al.* 1997). Classical protein secretion involves transport through the endoplasmic reticulum/Golgi complex, directed by the presence of a signal sequence within the protein (Kim, Jiyoon *et al.* 2018). Rammes *et al.* (1997) concluded that secretion of S100A8/A9 occurred was an energy-dependent process involving activation of protein kinase C (PKC). Labelling of S100A8/A9 with [^{38}S] methionine demonstrated their selective, steady secretion from monocytes. In addition, colocalisation analysis of S100A8/A9 heterodimers with microtubules suggested that their secretion was dependent on an intact microtubule network; by inhibiting tubulin polymerisation by use of nocodazole, release of S100A8/A9 into monocyte supernatants was inhibited. Following treatment of monocytes with 4β-phorbol 12-myristate 13-acetate (PMA), a phorbol ester known to stimulate S100A8/A9 secretion, S100A8/A9 was localised to the filamentous tubulin network. In contrast, depolymerisation of tubulin by nocodazole led to a diffuse S100A8/A9 localisation. Presence of the S100A8/A9 heterodimer has been observed in serum from patients with inflammatory conditions, such as rheumatoid arthritis, cystic fibrosis and bronchitis (Kerkhoff *et al.* 1998), although its exact role in these conditions have yet to be elucidated.

Kim *et al.* (2017) characterised the role of the S100A4 protein in osteoblast differentiation and function. Through *in vitro* recombinant S100A4 treatment, the authors demonstrated that exogenous S100A4 had no effects on osteoblast differentiation, with levels of a key transcription factor in

osteoblast differentiation, Runx2, remaining unchanged following treatment. However, the group did find inhibitory effects on matrix mineralisation by osteoblasts in culture. This was not due to changes in cellular proliferation or survival, but due to a decrease in levels of the transcription factor of osterix, a necessary transcription factor in the process of mineralisation. In addition, the authors reported S100A4-induced activation of the NFκB pathway, with increased phosphorylation of IKKα and IκBα detected, and attenuation of S100A4-dependent decreases in matrix mineralisation following treatment with a NFκB inhibitor.

Serum levels of certain S100 proteins have been implicated in disease progression. Cai *et al.* (2011) found increased levels of S100B, S100A6 and S100P in serum from patients suffering acute coronary syndrome compared to those with stable angina. S100A4 has been found to be significantly increased in serum from patients suffering from epithelial ovarian cancer compared to serum from both healthy patients, and those with benign ovarian disease (Lv *et al.* 2018). The authors also demonstrated a correlation between high serum S100A4 and metastasis to lymph nodes, in addition to cancer recurrence, making serum S100A4 levels a useful diagnostic and prognostic biomarker for epithelial ovarian cancer. Significantly elevated serum levels of S100A8/9 and S100A12 were found in patients with giant cell arteritis, a form of large vessel vasculitis, compared with healthy controls (Springer *et al.* 2018). Serum levels of S100A9 were found by to be significantly increased in prostate cancer patients compared to either healthy patients or benign prostate cancer patients (Hermani *et al.* 2005). In addition, S100A9 serum levels demonstrated a higher sensitivity between benign and malignant prostate cancers than the best current diagnostic marker for prostate cancer, prostate specific antigen, suggesting serum S100A9 may be a more reliable diagnostic marker for these patient groups. High levels of S100P in serum from cholangiocarcinoma patients were detected by Wu *et al.* (2016), a 3-fold increase in comparison to healthy individuals. S100P was also detected in serum from colorectal cancer patients, with the authors of the study establishing that colorectal cancer patients with normal S100P serum levels had a significantly more favourable prognosis than those with elevated serum levels (Wang *et al.* 2012). In addition, Peng *et al.* (2016) highlighted a correlation between high plasma S100P levels and poor survival in metastatic breast cancer patients. These works together suggest the potential for either serum or plasma levels of S100P as a biomarker for diagnosis and prognosis for various cancers.

1.1.1.1.2 S100 proteins and receptors

S100 proteins have been reported to bind several cell surface receptors, with the most thorough investigations surrounding S100 proteins binding to the receptor for advanced glycation end products (RAGE). RAGE is a member of the immunoglobulin superfamily, and is a transmembrane cell surface receptor that interacts with a variety of different ligands, including a number of the S100 proteins (Leclerc *et al.* 2009). RAGE ligation and activation is known to lead to activation of several cell signalling pathways, such as the ERK1/2 pathway (Lander *et al.* 1997), Cdc42/Rac pathway (Huttunen *et al.* 1999), and the p38 MAPK pathway, the latter of which was shown by Taguchi *et al.* (2000) to be suppressed following inhibition of RAGE-amphoterin interaction in glioma cells.

RAGE comprises an extracellular domain, containing one variable (V) domain, and two constant (C1 and C2) domains, in addition to a transmembrane domain that anchors RAGE to the plasma membrane, and a cytoplasmic tail that transduces signals intracellularly (Schmidt 2015). Two forms of soluble RAGE (sRAGE) have also been detected in circulation. These forms comprise a variant in which MMPs cleave RAGE present on the extracellular surface (cRAGE) leaving only domains V-C1-C2, and a differential mRNA splice variant termed endogenous secretory RAGE (esRAGE) which contains a unique amino acid sequence in its C2 domain and lacks both the cytosolic and C-terminal domains (Detzen *et al.* 2019). Interestingly, the soluble forms of RAGE are thought of as protective forms, due to their competition with RAGE ligands, therefore inhibiting RAGE-ligand interactions (Bucciarelli *et al.* 2006; Yan, Ramasamy and Schmidt, 2010). However, the consequences of sRAGE-S100 protein interactions in particular are yet to be characterised.

The binding of S100 proteins with different domains of RAGE has been explored by several authors. The majority of S100 proteins, such as S100A1, S100A2, S100A5, S100A12 and S100P have been shown to interact with RAGE's V domain (Leclerc *et al.* 2009). S100B interacts with the V and V-C1 domains with high affinity (K_D V = 0.5-0.6μM, K_D VC1 = 11nM-0.2μM). In contrast, S100A6 specifically interacts with the C1 and C2 domains (K_D VC1 = 0.6μM-5.8μM, K_D C2 = 28nM-1μM) (Leclerc *et al.* 2007), and its interaction with the V domain of RAGE was undetectable. In addition, both S100B and S100A6 proteins were found by Leclerc *et al.* (2007) to interact with sRAGE with high affinity.

Interestingly, oligomers of S100 proteins have been shown to bind to RAGE. Analytical ultracentrifugation studies suggest that the S100B tetramer can bind to two RAGE molecules (Ostendorp *et al.* 2007). This, in turn, could potentially lead to RAGE multimerisation and subsequent signal transduction. S100A12 is known to form a hexameric structure to enable its binding to RAGE tetramers (Moroz *et al.* 2002).

S100B and S100A12 were the first members of the S100 family demonstrated to interact with RAGE, with the latter originally named EN-RAGE (Hofmann *et al.* 1999). S100B has been demonstrated to act in concert with S100A1 and amphoterin to activate NFκB, in addition to promoting cellular survival through increased expression of Bcl-2, an anti-apoptotic protein. S100B and S100A1 together can induce the outgrowth of neurites in a RAGE-dependent manner (Huttunen *et al.* 2000). S100A12 secreted from inflammatory cells *in vitro* has been shown to interact with RAGE, leading to the production of NF-κB and pro-inflammatory cytokines such as IL-6 and IL-8 (Yang *et al.* 2007).

Interaction of RAGE with S100P has also been explored by several groups. Marcado-Pimentel *et al.* (2015) showed that addition of exogenous S100P to colon cancer cells leads to upregulation of miRNA-21, and that blocking RAGE by use of an anti-RAGE antibody abrogated S100P-dependent miRNA-21 upregulation. Much of the work surrounding S100P and RAGE occurs in the context of pancreatic cancer, where S100P stimulates cell proliferation and survival *in vitro* through RAGE (Arumugam *et al.* 2004). Downstream consequences of S100P-RAGE interactions will be discussed in further detail in 1.1.2.2.

Several receptors other than RAGE have been demonstrated to interact with S100 proteins. For example, regulation and expression of CC chemokine receptor 10 (CCR10), a member of a subfamily of GPCRs, on the surface of melanocytes is in fact regulated by S100A10, and S100A10 binds directly to the C-terminal cytoplasmic tail of CCR10 (Hessner *et al.* 2016). S100A10 also regulates the cell surface localisation of the serotonin receptor 5HT1B and of TRPV5, a protein involved in calcium reabsorption. In fact, overexpression of S100A10 results in increased 5HT1B at the cell surface and modulates signal transduction (Warner-Schmidt *et al.* 2009). S100A10 has also been implicated in Toll-like receptor (TLR) signalling, where S100A10 deficiency seemingly enhances signalling through TLR in macrophages. (Lou *et al.* 2019). The group observed enhanced phosphorylation of several kinases such as ERK and p38, in addition to phosphorylation of transcription factor IRF3, as determined by ELISA.

A subset of other S100 proteins also bind to TLRs. S100A12, expressed by granulocytes (Orczyk and Smolewska 2018), was found to be overexpressed in patients experiencing acute sepsis, and promoted the activation of monocytes through activation of TLR4 *in vitro* (Foell *et al.* 2013). S100A8 has been documented to stimulate formation and function of osteoclasts, again mediated by TLR4. The S100A8-dependent stimulation of osteoclast function was suggested to occur by stimulating the formation of actin rings, which have been shown to be a key marker of osteoclast capacity for bone resorption (Grevers *et al.* 2011).

1.1.1.1.3 Extracellular S100 protein interactions

The presence of S100A10 at the cell surface, in complex with annexin A2 as the S100A10-annexin A2 heterotetramer (AIIt) has been documented in fibrosarcoma cells (Choi *et al.* 2003). In addition, its expression at the cell surface was correlated with increases in invasion and degradation of the extracellular matrix (ECM).

The interaction of S100A10 with annexin A2 is well documented, however other S100 proteins such as S100A4, S100A6 and S100A11 have also been shown to bind to annexin A2. The S100A4-AnnexinA2 complex was suggested to be responsible induction of angiogenesis through formation of plasmin from plasminogen, through activation of tissue plasminogen activator (tPA) (Semov *et al.* 2005). Additionally, the authors demonstrated the importance of the C-terminal lysine residues of S100A4, which like S100A10, were also shown to be essential for plasminogen activation, as mutant S100A4 with two C-terminal lysines mutated to leucines retained only 15% of its activity in comparison to WT S100A4.

Interaction of S100A11 with the N-terminal region of annexin A2 was demonstrated by Rintala-Dempsey *et al.* (2006) through NMR experiments. S100A11 has also been shown to bind annexin A1 (Réty *et al.* 2000), however this interaction is at a much-reduced affinity to that of annexin A2. Regarding the biological consequences of the S100A11-annexinA2 complex, Jaiswal *et al*. (2014) have shown that S100A11 in complex with annexin A2 can direct membrane repair following external cell injury. The authors proposed that the S100A11-annexin A2 complex accumulates at the site of injury, binds to F-actin, and prevent its depolymerisation which in turn preserves levels of F-actin at the site of injury.

Binding of S100A6 to annexin A2 has been demonstrated in pancreatic cancer cells *in vitro* by mass spectrometry and reciprocal immunoprecipitation (Nedjadi *et al.* 2009). In addition, depletion of S100A6 by siRNA treatment led to a significant decrease in annexin A2 at the plasma membrane, together with impairment of pancreatic cancer cell motility assessed by Boyden chamber migration assays, suggesting a correlation in levels of S100A6 and annexin A2.

1.1.1.2 S100 proteins in cell motility and invasion

The role of S100 proteins in the processes of cellular motility and invasion have been covered extensively by Gross *et al.* (2014). Almost all S100 proteins discovered thus far have been implicated

in either progression or inhibition of cellular motility and invasion of a wide variety of cell types, in both physiological and pathophysiological tissues, through various pathways and effector proteins.

S100A4 has been extensively studied in regards to its role in migration and invasion. Expression of S100A4 has been demonstrated to enhance the migration of breast cancer cell lines MDA-MB-231 and MDA-MB-468 through promotion of EMT. Equally, knockdown of S100A4 induced expression of epithelial markers E-cadherin and vimentin (Xu *et al.* 2016). Through its interaction with non-muscle myosin IIA (NMIIA), S100A4 promotes disassembly of NMIIA filaments and inhibits the assembly of NMIIA monomers into filaments (Li *et al.* 2003) inhibiting cell migration. Overexpression of S100A4 has been observed in metastatic cells and tissues, where its expression level correlates with increased levels of motility and invasion of mammary tumour cells through Boyden chambers (Jenkinson *et al.* 2004). Transfection of MCF-7 breast cancer cells with anti-sense S100A4 led to decreased cellular motility mediated through connective tissue growth factor (CTGF), a protein whose expression is also seen to be elevated in advanced breast cancer (Chen *et al.* 2007).

Another well studied member of the S100 family that has been implicated in cellular motility and invasion is S100A10. Its localisation is cytosolic, however binding to is ligand annexin A2 leads to the formation of a S100A10-annexin A2 heterotetramer (AIIt), which results in the translocation of S100A10 to the plasma membrane, and its presence on the extracellular surface (O'Connell *et al.* 2010). The S100A10 subunit of AIIt is responsible for binding of plasminogen and tPA, and can regulate plasminogen activation by tPA. Silencing of S100A10 expression by use of siRNA in colorectal cancer cell line Colo 222 led to the abrogation of plasmin binding and generation, consequently leading to significant decreases in cellular invasion (Zhang, Libo *et al.* 2004). Similar observations regarding S100A10 expression and consequent changes in cellular motility and invasion were made by O'Connell *et al.* (2010). Macrophage migration across the peritoneal membrane in S100A10-deficient mice was significantly decreased compared to WT mice, in addition to a reduction in invasion through Matrigel-coated Boyden chambers that is dependent on plasmin. The authors found that macrophages from S100A10-deficient mice had lowered production of plasmin in addition to decreased activation of MMP-9, suggesting that the generation of plasmin by macrophages, and consequent invasion, is dependent on S100A10 expression.

Many S100 proteins have been associated with the invasive process in cancer, sometimes through mediating transcription or expression of MMPs. For example, the S100A14 protein can influence cellular migration and invasion of oesophageal squamous cell carcinoma cells through Boyden chambers through regulating the transcription of matrix metalloprotease 2 (MMP-2), assessed by the use of a transwell assay system (Chen *et al.* 2012). This process was shown to be mediated through

tumour suppressor protein p53, and increased MMP-2 expression was observed with a significant reduction in p53 expression and transcriptional activity in S100A14-overexpressing oesophageal squamous cell carcinoma cells.

Previous work by Rammes *et al.* (1997) demonstrated the colocalisation of the S100A8/A9 heterodimer with microtubules following monocyte activation. Vogl *et al.* (2004) further characterised this interaction through the use of spin-down binding assays, and found that the interaction with tubulin was calcium-dependent and did not depend on phosphorylation of S100A9 (K_D = 0.14 ± 0.05μM). Further analysis by the group found that the S100A8 subunit was principally responsible for the interaction with tubulin. Granulocytes from S100A9 knockout mice (S100A9-/-) were found to express less tubulin, in addition to decreased levels of Rac1 and Cdc42. Transendothelial migration of granulocytes from S100A9-/- mice did not increase following activation of p38 MAPK by use of arsenite. Conversely, S100A9+/+ mice demonstrated a significant 1.2-fold increase in their transendothelial migration capabilities following arsenite treatment. Activation of the MAPK pathway in granulocytes was dependent on S100A9 phosphorylation, suggesting the association of increases in transendothelial migration with both S100A9 phosphorylation and p38 MAPK activation.

1.1.1.3 Cellular localisation of S100 proteins

The subcellular localisations of proteins are essential for protein function; it determines the access of proteins to their target interactors, and consequently their effects. Protein mis-localisation has been demonstrated in several disease states (Hung and Link 2011) suggesting the importance of protein localisation to specific subcellular compartments.

The diverse nature of S100 protein expression and interaction partners allows for their diverse subcellular localisations in different tissues. The ability of S100 proteins to bind calcium is one key regulator of their localisation, as changes in cellular calcium concentration have been shown to lead to the alteration of S100 protein subcellular distribution.

Prior investigations of the localisation of several S100 proteins have been carried out by Mandinova *et al.* (1998). Immunolocalisation studies of two separate smooth muscle cell lines derived from human aorta showed that S100A1 was found to be primarily cytosolic and firmly associated with both actin stress fibres and sarcoplasmic reticulum. Similar results were demonstrated with S100A4 in the same cell lines; S100A4 colocalised with stress fibres in the cell periphery in addition to cytosolic staining. Staining of the same cell lines for S100A6 demonstrated that 90% of cells showed a cytoplasmic

staining, with the remaining 10% showing a strong nuclear staining with weak cytoplasmic signals. S100A2 staining, once again with the same cell lines, was shown to be confined to the nucleus of all cells studied. The authors compared the *in vitro* staining with *in vivo* arterial smooth muscle, finding identical patterns of immunostaining for all S100 proteins studied.

Orre *et al.* (2007) studied the immunolocalisation of S100A6 following irradiation in A549 human lung adenocarcinoma cells. Prior to irradiation, A549 cells demonstrated a nuclear localisation of S100A6. However, 24 hours post-irradiation, S100A6 was primarily cytosolic in nature and was colocalised with tropomyosin, a suggested cytoplasmic interaction partner of S100A6.

The specific localisations of S100A6, S100A4 and S100A2 in tumour cell lines MDA-MB-231 and HeLa have also been investigated (Mueller *et al.* 1999). Following immunostaining, S100A6 was localised to the cytosol in both cell lines, and low-level translocation to the rough endoplasmic reticulum and plasma membrane was observed after stimulation of intracellular calcium with thapsigargin (TG). Perinuclear localisation of S100A4 was observed in HeLa and MDA cells along with diffuse cytosolic staining, with TG treatment leading to relocation of perinuclear S100A4 to the cytoplasmic region. The S100A2 protein was found to be primarily nuclear in both cell lines, forming punctate structures. TG treatment did not drastically alter its cellular localisation, unlike the other S100 proteins studied. No differences in localisation of any S100 proteins studied were observed when using several other agents to increase intracellular calcium, such as ionophore A23187 or cyclic ADP-ribose.

Immunohistochemical analysis of adenocarcinoma tissue found that patients with membrane and nuclear S100A16 staining showed better prognostic outcomes in contrast to patients that demonstrated only membranous S100A16 staining (Kobayashi *et al.* 2018).

S100A4 has been observed by immunofluorescence to localise to the leading edge of migrating MDA-MB-231 breast cancer cells, and was demonstrated to colocalise at this location with NMIIA (Kim and Helfman 2003). Colocalisation of S100A4 with N-WASP, a regulator of actin polymerisation, was also observed at the lamellipodial region by the same group, suggesting a role for S100A4 in mediating processes of motility in these cells through interaction proteins in various subcellular compartments.

Post-translational modifications (PTMs) have also been demonstrated to alter S100 protein subcellular localisation. In human articular chondrocytes, S100A4 translocated from the cytosol to the nucleus following stimulation by interleukin-1β, however this translocation was dependent on sumoylation of S100A4's C-terminal lysines by sumo-1 (Miranda *et al.* 2010). Sumoylation and S100A4 translocation were prevented by mutating these C-terminal lysine residues, highlighting the importance of PTMs in modulating protein localisation.

1.1.2 S100P

The S100P protein, originally isolated from the placenta (Becker *et al.* 1992), is a 10.4kDa member of the S100 protein family that mediates a variety of processes, including cellular invasion, cell proliferation, drug resistance and differentiation (Dakhel *et al.* 2014). S100P is expressed in vertebrates, namely humans, chimpanzees, opossums and dogs. Interestingly, S100P is not expressed in rodent species such as mice and rats (Shang *et al.* 2008).

S100P has been shown to be expressed in normal tissues, such as in the placenta during embryo implantation, but the majority of literature on S100P explores its relation to cancer progression (Prica *et al.* 2016).

1.1.2.1 Structure of S100P

S100P, like all members of the S100 family, consists of two EF-hand domains at either end of the protein, connected by a hinge region (Figure 1.1.2). Each EF-hand domain consists of a "helix-loop-helix", in which a calcium-binding loop is surrounded by an alpha helix on each side. S100P has the ability to bind to multiple divalent cations, including Ca^{2+}, Zn^{2+} and Mg^{2+}. Zn^{2+} ions only bind to the C-terminal EF-hand of S100P, whereas Mg^{2+} only binds to the N-terminal EF-hand (Gribenko and Makhatadze 1998). Interestingly, both EF-hand domains have differing affinities for calcium; the N-terminal EF-hand of S100P has a lower affinity for calcium ions than the canonical C-terminal domain (K_d C-terminal EF hand ~ 10^{-7} M; K_d N-terminal EF hand ~ 10^{-4} M, Gribenko and Makhatadze, 1998). This may be due to the N-terminal domain binding calcium through main-chain carbonyl groups (Santamaria-Kisiel *et al.* 2006), or the limited structural changes S100P showcases upon binding calcium ions compared to the C-terminal domain (Marenholz and Heizmann, 2004). Changes in calcium ion concentration lead to a significant change in the tertiary structure of S100P, namely the orientation of the helical regions (Gribenko and Makhatadze 1998).

Koltzscher and Gerke (2000) characterised the residues involved in forming the dimer interface between S100P homodimers, demonstrating the importance of the F15 residue in this process, as although F15A S100P can be expressed and purified, no interaction with WT S100P was detected. When both monomers contain a F89A mutation, dimerisation is significantly limited. Austermann *et al.* (2008), on the other hand, concluded that the C-terminal extension of S100P, residues 88-95, are in fact dispensable for dimerisation. A crystal structure of S100P generated by Zhang *et al.* (2003) seems to confirm the limited contribution of these residues to the dimer interface.

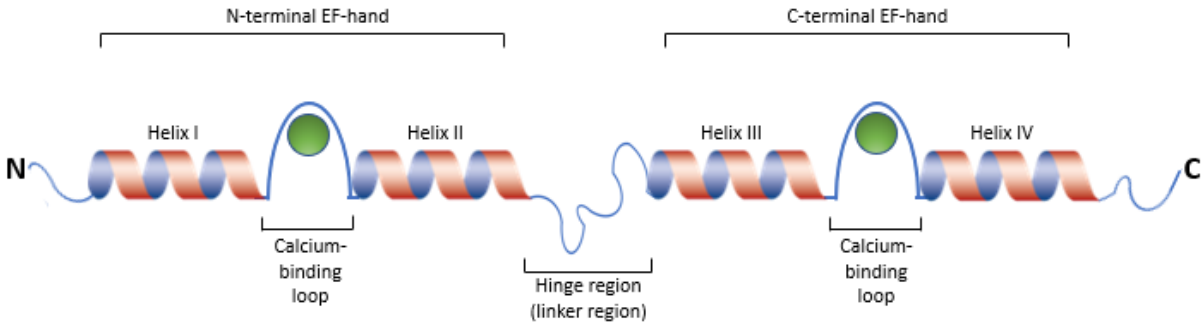

Figure 1.1.2 Secondary structure of S100P

The secondary structure of S100P consists of a pseudo EF-hand (N-terminus), a canonical EF-hand (C-terminal), two loop regions capable of binding calcium ions, each of which are surrounded by two alpha helices. A linker domain connects both EF-hands between helix 2 and helix 3.

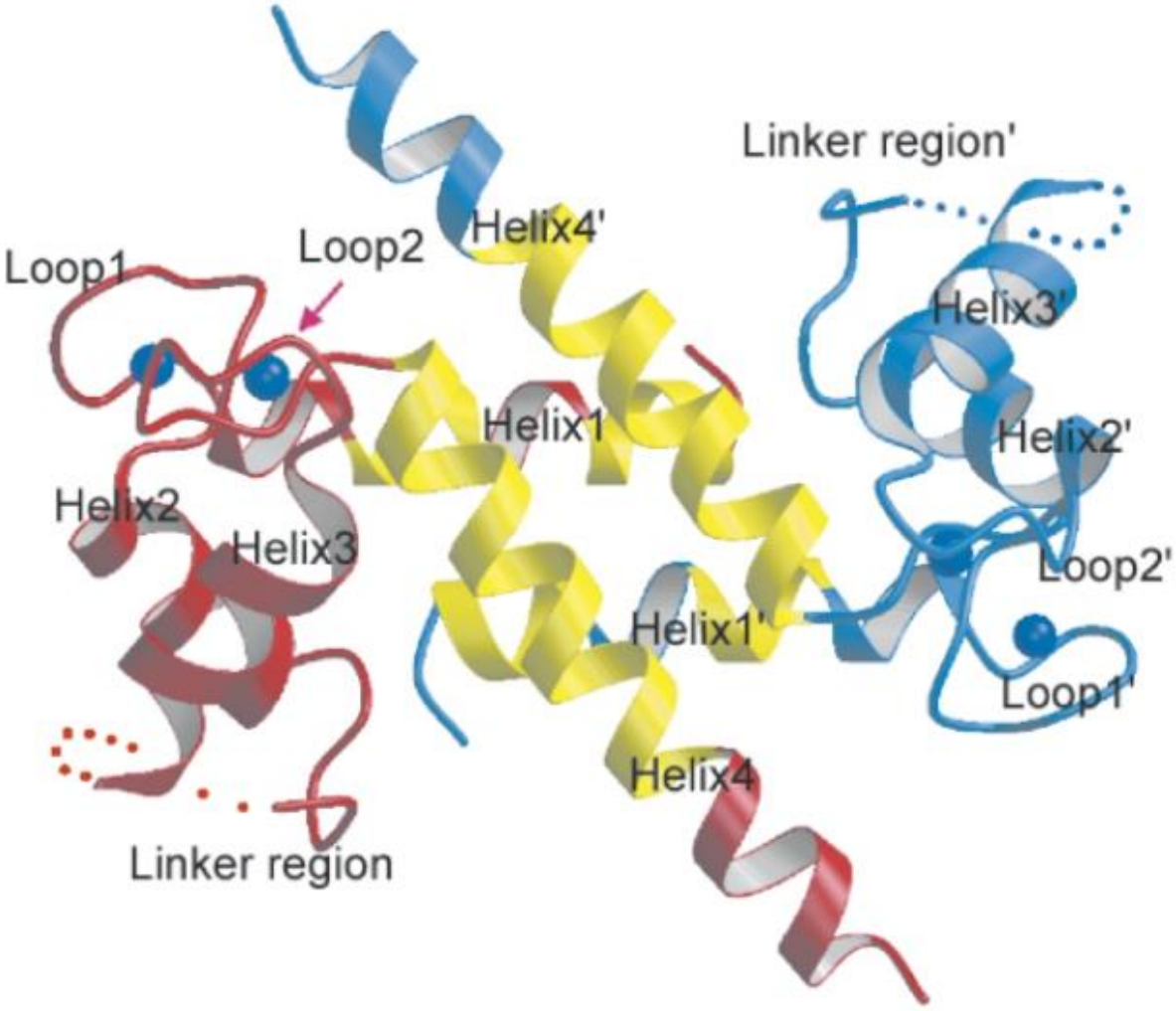

Figure 1.1.3: Ribbon model of S100P dimer

Ribbon model of the S100P dimer generated by X-ray crystallography, with PDB accession number 1J55. Adapted from Zhang *et al.* (2003).

1.1.2.2 Intracellular interacting partners of S100P

A variety of different proteins have been documented to associate with S100P to elicit different responses mainly, if not exclusively using cancer cell lines (Figure 1.1.4).

Ezrin is one such protein; it is a member of the ERM protein family that serves as a cross-linking protein between F-actin and the plasma membrane. (Austermann *et al.* 2008). This interaction is dependent on calcium and requires dimerised S100P. Austermann *et al.* (2008) characterised a variety of S100P mutants and their ability to interact with ezrin, and found that truncated versions of S100P at the C-terminus (S100P 91aa and S100P 87aa) could be expressed, form dimers, and demonstrated similar properties to WT S100P. However, binding of ezrin to the S100P 87aa mutant alone was abrogated, suggesting key contact residues for ezirn-S100P interactions are present within this region. In addition, the stimulatory effects of S100P-ezrin interactions on transendothelial migration were prevented following treatment with the S100P 87aa mutant, but not S100P WT or the S100P 91aa mutant.

Another protein observed to interact with S100P is IQGAP1. The actin binding protein IQGAP1 is ubiquitously expressed and has been shown to play a role in actin cytoskeleton regulation and microtubule reorganisation (Heil *et al.* 2011). Interestingly, IQGAP1 was found to bind to the N-terminal domain of S100P and does not require the higher affinity C-terminal EF-hand domain to elicit its function unlike other S100P target proteins. A number of other actin binding proteins have been documented to interact with IQGAP1, including but not limited to Arp2/3, N-WASP and Cortactin (White *et al.* 2013). The interaction between S100P and IQGAP1 requires S100P dimerisation and is calcium dependent. Colocalisation of the two proteins was found at the plasma membrane/cell cortex by immunofluorescence following stimulation with EGF, which is known to stimulate intracellular calcium levels. It was also found that S100P prevented EGF-induced tyrosine phosphorylation of IQGAP1, leading to impaired interaction between IQGAP1 and B-Raf, a part of the MAPK cascade.

Calcium-bound S100P has also been documented by Du *et al.* (2012) to interact with different isoforms of non-muscle myosin II (NMII) with differing affinities. One isoform, NMIIA, has been associated with a number of cytoskeletal elements linked to Rho kinase, including focal adhesion and stress fibre organisation (Even-Ram *et al.* 2007), and induction of S100P expression in HeLa cells leads not only to a change in distribution of NMIIA to the cellular periphery, but also decreases the number of vinculin-containing focal adhesion sites. The implication of S100P induction in this cell line, and its effects on NMIIA, was increased cell migration.

A novel protein was characterised by Dowen *et al.* (2005) through *in vitro* far western screening and found to interact with S100P, once again in a calcium dependent manner. It was consequently named

S100P binding protein (S100PBP) and was observed to be localised to the nucleus in transfected HeLa cells transiently transfected with GFP-tagged S100PBP. Endogenous expression of S100P in HeLa cells was localised to both nuclear and cytoplasmic regions, and it was suggested that S100PBP interacts with S100P in the nuclear compartment. Later work by the group determined the differential expression of S100PBP between healthy and tumour tissues; healthy prostate, lung and breast tissues demonstrated increased S100PBP expression compared to their relative cancerous tissues, whereas healthy liver and thyroid tissues were observed to express much lower levels of S100PBP than their cancerous counterparts (Lines *et al.* 2012). Interestingly, expression of S100PBP and S100P in either normal pancreas or pancreatic ductal carcinoma (PDAC) samples were found to be inversely correlated. In normal tissues, S100P was undetectable in all samples, whereas S100PBP exhibited strong immunoreactivity in 85% of samples. Regarding PDAC samples, high levels of S100P immunoreactivity were found in 82% of samples, compared to 9% of samples exhibiting strong S100PBP staining. The same study demonstrated that silencing of S100PBP in Panc1 cells by siRNA led to significant increases in their invasion, but not their migration. Furthermore, the authors found that upon S100PBP overexpression, the FA6 pancreatic cancer cell line demonstrated significant decreases in cell adhesion to various ECM proteins, including fibronectin and vitronectin. The same reduction in adhesion was not observed in non-S100P expressing pancreatic cancer cell line Panc1, suggesting a role for both S100PBP and S100P in mediating these processes.

A recent study suggests that interaction between S100P and αβ-tubulin occurs both *in vitro* and *in vivo* (Du *et al.* 2020). This interaction leads to a decrease in tubulin polymerisation and enhances cellular migration of COS-7 and HeLa cell lines. In addition, disruption of microtubule organisation by addition of colchicine led to suppression of S100P-dependent migration, suggesting a potential mechanism for S100P-enhanced cell migration.

Co-immunoprecipitation experiments by Filipek *et al.* (2002) led to the detection of complex formation between recombinant S100P and Calcyclin-binding protein, otherwise known as Siah-1-interacting protein (CacyBP/SIP). CacyBP/SIP was found to form complexes with other S100 proteins, including S100B in rat brain extract. The consequences of the interaction are not characterised; however, it has been proposed that since CacyBP is a component of a ubiquitinylation pathway involved in β-catenin degradation, S100P may play a role in or modulate this process.

Another component of ubiquitinylation pathways, CHIP (C-terminus of Hsc70-interacting protein), has also been observed to interact with S100P (Shimamoto *et al.* 2013). CHIP functions as an E3 ubiquitin-ligase, with the role of targeting misfolded proteins for proteasomal degradation in concert with chaperone proteins Hsc70 and Hsp90 (Murata *et al.* 2001). The tetratricopeptide (TPR) domain of CHIP

is responsible for CHIP's interactions with the above chaperone proteins, and it is this domain through which S100P can bind to CHIP. The study by Shimamoto *et al.* (2013) found that interaction of S100P with CHIP led to the prevention of its interaction with both Hsp90 and Hsc70 in a calcium-dependent manner and preventing their ubiquitinylation.

1.1.2.3 Extracellular interacting partners of S100P

The target proteins of S100P mentioned thus far are intracellular in nature. However, S100P has also been reported to act extracellularly by a number of studies (Arumugam *et al.* 2005, Fuentes *et al.* 2007) through its interaction with the receptor for advanced glycation end products (RAGE). RAGE overexpression has been documented in a variety of cancers, including pancreatic cancer (Kang *et al.* 2017), and its overexpression was shown to promote survival of these cells. S100P secreted from pancreatic cancer cells was shown to act through RAGE on the cell surface, stimulating the activation of NFκB and activating the MAP kinase pathway (Arumugam and Logsdon, 2011). The activation of these proteins and their pathways influences the progression of these cancers, as NFκB has been shown to stimulate cell proliferation and survival (Rayet and Gelinas, 1999).

In addition to RAGE, Clarke *et al.* (2017) demonstrated the interaction with and activation of tissue plasminogen activator (tPA) by S100P *in vitro.* Once again, this interaction is dependent on calcium ions, and it has been proposed that this interaction occurs through the C-terminal lysine of S100P, as mutation or deletion of residue K95 in S100P results in a significant reduction in tPA activation. tPA-dependent activation of plasminogen was also reduced in the presence of the above S100P mutants. In addition, binding of WT recombinant S100P to both tPA and plasminogen was significantly reduced upon the addition of 6-aminocaproic acid (6-ACA), a lysine analogue, seemingly confirming the involvement of S100P's lysine residues in tPA and plasminogen activation. Activation of tPA by another S100 family member, S100A10, has also been observed, leading to enhanced invasion of macrophages (O'Connell *et al.* 2010).

S100P has also been found by Kazakov *et al.* (2015) to interact with interleukin 11 (IL-11) *in* vitro in a calcium-dependent manner through surface plasmon resonance. IL-11 contains two binding sites for S100P with differing affinities, with the study suggesting that serum S100P may associate with circulating IL-11 and its associated receptor. However, the details of this interaction, namely the residues involved in the interaction and the biological consequences of said interaction, are yet to be elucidated.

Hsu *et al.* (2015) pulled down S100P from CL1-0 cancer cell membranes and detected presence of integrin α7 by mass spectrometry, and later confirming their interaction by coimmunoprecipitation. The interaction between these two proteins led to increased focal adhesion kinase (FAK) activation, in addition to the activation of transcription factor protein kinase B (PKB, otherwise known as AKT). This study highlights a role for S100P in the FAK/AKT pathway in lung cancer, however the relevance of this interaction in other cell types has not been explored.

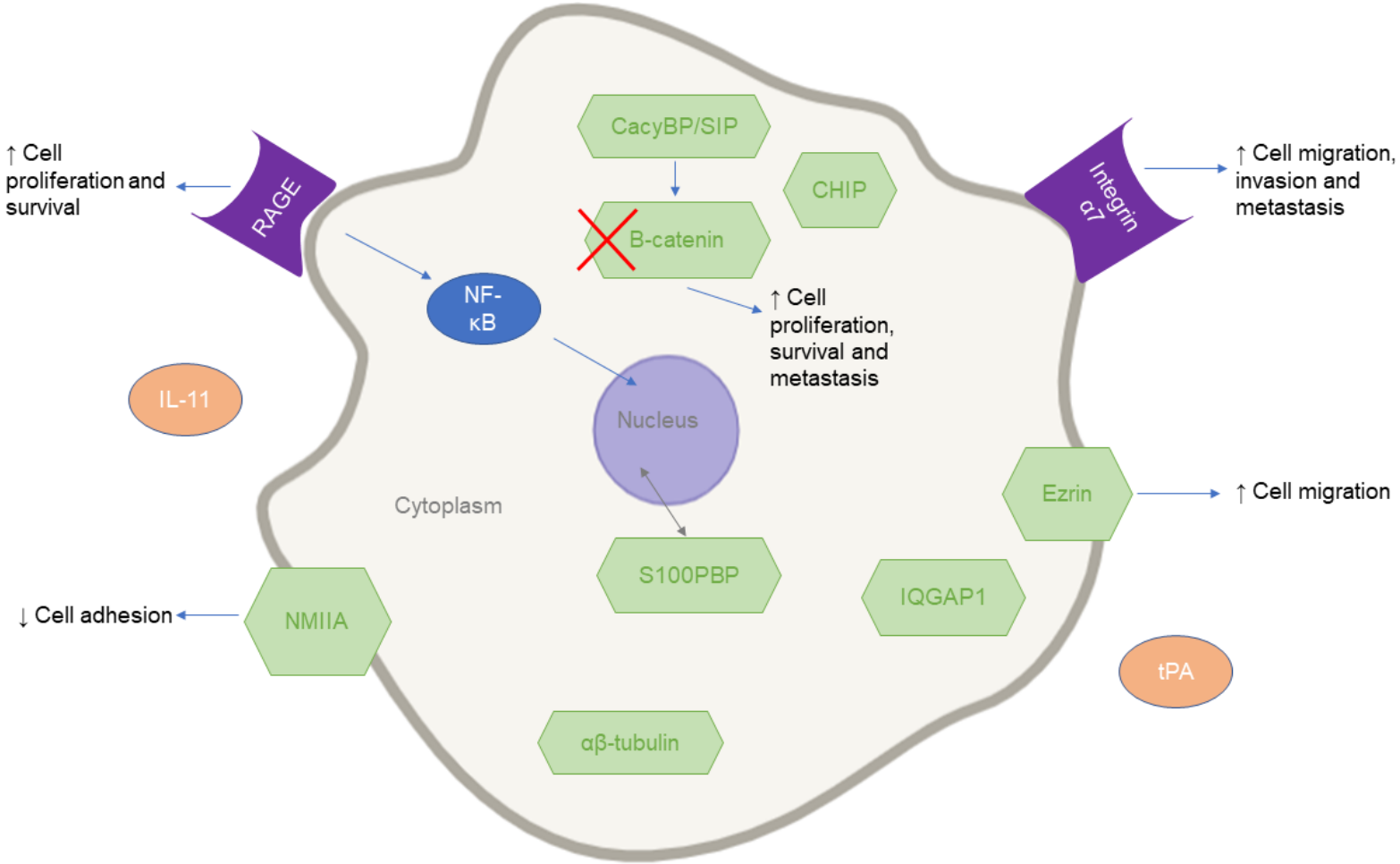

Figure 1.1.4: Interaction partners of S100P
Known interaction partners of S100P, and their associated cellular processes due to interaction with/regulation by S100P, are presented in relation to their cellular location, namely intracellular (green), cell surface receptors (purple), or extracellular (orange).

1.1.2.4 Tissue and subcellular distribution of S100P

S100P expression has been observed in both healthy and malignant tissues. Among healthy tissues, S100P is found to be expressed in the placenta, oesophagus, stomach, duodenum, large intestine, prostate and leukocytes (Parkkila *et al.* 2008). The highest levels of S100P protein expression in healthy organs has been seen in the placenta, stomach and bladder. Parkkila *et al.* (2008) also studied mRNA expression of S100P in a variety of normal and healthy tissues, finding that placental tissues demonstrate a 10-fold increase in S100P mRNA expression when compared to the next highest mRNA-expressing tissue, the oesophagus, and over 90 times the level of S100P mRNA expression found in housekeeping genes. Parkkila *et al.* (2008) suggest that differences in S100P mRNA and protein levels detected in various tissues may be due to changes in post-transcriptional regulation of S100P, or due to the presence of extracellular S100P through its interaction with RAGE. The half-life of several S100 proteins in NIH3T3 was found to be between 90-140 hours (Schwanhüusser *et al.* 2011), suggesting the potential for the S100P protein to have an equally long half-life which could also contribute to differences seen between mRNA and protein levels of S100P. In regards to malignant tissues, S100P has most commonly been implicated in tumour progression in a variety of cancer subtypes, mostly those of epithelial origins. Such carcinomas include that of the breast, lung, prostate and pancreas (Dowen *et al.* 2005; Schor *et al.* 2006; Rehbein *et al.* 2008). Much of the current knowledge about S100P has been gathered through the study of carcinomas, which will be detailed below (1.1.2.5 S100P in cancer).

The subcellular distribution of S100P has been studied using cell lines and tissues, mainly through the use of indirect immunofluorescence and immunohistochemistry, or through the use of overexpression/fluorescent tag systems. Through these studies, it is widely accepted that S100P is localised in either the nucleus, cytoplasm, or both in a variety of tissues and cell types. For example, Rehbein *et al.* (2008) demonstrated both cytoplasmic and nuclear localisation of S100P in a human lung adenocarcinoma cell line stably expressing GFP-S100P. In contrast, immunofluorescence analysis of human endometrium biopsies by Tong *et al.* (2010) found nuclear S100P expression in endometrial stroma. Contradictory data by (Zhang *et al.* 2012) found accumulation of S100P in the cytoplasm of primary endometrial stromal cells by immunofluorescence, suggesting variations in S100P detection.

Interestingly, so far, the majority proteins reported to interact with S100P are cytoplasmic or membrane-localised proteins, whilst most of the reports looking at its cellular localisation seem to suggest a predominantly nuclear segregation.

1.1.2.5 S100P in cancer

Expression of S100P has been documented in other healthy tissues apart from the organ of its origin, the placenta, including the stomach and oesophagus (Parkkila *et al.* 2008). However, the S100P protein has gained considerable attention in relation to its expression in various neoplasms (Table 1.1.1). S100P overexpression in several different types of cancers, including prostate, lung, and breast, has been demonstrated to correlate with increased tumour grade and poor patient prognosis (Wang *et al.* 2006). It was reported by Dowen *et al.* (2005) that as pancreatic neoplasm severity increased, the number of S100P positive neoplasms increased; 92% of the pancreatic ductal adenocarcinoma samples tested by the group were positive for S100P expression. Györffy *et al.* (2006) found that the S100P gene was associated with resistance against multiple anticancer drugs, whilst Surowiak *et al.* (2007) showed that malignant ovarian tumour cases associated with death displayed a higher level of S100P expression. Poor prognosis of patients with metastatic breast cancer was found to correlate with high levels of S100P in the blood plasma (Peng *et al.* 2016). Overexpression of S100P was found in lung adenocarcinoma samples in comparison to healthy samples, suggesting the usefulness of this protein as a biomarker for lung adenocarcinoma (Kim *et al.* 2007). The increased presence of S100P within tissues from a neoplastic origin suggest a role for this protein in the promotion of carcinogenesis.

This selection of studies demonstrates the potential for S100P to be used as a prognostic or diagnostic marker of various cancer subtypes. In addition, one study by Dakhel *et al.* (2014) has shown the potential of a specific function-blocking monoclonal S100P antibody in the treatment of pancreatic cancer, work which was demonstrated through blocking extracellular S100P activities in pancreatic tumour mice models using the BxPC3 cell line. In this way, S100P could be seen as a potential therapeutic target in the treatment of several types of carcinoma.

S100P has also been found to regulate motility and invasion in particular by its interaction with a variety of target proteins, once again in mostly cells of a cancerous background. Exogenous addition of S100P protein has been shown to enhance the invasion of Rama 37 cells *in vitro* (Clarke *et al.* 2017), in addition to induction of metastasis in rats injected with S100P-expressing cells (Wang *et al.* 2006). Stimulation of migration was observed by Fuentes *et al.* (2007) following exogenous S100P treatment of SW480 colon cancer cell line. Such work suggests exogenous addition of S100P, rather than endogenous expression or overexpression, is sufficient to induce changes in cellular migration and invasion in cells of a cancer background.

S100P overexpression in Panc1 cells, pancreatic cancer cell line, led to increases in transendothelial migration, whereas targeted knockdown of S100P in the same cell line by use of small interfering RNA

(siRNA) led to a significant decrease in the ability of Panc1 cells to migrate (Barry *et al.* 2013) . The same effect of S100P knockdown by siRNA technology was also observed in the BxPC3 cell line. A study by Arumugam *et al.* (2005) found similar results for both migration and invasion. Driving S100P expression in Panc1 cells led to significant increases in their invasion, and knockdown of S100P in BxPC3 cells led to invasive defects. S100P overexpression has also been demonstrated to lead to both increased cell migration and invasion in the Panc1 cell line by Whiteman *et al.* (2007), which was found in part to be mediated by upregulation of proisoforms of cathepsin D.

All of the above studies confirm a role for S100P in both motility and invasion of cells from a cancer background. Furthermore, these studies suggest S100P plays a part in promoting carcinogenesis, either by its involvement in the processes of cellular motility and invasion, or through its interaction with target proteins.

Cell type	Target protein	Cellular consequences	Reference
CL1-0 (human lung adenocarcinoma cell line)	Integrin α7	Increase in migration, invasion and EMT	Hsu *et al.* (2015)
COS-7 (African green monkey kidney cell line) and HeLa (human cervical carcinoma cell line)	Tubulin	Increase in cell migration	Du *et al.* (2020)
HMEC-1 (human endothelial cell line)	Ezrin	Increase in transendothelial migration	Austermann *et al.* (2008)
NIH3T3	RAGE	Increased cell proliferation and survival	Arumugam *et al.* (2004)
HeLa (human cervical carcinoma cell line)	NMIIA	Redistribution of focal adhesion sites leading to enhanced migration	Du *et al.* (2012)

Table 1.1.1: Table of S100P-target protein interactions and their outcomes

1.2 The placenta

1.2.1 The role of the placenta

The placenta is a transient foetomaternal organ formed from the outer layer of cells of the blastocyst, the trophectoderm. The trophectoderm will go on to differentiate into the different trophoblast cell lineages that together facilitate the remodelling of maternal spiral arteries, the exchange of nutrients and waste products, and the production of hormones required for a successful pregnancy (Gamage *et al.* 2016).

Implantation of the blastocyst begins with the degradation of the surrounding zona pellucida (Figure 1.2.1). The outer cells of the blastocyst, the trophectoderm, develops roughly 4-5 days after fertilisation (Knöfler *et al.* 2019). The polar trophectoderm, which is adjacent to the inner cell mass of the blastocyst, interacts with the endometrial epithelium and leads to the implantation of the embryo into the maternal endometrium (Gude *et al.* 2004). However, in order to facilitate implantation of the blastocyst, the maternal endometrium must go through several changes in a process known as decidualisation. During decidualisation, the production of the hormones oestradiol and progesterone by the ovaries occurs in response to implantation of the blastocyst in the secretory phase of the endometrial cycle (Plaisier 2011). This is followed by the formation of decidual cells from endometrial stromal cells, and vascular remodelling including angiogenesis (Dunn *et al.* 2003).

Defects in placental formation can lead to diverse complications. For instance, abnormally shallow implantation, due to inadequate trophoblast invasion, can lead to intrauterine growth restriction (IUGR), whereas preeclampsia is thought to be multifactorial in its causes. Early onset preeclampsia, which generally comprises the most serious of cases, can be characterised by increased resistance in maternal spiral arteries leading to abnormal blood flow (Huppertz 2008).

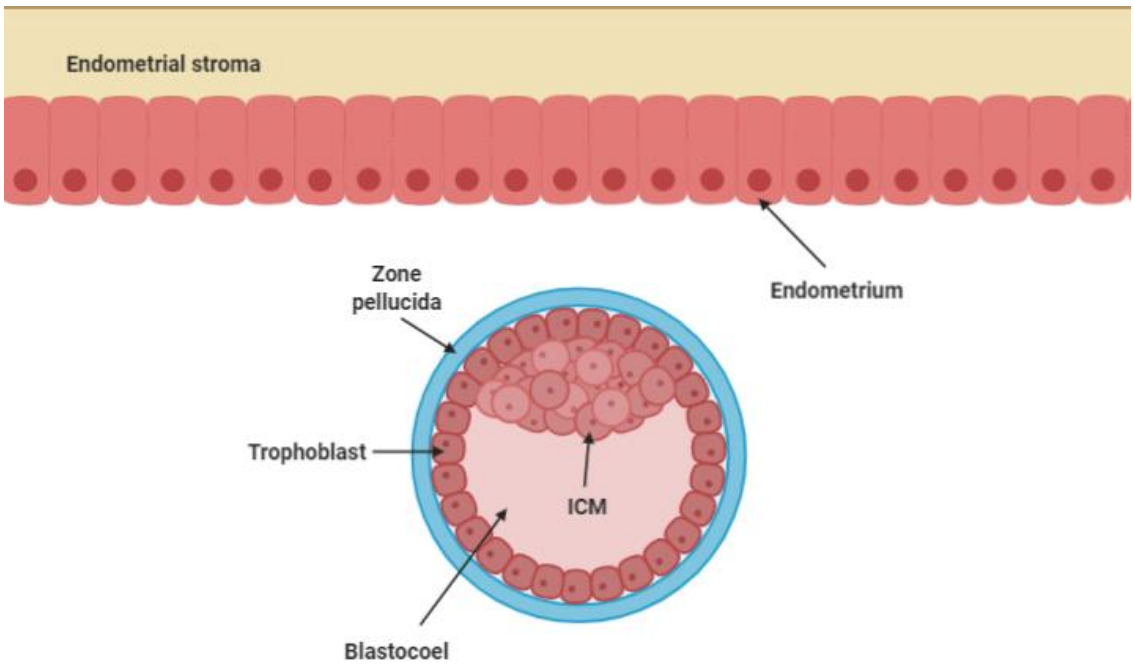

Figure 1.2.1: Structure of a human blastocyst
Following degradation of the zona pellucida, trophoblasts develop from the trophectoderm and begin the process of implantation into the maternal endometrium after its decidualisation. The inner cell mass (ICM) goes on to give rise to the foetus.

1.2.2 Trophoblasts

Following decidualisation and implantation of the blastocyst, the trophectoderm begins to differentiate into early trophoblast lineages (Figure 1.2.2).

Multinucleate primitive syncytium is formed from the trophectoderm at around 8 days post-fertilisation. This represents the earliest stage of placentation, where the primitive syncytium digests and expands towards the maternal decidua (Knöfler *et al.* 2019). Invasion of the decidua by primary syncytium aids in the formation of lacunar networks, in which uterine vessels are eroded and maternal blood can perfuse and establish uteroplacental circulation at day 12-13 post-fertilisation (Turco and Moffett, Ashley 2019).

During the expansion of the primitive syncytium, mononuclear cytotrophoblasts invade through the primitive syncytium leading to the formation of primary villi. Primary villi transform through pregnancy into secondary and tertiary villi, characterised by their levels of vascularisation, extension of the villi and extent of migration of extraembryonic mesoderm into the villi (Knöfler and Pollheimer 2013). Along with this transformation comes differential expression of certain ECM proteins, in addition to a lack of cell-associated ECM; Damsky, Fitzgerald and Fisher (1992) were unable to detect fibronectin or laminin A in association with the surface of uterine trophoblasts.

Mononuclear cytotrophoblasts, otherwise known as trophoblast stem cells, can differentiate into different populations of trophoblasts via the villous or extravillous pathways (Li, Zhuosi *et al.* 2019). The fusion of villous cytotrophoblasts (vCTB) results in the formation of multinucleate syncytiotrophoblasts (STBs) surrounding the primary villi surface. The STB layer, due to its proximity to placental vessels, are involved in nutrient and gas exchange between the maternal endometrium and the foetus (Fuchs and Ellinger, 2004). STBs are also responsible for the secretion of hormones such as human chorionic gonadotropin (hCG) (Handschuh *et al.* 2007), a hormone important in immune tolerance at the foetal-maternal interface in addition to stimulation of trophoblast invasion, mediated by secretion of MMPs by cytotrophoblasts (Fluhr *et al.* 2008).

Mononuclear cytotrophoblasts form a mass at the distal end of the villi, known as the cytotrophoblast cell column (CCC). STBs are not present at this site, allowing the CCC to make contact with the maternal decidua and spread outwards to form the cytotrophoblastic shell (CTS). The CTS provides an anchor for the placenta to attach to the maternal endometrium (Burton, Graham J. and Jauniaux 2017). Following CTS formation, the outer cell layer of the CTS at the distal end of the villi differentiates into invasive extravillous trophoblasts (EVTs), the main invasive population of trophoblasts (Gude *et al.* 2004).

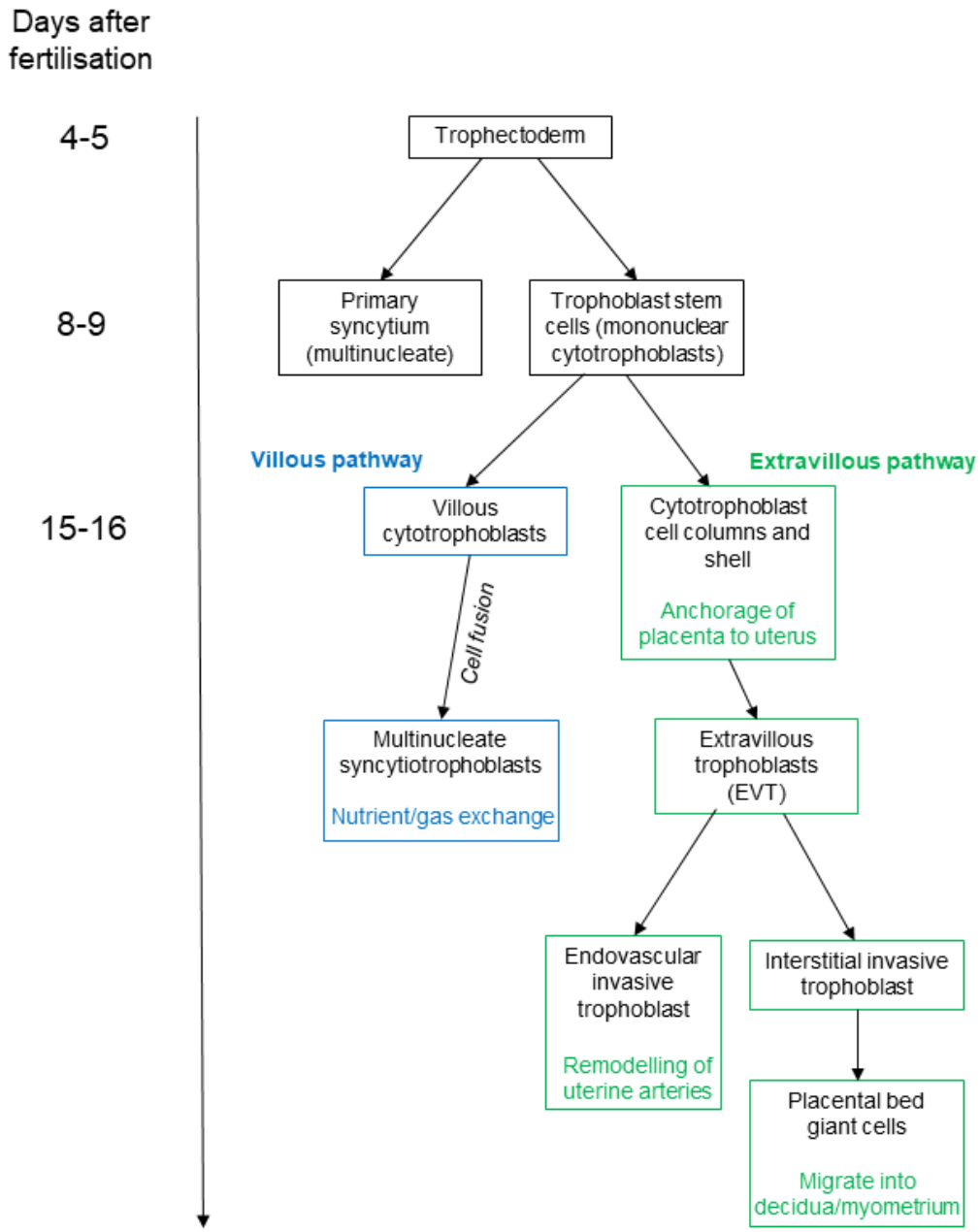

Figure 1.2.2: Human trophoblast differentiation
A depiction of the differentiation of the trophectoderm into the different trophoblast lineages, around 4 days after fertilisation. The extravillous pathway of differentiation is highlighted in green, whereas the villous pathway is highlighted in blue.

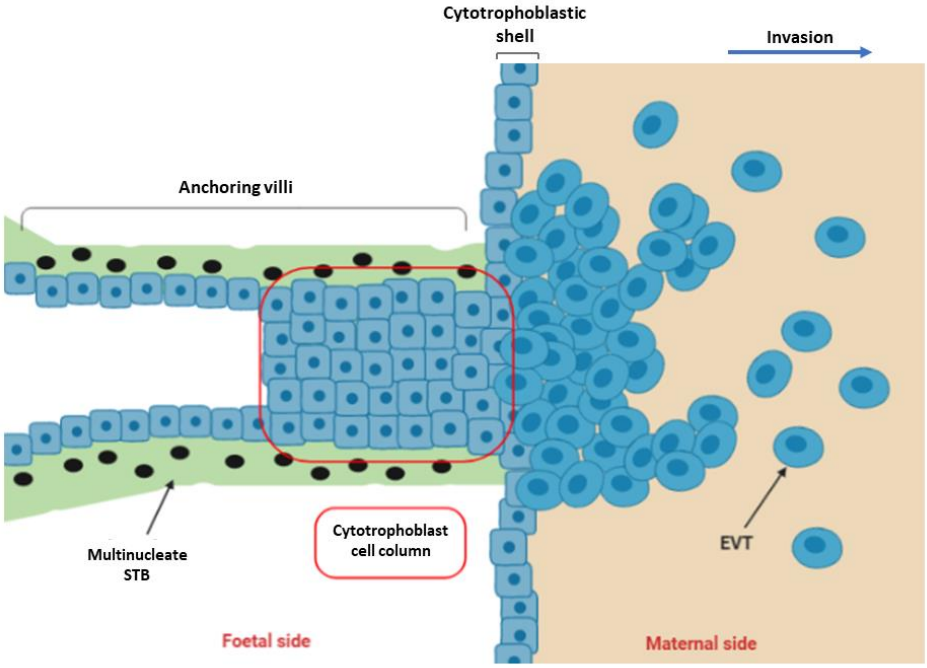

Figure 1.2.3: Differentiation of trophoblasts at the foetal-maternal interface
Cells at the distal tip of the villi begin to differentiate into invasive EVTs, penetrating the maternal decidua and underlying maternal myometrium.

STB, syncytiotrophoblast; *EVT,* extravillous trophoblast.

1.2.2.1 Extravillous trophoblasts

vCTBs at the proximal end of the villi are highly proliferative, however EVTs at the distal end of the villi eventually cease to proliferate. Instead, EVTs differentiate into one of two populations; endovascular trophoblasts or interstitial trophoblasts. As of yet, the specific signals driving the differentiation pathways of EVTs into either endovascular or interstitial trophoblasts is not known (Turco and Moffett, Ashley 2019).

Endovascular trophoblasts are primarily responsible for invading uterine spiral arteries to establish a blood supply to the growing foetus. The maternal spiral arteries are transformed by endovascular trophoblasts to a low-resistance high-capacity state, leading to increased placental perfusion and increased nutrient uptake by the growing foetus (Kaufmann *et al.* 2003).

The other differentiation pathway for extravillous trophoblasts is the interstitial trophoblasts. Interstitial trophoblasts must penetrate into the decidua and underlying endometrium, acting as an anchor to link the placental and maternal tissues (Davies *et al.* 2016). Interstitial trophoblasts secrete several proteases, including MMP-2 and MMP-9, to facilitate degradation of the ECM. Expression of PLAC8 in interstitial trophoblasts was recently found to promoting both motility and invasion of this trophoblast subset by increasing the activity of Cdc42 and Rac1 leading to the formation of filopodia, a structure characteristic of migratory cells (Chang *et al.* 2018).

After interstitial trophoblasts have completed their migration through the decidua into the myometrium, they terminally differentiate and fuse into multinucleated placental bed giant cells - these are thought to have no invasive activity (Knöfler *et al.* 2019). Both urokinase and plasminogen activator inhibitors 1 and 2 were found to be localised in cytoplasmic and membrane regions of interstitial trophoblasts, suggesting fine control of their invasion (Hofmann *et al.* 1994). Placental giant bed cells also express HLA-G, which may facilitate their interaction with maternal immune cells and prevent their attack by the maternal immune system (Al-Lamki *et al.* 1999).

Controlled EVT invasion is an important aspect of establishing a successful pregnancy. Invasion must be confined both spatially (in the decidua/myometrium) and temporally (at the early stages of pregnancy). Invasion by EVTs is thought to be at its maximum between 10-12 weeks, with EVTs not normally invading beyond the first third of the myometrium (Zhu, J.-Y. *et al.* 2012). Abnormalities in the invasive process in EVTs can lead to a wide array of complications. For example, shallow invasion of EVTs has been implicated in intrauterine growth restriction (IUGR) and early onset preeclampsia, in which endovascular trophoblasts fail to remodel spiral arteries leading to insufficient placental perfusion (Kaufmann *et al.* 2003).

In order for implantation to occur successfully, EVTs must maintain an invasive and highly motile phenotype. There are numerous striking similarities between the process of implantation (particularly in respect to invading EVTs) and malignant cells during cancer metastasis. Both cell subsets require proliferative and invasive capabilities, as well as the ability to evade the immune system, as the foetus is immunologically distinct from the mother (Holtan *et al.* 2009). Both trophoblasts and malignant tumours express proteases; EVTs have been shown *in vitro* to secrete several MMPs (Staun-Ram *et al.* 2004), and likewise MMPs have been implicated in cancer progression due to alteration of cell-cell and cell-extracellular matrix interactions (Gialeli *et al.* 2011). Several growth factors, their receptors, and signalling cascades have been demonstrated to be required for both placental development and cancer progression, including the MAPK and PI3K/AKT pathways (West, R. C. *et al.* 2018).

Differentiation of CTB to EVT is vital for successful implantation to occur. It has been hypothesised by Dasilva-Arnold *et al.* (2015) and several others that this differentiation is a form of epithelial-to-mesenchymal transition (EMT). The EMT process is well characterised in cancer (Roche 2018), in which cells of epithelial origin can convert into a mesenchymal phenotype. Disruption of cell-cell and cell-matrix contacts, in addition to cytoskeletal remodelling, enables increased cellular migration which, in cancer, aids the formation of secondary metastases.

With regards to trophoblast differentiation, Dasilva-Arnold *et al.* (2015) found downregulation of several epithelial markers, including occludin, which maintains stable tight junctions between cells. In addition, the group also found upregulation of several mesenchymal markers in EVT compared to CTB, namely vimentin and fibronectin1. Expression of proteases MMP-2 and MMP-9 were also found to be upregulated, suggesting the increased invasive capabilities of EVT compared to CTB that is required for breaking down ECM components. However, unlike cancer, trophoblast migration and invasion must be carefully regulated, both spatially and temporally.

1.2.3 S100 proteins in the placenta

The presence of several S100 proteins have been detected in placental tissues. Immunohistochemical studies of placental tissues have demonstrated the presence of S100A10 in syncytiotrophoblast brush border vesicles (Kaczan-Bourgois *et al.* 1996), and in syncytiotrophoblast microvillous plasma membranes by both confocal laser scanning microscopy and flow cytometry (Kristoffersen and Matre 1996). More recent studies by Abd El-Aleem and Dekker (2018) have observed high levels of expression of the S100A10/annexin A2 complex in amniotic membranes and endothelial cells lining blood vessels by use of proximity ligation. In addition, low levels of the complex were found in syncytiotrophoblast

brush borders and in trophoblasts. Non-complexed S100A10 was also found in similar locations within placental tissue, with higher expression documented in placental villi. S100A10 is also found within human endometrium, with decreased expression of S100A10 seen in the endometrium of infertile women compared to fertile women, suggesting that S100A10 plays a part in endometrial receptivity (Bissonnette *et al.* 2016). It was also established that silencing of S100A10 by siRNA reduced migration of human epithelial endometrial cells and resulted in decreased mRNA expression of prolactin and connexin 43, both markers of decidualisation, further suggesting a role for S100A10 in promoting the decidualisation process leading to successful pregnancies.

In addition to S100A10, S100A11 has been detected in apical microvillus membranes from syncytiotrophoblasts through proteomic analysis (Paradela *et al.* 2005). Furthermore, (Liu *et al.* 2006) identified a decrease in expression of S100A11 in placental villous tissues from patients suffering early pregnancy loss through the use of MALDI-TOF mass spectrometry. This finding was further validated by immunohistochemistry, where reduced cytoplasmic staining of both syncytiotrophoblasts and cytotrophoblasts was observed. S100A11 has also been detected in both human endometrium and stroma, with healthy control subjects expressing higher levels of S100A11 than those who suffered from early pregnancy loss (Liu *et al.* 2012). Further work by the authors found that knockdown of S100A11 using siRNA reduced mouse embryo implantation, suggesting that S100A11 may have a role in mediating the implantation process.

The S100A8/A9 heterodimer has also been implicated in early pregnancy loss (Nair *et al.* 2013). RT-PCR analysis demonstrated a significant increase in S100A8 and S100A9 mRNA in endometrial tissue of patients experiencing recurrent loss of pregnancy in early states when compared to healthy controls. Given the role of these proteins in enhancing the recruitment of immune cells to sites of inflammation, it may be that overexpression of S100A8/A9 at the maternal-foetal interface interferes with placental perfusion, consequently leading to loss of the pregnancy as part of the maternal immune response.

Expression of S100A6 in placental tissue was studied by (Schol *et al.* 2014) through immunohistochemistry. The group found a highly significant increase in expression of S100A6 in pre-eclamptic patients compared to healthy controls, with expression of S100A6 seen in predominantly in syncytiotrophoblasts, but also in cytotrophoblasts. Stromal cells did not exhibit significant differences in S100A6 expression between healthy and pre-eclamptic patients.

1.2.4 S100P in the placenta

Expression of S100P in the placenta was first documented by Becker *et al.* (1992), and it is the placenta in which S100P is found at the highest levels in the human body (Parkkila *et al.* 2008). Given its high expression level in the placenta, it is striking that little is known about its physiological role in this location. S100P has been detected in in *ex vivo* samples by Zhu *et al.* (2015a), with a significant decrease in S100P expression seen in villi obtained from spontaneous abortion versus normal pregnancy.

Zhu *et al.* (2015b) have studied the localisation of S100P in the placenta by immunohistochemistry, observing S100P protein in STBs, vCTBs and cytotrophoblast columns during the first trimester of pregnancy. The level of S100P expression was found to decrease as pregnancy progressed from first to third trimester. Interestingly, this mimics the proliferative and invasive capabilities of trophoblasts, which seem to diminish following the 12^{th} week of gestation (Fisher *et al.* 1989). Our recent work (Tabrizi *et al.* 2018) supports these findings by Zhu *et al.* (2015), in which S100P expression decreases throughout gestation. Furthermore, we demonstrated the presence of S100P in EVTs from first trimester *ex vivo* placental tissues, work that is corroborated by genome-wide expression profiling of EVTs by Apps *et al.* (2011). We additionally characterised a role for S100P in enhancing both the migration and invasion of model trophoblast cell lines, suggesting that S100P may play a role in trophoblast motility and invasion *in vivo.*

Given the high levels of S100P expression detected in a variety of cancers, in addition to the high levels of expression seen in trophoblast cells of the placenta, it is understandable to assume that there may be a link between S100P expression and the invasive/motile processes undertaken by EVTs during placentation. Curiously, placentation in the mouse is deemed to be shallow (Carter 2007). The lack of invasion by trophoblast cells into spiral arteries means that mice may not be the optimal choice for studies of placentation. Mice also do not express S100P; whether there is a link between levels of S100P expression in vertebrates and shallow implantation is yet to be fully elucidated.

1.3 Project aims

The aim of the first section of this thesis is to demonstrate the localisation of the S100P protein in a variety of cell backgrounds, including that of trophoblast cells, using a biochemical technique known as subcellular fractionation (Chapter 3).

Following the establishment of S100P's localisation in trophoblasts, we set out to characterise the role of membrane-associated S100P in the processes of motility and invasion by either gain or loss of function studies. In addition, we undertake analysis of the S100P structure that may lead to its membrane association capabilities (Chapter 4).

Finally, we aim to characterise changes in protein abundance as a result of S100P expression in trophoblast cells using a mass spectrometry-based approach, with the overall aim of identifying either possible interaction partners of S100P, or proteins that may be involved in the S100P-dependent processes either intracellularly or at the cell membrane (Chapter 5).

Chapter 2:

Materials and Methods

Chapter 2: Materials and Methods

Contents

2.1 Materials

2.1.1 Equipment

0.1-10µl tips (Sarstedt, Germany)

0.2µm filters (Sarstedt, Germany)

1.5ml microfuge tubes (Eppendorf, Germany)

2.0ml microfuge tubes (Fisher Scientific, Loughborough, UK)

35mm dishes (Sarstedt, Germany)

60mm dishes (Sarstedt, Germany)

10cm dishes (Thermofisher, UK)

10ml glass pipettes (Sarstedt, Germany)

1000µl tips (Starlab, UK)

24 well plates (Appleton Woods, UK)

96 well plates (Fisher Scientific, Loughborough, UK)

25ml glass pipettes (Fisher, UK)

30ml polypropylene universal containers (Starlab, UK)

5ml glass pipettes (Sarstedt, Germany)

60mm dishes (Thermofisher, UK)

96 well plates (Fisher, UK)

Acclaim™, PepMap™ C18, 3 µm, 100 Å, 75 µm × 150 mm analytical column (ThermoScientific, UK)

Acetonitrile (Fisher, UK)

Autoclave tape (Fisher, UK)

Autoclave bags (Fisher, UK)

Biosafety cabinet (Thermofisher Scientific, UK)

Cavitation bomb chamber (Parr Instruments, UK)

Cell culture flasks (Fisher Scientific, Loughborough, UK)

Centrifuge (2-6E, Sigma Aldrich, UK)

Centrifuge tubes, 15ml (Appleton Woods, UK)

Centrifuge tubes, 50ml (Corning, Sigma-Aldrich, Dorset, UK).

Cryotubes (Fisher Scientific, Loughborough, UK)

CytoFLEX flow cytometer (Beckmann Coulter, California, US)

Eppendorf tubes, 1.5ml (Fisher Scientific, Loughborough, UK)

Gauze, sterile (Boots, UK)

Gel tank (Bio-Rad Laboratories Ltd, UK)

Gel loading tips (Sarstedt, Germany)

Glass coverslips (Fisher, UK)

Gloves (Appleton Woods, UK)

Graduated 1ml Pasteur pipettes (Starlab, UK)

Incubator (Sanyo)

Mini LabRoller (LabNet)

Microflow Class II Biosafety Cabinet (Laboratory Analysis Ltd., Exeter, UK)

Microscope (Nikon Eclipse T5100)

Microcentrifuge (1-14, Sigma Aldrich, UK)

Mr Frosty freezing container (Fisher Scientific, Loughborough, UK)

Optima XPN-100 Ultracentrifuge (Beckmann Coulter, California, US)

PicoTip™ emitter (New Objective, Germany)

Pipettes (HTL Lab solutions, Poland)

Pipette filler (Bel-Art, SP Scienceware)

Plate Reader EL800 (Biotek, US)

Power pack (Bio-Rad Laboratories Ltd, UK)

Rocker, Gyratory, SSL3 (Stuart, UK)

Semi-dry Trans-Blot SD cell (Bio-Rad Laboratories Ltd, UK)

Tissue homogeniser, 1ml (GPE Scientific, UK)

ThinCert™ Transwell 24 well plate inserts (Greiner Bio-One, UK)

TripleTOF 5600 system (AB Sciex, UK)

Water bath (Clifton, Weston-Super-Mare, UK)

Western blot tank (Bio-Rad, UK)

2.1.2 Reagents

α-2-antiplasmin (Sigma, UK)

2-(n-morpholino) ethanesulfonic acid (Sigma, UK)

Acetic Acid (Fisher, UK)

Acrylamide (Melford, UK)

Aminocaproic acid (ACA) (Sigma, UK)

Ammonium Bicarbonate (Sigma, UK)

Ammonium Persulfate (APS) (Melford, UK)

Amphotericin B (Melford, UK)

Aprotinin (Sigma, UK)

B-mercaptoethanol (Sigma, UK)

Bis-Acrylamide (Melford, UK)

Bis-Tris (Melford, UK)

Bovine Serum Albumin ((Melford, UK)

Bromophenol Blue (Sigma, UK)

Calcium chloride (Melford, UK)

Coomassie Brilliant Blue G250 (Thermofisher, UK)

Cromolyn (Sigma, UK)

Dionex 3000 nLC system (ThermoScientific, UK)

Disodium hydrogen orthophosphate (Scientific Laboratory Supplies, UK)

DMSO (Fisher, UK)

Doxycycline hydrochloride (Melford, UK)

DTT (Melford, UK)

Dulbecco's Modified Eagle's Medium With 4500 mg/L glucose and sodium bicarbonate, without L-glutamine and sodium pyruvate (Sigma, UK)

EDTA (Sigma, UK)

EGTA (Melford, UK)

Ethanol (Fisher, UK)

Fibronectin, from human plasma (Sigma, UK)

Filter paper, extra thick (Bio-Rad, UK)

Foetal Bovine Serum (Sigma, UK)

Formic acid (Fisher, UK)

Gentamicin Sulfate (Melford, UK)

Giemsa stain (Sigma, UK)

Glacial Acetic Acid (VWR, UK)

Glucose (Fisher, UK)

Glycerol (Melford, UK)

Glycine (Melford, UK)

Goat Serum (Sigma, UK)

Ham's F12 medium with sodium bicarbonate, without L-Glutamine (Sigma, UK)

Ham's F12 Medium without L-Glutamine and Phenol Red (Pan Biotech, Germany)

HDAC2 primary antibody (Abcam,

HEPES powder (Sigma, UK)

Hygromycin B powder (Melford, UK)

INTERFERin siRNA Transfection Reagent (Polyplus, UK)

L-Glutamine solution 200mM (Sigma, UK)

Leptomycin B powder (Santa Cruz, Texas, USA)

Lipofectamine 3000 Transfection Kit (Invitrogen, UK).

Industrial Methylated Spirits (CEAC, Aston University, UK)

Magnesium Chloride (Melford, UK)

May-Grünwald solution (Sigma, UK)

Methanol (Fisher, UK)

Minimum Essential Medium Eagle, with Earle's salts, non-essential amino acids and sodium bicarbonate (Sigma, UK)

Native PAGE gels (Life Technologies, UK)

Non-Essential Amino Acids (Sigma, UK)

NP-40 (Sigma, UK)

OptiMEM (Sigma, UK)

PageRuler Prestained Protein Ladder (Thermofisher, UK)

Pancoll (Pan Biotech, Germany)

Paraformaldehyde (Sigma, UK)

PBS Tablets (Melford, UK)

Penicillin/Streptomycin solution, 10,000 units penicillin and 10mg streptomycin/ml (Sigma, UK)

Pierce Cell Surface Isolation Kit (Thermofisher, UK)

Potassium chloride (Melford, UK)

Potassium dihydrogen orthophosphate (Fisher, UK)

Progenesis QI for proteomics software (Version 4, Nonlinear Dynamics, UK)

Protease inhibitor cocktail III (Melford, UK)

PVDF membrane (Thermofisher, UK)

Reagent A (Fisher, UK)

Reagent B (Fisher, UK)

RPMI 1640 medium, with L-Glutamine (Sigma, UK)

SDS (Melford, UK)

siRNA sequences (Qiagen, UK)

Sodium chloride (Fisher, UK)

Sucrose (Melford, UK)

TEMED (Melford, UK)

Transwell inserts (Greiner Bio-One, Austria)

Tricine (Melford, UK)

Tris (Melford, UK)

Triton X-100 (Sigma, UK)

Trypan Blue (Sigma, UK)

Trypsin powder (Pan Biotech, Germany)

Trypsin-EDTA 10x solution (Sigma, UK)

Trypsin Gold, Mass Spectrometry Grade (Promega, UK)

Type F immersion oil (Leica, Germany)

Vectashield hard set mounting medium containing 4'-6-diamino-2-phenylindole (DAPI) (Vector Laboratories, UK)

2.2 Methods

2.2.1 Cell culture

2.2.1.1 JEG-3

The JEG-3 cell line is a human placental-derived trophoblastic choriocarcinoma cell line. This cell line, along with the BeWo cell line, is adherent with epithelial morphology, and has been widely used as a model for the placenta *in vitro.* JEG-3 cells endogenously express S100P (Tabrizi *et al.* 2018).

JEG-3 cells were cultured at 37^{o}C in an atmosphere of 5% (v/v) CO_2 and 20% (v/v) O_2, in Minimum Essential Medium (MEM) supplemented with 10% (v/v) foetal bovine serum, 1% (v/v) non-essential amino acids, 1x Penicillin/Streptomycin solution (100 units and 0.1mg/ml respectively), and 2mM L-Glutamine.

2.2.1.2 BeWo

The BeWo cell line is another human placental-derived trophoblastic choriocarcinoma cell line. They are adherent with epithelial morphology. This cell line expresses S100P endogenously, at a higher level than that of the JEG-3 cell line (Tabrizi *et al.* 2018).

BeWo cells were cultured at 37^{o}C in an atmosphere of 5% (v/v) CO_2 and 20% (v/v) O_2, in Ham's F12 medium supplemented with 10% (v/v) foetal bovine serum, 1x Penicillin/Streptomycin solution (100 units and 0.1mg/ml respectively), and 2mM L-Glutamine.

2.2.1.3 HTR8/SVneo

The HTR8/SVneo cell line are a first trimester extravillous trophoblast cell line that is regularly used as a model for implantation (Hannan *et al.* 2010). This cell line does not express S100P endogenously, and was therefore transfected with a wild type S100P protein (Tabrizi *et al.* 2018).

The HTR8 clones were kindly generated by Dr Thamir Ismail (University of Liverpool, UK), with levels of S100P in each clone confirmed by western blotting. The HTR8 cell clones used are as follows:

1) control cells transfected with the empty vector (Empty plasmid Clone 3), 2) cells transfected with plasmid SGB217, which was obtained by combining the pcDNA3.1 Hygro plasmid with a PCR amplified S100P product (SBG217 Clones 3, 5, 7, 9 and 10).

All HTR8 cell lines were cultured at 37^{o}C in an atmosphere of 5% (v/v) CO_2 and 20% (v/v) O_2, in RPMI 1640 medium supplemented with 5% (v/v) foetal bovine serum, 1x Penicillin/Streptomycin solution (100 units and 0.1mg/ml respectively), 2mM L-Glutamine and 50µg/ml Hygromycin B.

2.2.1.4 COS-7 and HeLa cells

The COS-7 cell line, derived from African green monkey kidney, and the HeLa cell line, derived from human cervical carcinoma, express S100P under the control of a doxycycline inducible promoter. The doxycycline inducible cell system has been previously described by Du *et al.* (2012) and Du *et al.* (2020).

The tetracycline induction system, Tet-On, utilises two plasmids. The first plasmid, pBTE, contains the rtTA2(S)-M2 regulatory element. The second plasmid, pTRE-ins, expresses the target protein (S100P), and is under the control of the tetracycline-response element (TRE). Both plasmids are required for target protein expression, and expression of the protein is initiated by tetracycline or its derivative, doxycycline. Doxycycline binds to the rtTA regulatory element, which allows it to bind to the *TetO* operator sequence upstream of the minimal promoter. This in turn allows for initiation of gene transcription (Figure 2.2.1). One inducible clone per cell line was utilised, named COS-7 s10 and HeLa A3 respectively. Induction of S100P expression in COS-7 s10 and HeLa A3 cells were promoted using 1µg/ml doxycycline, added to the culture media every 48 hours to maintain S100P expression.

Both COS-7 and HeLa cells were cultured at 37^{o}C in an atmosphere of 5% (v/v) CO_2 and 20% (v/v) O_2, in Dulbecco's Modified Eagle Medium (DMEM) supplemented with 10% (v/v) foetal bovine serum, 1x Penicillin/Streptomycin solution (100 units and 0.1mg/ml respectively), and 2mM L-Glutamine.

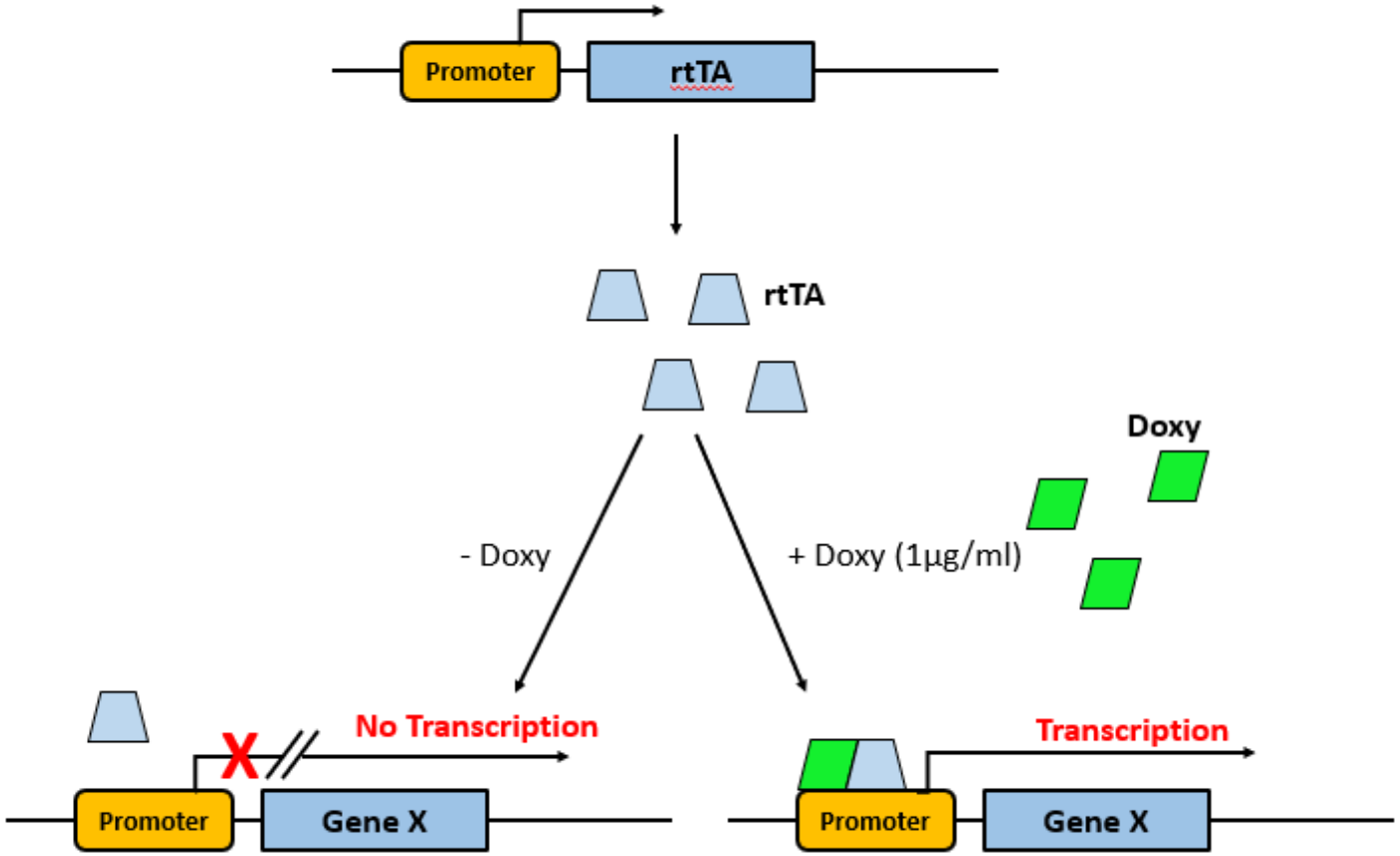

Figure 2.2.1: The Tet-On system

Cells were transfected with two plasmids, one of which expresses the regulatory element (rtTA) and one of which expresses the gene of interest (Gene X). In the presence of doxycycline (Doxy), rtTA can interact with a rtTA responsive promoter to drive the expression of the protein.

2.2.1.5 MDA-MB-231 cells

The MDA-MB-231 cell line is an invasive breast cancer cell line with endogenous S100P expression (Bigelow *et al.* 2009). MDA-MB-231 cells were cultured at 37^{o}C in an atmosphere of 5% (v/v) CO_2 and 20% (v/v) O_2, in Dulbecco's Modified Eagle Medium (DMEM) supplemented with 10% (v/v) foetal bovine serum, 1x Penicillin/Streptomycin solution (100 units and 0.1mg/ml respectively), and 2mM L-Glutamine.

2.2.1.6 Passaging of cells

Cells were grown to at least 80% confluency in a T25 flask. Cells were washed with warm PBS before incubation with warm trypsin (0.025% for JEG-3, BeWo, and HTR8 cell lines, and 0.25% for COS-7, HeLa and MDA-MB-231 cell lines) and 2.5mM EDTA for 5 minutes at 37^{o}c. Following their detachment, cells were resuspended in 4ml supplemented media and spun at 1000rpm for 5 minutes. The supernatant was removed and cells were resuspended in the same volume of fresh media. 1ml of the cell suspension was placed into a T25 flask and 6ml fresh media added. Excess cells were utilised in experiments.

2.2.1.7 Cryopreservation

Cells were grown to confluency and trypsinised as mentioned above (2.2.1.6). Following centrifugation, the supernatant was removed and cells were resuspended in 4ml freezing mix (10% DMSO in FBS). 1ml of the cell suspension was placed into one cryovial each and placed into the Mr Frosty container at -80^{o}c. The following day, the cryovials were transferred into liquid nitrogen for long term storage.

2.2.1.8 Cell thawing

Frozen cells were removed from liquid nitrogen and defrosted in a water bath. Following thawing, cells were transferred into a T25 cell culture flask and 6ml of culture media was added drop by drop. The culture media was changed the following day.

2.2.2 Cell counting

Prior to every experiment involving cultured cells, the number of cells present in the suspension were calculated. Following cell passaging (see 2.2.1.6), 10µl of excess cell suspension was added to a haemocytometer chamber. An average of four separate cell counts were taken, and the number of cells counted was multiplied by 10^4 to give the total amount of cells in 1ml of suspension.

2.2.3 Preparation of total cell lysate

Cells were grown to confluency in 2x 60mm dishes. Cell culture media was then removed, and cells were washed with 1x PBS before being collected by scraping into 1x PBS with 1x protease inhibitor cocktail. Lysates were collected in Eppendorf tubes and sonicated on the lowest power setting for 10 seconds with an interval of 30 seconds for three times. Lysates were spun for 20 seconds at 3000rpm to remove cell debris. 10µl of the lysate was used for protein quantification, and the rest of the lysate was frozen at -80^{o}c.

2.2.4 Protein Quantification

The amount of protein present within each sample was calculated using a modified protein assay based on the Lowry method (Lowry *et al.* 1951).

A BSA standard solution between the ranges of 0 and 10mg/ml and 2µl of samples were added in triplicate to a 96 well plate. 25µl of Reagent A and 250µl of Reagent B was added to each well, with care taken to avoid creating air bubbles. The samples were mixed and incubated for 10-15 minutes before being read at 750nm using a BioTek EL800 plate reader to produce a standard curve. Protein level in each sample was quantified by calculating the amount of protein in µg/µl.

2.2.5 SDS-PAGE

4x Laemmli buffer (200mM Tris pH 6.8, 40% (v/v) glycerol, 4% (v/v/) β-mercaptoethanol, 4% (w/v) SDS, 0.04% (w/v) bromophenol blue) was added to lysates before loading 15µg of protein lysates on a 16% (w/v) polyacrylamide tricine gel (Table 2.2.1). The voltage was set at 70V for 15 minutes, followed by

100V for 30 minutes and 150V for the remaining time. Reagents required for SDS-PAGE and western blotting are listed in Table 2.2.2.

	16% Separating gel	**4% Stacking gel**
3x Gel Buffer	3.3ml	1.2ml
Acrylamide/bisacrylamide	3.3ml	0.4ml
Water	1.36ml	3.36ml
50% Glycerol	2ml	0ml
10% Ammonium Persulphate (APS)	50µl	40µl
TEMED	6µl	4µl

Table 2.2.1: List of reagents required to make 16% SDS-PAGE tricine gels

Acrylamide/Bisacrylamide (48%:1.5%)	24g acrylamide and 0.75 bisacrylamide in 50ml dH_2O
Anode buffer	12.11g Tris in 1 litre dH_2O (pH 8.9)
Cathode buffer	12.11g Tris, 17.92g Tricine, 1g SDS in 1 litre dH_2O (pH 8.25)
3x Gel buffer	18.16g Tris, 0.75ml 20% SDS in 50ml dH_2O (pH 8.45)
Sealing gel	1ml of 16% separating gel, 20µl 10% APS and 2µl TEMED.
4x Laemmli buffer	20ml 0.5M Tris base (pH 6.8), 20ml Glycerol, 2ml β-mercaptoethanol, 2g SDS and 0.02g Bromophenol blue
10x Electroblot transfer buffer	30.25g Tris Base, 144g Glycine in 1 litre dH_2O (pH 8.3)
1x Electroblot transfer buffer	50ml 10x electroblot transfer buffer, 100ml 100% Methanol, 350ml dH_2O
ECL detection reagent	6ml dH_2O, 1.5ml 0.5M Tris (pH 8.5), 19µl 50mM Coumaric acid, 37µl 250mM Luminol, 2.2µl 37% H_2O_2

Table 2.2.2: List of buffers used in SDS-PAGE and western blotting

2.2.6 Western blotting

Proteins were transferred onto polyvinylidene fluoride (PVDF) membranes at 35mA per gel for 2 hours. Membranes were blocked in 3% (w/v) BSA in PBS, before incubating in the appropriate primary antibodies (Table 2.2.5) diluted in 3% (w/v) BSA in PBS overnight at 4^{o}c. Membranes were washed in PBS before incubation in secondary antibodies conjugated to horseradish peroxidase (HRP) diluted in 3% BSA for 2 hours. Membranes were developed using ECL detection reagent.

2.2.6.1 Blot stripping

Membranes containing proteins were subjected to blot stripping. Membranes were incubated in stripping buffer (Table 2.2.3) for 30-45 minutes at 50^{o}c with minimal agitation. Membranes were subsequently washed with distilled water for 2 minutes, before being washed with 1x PBS three times for 5 minutes each. Blots were subjected to blocking with 3% BSA prior to incubation with primary antibody.

Stripping buffer (100ml)	20ml 10% (w/v) SDS 12.5ml 0.5M Tris HCl pH 6.8 0.8ml B-mercaptoethanol 66.7ml distilled water

Table 2.2.3: List of reagents required for western blot stripping buffer

2.2.6.2 Quantification of band intensity

Intensity of the protein bands detected by western blotting were quantified with Image Studio Lite. The intensity of the protein bands of interest were normalised to the band intensity of their respective loading controls. Protein expression and isolation of subcellular cellular compartments were calculated following normalisation.

2.2.7 Indirect immunofluorescence

Cells were seeded at a density of 20,000 cells per well in a 24 well plate containing fibronectin-coated glass coverslips. Cells were incubated for 48 hours before washing with 1x cytoskeleton buffer (CB, see table 2.2.4 for recipe) and treatment with 4% paraformaldehyde in 1xCB for 10 minutes at 37^{o}c. 4% paraformaldehyde was removed and cells were incubated in 30mM glycine in 1x CB at room temperature, before permeabilising and solubilising the cells in 0.1% Triton X-100 in 1x CB for 10 minutes. Following this, cells were washed 3 times for 5 minutes each in 1x CB and blocked in 10% goat serum in 1x CB for 30 minutes. Cells were consequently incubated with the appropriate primary antibodies in 1x CB and 1% goat serum at room temperature for 45 minutes. Following primary antibody incubation, cells were washed 3 times for 5 minutes each in 1x CB and incubated with the appropriate secondary antibody labelled with a fluorophore (FITC or TRITC) as well as rhodamine phalloidin (dilution 1:100) to visualise F-actin when required in 1x CB and 1% goat serum at room temperature for 45 minutes. Cells were washed 3 times for 5 minutes each in 1x CB. Coverslips were washed in distilled water and mounted and fixed onto microscope slides with mounting medium, and sealed. Cells were visualised using the Leica DMI4000B microscope, and pictures taken with the DFC 360FX camera.

1x Cytoskeleton Buffer	150mM NaCl, 5mM MgCl2, 5mM EGTA, 5mM glucose, 10mM 2-(n-morpholino) ethanesulfonic acid pH 6.1
Rhodamine Phalloidin	1:100 dilution in 1x cytoskeleton buffer

Table 2.2.4: List of reagents required for indirect immunofluorescence staining

2.2.8 Subcellular fractionation using a Dounce homogeniser

Cells were fractionated as depicted in figure 2.2.2. Cells were grown to confluency in 2x 60mm dishes. Cell culture media was then removed, and cells were washed with 1x PBS before being collected by scraping into subcellular fractionation buffer (see table 2.2.5). The cell suspension was passed through a Dounce homogeniser 10 to 15 times to lyse cells. The homogenate was centrifuged at 720 x *g* for 5 minutes to pellet nuclei. The supernatant containing cytoplasm, membrane and mitochondria was removed and placed into a fresh Eppendorf tube kept on ice. The nuclear pellet was washed with subcellular fractionation buffer before being passed through the Dounce homogeniser another 10 to 15 times. This was centrifuged at 720 x *g* for 10 minutes. The supernatant was discarded and the nuclear pellet resuspended in a final volume of 150µl subcellular fractionation buffer. The supernatant containing cytoplasm, membrane and mitochondria fractions was centrifuged at 10,000 x *g* for 5 minutes to pellet the mitochondria. The supernatant containing cytoplasm and membrane fractions was removed and placed into a fresh Eppendorf tube. All fractions were sonicated and a small volume was taken for protein quantification, prior to storage at -80^{o}c.

Subcellular fractionation buffer	**5µM $CaCl_2$ Subcellular fractionation buffer**
250mM Sucrose	250mM Sucrose
20mM HEPES pH 7.4	20mM HEPES pH 7.4
10mM KCl	10mM KCl
2mM $MgCl_2$	2mM $MgCl_2$
1mM EDTA	1x protease inhibitors
1mM EGTA	1mM DTT
1x protease inhibitors	5µM $CaCl_2$
1mM DTT	

Table 2.2.5. Recipe for various subcellular fractionation buffers for use with a Dounce homogeniser.

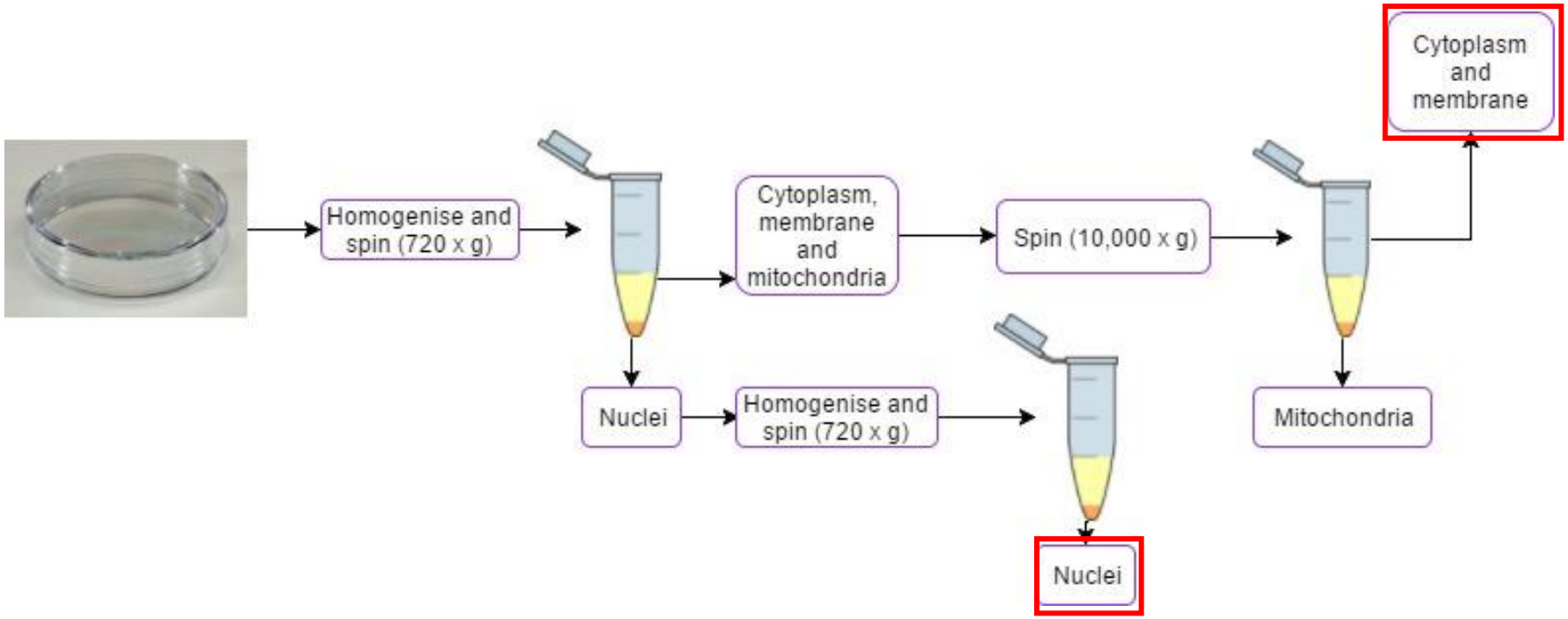

Figure 2.2.2: Flow chart depicting steps taken in subcellular fractionation protocol. Fractions of interest are marked with a red border.

2.2.8.1 Quantification of protein in cellular fractions

Following western blotting of subcellular fractions, densitometric analysis was carried out on bands of interest using Image Studio Lite. The relative densities of both nuclear and cytoplasmic fractions were taken as a proportion of their sum (eg. % of nuclear S100P = density of nuclear S100P/ [density of nuclear S100P + density of cytoplasmic S100P] x 100).

2.2.9 Subcellular fractionation using NP-40 detergent

Cells were fractionated as depicted in Figure 2.2.3. Cells were grown to confluency in 2x 10cm dishes. Cell culture media was then removed, and cells were washed with 1x PBS before being collected by scraping into 500µl of Buffer A on ice (see table 2.2.6). The cell suspension was transferred into an Eppendorf tube before centrifugation at 10,000 x *g* for 2 minutes at 4^{o}C. The supernatant containing the cytosolic extract was centrifuged at 14500 x *g* for 10 minutes at 4^{o}C, following which the supernatant was transferred into a new tube and labelled as the "cytosolic" fraction.

The pellet left from the first centrifugation was resuspended in 500µl of Buffer A and incubated on a rocker, on ice, for 30 minutes. Following incubation, the sample was spun at 10,000 x *g* for 2 minutes at 4^{o}C and the pellet was once again resuspended in 500µl Buffer A. The nuclear fraction was sonicated for 5 seconds at minimum power.

Reagents required for Buffer A
10mM HEPES pH 8
1.5mM $MgCl_2$
10mM KCl
200mM Sucrose
0.5mM DTT
0.5% NP-40
1x protease inhibitors

Table 2.2.6: Reagents required to make Buffer A

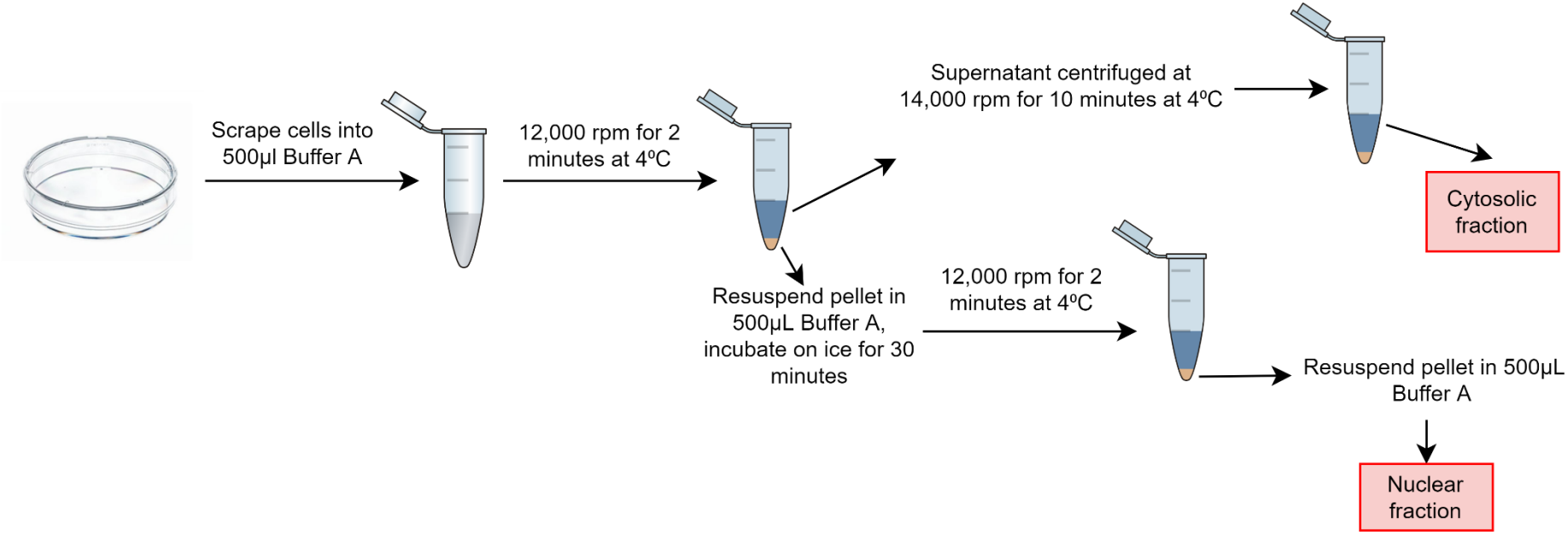

Figure 2.2.3: Flow chart depicting steps taken in the subcellular fractionation protocol utilising NP-40 detergent. Fractions of interest are marked with a red border.

2.2.10 Transient transfection

Depending on the experiment to be carried out, cells were first seeded at the appropriate density onto a variety of culture dishes/plates (either 24 well plates for immunofluorescence or 60mm dishes for western blotting). After 24 hours, the culture media was removed, discarded, and replaced with the antibiotic-free equivalent for 1-2 hours prior to transfection. Cells were transfected using the Lipofectamine 3000 Transfection Reagent according to the manufacturer's instructions.
Plasmid SGB214 contains the N-terminal YFP-tagged S100P. 500ng of plasmid DNA (SGB214) was used per well of a 24 well plate, and 2.5µg of plasmid DNA was required per 60mm dish. Tubes containing the transfection reagents were added dropwise to each well and left to incubate for 48 hours before cell fractionation or fixation.

2.2.10.1 Calculation of transfection efficiency

Round glass coverslips were coated with fibronectin at a concentration of 10µg/ml. Coverslips were covered and left to incubate for 1 hour at room temperature before being washed twice with 1x PBS and lifted into a 24 well plate. The plate was exposed to UV light for 10 minutes before cells were seeded at the required density. Cells were transfected as previously (2.2.10) and left for 24 hours. Following the 24-hour incubation, cells were washed once with PBS before fixation with 4% (w/v) paraformaldehyde in PBS for 10 minutes at 37^{o}c. PFA was removed and replaced with 30mM glycine in PBS to neutralise the leftover PFA. Cells were mounted onto glass microscope slides with DAPI mounting medium and sealed with clear nail varnish. Images of the transfected cells were taken with an inverted epifluorescence microscope (Leica DM14000B) using 63 x oil objective. The total cell count was obtained per field by counting the number of DAPI-stained nuclei. The transfection efficiency was calculated as an average of the percentage of cells expressing the YFP-tagged S100P out of the total cell count per field.

2.2.11 Quantification of S100P nuclear to cytoplasmic ratio

Following transfection, fixation and staining of cells (see 2.2.7 and 2.2.10), images were taken on the Leica DM14000B epifluorescence microscope and quantified with the program ImageJ. A region of interest was drawn in either cytoplasmic or nuclear regions of the cell and the pixel intensity was recorded. Multiple regions of interest were recorded per cell, and at least 50 cells were examined.

2.2.12 Leptomycin B treatment

For experiments requiring Leptomycin B (LMB), cells were treated at varying concentrations (0, 5 and 10ng/ml) in order to calculate the optimal dosage. LMB was dissolved into 100% ethanol at a concentration of 5µg/ml and further diluted to the required concentrations (0, 5 and 10ng/ml) in cell culture media.

To treat cells, culture media was removed and replaced with LMB-containing media for either 3 or 6 hours prior to fixation or subcellular fractionation.

2.2.13 Plasma membrane extraction by nitrogen cavitation

Plasma membranes were isolated from cell lines using adapted protocols (Kaoutzani *et al.* 1993; Simpson, 2010, see figure 2.2.4 for flow chart). Cells were grown to confluency in between 4 and 8 10cm dishes. Cell culture media was removed before washing cells twice with 1x PBS. Cells were scraped into 1 x PBS before centrifugation at 300 x *g* for 5 minutes. Following removal of the supernatant, the pellet was resuspended in homogenisation buffer (250mM sucrose, 50mM Tris, 0.25mM CaCl2 pH 7.4), and centrifuged at 600 x *g* for 5 minutes, twice. The cell pellet was resuspended in homogenisation buffer and passed through the cell disruption bomb chamber at 4^{o}C. Cells were equilibrated in the cell disruption bomb chamber at 800-1000 PSI for 20 minutes. Following release from the bomb, the suspension was centrifuged at 550 x *g* for 10 minutes to remove remaining whole cells and nuclei. The supernatant was collected and layered over 35% (w/v) sucrose/50mM Tris and spun at 100,000 x *g* for 1 hour. The interface was collected and topped up with 25mM sucrose/50mM Tris pH 7.4 before spinning at 100,000 x *g* for 30 minutes. The pellet containing plasma membranes was resuspended in 250mM Sucrose/50mM Tris pH 7.4.

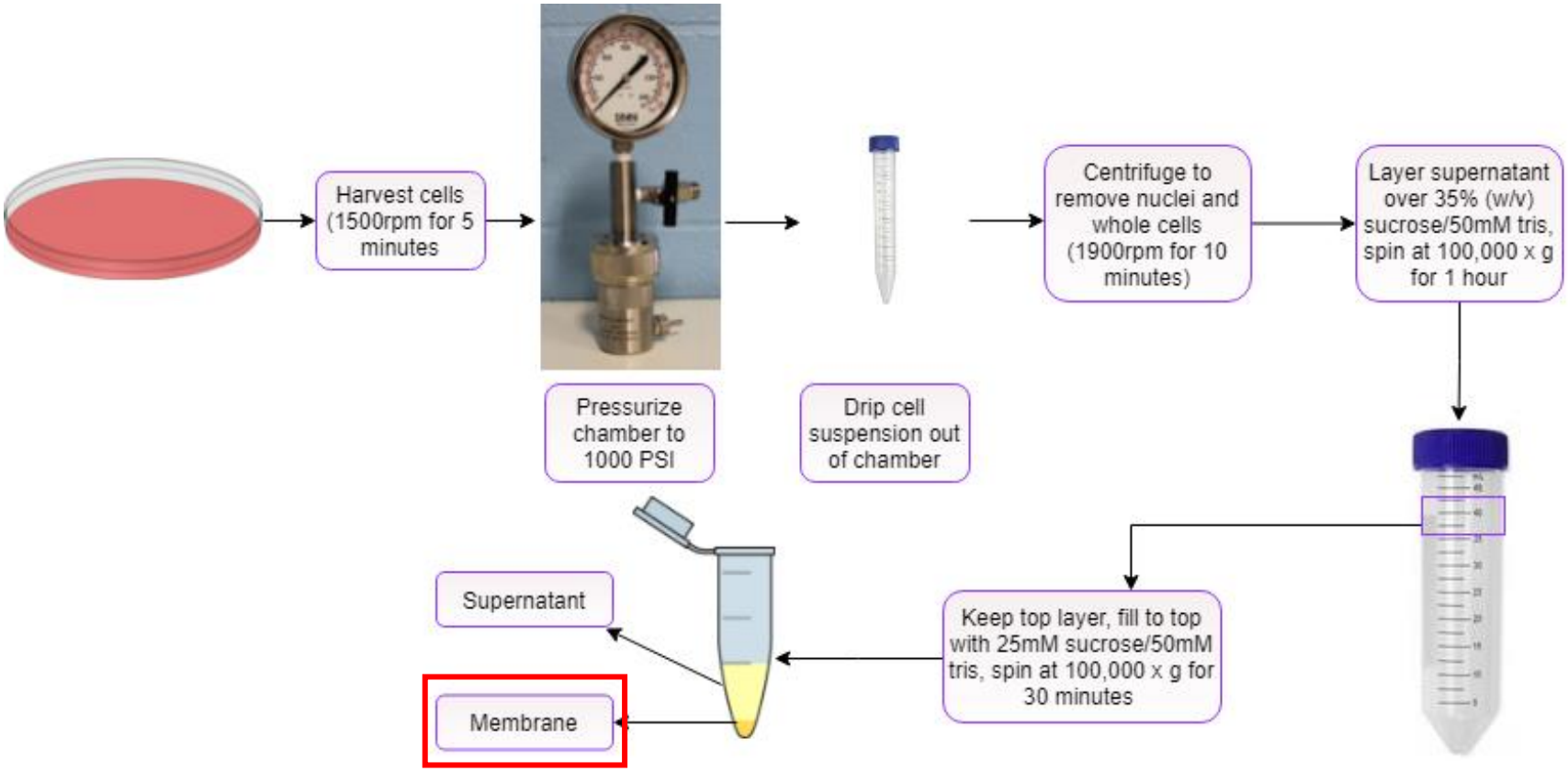

Figure 2.2.4: Flow chart depicting steps taken in nitrogen cavitation protocol. Fraction of interest is marked with a red border.

2.2.14 Biotinylation of cell surface proteins

Cell surface proteins were biotinylated and extracted using the Pierce Cell Surface Isolation Kit according to the manufacturer's instructions (Jang and Hanash 2003). Cells were grown to 90% confluency in 2x T75 flasks. Cell media was removed and cells were washed twice with ice-cold PBS. Sulfo-NHS-SS-Biotin solution was prepared at a concentration of 250µg/ml. 10ml of the biotin solution was added per T75 flask and flasks were incubated on a rocking platform, on ice, for 30 minutes. 500µl of quenching solution was added to each flask and swirled around to stop the reaction. Cells were then scraped into solution and transferred to a 50ml tube. Each flask was washed with 10ml TBS, which was then added to the same 50ml tube containing the cell suspension. Cells were centrifuged at 500 x *g* for 3 minutes and the supernatant discarded. The cell pellet was resuspended in 5ml TBS, and was again centrifuged at 500 x *g* for 3 minutes. The supernatant was discarded and 250µl of lysis buffer, containing protease inhibitor, was added to the cell pellet. Cells were resuspended and sonicated on ice for 10 seconds using 1 second bursts. Cells were incubated on ice for 30 minutes, and were vortexed every 5 minutes for 5 seconds. The lysate was then centrifuged at 10,000 x *g* for 2 minutes at 4^{o}C.

NeutrAvidin agarose was prepared by adding 250µl of NeutrAvidin slurry to a column and spinning at 1000 x *g* for 1 minute. The flow through was discarded before adding 250µl wash buffer, followed by centrifugation at 1000 x *g* for 1 minute. This step was repeated twice. The lysate was added to the capped column and left for 60 minutes at room temperature in a rotating platform. Following incubation, the caps were removed from the column and the column was placed into a fresh collection tube. The column was centrifuged at 1000 x *g* for 1 minute, and the flow through discarded. The column was then washed with wash buffer (containing protease inhibitors). The column was inverted several times to fully mix the sample. The column was then centrifuged again at 1000 x *g* for 1 minute. The washing step was repeated three times before beginning the elution of cell surface proteins.

To elute proteins bound to the Sulfo-NHS-SS-Biotin, 200µl of sample buffer (62.5mM Tris HCl pH 6.8, 1% (w/v) SDS, 10% (v/v) glycerol, 50mM DTT) was added to the column and heated on a heat block for 5 minutes at 95^{o}C. The column was then added to a new collection tube, the totality of which was centrifuged for 2 minutes at 1000 x *g*. A trace amount of bromophenol blue was added to the eluate following protein quantification. Samples were stored at -20^{o}C prior to analysis via western blotting, where 1/10th of the final sample volume was loaded onto the gel.

2.2.15 Flow cytometry of cell surface S100P

Cells were resuspended at a concentration of 400,000 cells/ml. 250µl of the cell suspension, containing 100,000 cells, was required per condition and pipetted into Eppendorf tubes. The tubes were centrifuged at 1000 rpm for 5 minutes to pellet the cells. The supernatant was discarded and the pellet resuspended in P2 (2% (v/v) FBS in PBS). The tubes were vortexed for 5 seconds before repeating centrifugation. The supernatant was again discarded before adding S100P primary antibody (see table 4.2.1) at a concentration of 1µg/ml. The samples were vortexed for a few seconds before being incubated for 30 minutes at 4^{o}C. 500µl of P2 was then added to each sample before vortexing and centrifuging at 1000 rpm for 5 minutes, following which the supernatant was discarded. This step was repeated twice more. The supernatant was removed and a secondary antibody (see table 4.2.1) at dilution 1:10 was added to each sample. The samples were vortexed before incubating at 4^{o}C for 30 minutes. 500µl of P2 was added to each sample before vortexing and centrifugation as previously. The supernatant was removed and samples were run through the CytoFLEX flow cytometer.

Antibody	Type	Clone	Supplier	Dilution	Incubation	Buffer
S100P primary antibody	Monoclonal	IgG Rabbit	Abcam (EPR6143)	1µg/ml	30 minutes at 4^{o}C	P2
α- Rabbit FITC secondary antibody	Polyclonal	Swine polyclonal	Dako (F0054)	1:10	30 minutes at 4^{o}C	P2

Table 2.2.7 List of antibodies required for flow cytometry of cell surface S100P

2.2.16 siRNA transfection of JEG-3 cell line

Two siRNA sequences were selected to allow for knockdown of S100P; siRNA 4 (sequence TAGCACCATGACGGAATAGA) and siRNA 6 (sequence TAGGCTGAGCCTGCTCATGTA). JEG-3 cells were seeded in 24 well plates and grown to 50% confluency before changing the medium. The plate was incubated at 37^{o}c for 30 minutes to allow cells to settle. A mixture containing 100µl Opti-MEM, 2µl INTERFERin and 0.5µl 5µM siRNA (either 4 or 6) was added to each well after mixing. Control wells contained only Opti-MEM, mock-treated wells contained only Opti-MEM and INTERFERin. Cells were left to grow for 2 days before changing medium.

2.2.17 Transwell assay for motility and invasion

In order to assess the migration and invasion of cell lines, Boyden chamber assays were utilised (Justus *et al.* 2014). In this technique, cells are seeded into an 8µm polycarbonate Boyden chamber placed into a well of a 24 well plate. The cells are left to migrate through the membrane, following which the transwells are fixed and the cells counted.

Following 24 hours of serum deprivation by growing cells in 0.5% (v/v) FBS -containing medium, cells were seeded at a density of 25,000 cells into each transwell containing fully supplemented medium (5% (v/v) FBS). For invasion experiments, transwells were coated with Matrigel (diluted 1:3 into serum free RPMI) and left to set for 2 hours prior to seeding cells. For motility experiments, cells were seeded directly onto the transwells. Cells were then incubated for 24 hours to allow the cells to migrate/invade through the membrane.

Following 24 hours, media was removed from the transwells prior to incubation in 4% (w/v) PFA, diluted in PBS, for 10 minutes at room temperature. PFA was removed and cells were gently washed with PBS twice. Cells on the transwell membrane were permeabilised using 0.1% (v/v) triton in PBS for 10 minutes at room temperature. Cells were washed twice further with PBS before staining the cells with May-Grünwald solution for 10 minutes at room temperature. Following this, cells were again washed twice with PBS prior to staining the cells with Giemsa for 10 minutes at room temperature. The transwells were then washed gently with distilled water before removing any stained cells on the upper surface of the transwell membrane with a cotton bud. Cells on the lower side of the membrane were counted using a Nikon Eclipse TS100 inverted microscope and a 40x objective lens in at least 5 random fields per transwell.

2.2.17.1 S100P antibody treatment

To assess the effect of the S100P in the cell surface/membrane on cell migration or invasion, addition of S100P antibody was carried out as previously done in the context of cancer cells (Clarke *et al.* 2017; Ismail *et al.* in preparation). Cells were seeded as above (see section 2.2.17) into the transwells, and S100P antibody was added to the culture media in both the transwells and the outer wells at dilution 1:1000. Following 24 hours of incubation, the transwells were processed as above (see section 2.2.17).

2.2.17.2 Cromolyn treatment

To assess the effect of the cromolyn on cell migration or invasion as previously done by Arumugam, Ramachandran and Logsdon (2006), cells were seeded as above (see section 2.2.17) into the transwells, with cromolyn added into the transwell and outer well at a concentration of 10µM and 100µM. Following 24 hours of incubation, the transwells were processed as above (see section 2.2.17).

2.2.18 Quantification of focal adhesion complexes

Following indirect immunofluorescent staining of cells for paxillin (see section 2.2.7), pictures were taken of cells with the Leica DMB400 using a 63x oil objective. The number of focal adhesions per cell (randomly selected) were counted for each condition, with an excess of 50 cells being counted per condition.

2.2.19 Isolation of extravillous trophoblasts from first trimester placenta

Written informed consent was obtained from all women recruited into the study. Samples of placental tissues for EVT isolation were obtained immediately after elective termination of pregnancy from first trimester of gestation (8-12 weeks). Placental samples were collected with approval of Health Research Authority - West Midlands, Edgbaston Research Ethics Committee (NHS REC 15/WM/0284 and AHRIC REF 1245-SG).

All work was carried out with sterile equipment in a sterile tissue culture hood. Blood clots were removed from the placental tissue before washing with Ham's F12 (without phenol red) for 10 minutes whilst stirring gently. Pieces of tissue were sorted through to obtain chorionic villi. The chorionic villi

were scraped using forceps and a scalpel, and excess placental membrane was removed. Several millilitres of pre-warmed 0.25% trypsin solution (0.03% glucose, 1.2% NaCl, 0.03% KCl, 0.1725% disodium hydrogen orthophosphate, 0.03% potassium dihydrogen orthophosphate, 0.2% trypsin powder, 0.02% EDTA) was poured onto the scraped material. The placental tissue mixed with trypsin was transferred into a 250ml bottle with a magnetic stirrer using a cut Pasteur pipette. The solution was mixed along with 75ml 0.25% trypsin for 9 minutes on a heat stirrer at 37^{o}c. A funnel and gauze were assembled over a fresh sterile 250ml bottle filled with 25% newborn foetal calf serum in Ham's F12, and after 9 minutes of digestion, the placental tissue was filtered into this bottle, allowing for neutralisation of the trypsin solution. The bottle was rinsed with 15ml Ham's F12, and the gauze twisted, to obtain as many cells as possible. The filtrate was aliquoted into universal tubes and centrifuged for 5 minutes at 450 x g. The supernatant was discarded and the pellets were resuspended by flicking the tubes. Pellets were pooled and resuspended in a total volume of 15ml Ham's F12. Universal tubes were rinsed with 5ml Ham's F12 which was then added to the 15ml of pooled pellets. 8ml of Pancoll was aliquoted into two fresh sterile universal tubes, and equal volumes of sample were layered over the Pancoll (Figure 2.2.5, panel A). The tubes were spun at 750 x *g* for 20 minutes with the brake off. Following centrifugation, a white band of cells should be visible at the interface (Figure 2.2.5, panel B). 4-5ml of the interface was aspirated using a Pasteur pipette and collected into clean universal tubes. The universal tubes were topped up with Ham's F12 and spun at 500 x *g* for 5 minutes. The supernatant was discarded and pellets were resuspended by flicking the tube. All cell pellets were pooled into one tube and 1ml of Trophoblast Complete Medium (TCM: Ham's F12 without Phenol red, 20% FBS, 1x Pen/Strep solution, 2mM L-Glutamine, 6.25µg/ml amphotericin, 50µg/ml gentamicin sulfate) was added before performing a viable cell count. Cells were seeded onto fibronectin coated 35mm dishes (20µg/ml) and left to settle. Cells were left overnight before changing the media with fresh TCM, both to allow EVT cells to settle and to wash away other contaminating cells (placental macrophages, foetal red cells, mesenchymal core cells). The yield of EVT cells was calculated immunofluorescent staining for HLA-G.

A

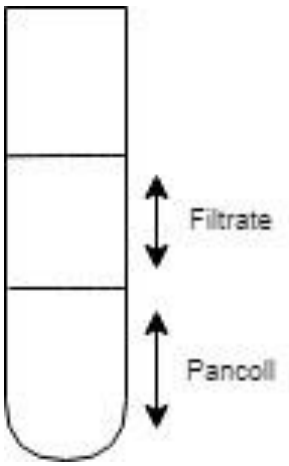

B

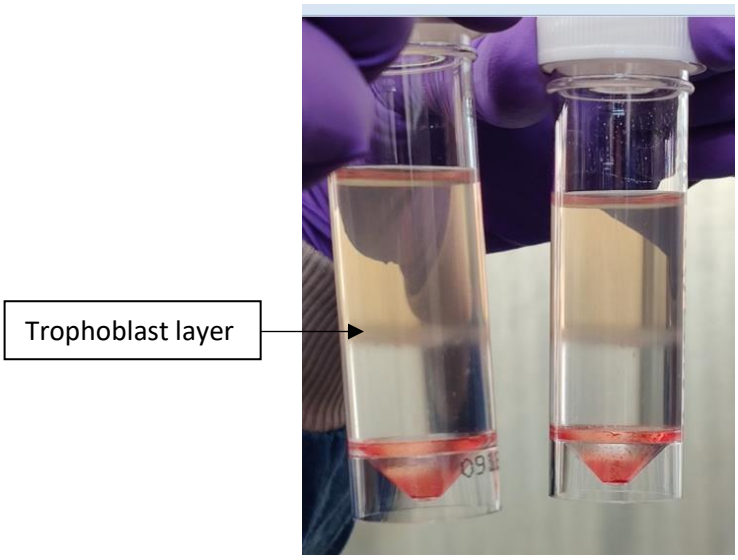

Figure 2.2.5: Isolation of EVT cells from first trimester placenta

A) Schematic representing layering of cell filtrate onto Pancoll to allow for separation of EVT cells from other cell types

B) Resulting interface containing EVT cells following centrifugation at 720 x *g* for 20 minutes.

2.2.20 Antibodies

Primary Antibodies	Experiment	Supplier	Species	Type	Dilution	Reference
Actin	WB	Sigma-Aldrich (Dorset, UK)	Mouse	Monoclonal	1:3000	A2228
Lamin	WB	Sigma-Aldrich (Dorset, UK)	Rabbit	Polyclonal	1:1000	SAB4501764
S100P	WB	R&D Systems (Oxford, UK)	Goat	Polyclonal	1:2000	AF2957
Tubulin	WB	Sigma-Aldrich (Dorset, UK)	Mouse	Monoclonal	1:5000	T5168
HDAC2	WB	Abcam (Cambridge, UK)	Rabbit	Monoclonal	1:2000	ab32117
Paxillin	WB	Invitrogen (Altrincham, UK)	Mouse	Monoclonal	1:2000	MA5-13356
Caveolin I	WB	Santa Cruz (Texas, USA)	Rabbit	Monoclonal	1:750	N-20, sc-894
S100PBP	WB	Sigma-Aldrich (Dorset, UK)	Rabbit	Polyclonal	1:1000	HPA027328
S100P	IF	Abcam (Cambridge, UK)	Rabbit	Monoclonal	1:200	EPR6143
Paxillin	IF	Invitrogen (Altrincham, UK)	Mouse	Monoclonal	1:100	AH00492
HLA-G	IF	Abcam (Cambridge, UK)	Mouse	Monoclonal	1:100	4H84
Secondary Antibodies		**Supplier**	**Species**	**Type**	**Dilution**	**Reference**
Anti-mouse IgG, HRP-linked	WB	New England Biolabs (Hertfordshire, UK)	Horse	Polyclonal	1:3000	7076S

Anti-goat IgG, HRP-linked	WB	Dako (California, US)	Rabbit	Polyclonal	1:3000	P0449
Anti-rabbit IgG, HRP-linked	WB	New England Biolabs (Hertfordshire, UK)	Gat	Polyclonal	1:3000	7074S
α- Mouse FITC secondary antibody	IF	Dako (California, US)	Rabbit	Polyclonal	1:100	F0261
α- Rabbit FITC secondary antibody	IF	Dako (California, US)	Swine	Polyclonal	1:100	F0205

Table 2.2.8: List of primary and secondary antibodies used in these studies
WB, Western blotting; *IF,* immunofluorescence

2.2.21 Blue Native PAGE

Cell lysates and fractions were added to native gel loading buffer with a final concentration of 50% (v/v) glycerol (Table 2.2.9). Electrophoresis equipment was assembled before pouring 1x BN blue cathode running buffer and 1x BN anode running buffer into the inner and outer chambers of the tank respectively. 30µg of cell lysates and fractions were loaded on a NativePAGE 4-16% (w/v) Bis-Tris gel and run for 60 minutes at 150V. After 60 minutes, the 1x BN blue cathode running buffer was replaced with 1x BN colourless cathode running buffer and run for another 60 minutes. After 60 minutes, the voltage was increased to 250V and run until the blue front reached the bottom of the gel. The gel was then transferred to PVDF membrane prior to western blotting for S100P (see 2.2.6) or mass spectrometric analysis.

BN loading buffer	750mM ACA, 50mM bis-tris pH7, 5% (w/v) CBB G250, stored at -20^{o}c
10x BN blue cathode running buffer	500mM tricine, 150mM bis-tris pH7, 0.2% (w/v) CBB G250, stored at 4^{o}c
10x BN colourless cathode running buffer	500mM tricine, 150mM bis-tris pH7, stored at 4^{o}c
10x BN anode running buffer	500mM tricine, stored at 4^{o}c

Table 2.2.9 List of reagents required for blue native PAGE electrophoresis

2.2.22 Mass spectrometry analysis

All mass spectrometry work was performed by Ms Ivana Milic following the methodology of Shevchenko *et al.* (2007) with minor modifications, as described by Pallett *et al.* (2019).

Following separation of cell lysates and fractions by BN-PAGE (see section 2.2.21), gels were disassembled from the gel apparatus and stained with Coomassie G250 blue (0.5% (w/v) in 40% methanol and 10% glacial acetic acid) for 1 hour. Gels were subsequently destained in 10% ethanol and 7.5% glacial acetic acid.

For the in-gel digestion of proteins, each sample was divided into 4 fragments per lane according to their approximate molecular weight (Figure 2.2.6). Each gel fragment was excised and diced in a clean Eppendorf tube using a sterile scalpel. Gel pieces were consequently destained with 50% acetonitrile in 50 mM ammonium bicarbonate, after which they were dehydrated with acetonitrile and vacuum dried. In-gel digestion of proteins was carried out using trypsin Gold in 3 mM ammonium bicarbonate using a 25:1 protein:trypsin ratio on a shaking platform at 550 rpm at 37 °C overnight. The next day, peptides were extracted for 15 minutes in an ultrasonic bath using acetonitrile, with the volume used equivalent to 50% of the sample volume. Peptides were washed twice with 150µl of 50% acetonitrile in 50mM ammonium bicarbonate. Full dehydration of the gel pieces and maximisation of peptide extraction was achieved using 400µl of acetonitrile. Peptide extracts were pooled into the appropriate Eppendorf tubes, vacuum dried and stored at −20 °C prior to analysis.

Sample reconstitution was achieved by resuspension of peptides in 50µl 3% aqueous acetonitrile, 0.1% formic acid prior to liquid chromatography-coupled tandem mass spectrometry analysis (LC-MS/MS). Separation and analysis of peptides was carried out using the nLC system coupled to the TripleTOF 5600 system operation in information dependent mode (IDA). The peptide solutions were injected onto a PepMap column using 2% Eluent B (98% acetonitrile in 0.1% formic acid) at a 30µL/minute flow rate. Separation of peptides on the PepMap column was carried out under the following gradient conditions: 0-3 minutes 2% B, 3–48 minutes 2–45% B, 48–52 minutes 45–90% B, 52–55 minutes 90% B, 55–70 minutes 2% B.

To form the electrospray, nLC eluate was sprayed at 2500V using a PicoTip emitter, and the 10 most intense ions from each MS survey scan were selected for MS/MS. Acquired ions were temporarily excluded from acquisition by MS/MS for 30 seconds. Calibration of the mass spectrometer was carried out prior to ion acquisition to ensure high mass accuracy of <10 ppm on both MS and tandem mass spectrometry (MS/MS) levels. Relative quantification of unique peptides was done using Progenesis QI for proteomics software. The acquired MS/MS data was then searched against the SwissProt database using MascotDaemon software (version 2.5) using the following search parameters: mass tolerance of 0.1 Da for MS and 0.6 Da for MS/MS spectra, a maximum of 2 trypsin miscleavages, *Homo Sapiens* taxonomy, variable modifications of methionine oxidation and cysteine carbamidomethylation.

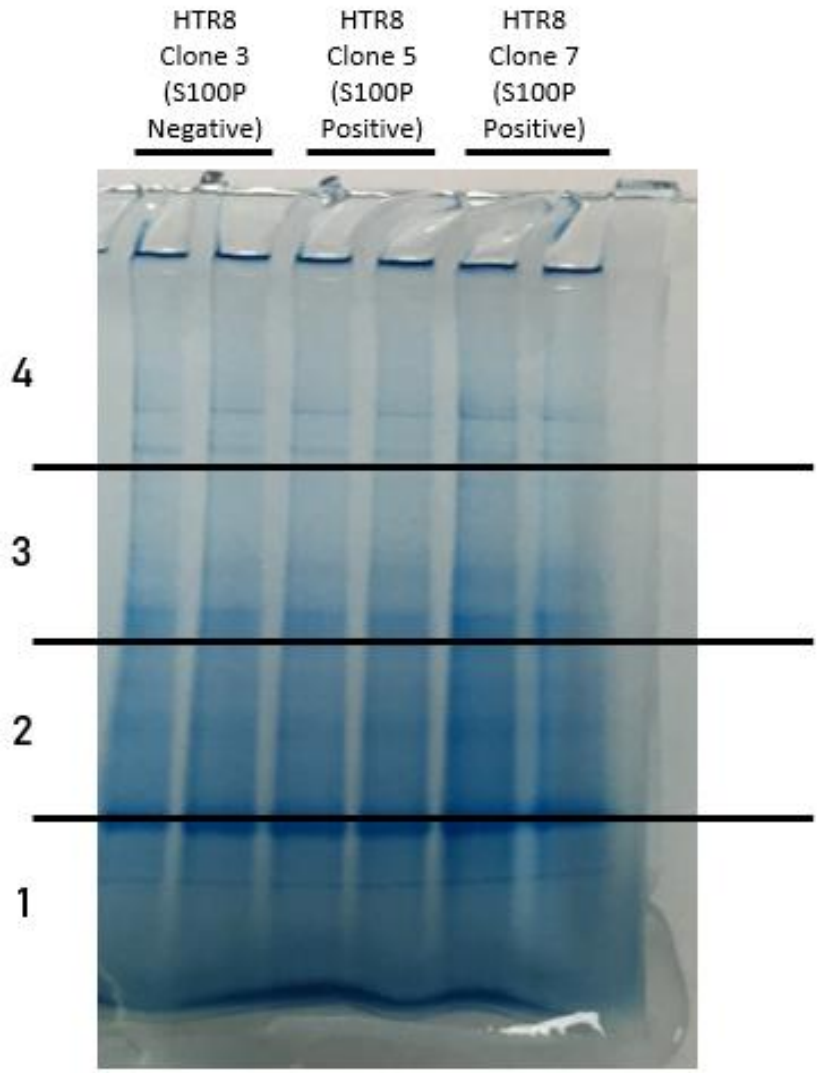

Figure 2.2.6: Representative image depicting slicing of NativePAGE gels prior to mass spectrometry analysis of cytoplasm/membrane fractions from S100P-negative and S100P-positive cells for changes in protein abundance

NativePAGE 4-16% (w/v) Bis-Tris gel was stained with InstantBlue to allow for visualisation of total protein within each lane prior to cutting the gel into 4 fragments.

2.2.23 Data analysis

Statistical analysis of significant changes of protein abundance was carried out using multiple T-tests in GraphPad 6.0 software, and evaluated at a 95% confidence interval where $p<0.05$. Gene Ontology (GO) enrichment analysis was performed using the Database for Annotation, Visualisation and Integrated Discovery (DAVID) v6.8 (Huang *et al.* 2007).

2.2.24 Statistical Analysis

Data presented within this work are listed as mean ± SEM (standard error) or ± SD (standard deviation). All statistical analysis, either one-way/two-way ANOVA or Student's T test, was carried out using GraphPad v 6.0 software, and evaluated at a 95% confidence interval where $p<0.05$. Data was considered statistically significant when represented with * where $p<0.05$, ** $p<0.01$, *** $p<0.001$, or **** $p<0.0001$.

Chapter 3:

Biochemical analysis of S100P cellular localisation in multiple cell lines

Chapter 3: Biochemical analysis of S100P cellular localisation in multiple cell lines

Contents

3.1 Introduction

The S100P protein, first isolated from the placenta, has been the focus of several groups due to its high expression in many diverse tumour types, and its role in a myriad of cellular processes (Prica *et al.* 2016). Whilst much has been reported regarding the expression of S100P in numerous tissues, significantly less is known about the specific localisation of S100P at the subcellular level, with only a small number of studies highlighting this (Table 3.1.1). The majority of tissues and cell lines that have been assessed for S100P subcellular localisation in previously published literature happen to be of pathophysiological origin, largely from a cancer background (Whiteman *et al.* 2007; Hsu *et al.* 2015).

Whilst the knowledge of S100P subcellular localisation in a disease background is important, few studies exist that report the localisation of S100P in a normal physiological background. In addition, the localisation of the S100P protein in cells could lead to more information about its role or interacting partners. Several previous studies have examined or isolated a variety of different proteins that interact or associate with S100P (Austermann *et al.* 2008; Heil *et al.* 2011; Du *et al.* 2012). This research has utilised mainly, if not exclusively, cancer cell lines, again highlighting the lack of research into S100P in normal healthy tissues. Several of the S100P interacting partners, namely IQGAP1 and ezrin, play a role in cytoskeletal organisation and regulation and act as key signalling intermediates in a variety of pathways (Heil *et al.* 2011; Neisch and Fehon, 2011). Others, such as RAGE, are present on the cell surface suggesting S100P has extracellular activities (Arumugam *et al.* 2004).

What is puzzling nonetheless, is the fact that in most cases up to date, assessments of S100P localisation have been carried out using immunohistochemistry, which has the disadvantage of variance in both specificity and sensitivity in addition to a lack of a standard scoring system (Kim, S.-W. *et al.* 2016, Johnson, C. W. 1999). These studies highlighted in the table below suggest that S100P is predominantly found in the nucleus without clear explanation for such localisation in the context of its interactome, which consists of mostly cytoplasmic/membrane associated proteins.

In this chapter, we aim to assess the specific subcellular localisation of the S100P using biochemical subcellular fractionation, a direct biochemical technique that allows for separation of cells into their constituent compartments using differential centrifugation. This will be achieved by the use of cell lines endogenously expressing S100P, as well as those that have regulatable expression. We also aim to assess the effect of modifications to the fractionation assay, including the addition of excess calcium, removal of calcium chelators, and the use of a non-ionic detergent (NP-40). In addition, the effect of both a YFP tag on the N-terminus of S100P, and the nuclear export inhibitor leptomycin B on S100P subcellular localisation will be evaluated.

Tissue type	S100P localisation	Technique used	Reference
Breast cancer (primary stage II tumours)	Predominantly nuclear (strong) Cytoplasmic (weak)	Immunohistochemistry	Maciejczyk *et al.* (2013)
Breast cancer (typical and atypical ductal hyperplasia epithelial cells)	Cytoplasmic (accumulation in apical and supranuclear regions)	Immunohistochemistry	Russo and Russo (2004)
Breast cancer (invasive ductal carcinoma)	Cytoplasmic	Immunohistochemistry	Russo and Russo (2004)
Pancreatic ductal adenocarcinoma	Nuclear and cytoplasmic	Immunohistochemistry	Dowen *et al.* (2005)
Lung adenocarcinoma (stably expressing GFP-S100P)	Nuclear and cytoplasmic	Immunofluorescence following transfection	Rehbein *et al.* (2008)
Epidermoid carcinoma (expressing GFP-S100P)	Nuclear and cytoplasmic	Immunofluorescence following transfection	Koltzscher *et al.* (2003)
Colorectal cancer	Low-grade adenomas: Nuclear (strong) High-grade adenomas: Nuclear (strong) and cytoplasmic (moderate)	Immunohistochemistry	Chiang *et al.* (2015)
Placenta	First trimester syncytiotrophoblasts: Nuclear and cytoplasmic (strong)	Immunohistochemistry	Zhu *et al.* (2015)
	First trimester villous cytotrophoblasts and cytotrophoblast columns: Cytoplasmic		
	Third trimester trophoblasts: Nuclear (strong) and cytoplasmic (weaker)	Immunohistochemistry	Zhang *et al.* (2011)

Human oesophageal epithelium	Cell membrane and cytoplasm	Immunohistochemistry	Sato and Hitomi (2002)
Duodenum	Enterocytes: Nuclear	Immunohistochemistry	Parkkila *et al.* (2008)
Urothelial carcinoma	Nuclear (strong) and cytoplasmic	Immunohistochemistry	Gulmann *et al.* (2013)
Human endometrium	Nuclear	Immunofluorescence	Tong *et al.* (2010)
Primary human endometrial epithelial cells	Cytoplasm	Immunofluorescence	Zhang *et al.* (2012)
Primary human endometrial stromal cells	Cytoplasm	Immunofluorescence	
Low differentiation endometrial cancer	Cytoplasm	Immunohistochemistry	Guo *et al.* (2014)
Bladder cancer tissues and T24/KK47 cell lines (urinary bladder carcinoma)	Nuclear	Immunohistochemistry, immunofluorescence and fractionation	Shiota *et al.* (2011)
HeLa cell line	Nuclear and cytoplasmic	Immunofluorescence	Dowen *et al.* (2005)
	Nuclear and cytoplasmic	Immunofluorescence	Heil *et al.* (2011)
	Nuclear, cytoplasmic, and in membrane ruffles following EGF stimulation		
Human breast carcinoma	Predominantly nuclear, cytoplasmic	Immunocytochemistry	Wang *et al.* (2006)

Table 3.1.1: Table of tissues and their subcellular distribution of S100P

3.2 Results

3.2.1 S100P is expressed by various cell lines of differing origin

Prior to assessing the subcellular localisation of S100P, a variety of different cell lines were first tested to establish the levels of S100P expression (Figure 3.2.1). To this end, we used a panel of cell lines; some non-tumourigenic (COS-7), as well as cancer systems (HeLa and MDA-MB-231), and models where S100P is known to be expressed (JEG-3 and BeWo). In some cases, S100P was endogenously produced by cell lines to a certain level without intervention (JEG-3, BeWo and MDA-MB-231), whilst in others, S100P levels can be regulated (COS-7 and HeLa). Western blotting for S100P and tubulin of total cell lysates was performed after separation on a 16% (w/v) SDS-PAGE on several different cell lines; trophoblast model cell lines JEG-3 and BeWo, cancer cell line MDA-MB-231, and two cell lines transfected with the inducible system HeLa A3 and COS-7 s10 (Figure 3.2.1, panel A). Quantification of the band intensity for both S100P and tubulin was carried out on all cell lines (Figure 3.2.1, panel B).

Results demonstrated that levels of S100P across these cell lines was somewhat variable, with the JEG-3 cell line exhibiting on average the lowest levels of S100P expression. The invasive breast cancer cell line MDA-MB-231 showed the highest level of S100P expression which was 80% higher than that of JEG-3 cells (±78.99 SD), followed by the BeWo choriocarcinoma cell line, which was on average almost 50% higher than JEG-3 cells (±28.73 SD). HeLa A3 and COS-7 s10 inducible cell lines showed similar levels of S100P expression to each other (both 31% higher S100P expression than JEG-3 cells; COS-7 s10 ±78.13 SD; HeLa ±37.75 SD). Levels of S100P expression in these five cell lines were not found to be statistically significantly different from each other ($p>0.89$, one-way ANOVA).

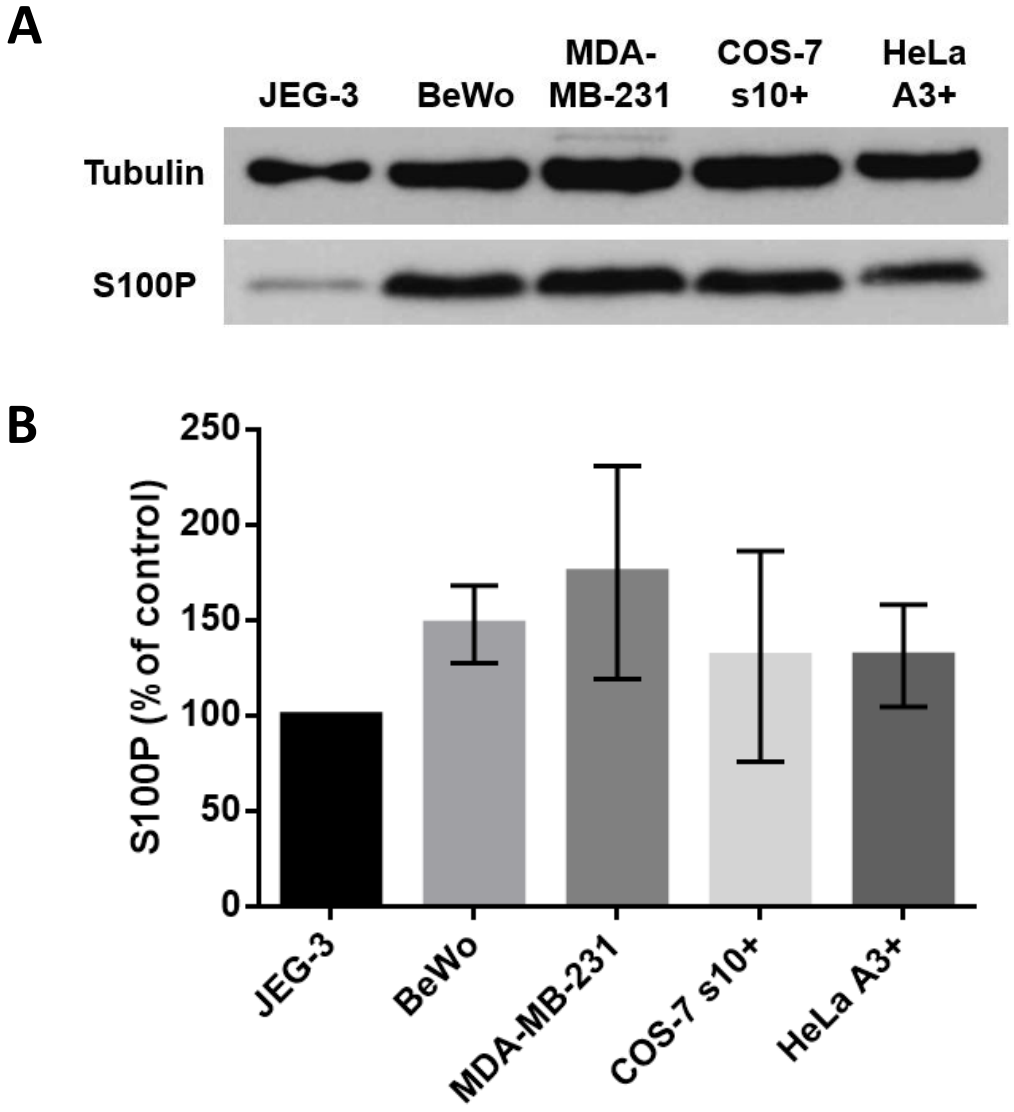

Figure 3.2.1: Levels of S100P in a wide variety of cell lines

A) Cell lysates from JEG-3, BeWo, MDA-MB-231, COS-7 s10+ and HeLa A3+ cells were collected and separated on a 16% (w/v) SDS-PAGE before western blotting for S100P and tubulin.

B) Levels of S100P within cell lysates were quantified by densitometry using Image Studio Lite and normalised to tubulin. Data represents the mean ±SD from at least 3 independent replicates (one-way ANOVA).

As mentioned, several cell lines were utilised in which S100P levels could be regulated. S100P expression in the HeLa A3 and COS-7 s10 cell lines could be variable depending on the length of treatment with 1µg/ml doxycycline. To assess the variability of S100P expression in the two cell lines transfected with the inducible system, western blotting was performed on HeLa A3 and COS-7 s10 cell lysates that had been treated with 1µg/ml doxycycline, the gene expression-inducing agent, for different lengths of time, ranging from 24 to 336 hours. Cells were collected prior to separation on a 16% (w/v) SDS-PAGE, followed by western blotting for S100P and tubulin (Figure 3.2.2, panel A). Quantification of band intensity for both tubulin and S100P was carried out on each sample (Figure 3.2.2, panel B).

Data from these experiments show that S100P levels in the HeLa A3 cell line gradually increase with longer doxycycline treatment up to 120 to 144 hours, to a level that is statistically significantly different than non-induced HeLa A3 lysates ($p<0.01$). The HeLa A3+ lysates induced for 144 hours demonstrated an S100P expression level over 5.5-fold higher than that of HeLa A3+ lysates induced with doxycycline for 24 hours ($p<0.034$). Following the 144-hour time point, there is a general decrease in the level of S100P expression, in which the 336-hour HeLa A3+ lysate demonstrated 45% less S100P expression than the 144-hour HeLa A3+ lysate.

In the COS-7 s10 cell line, there is a sharp increase in S100P expression between COS-7 s10 lysates induced with 1µg/ml doxycycline for 24 hours until the 72-hour time point ($p<0.04$). Induction of S100P expression for 96 hours or longer does not generate the same level of S100P expression seen in COS-7 s10 cell lysates induced for 72 hours; on average, there is a 30% decrease in S100P expression following 96 hours of induction with doxycycline when compared to COS-7 s10 lysates induced for 72 hours. COS-7 s10 lysates induced for 96 or 120 hours exhibit a statistically significantly different level of S100P expression compared to the non-induced COS-7 s10 lysates ($p<0.03$). However, COS-7 s10 lysates induced for 96 hours or longer do not demonstrate a statistically significant difference in S100P expression when compared to their 24-hour counterpart ($p>0.5$).

Both HeLa A3 and COS-7 s10 cell lines showed a 2.6-fold or 4.3-fold increase, respectively, in their S100P expression level following induction with 1µg/ml doxycycline for 72 hours compared to the 24-hour counterpart. As a result, for fractionation experiments utilising the inducible cell lines, it was decided to induce cells with 1µg/ml doxycycline for 72 hours to ensure that S100P expression was at a sufficiently high level for localisation studies using both HeLa A3 and COS-7 s10 cell lines.

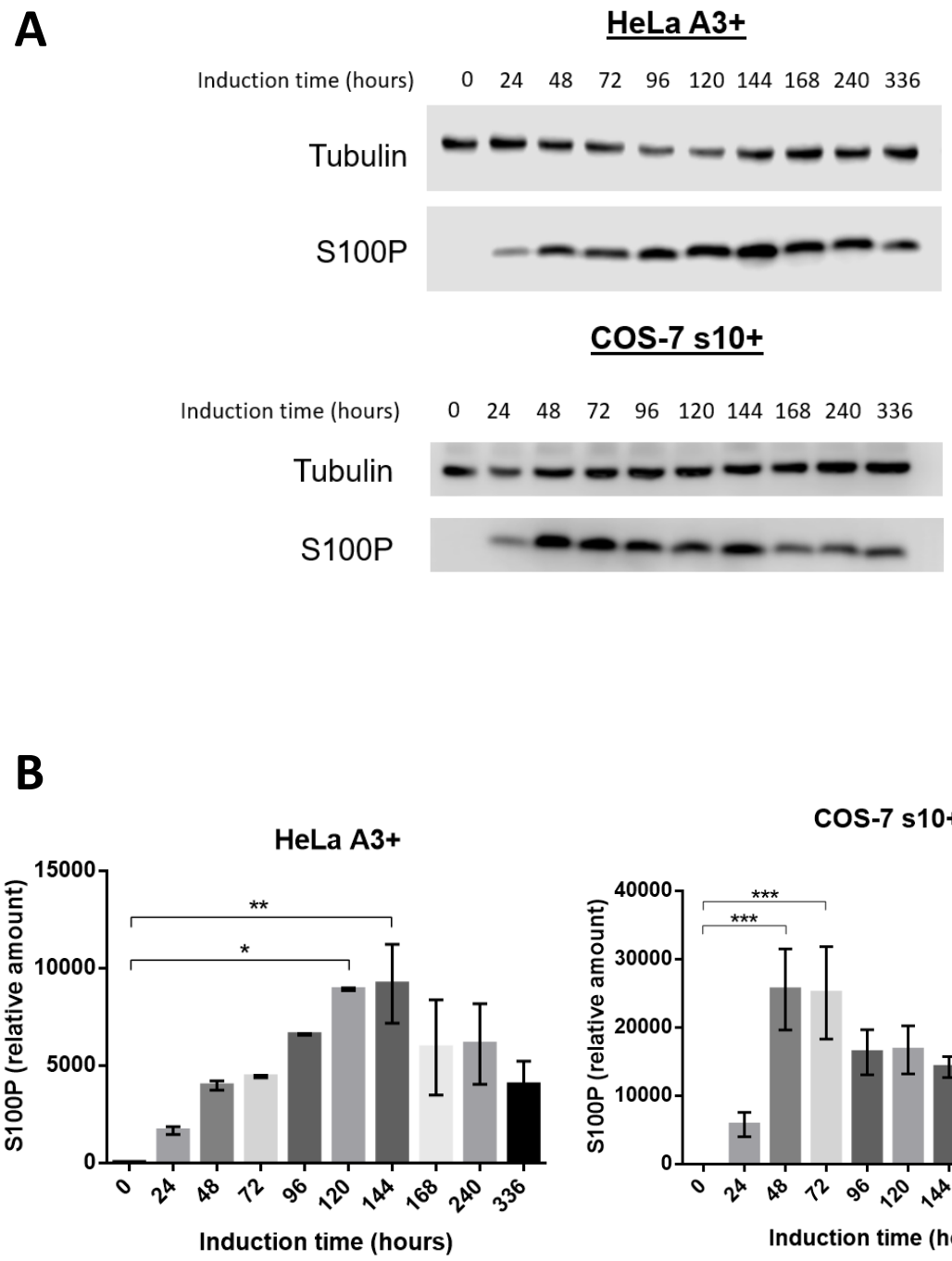

Figure 3.2.2: Induction of S100P expression over time leads to increased S100P expression in HeLa A3 and COS-7 s10 cell lines

A) Cell lysates from COS-7 s10+ and HeLa A3+ cells induced for different lengths of time (from 0 to 336 hours) were collected and separated by 16% (w/v) SDS-PAGE before western blotting for S100P and tubulin.

B) Levels of S100P within cell lysates were quantified by densitometry using Image Studio Lite and normalised to tubulin. Data represents the mean ±SEM from at least 3 independent replicates (one-way ANOVA, * $p<0.05$, ** $p<0.01$, *** $p<0.001$)

In addition to the cell lines previously mentioned and used to study S100P expression, the HTR8/SVneo trophoblast cell line was utilised. Despite the work we have done showing that S100P appears to play an important role in trophoblast cell motility and invasion, this first trimester extravillous trophoblast cell line does not express S100P at detectable levels (Figure 3.2.3, see Tabrizi *et al.* 2018). Therefore, a HTR8 cell line stably expressing S100P was created, generating a range of clones with varying levels of S100P expression. HTR8 clone lysates were collected prior to separation on 16% (w/v) SDS-PAGE and western blotting for S100P and tubulin (Figure 3.2.3 panel A). Quantification of the band intensity was carried out on S100P and tubulin for each HTR8 clone (Figure 3.2.3 panel B). As expected, HTR8 cells transfected with the control plasmid showed no S100P expression. Out of the clones transfected with plasmid containing S100P, HTR8 clones 3 and 5 demonstrated the lowest levels of S100P expression, with clone 5 exhibiting on average a 30% higher level of expression than S100P-expressing clone 3. S100P-expressing clones 7, 9 and 10 showed similar levels of expression to each other, in which S100P expression in clones 7, 9 and 10 was 349%, 359% and 393% higher respectively than S100P expression seen in clone 5. HTR8 clones 7, 9 and 10 demonstrated a statistically significant difference in S100P expression compared to S100P-expressing clone 3 ($p<0.0021$) and S100P-expressing clone 5 ($p<0.0035$). There is no statistically significant difference in S100P expression between HTR8 clones 7, 9 and 10 ($p>0.81$). The HTR8 stable cell line is therefore an invaluable tool for assessing the impact of expression level on S100P subcellular localisation, as it removes the requirement of inducing cells with doxycycline. Most importantly, the HTR8 cell line is a model first trimester extravillous trophoblast cell line, and therefore more relatable to the role of S100P in placenta, unlike the inducible cell lines HeLa A3 and COS-7 s10.

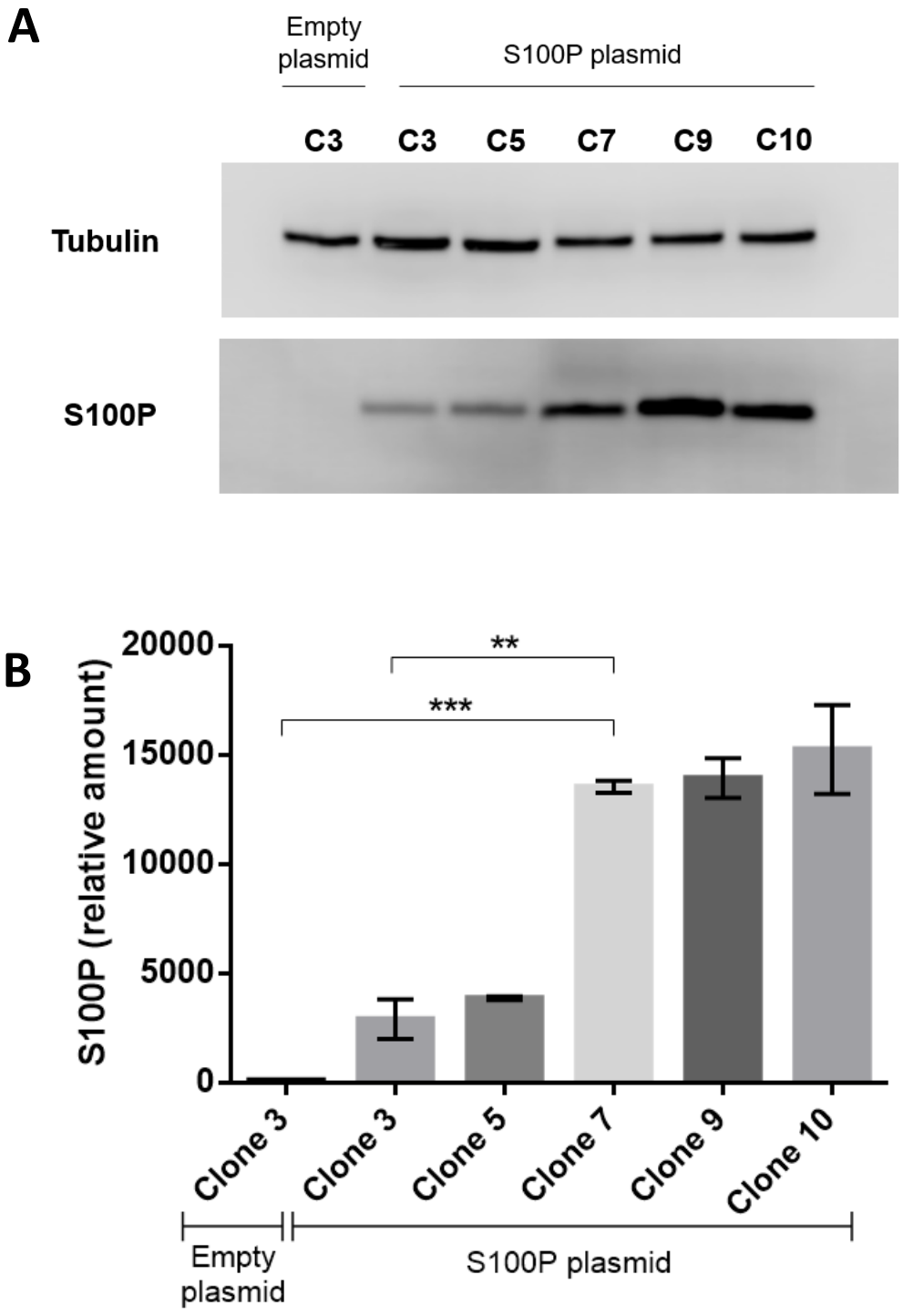

Figure 3.2.3: S100P is stably expressed by HTR8 clones following transfection

A) Cell lysates from different HTR8 clones generated by transfection with a plasmid containing S100P, SGB217, were collected and run on 16% (w/v) SDS-PAGE before western blotting for S100P and tubulin. HTR8 cells transfected with a non-S100P containing plasmid, SGB16, were utilised as a negative control.

B) Levels of S100P within cell lysates were quantified by densitometry using Image Studio Lite and normalised to tubulin. Data represents the mean ±SEM from at least 3 independent replicates (one-way ANOVA, ** $p<0.01$, *** $p<0.001$)

3.2.2 S100P immunofluorescence demonstrates nuclear and cytoplasmic localisation

Many studies, including our own work (Tabrizi *et al.* 2018), have shown the presence of S100P in the nucleus and the cytoplasm through immunostaining and immunofluorescence of different cell lines and tissues (see table 3.1.1 for references). In order to assess the localisation of S100P, HeLa A3+ cells were fixed and stained with an antibody to S100P by indirect immunofluorescence (see Table 2.2.8 for antibody dilutions). Cells were also stained for actin and DAPI to visualise the cellular cytoskeleton and nuclei respectively (Figure 3.2.4, panel A).

Immunostaining of non-induced HeLa A3 cells for S100P demonstrated a small level of background staining. Concurrent immunostaining of HeLa A3+ cells showed a fairly homogenous, non-specific distribution of S100P, with a generally higher intensity of staining within the nuclear and perinuclear regions (Figure 3.2.4). Overall, the signal achieved for S100P appears to be quite diffuse and perhaps somewhat non-specific, even though no significant signal for S100P can be detected in non-induced HeLa A3 cells.

In order to gain further information regarding the cellular localisation of the staining, image analysis was carried out using integrated density in ImageJ (figure 3.2.4, panel B). The distribution of S100P signal in HeLa A3+ cells was found to be 74.11% nuclear, and 25.89% cytoplasmic (±5.23 SD).

A

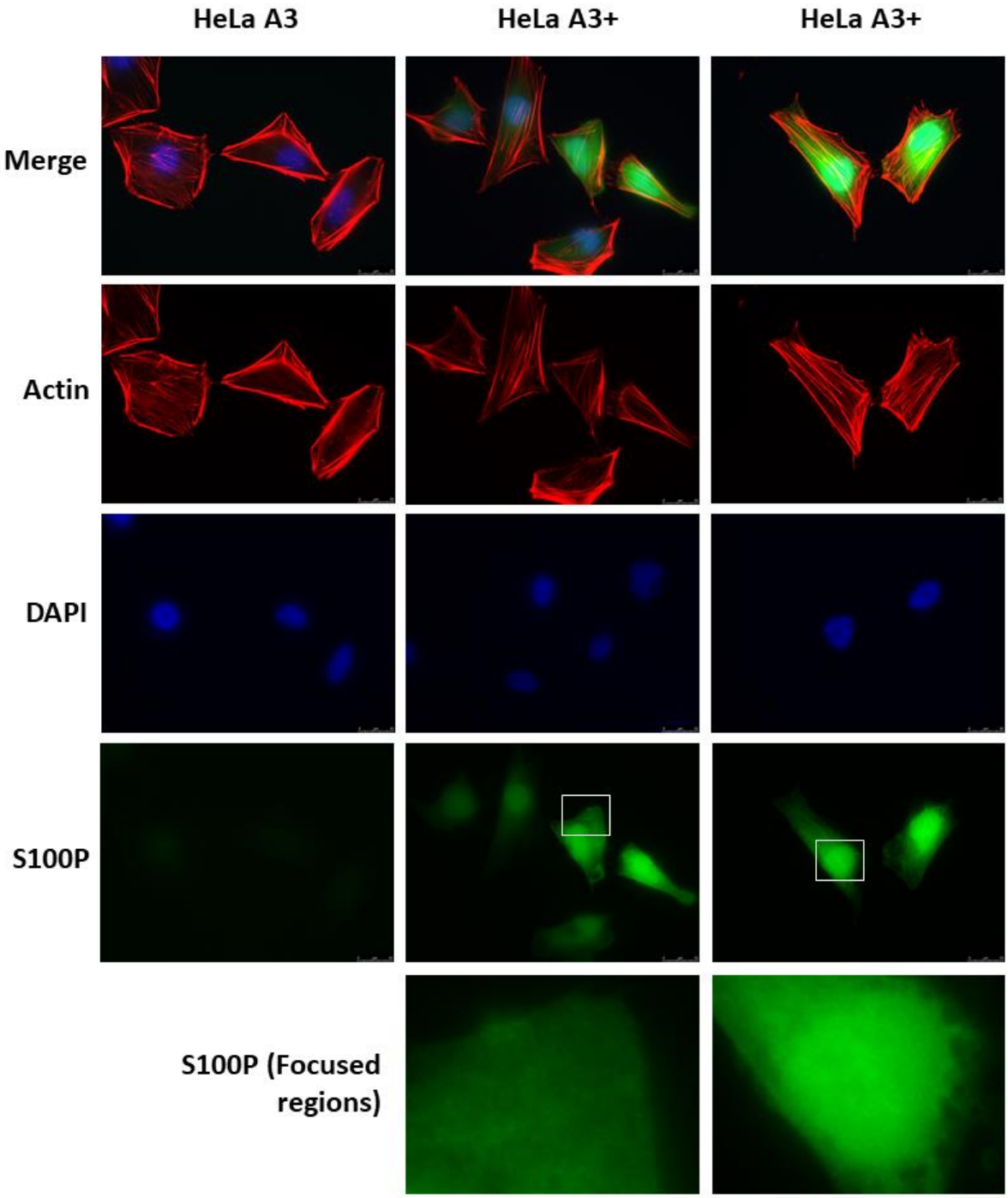
HeLa A3
HeLa A3+
HeLa A3+
Merge
Actin
DAPI
S100P
S100P (Focused regions)

B

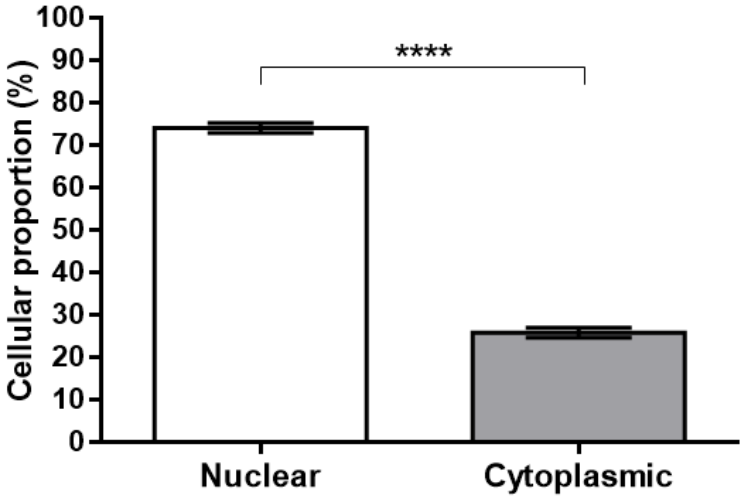

Figure 3.2.4: S100P is mainly nuclear in HeLa A3 cells when studied by immunostaining

A) Following induction with 1µg/ml doxycycline for 48 hours, non-induced HeLa cells and HeLa A3+ cells were seeded onto glass coverslips and grown for 24 hours prior to fixation with 4% (w/v) PFA, followed by permeabilization with 0.1% Triton X-100 in CB buffer. Cells were stained for S100P (green) using a FITC-conjugated secondary antibody, and actin (red) using rhodamine phalloidin at a concentration of 0.6µM. Focused regions of cytoplasmic and nuclear S100P staining are highlighted with a white box. Cells were mounted onto glass slides with DAPI and viewed using an epifluorescence microscope.

B) HeLa A3+ cells from Figure 3.2.4 panel A were stained with S100P and quantified to calculate the ratio of nuclear to cytoplasmic S100P using ImageJ. Data represents the mean ±SD from 3 independent replicates (Student's unpaired t-test, **** $p<0.0001$).

Whilst the S100P staining was found to be specific, we wanted to see how expression and localisation would vary between cell lines and in relation to their different levels of S100P.

In this view, one cell line that endogenously expresses S100P (JEG-3) was compared against HeLa A3+ cells at a variety of different time points following induction of S100P expression, including non-induced cells as a negative control. Cells were stained for S100P as previously (see Table 2.2.8 for antibody dilutions), as well as for actin and DAPI to visualise the cellular cytoskeleton and nuclei respectively before viewing with an epifluorescence microscope (Figure 3.2.5).

The resulting S100P staining showed similar distributions of S100P between all cell lines; both JEG-3 and induced HeLa A3 cells showed a high proportion of S100P within the nuclear region, and a diffuse presence of S100P within the cytoplasm. As expected, the non-induced HeLa A3 cells (HeLa A3-) showed no signal for S100P.

The S100P images from each cell line were further analysed to quantify the respective level of S100P in relation to their expression. This was performed as previously, using ImageJ to calculate the integrated density of a selected region of interest encompassing the stained area for multiple cells. The resulting quantification demonstrated that JEG-3 cells had a lower intensity of S100P staining; this is in agreement with previous data acquired by western blot, in which JEG-3 express on average 30% less S100P than HeLa A3+ cells (see figure 3.2.1). However, HeLa A3+ cells induced for 24 hours demonstrated a 2.8% increase in fluorescence intensity than HeLa A3+ cells induced for 96 hours; an unexpected increase that was not deemed statistically significant ($p=0.994$). This data suggests that intensity of S100P staining between HeLa A3+ cells induced with 1µg/ml doxycycline for either 24 hours or 96 hours are almost equal, as their respective increases in fluorescence when compared to JEG-3 are 48% and 45%. This is in direct contrast with previously generated data that showcases an almost 4-fold increase in S100P expression between HeLa A3+ samples induced for 24 and 96 hours respectively (Figure 3.2.2). A 4-fold increase in fluorescence intensity between HeLa A3+ cells induced for 24 and 96 hours is not detected when immunostaining for S100P.

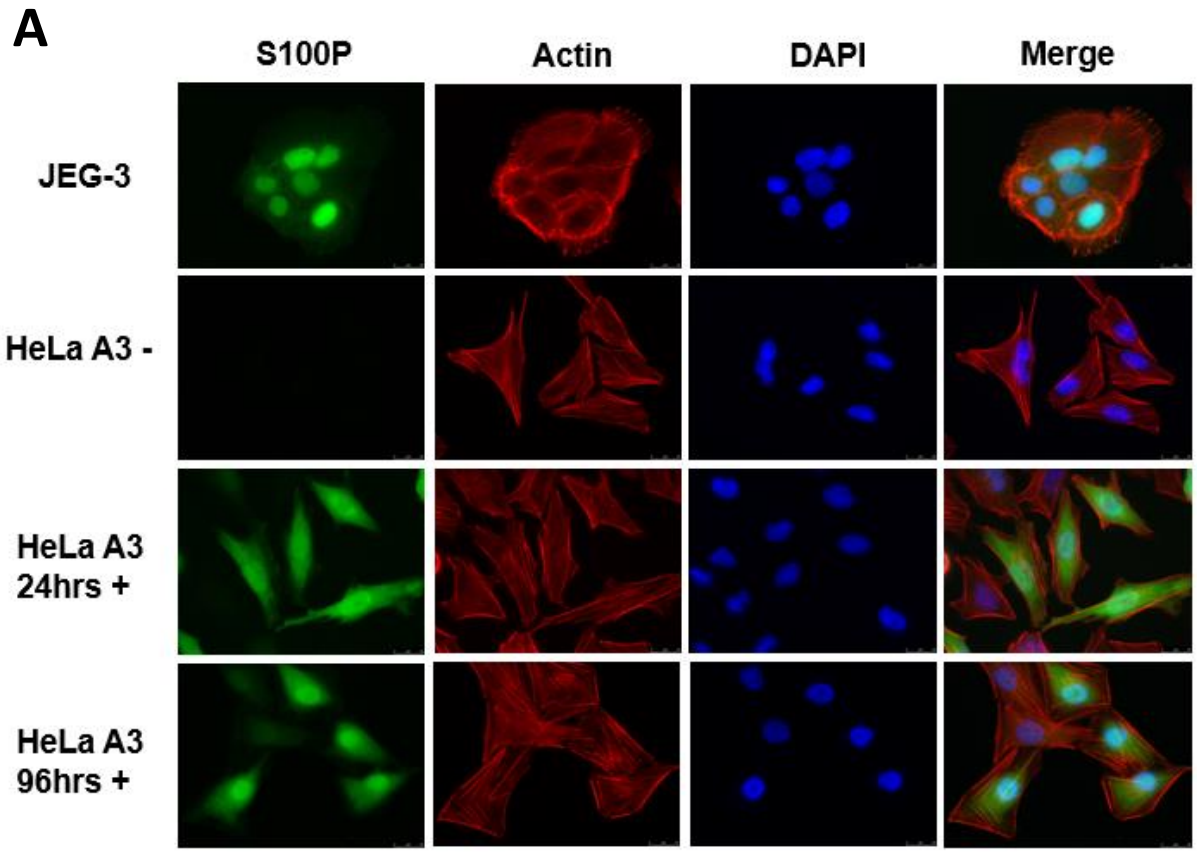
A
S100P
Actin
DAPI
Merge
JEG-3
HeLa A3 -
HeLa A3 24hrs +
HeLa A3 96hrs +

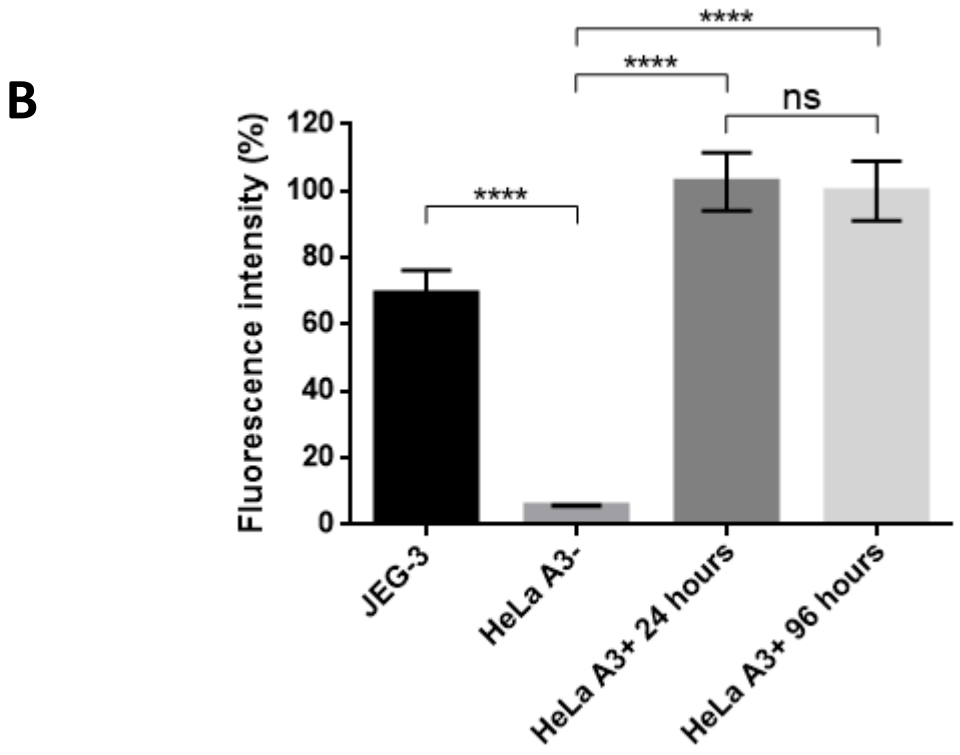
B
****
****
ns
****
Fluorescence intensity (%)
120
100
80
60
40
20
0
JEG-3
HeLa A3-
HeLa A3+ 24 hours
HeLa A3+ 96 hours

Figure 3.2.5: S100P fluorescence intensity in HeLa A3 cells induced for 24 or 96 hours are almost equivalent

A) JEG-3 and HeLa A3+ cells induced with doxycycline for 24 or 96 hours were seeded onto glass coverslips and grown for 24 hours prior to fixation, permeabilization, and staining for S100P and actin. Cells were mounted onto glass slides with DAPI and viewed using an epifluorescence microscope. Non-induced HeLa A3 cells were used as a negative control for S100P.

B) Cells stained with S100P were quantified to calculate fluorescence intensity using ImageJ. HeLa A3+ 96 hours sample was set to 100% as a positive control, with each sample being a percentage of the positive control. Data represents the mean ±SD from 3 independent replicates (one-way ANOVA, **** $p<0.0001$).

To confirm the discrepancy between the immunofluorescence intensity data and the initial western blot work, cell lysates were taken concurrently from JEG-3 cells and HeLa A3+ cells at 24 hour and 96-hour time points following induction of S100P expression with 1µg/ml doxycycline. Lysates were separated on a 16% (w/v) SDS-PAGE, alongside a non-induced HeLa A3 negative control, followed by western blotting for tubulin and S100P to analyse S100P levels (Figure 3.2.6). Quantification of the band intensity achieved for both S100P and tubulin was carried out using Image Studio Lite.

Western blotting for S100P demonstrated once again that JEG-3 cells express a lower level of S100P than induced HeLa A3 cells, with HeLa A3+ cells induced for 24 hours demonstrating a 2.5-fold increase in S100P expression over JEG-3 cells. No signal for S100P was obtained in HeLa A3 cells that were not induced with doxycycline.

Following induction over a 4-day time course, a higher level of S100P was seen in HeLa A3 cells induced for 96 hours than in cells induced for 24 hours, with the HeLa A3+ lysates induced for 96 hours demonstrating a 3-fold increase in S100P expression compared with the 24 hours counterpart. This is in line with previous western blot data (see figure 3.2.2), but contrasts to immunostaining of HeLa A3+ cells presented in figure 3.2.5, in which S100P levels in cells induced for both 24 hours and 96 hours are almost equivalent. These results highlight a degree of unspecificity and non-linearity when staining cells for S100P using indirect immunofluorescence, when compared with western blotting.

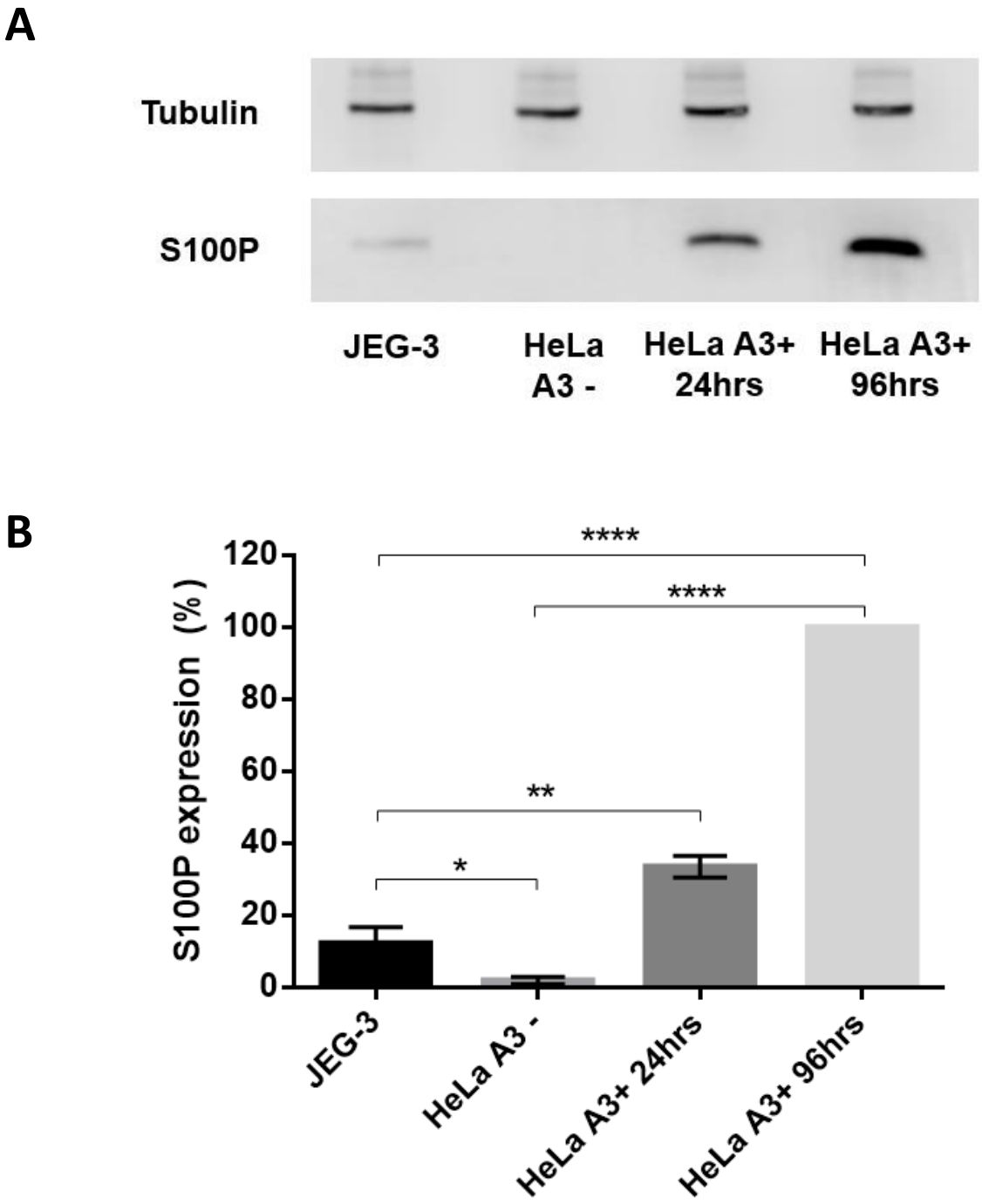

Figure 3.2.6 Western blotting for S100P does not correlate with S100P immunostaining

A) JEG-3 and HeLa A3+ cells lysates induced with 1µg/ml doxycycline for 24 or 96 hours were collected before running samples on SDS-PAGE and western blotting for S100P. Non-induced HeLa A3 cells were used as a negative control for S100P.

B) S100P expression in cell lysates from JEG-3, HeLa A3-, HeLa A3+ 24 hours and HeLa A3+ 96 hours was quantified using ImageJ. Levels of S100P were normalised to tubulin. The HeLa A3+ 96 hours was set to 100% as a positive control, with each sample being a percentage of the positive control. Data represents the mean ±SD from 3 independent replicates (one-way ANOVA, * $p<0.05$, ** $p<0.01$, *** $p<0.001$, **** $p<0.0001$)

3.2.3 Fractionation of cell lines show cytoplasmic and membrane S100P localisation

Cellular distribution of S100P suggests that it is majoritarily found in the nuclear region when studied by immunostaining (see Chapter 3.1 Introduction and figure 3.2.5). Having highlighted a discrepancy between its levels when using immunostaining compared to western blot analysis, we next sought to gain further understanding about its specific physiological subcellular localisation in various cell lines, using biochemical subcellular fractionation. Cell lysates were passed through a Dounce homogeniser, followed by the separation of cellular compartments by differential centrifugation. This technique is possible as the cellular compartments differ in both size and density. The fractions of particular interest were the nuclear fraction and the fraction containing cytoplasm and membrane. Following fractionation of cell lines, the cell fractions were subjected to 16% (w/v) SDS-PAGE prior to western blot analysis for S100P, as well as for nuclear and cytoplasmic protein markers (lamin A/C and HDAC2, and tubulin, respectively) (Barbetti *et al.* 2014; Vanli, Cuesta-Marban and Widmann, 2017; Flather *et al.* 2018). These protein markers make it possible to assess the level of contamination within each fraction (Figure 3.2.7).

Lamin A/C is a component of the nuclear envelope and should therefore not be present within the cytoplasm and membrane fractions. Several bands are detected by western blot in the nuclear fraction; a band at around 70kDa indicates the presence of lamin-A, with the second lower molecular weight band being attributed to lamin-C.

Tubulin is a major component of microtubules, cytoskeletal filaments that form the structure of the cell. Microtubules are formed from the association of α and β tubulin monomers, and form part of the cell cytoskeleton. α-tubulin was utilised as a cytoplasmic marker protein, since α-tubulin is not present within the nucleus and has only been found in the cytoplasm (Akoumianaki *et al.* 2009).

Another nuclear marker, HDAC2, was utilised as it is a small, soluble protein, and not a structural marker. HDAC2 is a soluble enzyme that is responsible for the removal of acetyl groups on histones. HDAC2 has mostly been found to be localised to the nucleus, but has also been documented to be present within the cytoplasm (Liu *et al.* 2014). The HDAC2 protein was used to demonstrate that soluble nuclear proteins are retained in nuclei during the process of fractionation. Evidence of high levels of HDAC2 in the cytoplasm and membrane fractions would demonstrate potential damage to nuclear structures and invalidate the results.

Quantification of the band intensity achieved by western blotting for all proteins (lamin A/C, tubulin, HDAC2 and S100P) was carried out using Image Studio Lite.

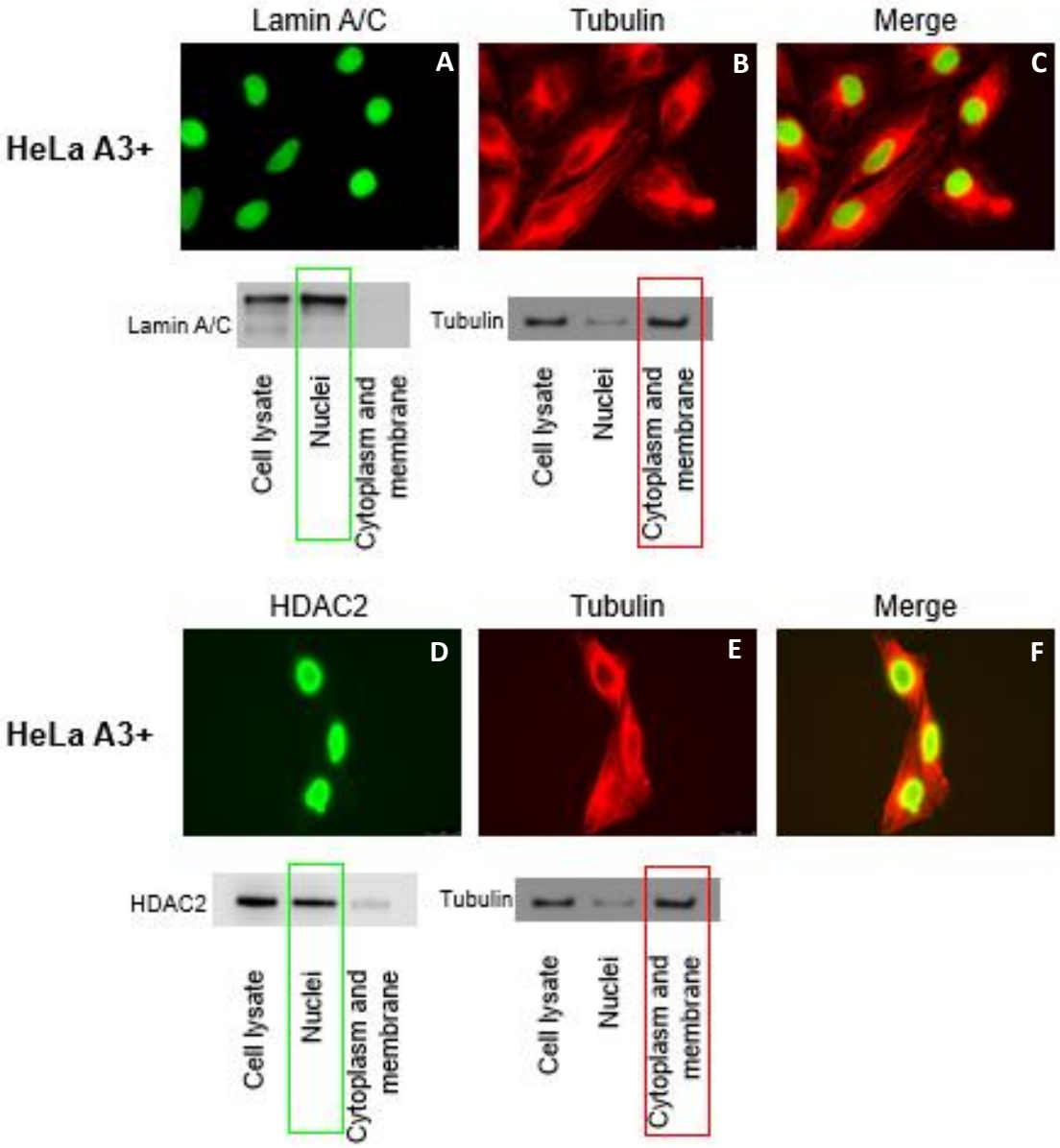

Figure 3.2.7: Visualisation of nuclear marker proteins lamin A/C and HDAC2, and cytoplasmic marker protein tubulin by indirect immunofluorescence and western blotting

HeLa A3+ cells were fixed as above (see figure 3.3.4) and stained for nuclear envelope protein lamin A/C (A), soluble nuclear marker protein HDAC2 (D), and cytoplasmic marker protein tubulin (B). Example western blots are shown for each of the protein markers depicting the expected localisation of each protein, allowing for assessment of potential contamination within each isolated fraction.

Western blotting for lamin A/C (Figure 3.2.8a) in JEG-3, BeWo, MDA-MB-231, HeLa A3 and COS-7 s10 cell lines demonstrated that nuclei were properly isolated with negligible traces in other cell compartments.

The JEG-3 cell line had 97.31% (±2.11 SD) of the total cellular proportion of lamin A/C within the nuclear fraction with the remaining 2.69% found within the cytoplasm and membrane fraction. The BeWo cell line by comparison contained 89.87% (±9.57 SD) of the total cellular proportion of lamin A/C within the nuclear fraction, the HeLa A3+ nuclear fraction contained 99.33% (±0.41 SD) of the total cellular proportion of lamin A/C, and the nuclear fraction isolated from the COS-7 s10+ cell line contained 98.55% (±0.79 SD) of the total lamin A/C. The MDA-MB-231 nuclear fraction contained 92.76% (±5.62 SD) of the total cellular lamin A/C.

Western blotting for HDAC2 in the five cell lines showed almost solely a nuclear localisation, with JEG-3 cells containing 91.93% (±7.52 SD) of the total cellular proportion of HDAC2 in the nuclear fraction. BeWo and HeLa A3+ cell lines were shown to contain a similar percentage of total HDAC2 within their nuclear fractions (92.08%, ±10.79 SD and 93.96%, ±10 SD respectively). The nuclear fraction isolated from COS-7 s10+ cells contained 97.47% (±2.3 SD) of the total cellular HDAC2, and the MDA-MB-231 cell line contained 96.61% of the total cellular HDAC2 in its nuclear fraction.

In these cell lines, tubulin was present at high levels within the total cell lysate and the cytoplasm and membrane fraction. There are small traces of tubulin detected within the nuclear fraction of the majority of cell lines tested, indicating a small level of cytoplasmic contamination within the nuclear fraction. This is somewhat to be expected due to the high titre of the tubulin antibody used within these studies. The cytoplasmic fraction isolated from JEG-3 cells contained on average 94.71% (±3.99 SD) of the total cellular tubulin, similarly to the COS-7 s10+ cytoplasmic fraction which contained on average 93.64% (±5.47 SD) of the total cellular proportion of tubulin. The BeWo cytoplasmic fraction on average contained a lower total proportion of tubulin (87.35%, ±10.75 SD), whereas the HeLa A3+ and MDA-MB-231 cell lines contained 75.78% (±8.75 SD) and 75.98% (±3.38 SD) of the total cellular proportion of tubulin within the cytoplasmic fractions respectively.

Having confirmed the suitable fractionation of the different cellular compartments through use of marker proteins lamin A/C and tubulin, it was possible to analyse the levels of S100P within each cell fraction by the same methodology. Western blots for S100P across all cell lines showed a strong signal within both the total cell lysate and the cytoplasm and membrane fractions. However, only barely detectable traces of S100P were detected in the nuclear fraction of any cell line tested. It was possible to confirm that this minute level of S100P was due to the cytoplasmic contamination of the nuclear fraction using densitometry analysis (Figure 3.2.8.b). The JEG-3 cell line on average contained 96.81%

(±2.11 SD) of the total cellular proportion of S100P within the cytoplasmic fraction, with the remaining 3.2% contained within the nuclear fraction. Total S100P within the BeWo cell line was found to be 96.2% cytoplasmic (±1.93 SD) and 3.79% nuclear. The cytoplasmic fraction isolated from HeLa A3+ cells contained 98.73% (±0.99 SD) of the total cellular pool of S100P, and the COS-7 s10+ cell line contained on average 97.33% (±3.06 SD) of the total proportion of S100P within the cytoplasmic fraction. Cytoplasmic fractions isolated from MDA-MB-231 cells contained on average 93.25% (±4.98 SD) of the total cellular proportion of S100P.

Densitometry allows for the quantification of all proteins of interest within each fraction; therefore, following this analysis, it was established that the level of tubulin within the nuclear fractions was in fact greater than the level of S100P within the nuclear fractions. This suggests that then small levels of S100P that are sometimes present within the nuclear fractions are in fact due to cytoplasmic contamination of the nuclear fraction. Regardless, S100P is present at high levels (between 93-99% of the total pool of S100P) in the cytoplasm and membrane fraction under these conditions.

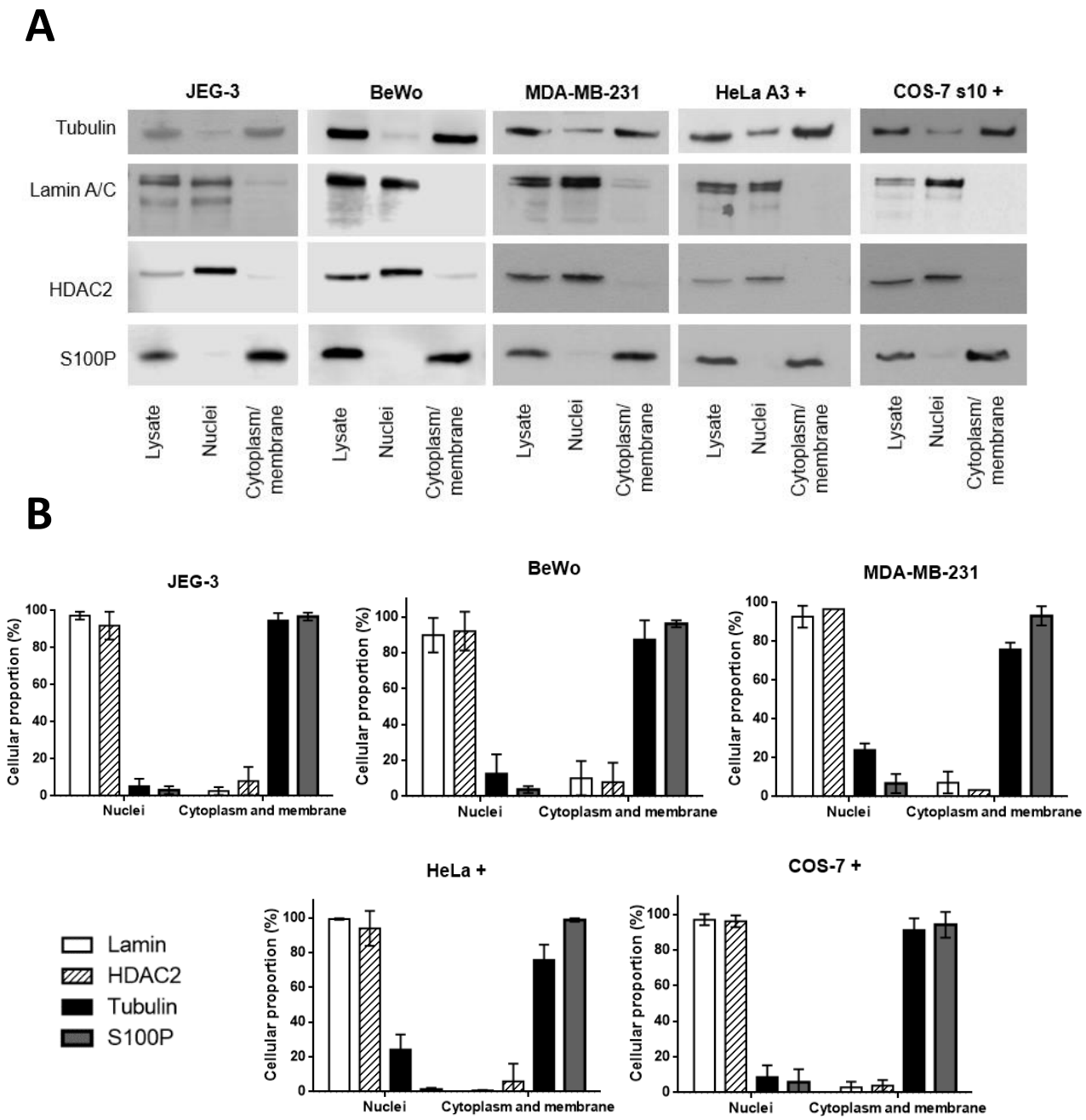

Figure 3.2.8: S100P is localised to the cytoplasm/membrane fraction of cell lines.

A) Lysed cells (JEG-3, BeWo, MDA-MB-231, HeLa A3+ and COS-7 s10+) were homogenised using a Dounce homogeniser before differential centrifugation. Samples were run on 16% (w/v) SDS-PAGE followed by western blotting to detect S100P, cytoplasmic marker tubulin, and nuclear markers lamin A/C and HDAC2 within each fraction. Fractions were isolated from cell lines that endogenously express S100P or cell lines that have been engineered to express S100P after induction of expression using doxycycline.

B) The cellular proportion of the various proteins were quantified by densitometry using Image Studio Lite. Data represents the mean ±SD from at least 3 independent replicates.

Western blotting confirms that nuclear marker proteins lamin A/C and HDAC2 are present within the nuclear fraction, but not that the nuclei themselves are still intact and undamaged. To confirm that the isolated nuclei were intact, a small sample of the nuclear fraction was mixed with DAPI for visualisation under the Leica DMI400B epifluorescence microscope (Figure 3.2.9). Imaging confirmed that the nuclei isolated from various cell lines were intact, further demonstrating that S100P was not leaked out due to their destruction.

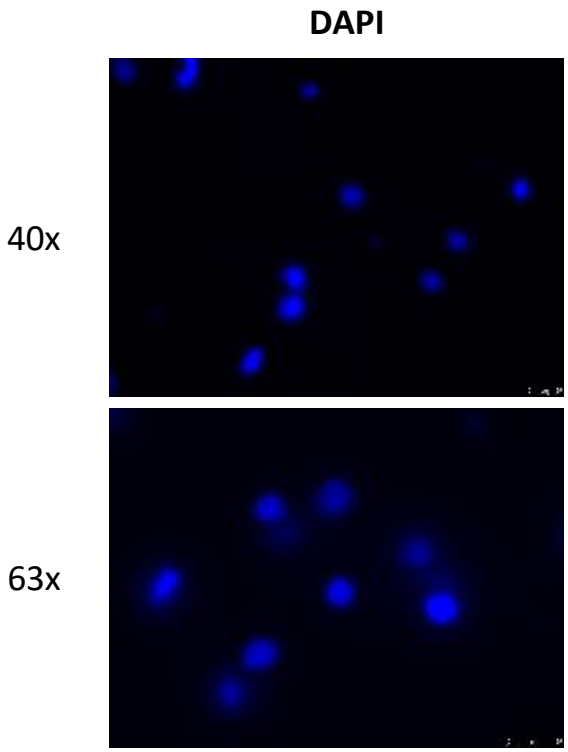

Figure 3.2.9: Subcellular fractionation using a Dounce homogeniser allows for isolation of intact nuclei from cell lines

Isolated nuclei from COS-7 cells were stained with DAPI before imaging at 40x and 63x magnifications.

To verify whether levels of stable and long term S100P expression had any effect on S100P localisation, we used different S100P stably expressing HTR8 clones. The HTR8 clones were also fractionated using a Dounce homogeniser (Figure 3.2.10). Cell fractions were separated on a 16% (w/v) SDS-PAGE, followed by western blotting for S100P and the various marker proteins. Quantification of the band intensity was carried out using Image Studio Lite.

As before, detection of lamin A/C in all HTR8 cell clones illustrated the correct isolation of all nuclear fractions. The control cell line, SGB16 Clone 3, contained 96.27% (±3.91 SD) of the total proportion of lamin A/C in the nuclear fraction, with the remaining 3.73% found in the cytoplasmic fraction, The nuclear fraction isolated from SGB217 Clone 3 contained 98.84% (±1.36 SD) of total cellular lamin A/C, and the nuclear fraction from SGB217 Clone 5 contained 99.36% (±0.25 SD) of the total cellular proportion of lamin A/C. The clone 7 nuclear fraction contained 99.59% (±0.41 SD) of the total cellular lamin A/C, and clones 9 and 10 contained 98.16% (±1.65 SD) and 98.42% (± 0.36 SD) of the total cellular lamin A/C in their nuclear fractions respectively.

Further confirmation of the isolation of the nuclear fractions was given by detection of the soluble nuclear protein, HDAC2, in each cell fraction isolated from the HTR8 clones. The control SGB16 Clone 3 contained 98.07% of the total cellular proportion HDAC2, with the remainder found in the cytoplasmic fraction. Similar results were seen for the rest of the HTR8 clones, with the nuclear fractions of SGB217 Clone 3 and Clone 5 containing 99.82% and 87.2% of the total cellular proportion of HDAC2 respectively. The nuclear fractions of SGB217 Clones 7, 9 and 10 contained 98.32%, 99.79% and 72.36% of the total cellular HDAC2, once again confirming that the nuclear fractions isolated from these cell lines demonstrate minimal leakage of nuclear proteins and that cell nuclei have been correctly isolated.

Isolation of cytoplasmic and membrane fractions was confirmed by western blotting for tubulin, a cytoplasmic marker protein. The cytoplasmic fraction of the control cell line SGB16 Clone 3 contained 74.31% of the total cellular tubulin (±3.78 SD), with the remaining 25.69% detected within the nuclear fraction. The cytoplasmic fraction of SGB217 Clones 3 and 5 contained 76.7% (±22.42 SD) and 81.69% (±10.24 SD) of the total cellular proportion of tubulin respectively, similar to SGB217 Clones 7, 9 and 10 which contained 80.39% (± 4.09 SD), 73.85% (±4.88 SD) and 75.96% (±5.89 SD) of the total cellular proportion of tubulin respectively. The level of cytoplasmic contamination in the nuclear fractions of the HTR8 clones, as detected by the tubulin antibody, is to be expected due to the high titre of the tubulin antibody.

As expected, the non-S100P expressing cell line, SGB16 Clone 3, demonstrated no detectable S100P within any cell fraction. SGB217 Clone 3 contained 98.09% (±2.44 SD) of the total cellular S100P within

the cytoplasmic and membrane fraction, with the remaining 1.91% found in the nuclear fraction. The majority of S100P was found in the cytoplasmic and membrane fraction of SGB217 Clone 5 (99.25%), with 0.75% (±0.59 SD) being detected in the nuclear fraction. The cytoplasm and membrane fraction of Clone 7 contained 93.67% of the total cellular proportion of S100P, and the nuclear fraction contained on average 6.33% (±3.93 SD) of the total cellular proportion of S100P. The cytoplasm and membrane fractions of clones 9 and 10 contained 96.27% (±4.21 SD) and 92.9% (±4.53 SD) of the total cellular proportion of S100P respectively. In a similar fashion to previous fractionation experiments, these results demonstrate that S100P is not present in the nucleus of any of the HTR8 clones, regardless of S100P expression levels. This is in line with results obtained using other S100P-expressing cell lines, and suggests that cellular S100P level does not have an effect on its localisation within cells.

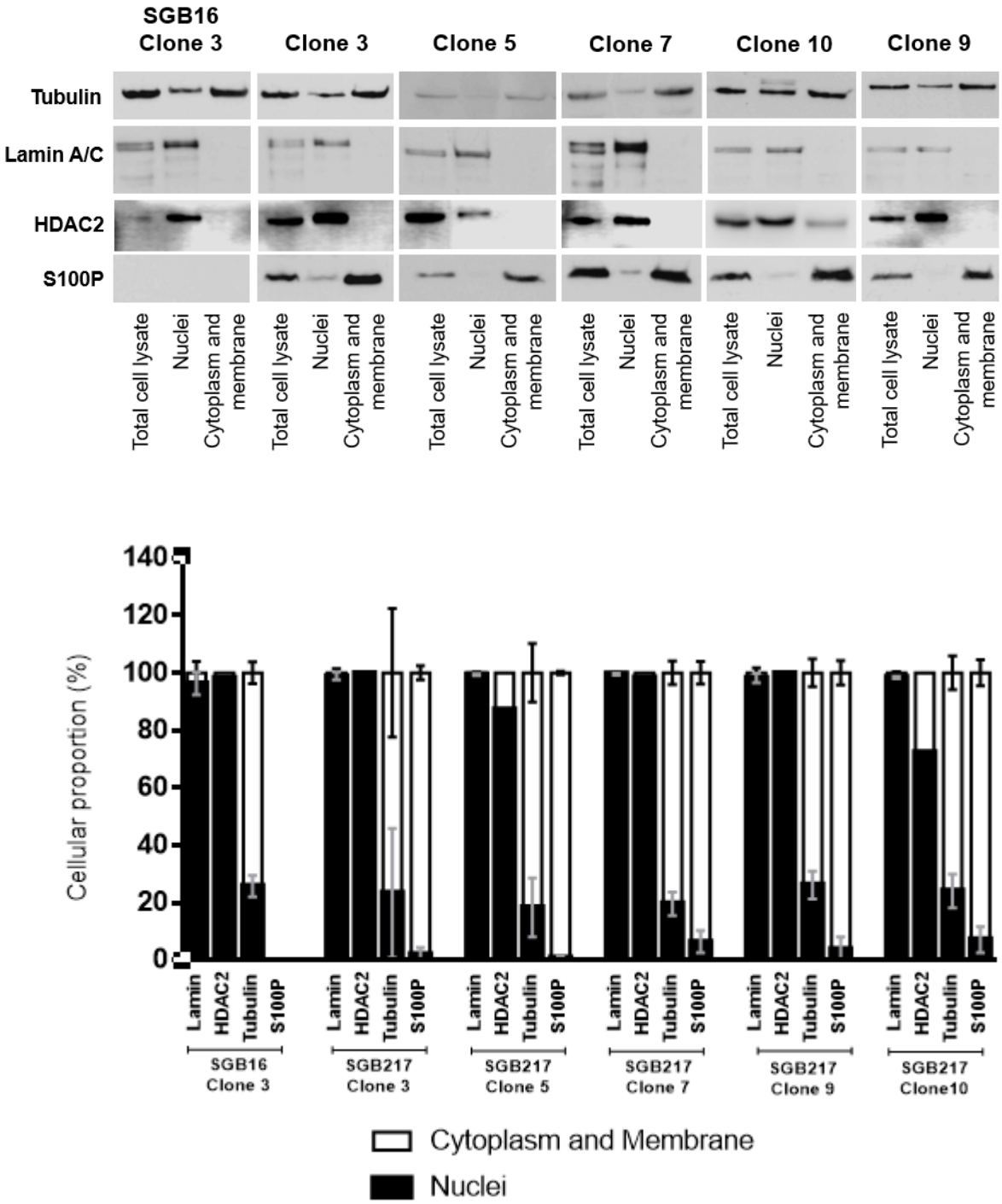

Figure 3.2.10: S100P is localised to the cytoplasm/membrane fraction of stably S100P-expressing HTR8 clones

A) Lysed cells from each HTR8 clone cell line were passed through a Dounce homogeniser before differential centrifugation. Cell fractions were isolated from HTR8 clones transfected with plasmid SGB217 or control plasmid SGB16. Samples were run on SDS-PAGE before Western blotting to detect S100P, cytoplasmic marker tubulin, and nuclear markers lamin A/C and HDAC2 within each cell fraction.

B) The cellular proportion of the various proteins were quantified by densitometry using Image Studio Lite. Data represents the mean ±SD from at least 3 independent replicates.

3.2.4 Differential fractionation methods do not alter S100P localisation

To assess the specificity of the Dounce homogeniser-based fractionation assay, modifications to the existing assay and an alternative fractionation assay were employed. Calcium is a requirement for S100P function, and the absence of calcium in the buffers could have the propensity to interfere with S100P function, and therefore its localisation as a consequence. In addition, the fractionation buffer contained EDTA and EGTA; these reagents are calcium chelators and would therefore sequester free calcium within the sample. To this end, the Dounce homogeniser-based fractionation assay was altered to include a concentration of 5µM calcium chloride, and calcium chelators EDTA and EGTA were removed. 5µM was chosen as the desired concentration of calcium chloride to be used in this assay, as this value is fifty times greater than the concentration of free calcium inside the cell (Bagur and Hajnóczky 2017), and should therefore facilitate interactions between S100P and its target proteins that could affect its localisation.

Following these modifications, the assay was performed on JEG-3 and HeLa A3 cell lines prior to the separation of cell fractions on a 16% (w/v) SDS-PAGE and western blotting for S100P and the various protein markers (Figure 3.2.11, panel A). Quantification of the band intensity was characterised by Image Studio Lite (Figure 3.2.11, panel B).

As before, correct isolation of the cellular fractions was confirmed using the marker proteins lamin A/C, HDAC2 and tubulin. In untreated JEG-3 nuclear fractions, 97.4% (±1.74 SD) of the total cellular lamin A/C was detected, whilst 2.6% of total cellular lamin A/C was detected in the cytoplasm and membrane fraction. A similar level of lamin A/C was detected in cellular fractions of JEG-3 cells treated with 5µM calcium chloride; 91.4% (±5.22 SD) of total cellular lamin A/C was detected in the nuclear fraction, with the remainder being detected in the cytoplasm and membrane fraction. 95.64% of total cellular HDAC2, the soluble nuclear marker protein, was detected in the nuclear fraction of untreated JEG-3 cells, compared to 76.12% detected in the nuclear fraction of JEG-3 cells treated with 5µM calcium chloride. High levels of tubulin were detected in the cytoplasm and membrane fraction of both treated (93.16%, ±4.51 SD) and untreated JEG-3 cells (83.83%, ±8.45 SD), demonstrating minimal cytoplasmic contamination of the nuclear fractions. Densitometric analysis of S100P within each fraction was performed following detection of the required marker proteins. In untreated JEG-3 cells, 95.46% (±2.92 SD) of the total cellular S100P was detected within the cytoplasm and membrane fraction. Similarly, 94.89% (±2.24 SD) of the total cellular proportion of S100P was detected within the cytoplasm and membrane fraction of JEG-3 cells treated with 5µM calcium chloride.

Western blotting of induced HeLa cells was carried out as above. In untreated HeLa cells, the nuclear fraction contained on average 97.96% (±1.06 SD) of the total cellular lamin A/C, with the remainder

being detected in the cytoplasm and membrane fraction. The total cellular proportion of lamin A/C found in the nuclear fraction of induced HeLa cells treated with 5µM calcium chloride was 97.81% (±2.56 SD). Western blotting for the soluble nuclear marker, HDAC2, found that the nuclear fraction of untreated HeLa cells contained 88.94% of the total cellular proportion of HDAC2, whereas the 5µM calcium chloride-treated HeLa nuclear fraction contained 98.84% of total cellular HDAC2. The cytoplasmic fraction of untreated HeLa cells contained 78.15% (±18.07 SD) of the total cellular proportion of tubulin, the cytoplasmic marker protein, whilst the treated counterpart contained 74.28% (±16.22 SD) of total cellular tubulin. Western blotting of untreated HeLa cell fractions for S100P found that 95.79% (±1.85 SD) of total cellular S100P was detected in the cytoplasm and membrane fraction, with the remaining 4.21% detected within the nuclear fraction. Likewise, in the HeLa cell fractions treated with 5µM calcium chloride, 91.81% (±3.2 SD) of the total cellular S100P was detected within the cytoplasm and membrane fraction, compared to the 8.19% detected in the nuclear fraction.

This data suggests that regardless of the presence of calcium or its chelators, S100P is not found associated with the nuclear fraction and can only be found within the cytoplasm and membrane fractions of cells fractionated using this assay.

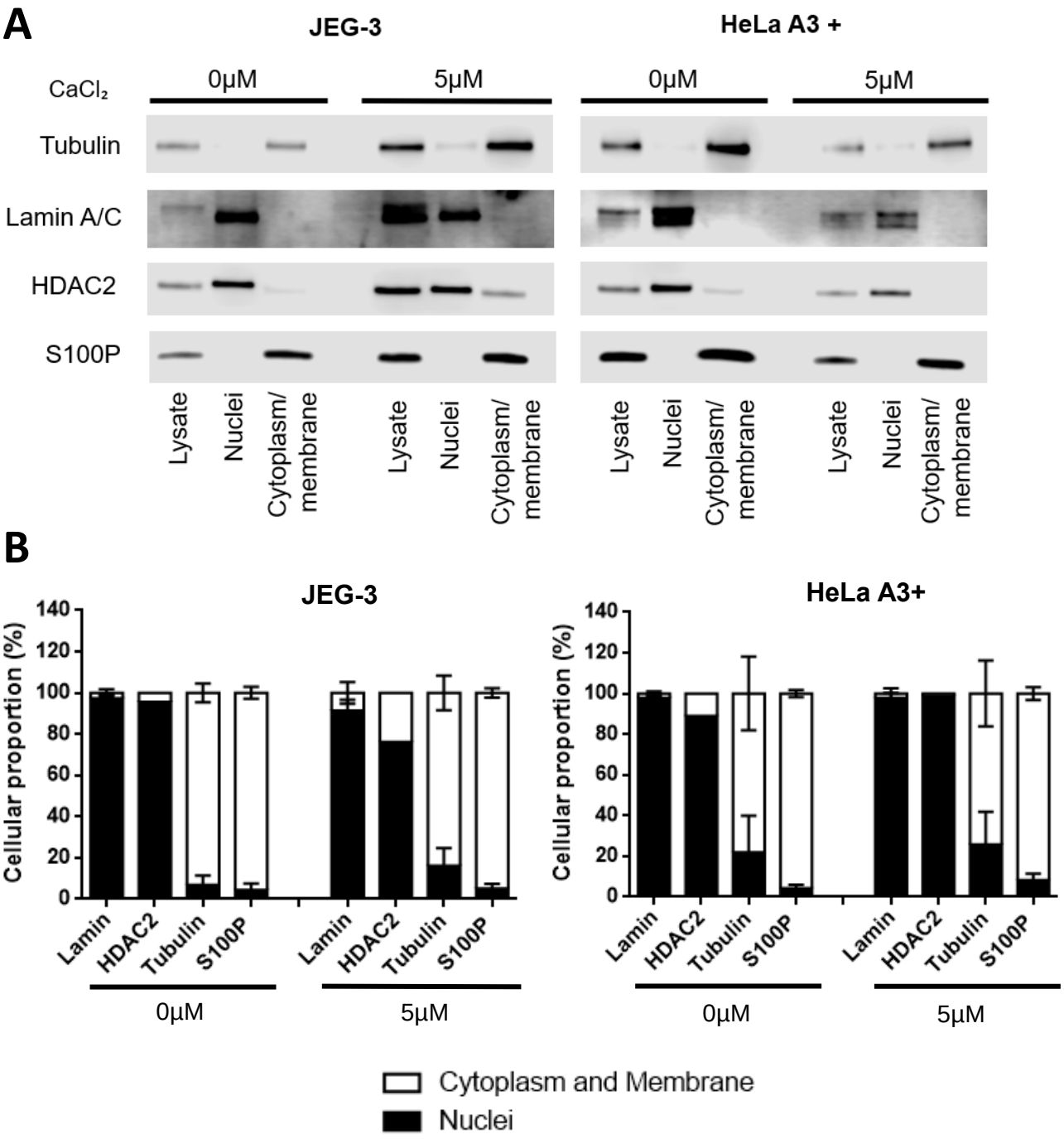

Figure 3.2.11: Addition of 5μM calcium chloride does not alter S100P subcellular localisation

A) Lysed cells from JEG-3 and HeLa A3+ cell lines were passed through a Dounce homogeniser with and without the addition of calcium chloride, before differential centrifugation. Samples were run on SDS-PAGE before western blotting was carried out to detect S100P, cytoplasmic marker tubulin, and nuclear markers lamin A/C and HDAC2 within each cell fraction.

B) The cellular proportion of the various proteins were quantified by densitometry using Image Studio Lite. Data represents the mean ±SD from at least 3 independent replicates.

Whilst the physical destruction of cells has been shown not to affect, microscopically, nuclear structure and organisation (Figure 3.2.9) or the correct localisation of the specific nuclear markers such as lamin A/C and HDAC2, and is therefore not thought to be responsible for the absence of S100P in the nuclear fraction, we sought to lyse cells and release the different compartments by utilising an alternative methodology, through use of a low concentration of the non-ionic detergent NP40 to lyse cell membranes instead. Cell fractions isolated using the detergent-based assay were collected and separated on a 16% (w/v) SDS-PAGE prior to western blotting (Figure 3.2.12, panel A). Quantification of the band intensity was carried out using Image Studio Lite (Figure 3.2.12, panel B).

As with the Dounce homogeniser-based fractionation assay, it was imperative to assess the purity of each isolated fraction by performing a western blot for cell compartment-specific marker proteins tubulin, lamin A/C and HDAC2 in addition to S100P. The western blot was performed alongside samples from Dounce homogeniser-based assays (henceforth referred to as manual fractionation) in order to compare each method to one.

Detergent-based fractionation of HeLa A3+ cells show an increased level of tubulin within the nuclear fraction compared to the manual fraction assay; nuclear tubulin was found to be 19.76% using manual fractionation, but showed an increased level of 37.86% in the detergent-based assay. The total cellular proportion of tubulin within the cytoplasmic fraction is 80.24% when using manual fractionation, whereas it is 62.14% whilst using the detergent-based fractionation assay. There does not appear to be much difference in the purity of the nuclear fraction between both assays, as both nuclear fractions achieved a high signal for lamin A/C (99.33% and 95.92% for manual and detergent-based assays respectively) and HDAC2 (98.06% and 97.43% for manual and detergent-based assays respectively), with little to no signal achieved in the cytoplasmic compartments. There is an increase in the intensity of S100P in the nuclear fraction of the detergent-based assay, from 0.91% of the total cellular proportion of S100P to 19.38% in the detergent-based assay. However, as with the manual fractionation assay, the higher level of tubulin within the nuclear fraction is most likely responsible for the increased nuclear S100P levels. Therefore, this experiment illustrates using two different assays generates the same result; that S100P is solely localised to the cytoplasm and membrane fractions and is not a part of the nucleus.

Both manual and detergent-based fractionation assays were also performed on the trophoblast cell line JEG-3 to assess if results obtained with HeLa A3+ cells were cell line specific. Cell fractions from both manual and detergent-based fractionation assays were separated on a 16% (w/v) SDS-PAGE gel prior to western blotting for cell compartment-specific marker proteins tubulin, lamin A/C and HDAC2, in addition to S100P (Figure 3.2.13).

In a slight departure from results obtained with the HeLa A3+ cell line, both fractionation assays resulted in a similar level of tubulin detected within the cytoplasm and membrane fraction; 92.46% (±1.08 SD) of total cellular tubulin was detected in the cytoplasm and membrane fraction of JEG-3 cells when using manual fractionation methods, compared to 96.26% (±2.77 SD) when using detergent-based fractionation.

Isolation of nuclear fractions from JEG-3 cells showed slight differences when utilising the two different fractionation methods. 83.5% of the total cellular lamin A/C (±5.36 SD) was detected in the nuclear fraction of manually fractionated JEG-3 cells, and 80.98% of total cellular lamin A/C (±11.71 SD) was detected in the nuclear fraction when using detergent-based fractionation. Similar levels of lamin A/C were detected in the nuclear fractions in both assays, suggesting appropriate separation of cellular components. Levels of the soluble nuclear marker, HDAC2 were also assessed. When utilising a manual fractionation method, 93.59% (±8.29 SD) of total cellular HDAC2 was detected within the nuclear fraction of JEG-3 cells. In contrast, 75.98% (±20.96 SD) of total cellular HDAC2 was detected in the nuclear fraction of JEG-3 cells fractionated using the detergent-based method.

Levels of S100P within each cell fraction were assessed by densitometry in order to assess differences in S100P localisation due to fractionation methods. Following manual fractionation, 93.88% (±5.4 SD) of total cellular S100P was detected within the cytoplasm and membrane fraction of JEG-3 cells, with the remainder being detected within the nuclear fraction. 96.89% (±3.71 SD) of total cellular S100P was detected in the cytoplasm and membrane fraction of JEG-3 cells fractionated using the detergent-based method. The level of S100P detected in the nuclear fraction using both fractionation methods is at a lower level than the percentage of total tubulin detected within the nuclear fractions. Both fractionation assays, in both HeLa A3+ and JEG-3 cell lines, demonstrate the cytoplasmic and membrane localisation of the S100P protein, and illustrate the lack of its presence within isolated nuclear fractions.

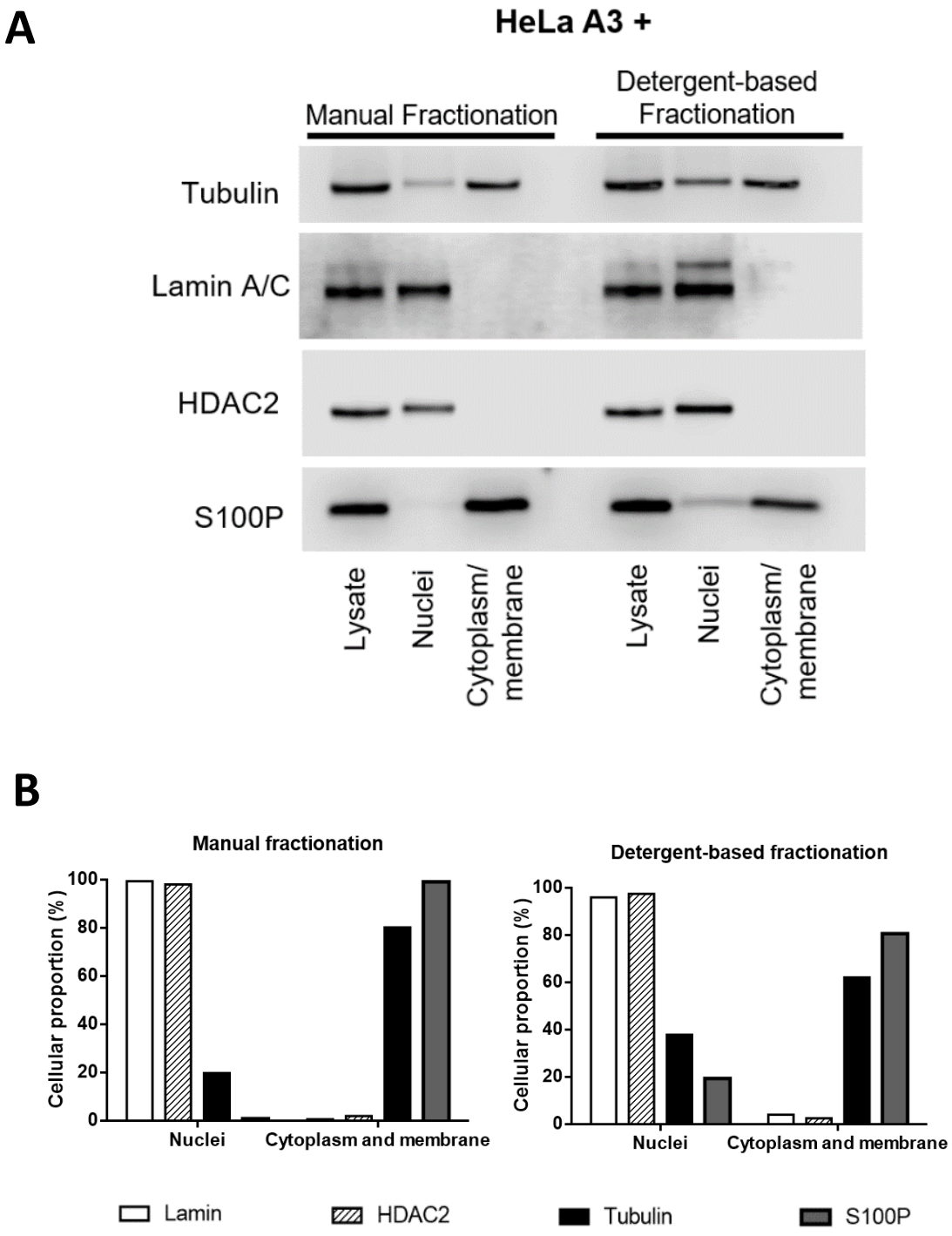

Figure 3.2.12: Two different subcellular fractionation assays show S100P is localised to the cytoplasm and membrane fraction in HeLa A3+ cells

A) Cell fractions were isolated from HeLa A3+ cells using two different assays (Dounce homogenisation, referred to as "manual fractionation", and fractionation using NP-40 detergent, referred to as "detergent-based fractionation"). Samples were run on 16% (w/v) SDS-PAGE before western blotting to detect S100P, cytoplasmic marker tubulin, and nuclear markers lamin A/C and HDAC2 within each cell fraction.

B) The cellular proportion of the various proteins were quantified by densitometry using Image Studio Lite.

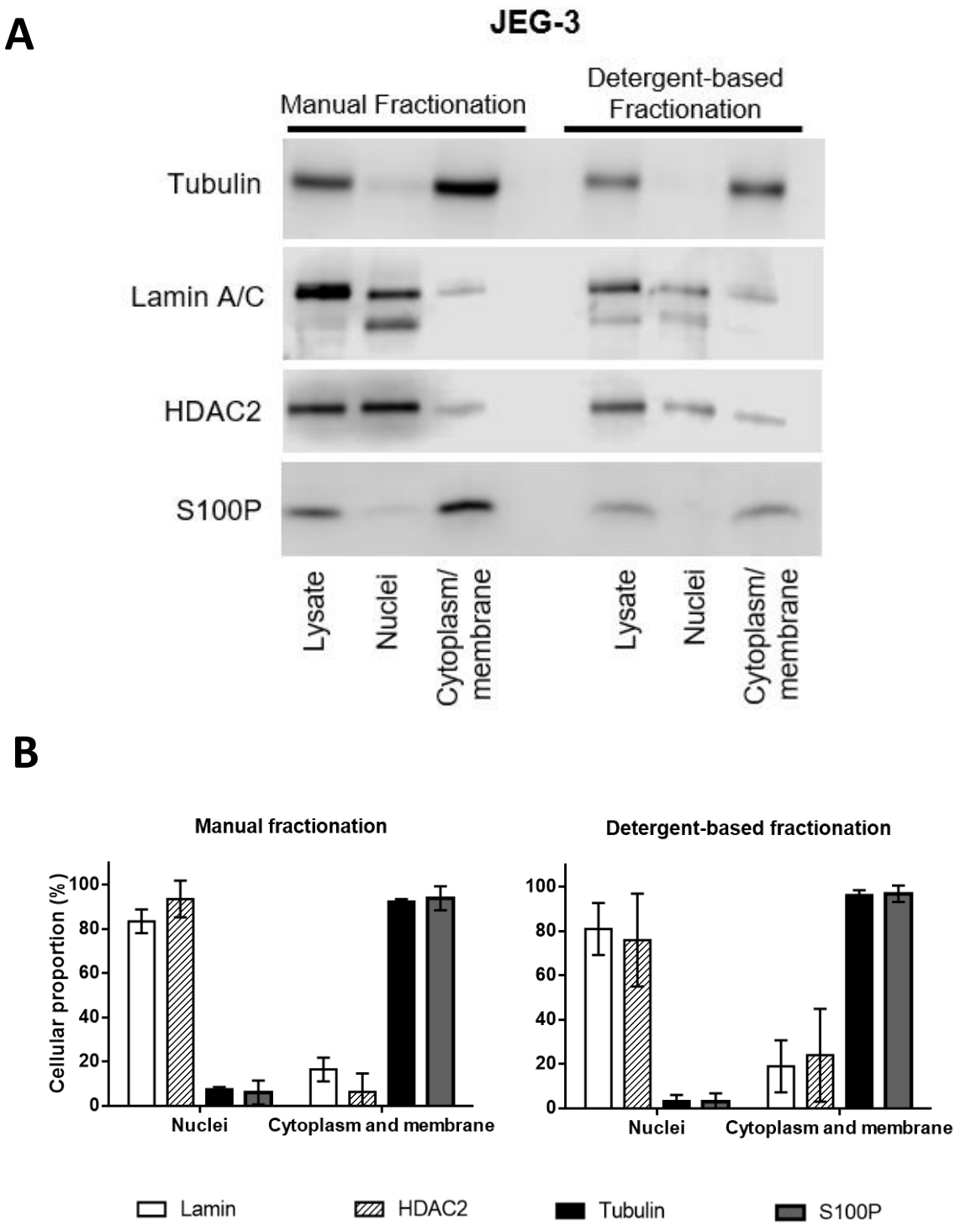

Figure 3.2.13: Two different subcellular fractionation assays show S100P is localised to the cytoplasm and membrane fraction in JEG-3 cells

A) Cell fractions were isolated from JEG-3 cells using two different assays (Dounce homogenisation, referred to as "manual fractionation", and fractionation using NP-40 detergent, referred to as "detergent-based fractionation"). Samples were run on 16% (w/v) SDS-PAGE before western blotting to detect S100P, cytoplasmic marker tubulin, and nuclear markers lamin A/C and HDAC2 within each cell fraction.

B) The cellular proportion of the various proteins were quantified by densitometry using Image Studio Lite.

3.2.5 Addition of a YFP tag to S100P disturbs its localisation

Whilst we have shown that there is a poor correlation between S100P expression levels using western blotting and immunostaining, other studies have shown nuclear localisation of S100P using GFP-tagging as a reporter system (Rehbein *et al.* 2008 and Koltzscher *et al.* 2003). In order to elucidate if adding a fluorescent tag to S100P can affect its subcellular localisation, HeLa A3 cells, already expressing S100P under the control of an inducible system, were transiently transfected with a plasmid containing YFP-S100P (SGB214), where S100P expression is driven by the rtTA inducible promoting element. HeLa A3+ cells were seeded onto glass coverslips and fixed using 4% PFA to assess transfection efficiency and YFP-S100P localisation (Figure 3.2.14). Upon the addition of doxycycline, induction of both the wild type (WT) S100P as well as that of the YFP-fusion were obtained.

Immunostaining of HeLa A3+ cells transfected with the YFP-S100P-containing plasmid demonstrated a somewhat similar distribution to that of WT S100P; high intensity S100P staining was seen in the nuclear and perinuclear regions of a large number of cells, with diffuse staining throughout the cell cytoplasm.

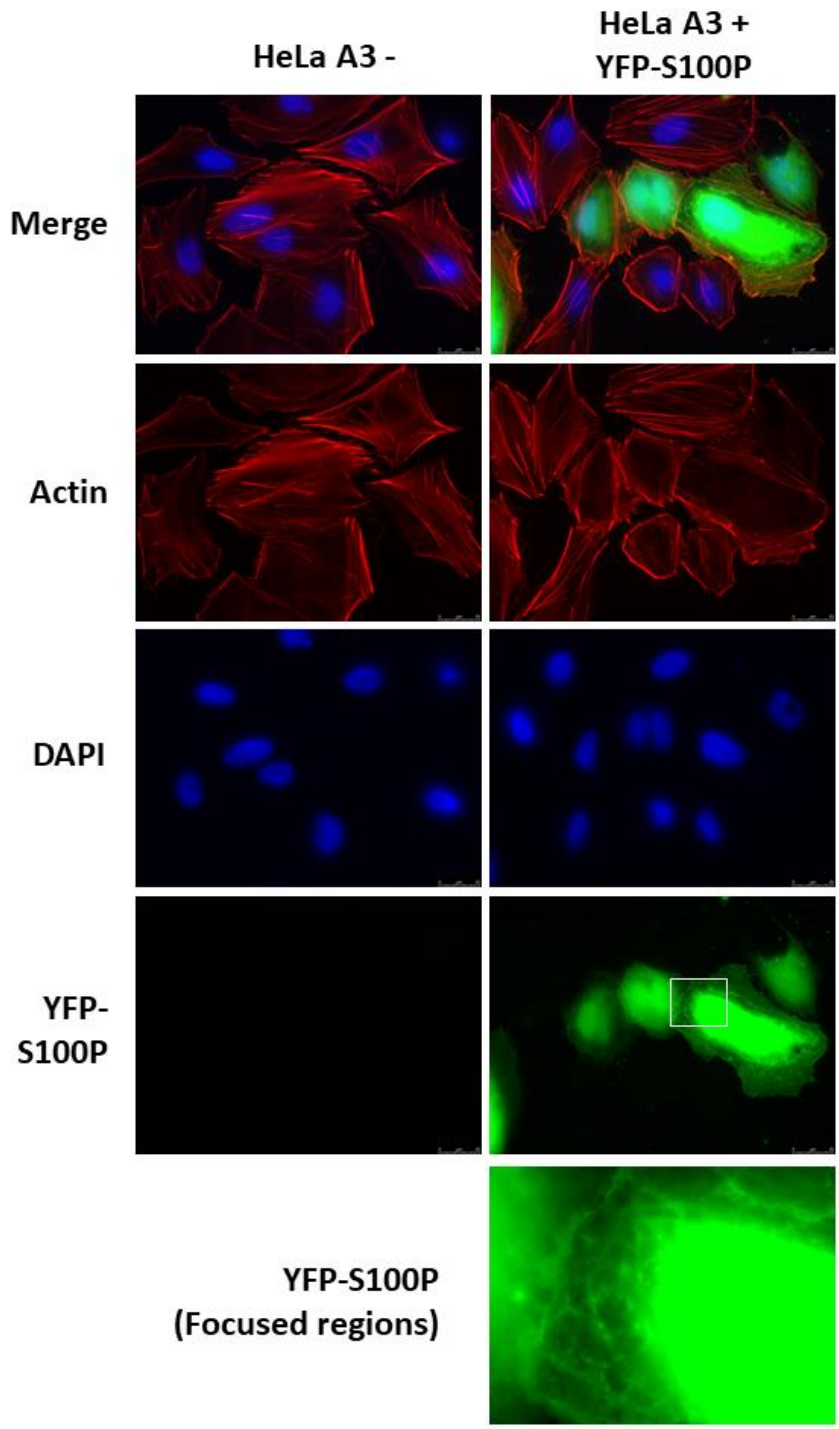

Figure 3.2.14: YFP-S100P demonstrates a mainly nuclear localisation within transiently transfected HeLa A3+ cells when studied by immunostaining

A) HeLa A3+ cells were transfected with plasmid SGB214, containing YFP-S100P, using Lipofectamine 3000 prior to seeding onto glass coverslips. Cells were left to grow for 24 hours prior to fixation with 4% PFA. Cells were visualised using an epifluorescence microscope.

Following visual confirmation that YFP-S100P has been transfected into HeLa A3+ cells, it was necessary to assess if tagging the N-terminus of S100P with YFP could alter its localisation within cells.

To this end, non-induced HeLa cells (HeLa A3-), non-induced HeLa cells transfected with the YFP-S100P containing plasmid (HeLa A3- +SGB214), induced HeLa cells (HeLa A3+) and induced HeLa cells transfected with the YFP-S100P containing plasmid (HeLa A3+ +SGB214), were fractionated with a Dounce homogeniser and separated by 16% (w/v) SDS-PAGE before western blotting for S100P and other marker proteins (Figure 3.2.15). Quantification of band intensity for all proteins of interest was carried out using Image Studio Lite.

Western blotting of all cell fractions for lamin A/C showed that nuclei were properly isolated in each condition with minimal contamination in the cytoplasmic fractions. The total cellular proportion of lamin A/C found in the nuclear fraction of each of the conditions are as follows: HeLa A3- fraction contained 92.48%, HeLa A3- + SGB214 fraction contained 96.78%, HeLa A3+ fraction contained 99.71%, and HeLa A3+ + SGB214 nuclear fraction contained 96.73%. This confirms the retention of the cell nuclei within the nuclear fraction, as more than 95% of the total cellular proportion of lamin A/C is found in each of the nuclear fractions in each condition.

Western blotting was also carried out for tubulin to ascertain the correct isolation of the cell fractions. Tubulin is present at high levels in both the total cell lysates and in the cytoplasm and membrane fractions of all conditions; 88.79% of total cellular tubulin was found within the cytoplasm and membrane fraction of HeLa- cells, 85.09% within HeLaA3- + SGB214 cells, 97.29% within the HeLa A3+ cells, and 92.2% within the cytoplasm and membrane fraction of HeLaA3+ +SGB214 cells.

As expected, non-induced HeLa cells (HeLa A3-) did not show any expression of S100P in any fraction. Non-induced HeLa cells that have been transfected with a plasmid containing YFP-S100P (HeLa A3- +SGB214) also do not express S100P, as induction of expression using doxycycline is required not just for WT S100P expression, but also for YFP-S100P expression. This is because the introduced plasmid is under the control of a rtTA inducible promoter.

S100P is detected in HeLa A3 cells induced with doxycycline (HeLa A3+), both in the total cell lysate and the cytoplasm and membrane fraction, at a molecular weight of 10kDa. This form of S100P corresponds to the non-tagged, native form of S100P (WT) that is expressed once cells are induced with doxycycline. No S100P could be detected within the nuclear fraction of these cells, which is in line with previously recorded data.

Induced HeLa A3+ cells that have been transfected with the plasmid containing YFP-S100P (denoted HeLa A3+ + SGB214) show comparatively a lower signal for 10kDa S100P in the total cell lysate

compared to HeLa A3+ cells. 10kDa S100P is found within the cytoplasm and membrane fraction within HeLa A3 + SGB214 cells, but not within the nuclear fraction. This again is in line with previously obtained data.

The molecular weight of the YFP tag is roughly 27kDa, and therefore the addition of a YFP tag to S100P increases its molecular weight from 10kDa to 37kDa. As a result, the YFP-tagged S100P can be found in HeLaA3+ + SGB214 at 37kDa. YFP-S100P is found within the total cell lysate, and in the cytoplasm and membrane fraction, as shown previously. However, in addition to this there is also a significant signal found for YFP-S100P within the nuclear fraction. There is a band detected by the S100P antibody at around 47kDa in each of the fractions of HeLa A3+ +SGB214 cells; this most likely corresponds to dimer formation between the WT 10kDa form of S100P and the YFP-tagged S100P. The signal for S100P in the nuclear fraction at around 47kDa is much fainter in comparison to the cytoplasm and membrane fraction.

Densitometry analysis allows for the quantification of S100P distribution in each of the cell fractions, in addition to quantification of YFP-S100P distribution. Figure 3.2.15, panel B, summarises the densitometry analysis carried out on HeLa A3+ cell fractions and on HeLa A3+ +SGB214 cell fractions, as these are the only experimental conditions which express S100P. The HeLa A3+ cytoplasmic and membrane fraction contains 99.63% of the total cellular S100P, reinforcing that S100P is only present within the cytoplasm and membrane fraction of HeLa A3+ cells. These cells were not transfected with YFP-S100P, so no quantification of YFP-S100P distribution was carried out on this experimental condition. The cytoplasmic and membrane fraction of HeLa A3+ +SGB214 cells contained 98.77% of the total cellular S100P, much like HeLa A3+ cells. For YFP-S100P quantification purposes, the density of only the 37kDa bands were assessed as these pertain to YFP-S100P alone. Densitometry analysis confirmed that 76.84% of the total proportion of YFP-S100P was present within the cytoplasm and membrane fraction, whereas 23.16% was present within the nuclear fraction. The total proportion of tubulin found within the nuclear fraction of HeLa A3+ +SGB214 cells was 7.8%, which is much lower than the level of YFP-S100P found in the nuclear fraction.

This data illustrates that the addition of a YFP tag can either facilitate shuttling of S100P into the nucleus, or at least perturb its cellular localisation in some way.

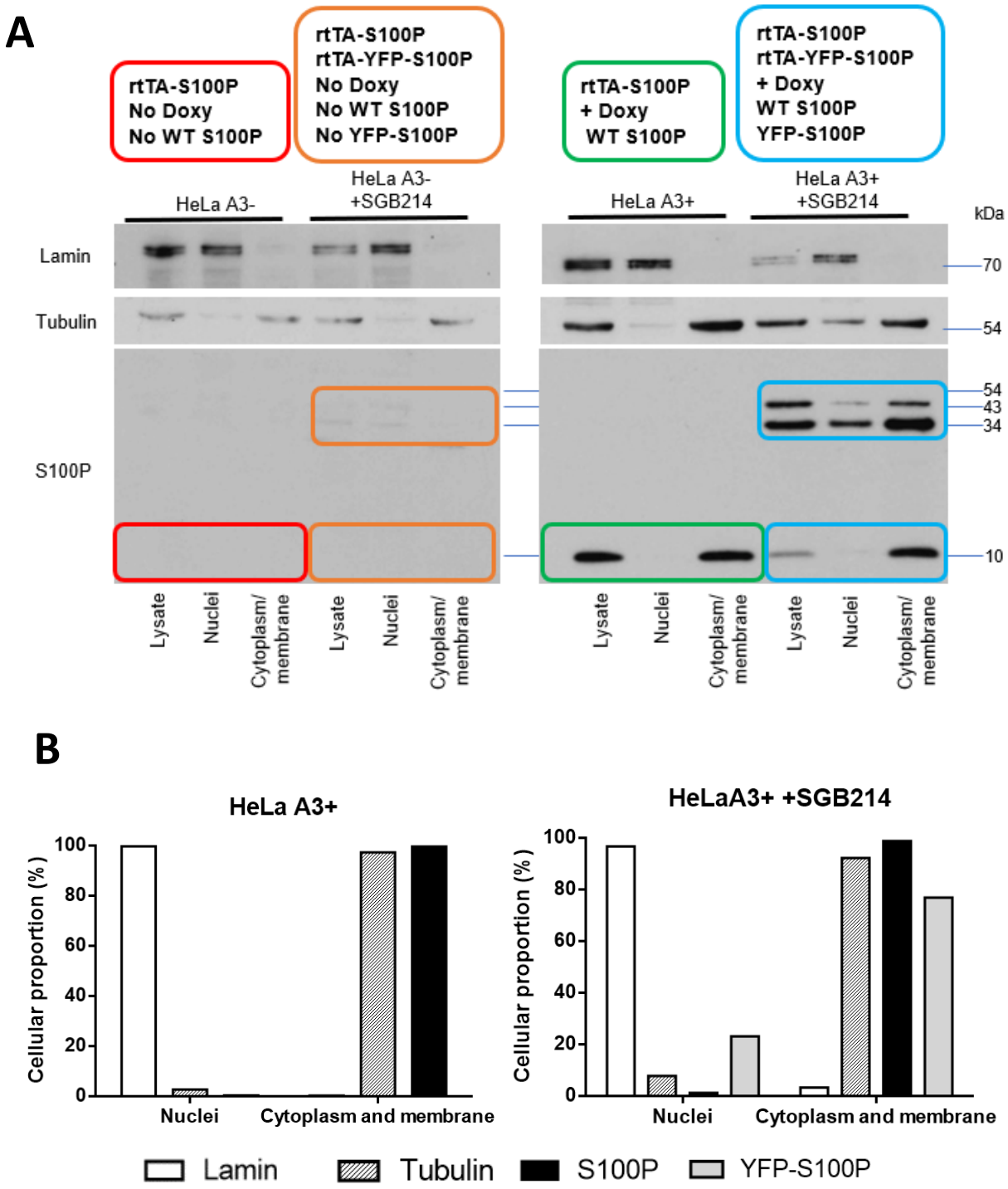

Figure 3.2.15: The addition of a YFP tag to S100P disturbs its subcellular localisation

A) HeLa A3 cells transfected with the rtTA-S100P plasmid, either induced or non-induced, were transfected with another plasmid containing YFP-S100P (rtTA-YFP-S100P) prior to fractionation with a Dounce homogeniser. Samples were run on 16% (w/v) SDS-PAGE before western blotting to detect S100P, cytoplasmic marker tubulin, and nuclear marker lamin A/C within each cell fraction.

B) The cellular proportion of the various proteins were quantified by densitometry using Image Studio Lite.

3.2.6 Leptomycin B does not induce S100P nuclear accumulation

Previous experiments have shown that S100P is exclusively found in the cytoplasm and membrane fraction of cell lines when fractionated using two different assays and alterations in calcium concentration, and that despite all our best efforts, we have been unable to establish S100P as a nuclear protein. To confirm that S100P is not being actively transported out of the nucleus during the fractionation process, Leptomycin B (LMB) was utilised. LMB is antibiotic and antifungal produced by streptomyces (Hamamoto *et al.* 1983). LMB directly binds to and inhibits chromosomal maintenance 1 (CRM1), otherwise known as exportin 1, which is required for export of cellular proteins out of the nucleus that contain leucine-rich nuclear export signal (NESs).

Nucleocytoplasmic transport is a process which involves exchange of molecules between the nucleus and the cytoplasm. This exchange is facilitated by 50nm channels known as nuclear pore complexes (NPCs) which are embedded in the nuclear envelope. NPCs provide two primary modes of molecular exchange; passive diffusion of small molecules, and active transport of molecules across the NPC.

Passive diffusion is the movement of small, inert molecules between the nucleus and the cytoplasm, without the need for a chaperone. Currently, it is thought that the nuclear pore complex has a limit on passive diffusion; macromolecules exhibit decreased passage through the nuclear pore complex as a function of their molecular mass. In addition, there is competition between macromolecules for volume within the nuclear pore cavity, another factor that can limit their transport through NPCs (Timney *et al.* 2016). There is some debate over the size of the NPC channel radius; several studies assert that the passive diffusion can take place only when molecules are less than 5nm in diameter, however Mohr *et al.* (2009) have observed the passive transport barrier of NPCs to be 2.6nm.

Active nuclear transport, on the other hand, is the guided transport of macromolecules by proteins known as transport receptors. Many proteins that are transported across the NPC into the cytoplasmic space contain a NES that is recognised by transport receptors. Regulation of transport receptors is possible through Ran GTPase; for nuclear export in particular, RanGTP, which is present at a high concentration in the nucleus, binds to transport receptors and alters their affinity for cargo. This cargo-transport receptor-RanGTP complex can cross the NPC into the cytoplasmic space, where the presence of Ran GTPase facilitates the conversion of Ran GTP into Ran GDP, thus dissociating the protein cargo complex (Güttler and Görlich 2011).

To firstly show the efficacy of LMB as a potent inhibitor of nuclear export, it was necessary to document its effect on a protein known to be affected by LMB. To this end, paxillin was chosen as a control as this protein has previously been reported to be affected by LMB treatment (Burgess and Gray 2012).

Cells were treated with differing concentrations of LMB (from 0 to 10ng/ml) and for either 0, 3 or 6 hours, to establish the optimal concentration and time required to prevent protein export. This optimisation was carried out in the COS-7 s10+, JEG-3 and BeWo cells.

Following treatment with LMB, cells were fixed, permeabilised and stained with an antibody to paxillin. Immunofluorescent staining of COS-7 s10+ cells demonstrate that paxillin is by default present within the perinuclear region and the cytoplasm at a high level, with small background staining within the nucleus (Figure 3.2.16). There are also distinct paxillin foci observed within the cytoplasmic regions of the cell, denoting focal adhesion plaques. Following LMB treatment for 3 hours at 5ng/ml, paxillin is seen within the nuclei of COS-7 S10+ cells at a high level. There does not seem to be an obvious difference in the nuclear localisation of paxillin between the 5ng/ml and 10ng/ml doses at 3 hours post-LMB treatment. There also does not seem to be distinct differences in paxillin localisation between 3 hours and 6 hours of treatment with LMB.

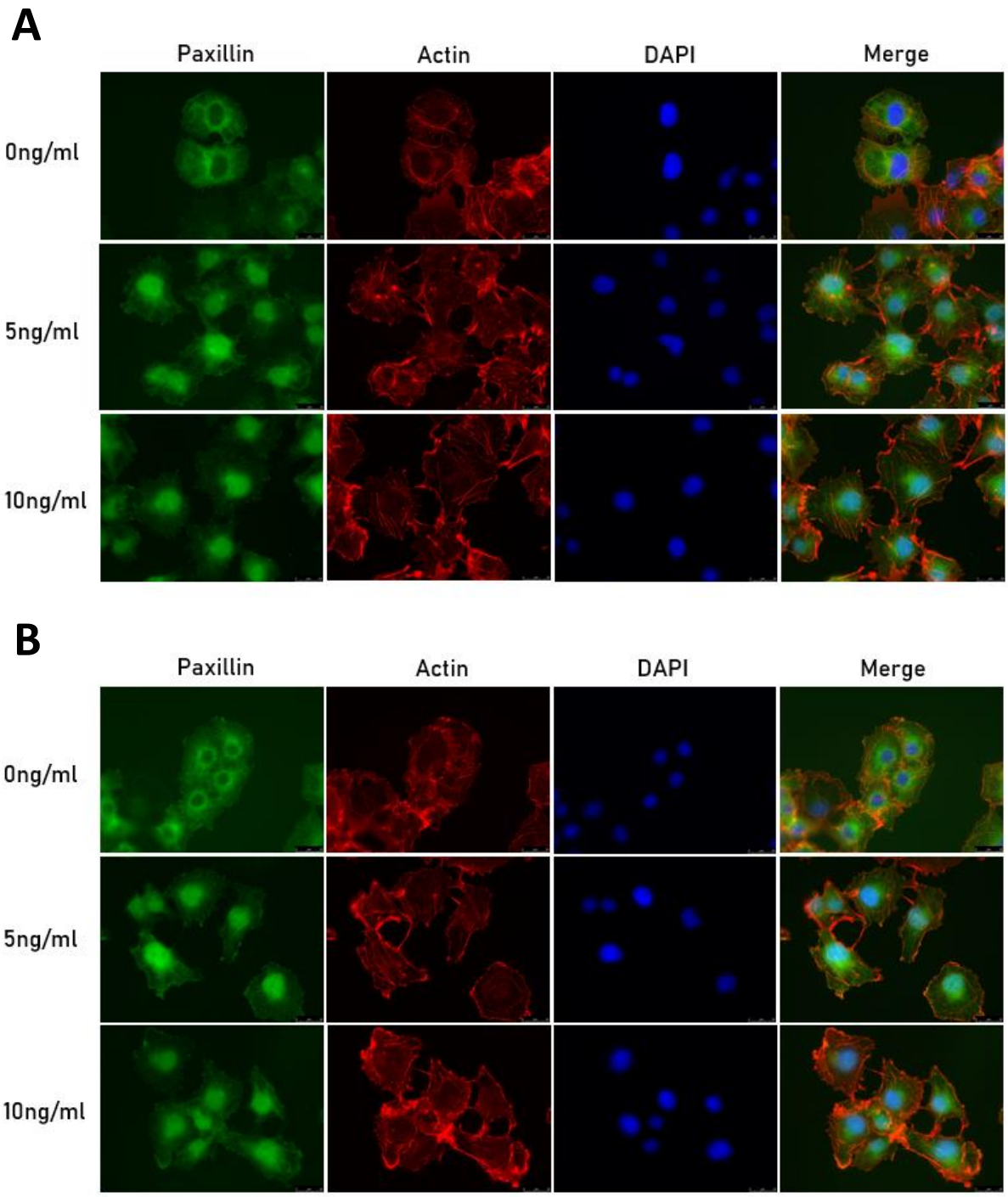

Figure 3.2.16: Leptomycin B prevents nuclear export of paxillin in COS-7 s10+ cells

COS-7 s10+ cells were induced and seeded onto glass coverslips, and grown for 24 hours prior to treatment with LMB at either 0, 5 or 10ng/ml for 3 (A) or 6 (B) hours. Cells were fixed, permeabilised and stained for paxillin and actin. Cells were mounted onto glass slides with DAPI and viewed using an epifluorescence microscope.

JEG-3 and BeWo cell lines without LMB treatment were observed to show a comparable localisation of paxillin to untreated COS-7 s10+ cells (figures 3.2.17 and 3.2.18). Paxillin is also present within the cytoplasm and in distinct foci mostly around the borders of the cell cytoskeleton, but without an increased perinuclear localisation as was seen in COS-7 s10+ cells. Nevertheless, following LMB treatment for 3 hours, paxillin was observed in the nucleus after treating with either 5ng/ml or 10ng/ml of LMB. However, the presence of paxillin in the nucleus is slightly increased following 6 hours of treatment with LMB at a concentration of 10ng/ml. There does not seem to be a marked increase in nuclear paxillin between 5ng/ml and 10ng/ml in either cell line.

The results of this study indicate that the optimal time and dosage of LMB treatment is 6 hours at a concentration of 10ng/ml, as this concentration was effective at preventing nuclear export of paxillin in all cell lines tested.

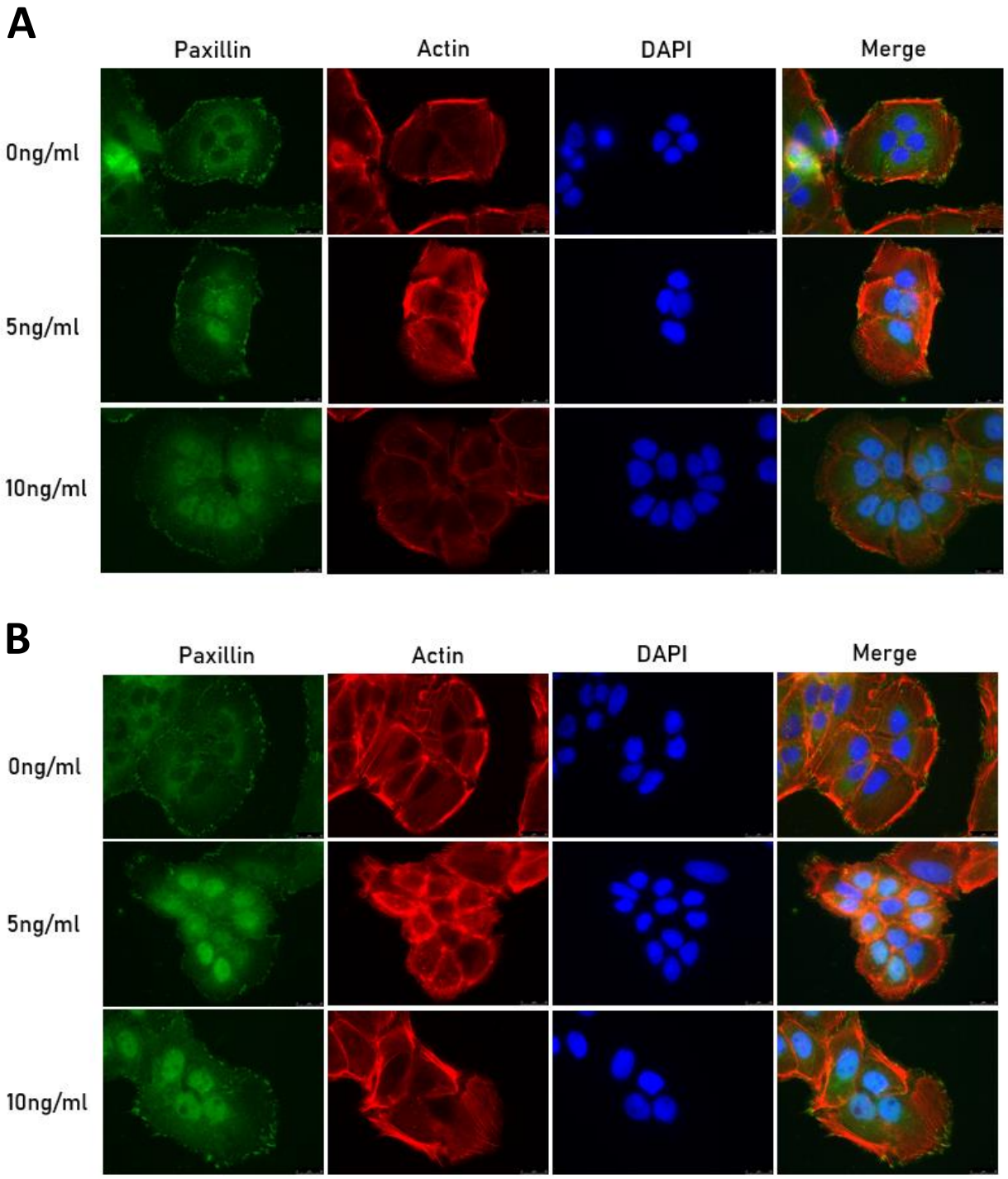

Figure 3.2.17: Leptomycin B prevents nuclear export of paxillin in JEG-3 cells

JEG-3 cells were seeded onto fibronectin-coated coverslips and grown for 24 hours prior to treatment with LMB at either 0, 5 or 10ng/ml for 3 (A) or 6 (B) hours. Cells were fixed, permeabilised and stained for paxillin and actin. Cells were mounted onto glass slides with DAPI and viewed using an epifluorescence microscope.

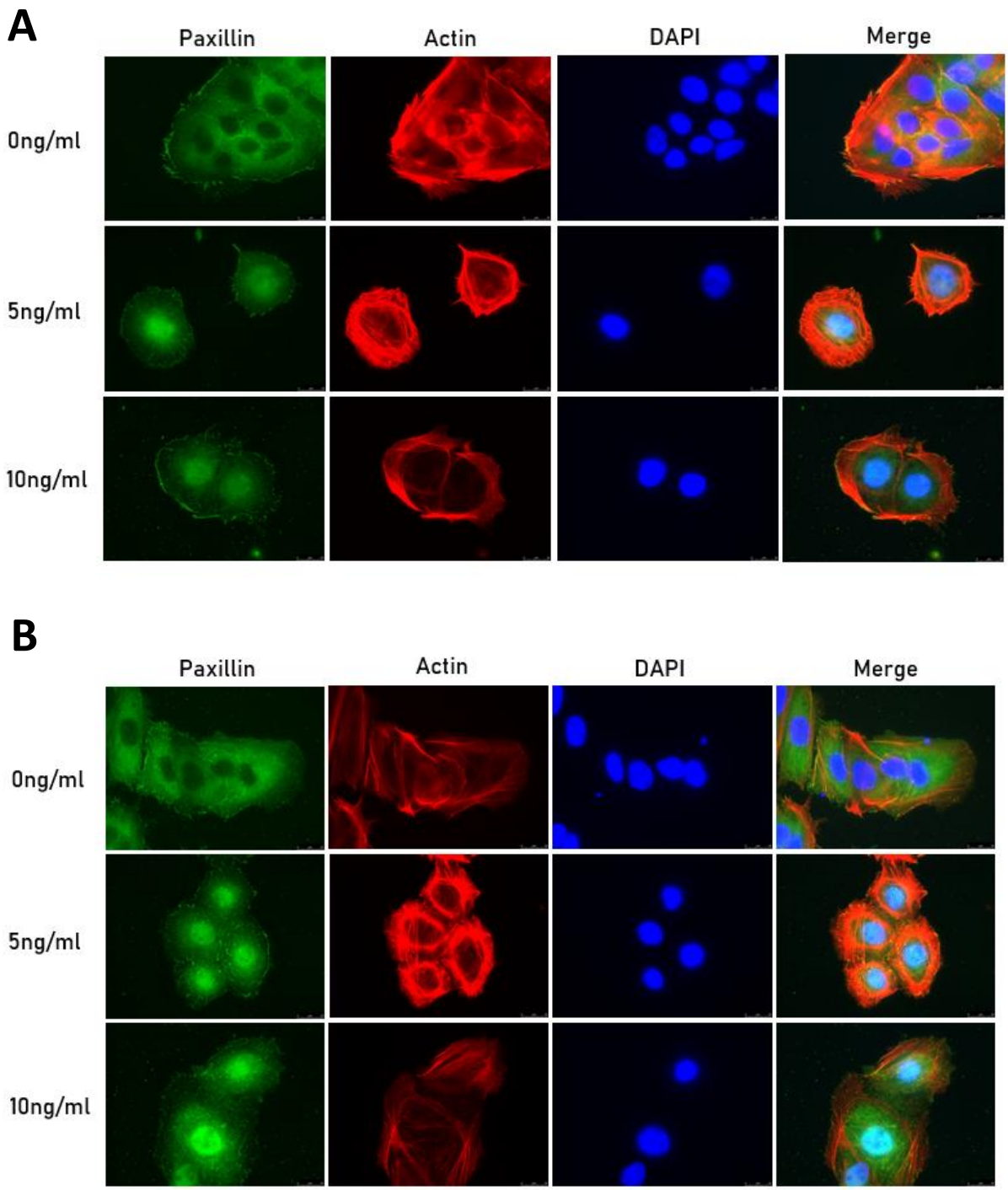

Figure 3.2.18: Leptomycin B prevents nuclear export of paxillin in BeWo cells

BeWo cells were seeded onto fibronectin-coated coverslips and grown for 24 hours prior to treatment with LMB at either 0, 5 or 10ng/ml for 3 (A) or 6 (B) hours. Cells were fixed, permeabilised and stained for paxillin and actin. Cells were mounted onto glass slides with DAPI and viewed using an epifluorescence microscope.

Having optimised the dosage and treatment time of LMB for each cell line, we sought to fractionate cell lysates by Dounce homogenisation in order to assess if S100P localisation is influenced in response to this drug.

Figure 3.2.19 presents western blotting of JEG-3 cell fractions following LMB treatment (10ng/ml for 6 hours) and Dounce homogenisation to separate cellular compartments. Western blotting for lamin A/C found that 91.04% (±0.34 SD) of total cellular lamin A/C was detected in the nuclear fraction of untreated JEG-3 cells, compared to 89.48% (±1.87 SD) detected in the nuclear fraction of cells treated with LMB. 90.35% (±10 SD), of the total cellular HDAC2 was detected within the nuclear fraction of untreated JEG-3 cells, compared to 90.12% (±9.56 SD) detected in the nuclear fraction of the LMB-treated JEG-3 cells. The total cellular proportion of tubulin detected in untreated JEG-3 cell cytoplasm and membrane fractions was 92.17% (±5.72 SD), whereas JEG-3 cells treated with LMB contained 78.96% (±2.89 SD) of total cellular tubulin within the cytoplasm and membrane fraction. Paxillin was detected by western blotting to ensure that LMB was working as previously established. Without LMB treatment, 92.28% (±1.69 SD) of total cellular paxillin was detected within the cytoplasm and membrane fraction of JEG-3 cells. However, upon treatment with LMB, 74.03% (±8.11 SD) of paxillin is detected within the cytoplasm and membrane fraction, with the remaining 25.97% detected in the nuclear fraction. This suggests that paxillin export from the nucleus is being inhibited by LMB, as levels of paxillin present in the nuclear fraction following LMB treatment (25.97%) exceed the levels of tubulin (21.04%). After confirming that LMB treatment sufficiently inhibits nuclear export of paxillin, it was possible to analyse S100P levels in the respective cell fractions to assess if S100P is also exported following treatment. Without LMB treatment, 99.06% of S100P was detected within the cytoplasm and membrane fraction (±1.33 SD). Following LMB treatment, 84.99% of total cellular S100P was detected within the cytoplasm and membrane fraction by densitometry, with the remaining 15.01% being detected in the nuclear fraction (±4.42 SD). However, 21.04% of total cellular tubulin was detected in the nuclear fraction of treated JEG-3 cells, suggesting the 15.01% of total S100P detected in the nuclear fraction is a by-product of contamination of the nuclear fraction with cytoplasmic proteins. This data suggest treatment of JEG-3 cells with LMB at a commonly used concentration of 10ng/ml does not influence S100P localisation by preventing its export from the nucleus.

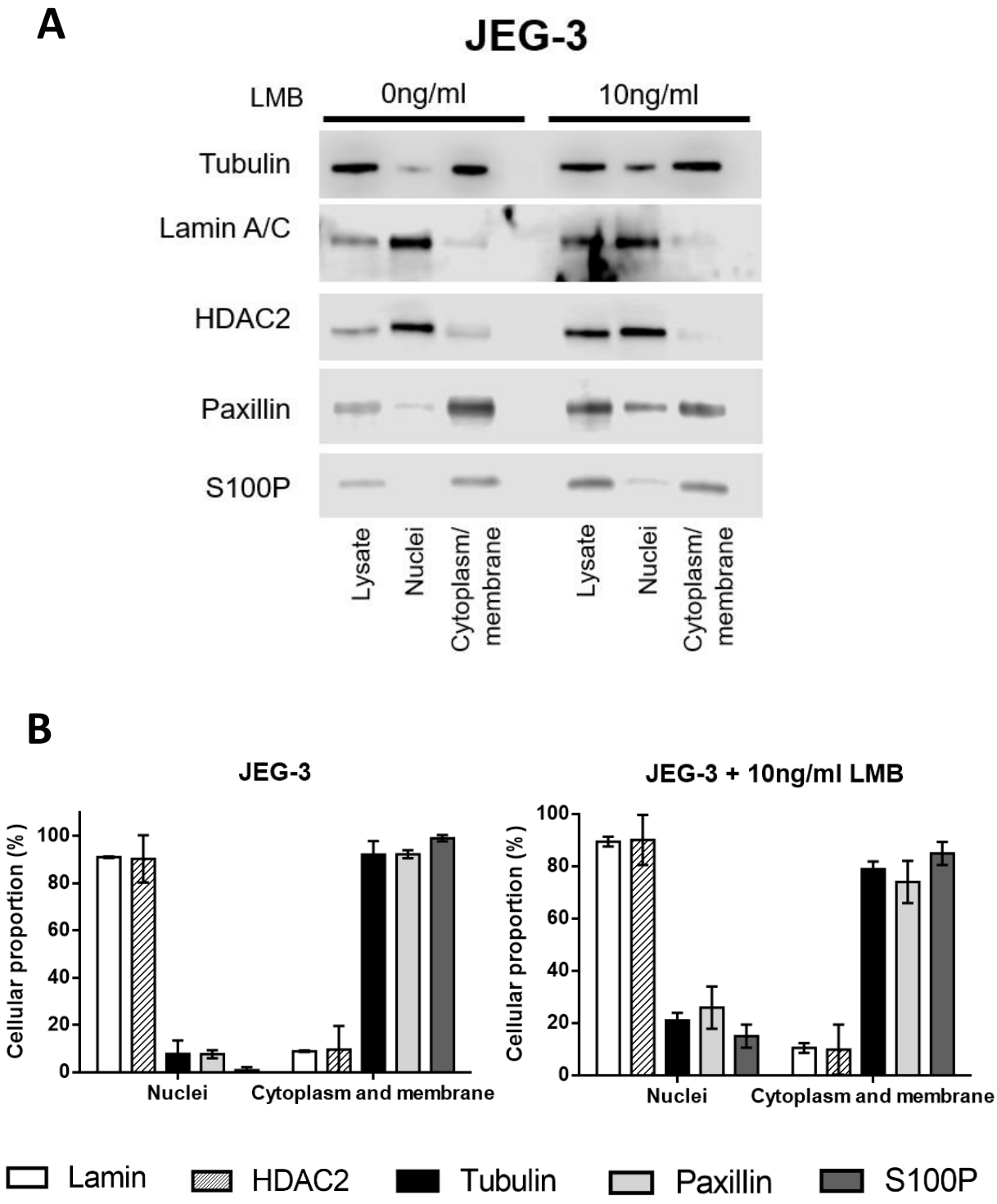

Figure 3.2.19: Leptomycin B does not alter the subcellular localisation of S100P in trophoblast cell line JEG-3

JEG-3 cells (A) were treated with 10ng/ml LMB for 6 hours prior to fractionation with a Dounce homogeniser and differential centrifugation. Cell fractions were run on SDS-PAGE followed by western blotting to detect S100P, cytoplasmic marker tubulin, and nuclear markers lamin A/C and HDAC2 within each fraction. Paxillin was also detected by western blot as confirmation of LMB efficacy. The cellular proportion of the various proteins were quantified by densitometry using Image Studio Lite (B). Data represents the mean ±SD from at least 3 independent replicates.

The BeWo cell line was also fractionated with and without LMB treatment, followed by western blotting for marker proteins of cellular compartments (Figure 3.2.20). The nuclear fraction of untreated BeWo cells contained on average 88.76% of the total cellular lamin A/C (±8.28 SD) and 84.52% of the total cellular HDAC2 (±0.11 SD). The nuclear fraction of BeWo cells treated with LMB contained on average 85.47% of the total cellular lamin A/C (±10.45 SD) and 89.75% of the total cellular HDAC2 (±14.09 SD), confirming the correct isolation of nuclear fractions in both treated and untreated conditions. Western blotting for tubulin demonstrated that 94.83% of the total cellular tubulin was detected within the cytoplasm and membrane fraction of untreated BeWo cells (±4.43 SD), whereas 92.62% of total cellular tubulin was detected within the cytoplasm and membrane fraction of BeWo cells treated with LMB (±4.41 SD). Western blotting for paxillin showed that the cytoplasm and membrane fraction of untreated BeWo cells contained 98.54% of cellular paxillin (±2.06 SD). Upon LMB treatment, the level of paxillin detected in the cytoplasm and membrane fraction was 88.48% (±3.02 SD).

Without any treatment, the total cellular proportion of S100P detected within the cytoplasm and membrane fraction was on average 95.64% (±5.32 SD). For BeWo cells treated with LMB for 6 hours, the cytoplasm and membrane fraction contained 95.75% of the total cellular proportion of S100P (±1.38 SD). Like the JEG-3 cells, the proportion of tubulin within the nuclear fraction was greater than the level of S100P within the nuclear fraction, once again suggesting that S100P is found in the cytoplasm and membrane fraction, even when blocking nuclear export in both of the trophoblast cell lines.

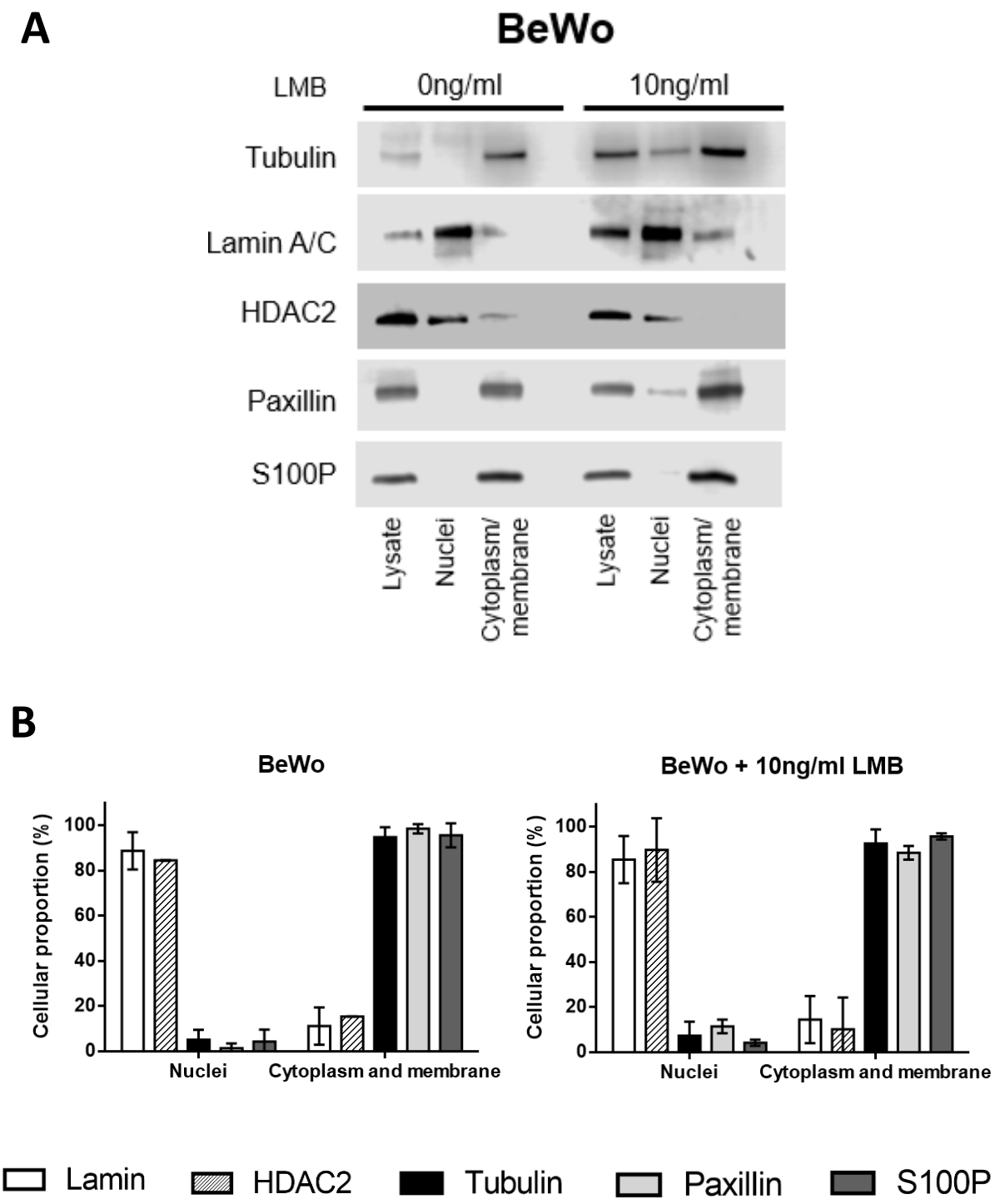

Figure 3.2.20: Leptomycin B does not alter the subcellular localisation of S100P in trophoblast cell line BeWo

BeWo cells (A) were treated with 10ng/ml LMB for 6 hours prior to fractionation with a Dounce homogeniser and differential centrifugation. Cell fractions were run on SDS-PAGE followed by western blotting to detect S100P, cytoplasmic marker tubulin, and nuclear markers lamin A/C and HDAC2 within each fraction. Paxillin was also detected by western blot as confirmation of LMB efficacy. The cellular proportion of the various proteins were quantified by densitometry using Image Studio Lite (B). Data represents the mean ±SD from at least 3 independent replicates.

Non-trophoblast cell lines, including COS-7 s10+, were also fractionated following LMB treatment. Figure 3.2.21a shows the resulting western blot for nuclear marker proteins lamin A/C and HDAC2, cytoplasmic marker tubulin, paxillin, and S100P. Nuclei were sufficiently fractionated from treated and non-treated cells, as the total cellular proportion of lamin A/C found in the nuclear fraction was 96.24% (±5.31 SD) and 92.03% (±5.13 SD) in non-treated and LMB-treated COS-7 s10+ cells respectively. The total cellular proportion of HDAC2 in the nuclear fraction of non-treated and LMB-treated COS-7 cells was 94.5% (±6.48 SD) and 90.18% (±2.8 SD) respectively, again confirming the proper isolation of cell nuclei. On average, western blotting and densitometry for tubulin showed that the total cellular proportion of tubulin found in the cytoplasm was 79.64% in non-treated cells (±10.92 SD), and 76.51% in LMB-treated cells (±10.38 SD), with the remainder of tubulin being found in the cell nuclei. The small traces of tubulin detected within the nuclear fraction indicates a small level of cytoplasmic contamination within the nuclear fraction, which is somewhat to be expected due to the high titre of the tubulin antibody used within these studies. The paxillin protein is known to be responsive to LMB treatment, in which paxillin export from the nucleus is prevented. This was confirmed by western blotting for paxillin, which demonstrated a ratio of 77.93% cytoplasmic to 22.07% nuclear in non-treated cells (±16.36 SD). Upon treatment with LMB, this ratio shifts in favour of cell nuclei, where 43.38% of the total cellular paxillin is now nuclear, and the remaining 56.62% is cytoplasmic (±10.74 SD). This confirms the cells' responsiveness to LMB and the ability of LMB to disrupt the nuclear export process. Western blotting of all marker proteins allowed for the analysis of S100P levels in each cellular compartment, with the ability to quantify if S100P has been retained in the cell nuclei following treatment with LMB. Non-treated COS-7 s10+ cells contained 93.45% of the total proportion of S100P within the cytoplasmic fraction (±4.78 SD). Following treatment with LMB, the cytoplasmic fraction of COS-7 s10+ cells contained 96.14% of the total cellular S100P (±3.57 SD). Despite treating COS-7 S10+ cells with LMB, S100P localisation does not shift from the cytoplasm and membrane fraction to the nuclear fraction as paxillin does, suggesting S100P export from the nucleus, if it were to be localised there, is not dependent on CRM1.

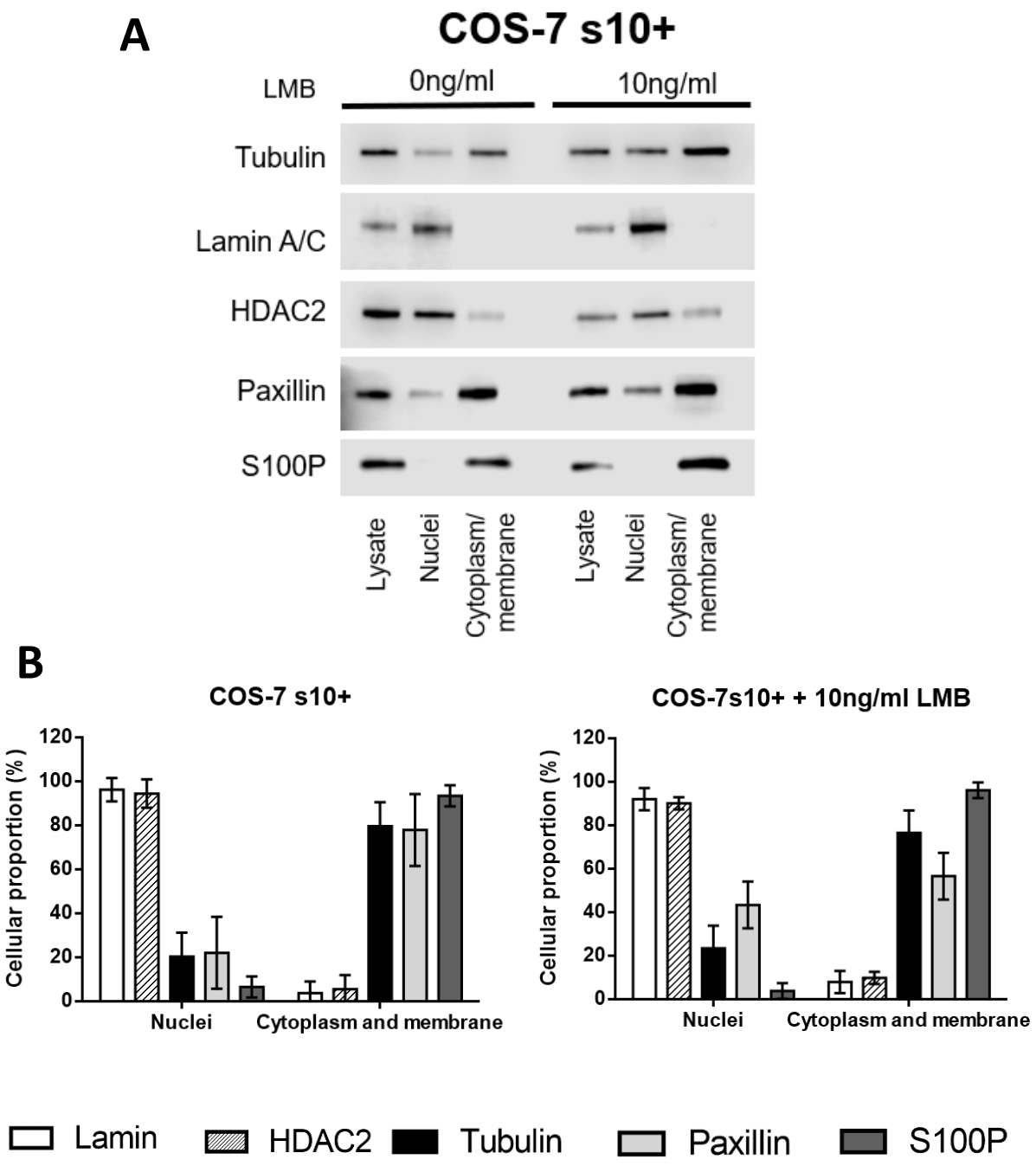

Figure 3.2.21: Leptomycin B does not alter the subcellular localisation of S100P in the COS-7 s10+ inducible cell line

COS-7 s10+ cells (A)were treated with 10ng/ml LMB for 6 hours prior to fractionation with a Dounce homogeniser and differential centrifugation. Cell fractions were run on SDS-PAGE followed by western blotting to detect S100P, cytoplasmic marker tubulin, and nuclear markers lamin A/C and HDAC2 within each fraction. Paxillin was also detected by western blot as confirmation of LMB efficacy. The cellular proportion of the various proteins were quantified by densitometry using Image Studio Lite (B). Data represents the mean ±SD from at least 3 independent replicates.

HeLa A3+ cells were fractionated as above, with and without LMB treatment at a dose of 10ng/ml for 6 hours. Figure 3.2.22a shows the resulting western blot for nuclear marker proteins lamin A/C and HDAC2, cytoplasmic marker tubulin, paxillin, and S100P. Without any treatment, the total cellular proportion of lamin A/C detected in the nuclear fraction was 96.2% (±5.37 SD). In comparison, the total cellular proportion of lamin A/C detected in the nuclear fraction of HeLa A3+ cells treated with LMB was 99.05% (±0.8 SD). For soluble marker HDAC2, the average total cellular proportion detected within the nuclear fraction of untreated HeLa A3+ fractions was 90.89% (±8.78 SD). In LMB-treated HeLa A3+ cells, the total cellular proportion of HDAC2 found in the nuclear fraction was on average 89.18% (±12.52 SD). The total cellular proportion of tubulin, the cytoplasmic marker protein, detected in the cytoplasm and membrane fraction of untreated HeLa A3+ cells was 87.9% (±0.1 SD), compared to 74.53% (±2.19 SD) in the respective cytoplasmic fraction of LMB-treated cells.

Following western blotting for paxillin on both treated and untreated HeLa A3+ cells, the average total cellular proportion of paxillin present in the cytoplasmic fraction of untreated HeLa A3+ cells was found to be 64.03% (±3.92 SD), with the remaining 35.96% detected within the nuclear fractions. Upon treatment of HeLa A3+ cells with LMB, the total average proportion of cytoplasmic paxillin was found to be 25.86% (±0.31 SD), a decrease of almost 40%. The remaining cellular paxillin, 74.14%, was detected within the nuclear fraction. This suggests once again that paxillin export from the nucleus can be inhibited by LMB.

After detection of the various marker proteins present within HeLa A3+ cell fractions by western blotting, it was possible to quantify levels of S100P in both treated and untreated HeLa A3+ cells in order to assess if LMB treatment leads to accumulation of nuclear S100P. In untreated HeLa A3+ cells, 90.37% of total cellular S100P was detected in the cytoplasm and membrane fraction (±13.58 SD), whereas in LMB-treated HeLa A3+ cells, the total cellular proportion of S100P detected in the cytoplasm and membrane fraction was 91.58% (±11.93 SD). The difference in cytoplasmic S100P localisation between treated and non-treated samples, a small level of less than 1%, is most likely due to cytoplasmic contamination of the nuclear fraction.

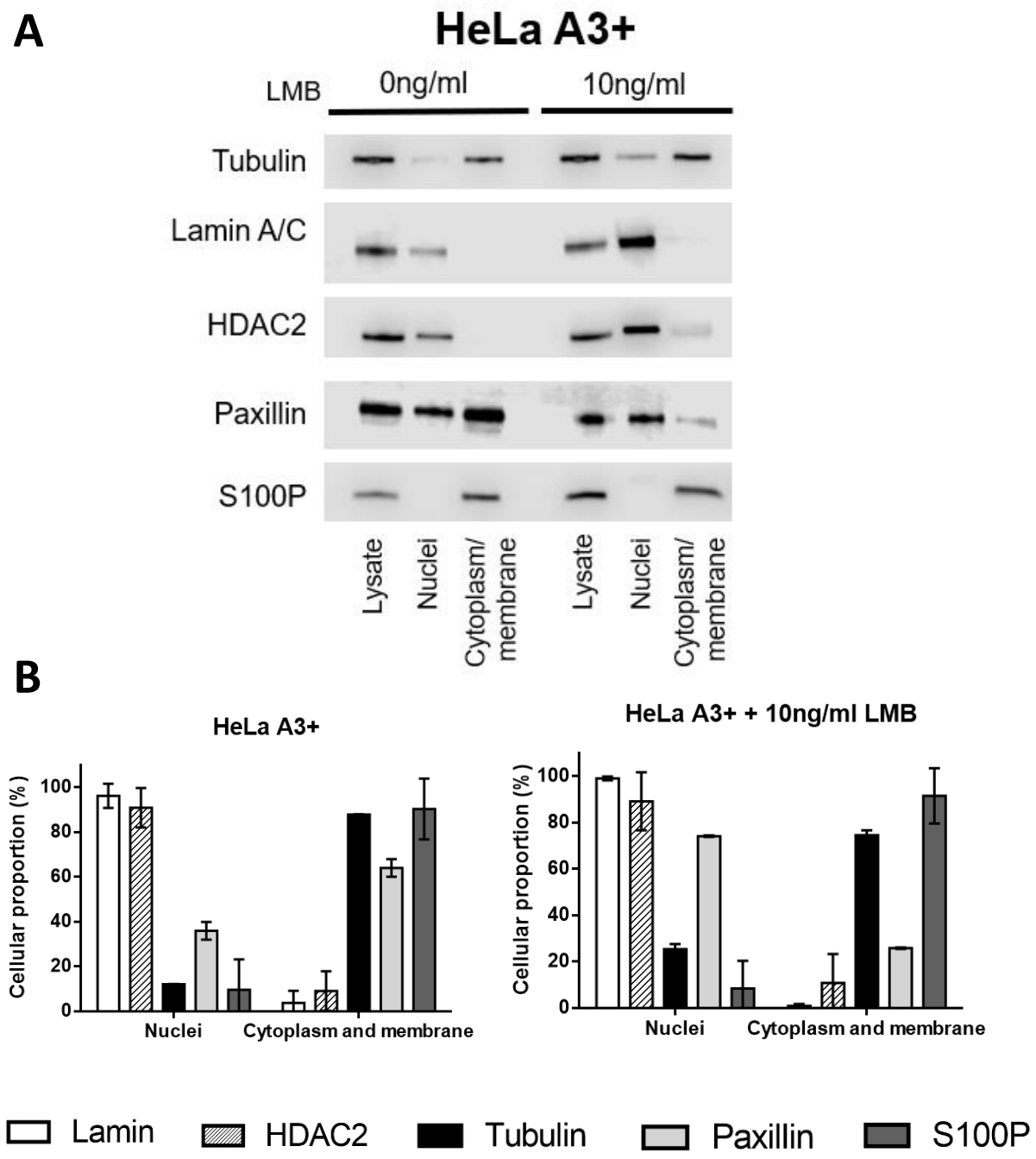

Figure 3.2.22: Leptomycin B does not alter the subcellular localisation of S100P in the HeLa A3+ inducible cell line

HeLa A3+ cells (A) were treated with 10ng/ml LMB for 6 hours prior to fractionation with a Dounce homogeniser and differential centrifugation. Cell fractions were run on SDS-PAGE followed by western blotting to detect S100P, cytoplasmic marker tubulin, and nuclear markers lamin A/C and HDAC2 within each fraction. Paxillin was also detected by western blot as confirmation of LMB efficacy. The cellular proportion of the various proteins were quantified by densitometry using Image Studio Lite (B). Data represents the mean ±SD from at least 3 independent replicates.

Nuclei isolated from COS-7 s10+ cells were stained with DAPI to assert that minimal rupturing of nuclear membranes had taken place (Figure 3.2.23). These images demonstrate intact nuclear membranes with minimal disruption.

All in all, the data obtained shows that treatment of cell lines, both trophoblast and non-trophoblast in nature, with LMB at a concentration of 10ng/ml leads to the nuclear accumulation of paxillin, due to prevention of nuclear export by blocking the CRM1 pathway. Most importantly, LMB treatment does not alter the subcellular localisation of S100P in any of the cell lines tested, suggesting that S100P is not exported from the nucleus and is instead localised to the cytoplasm and membrane.

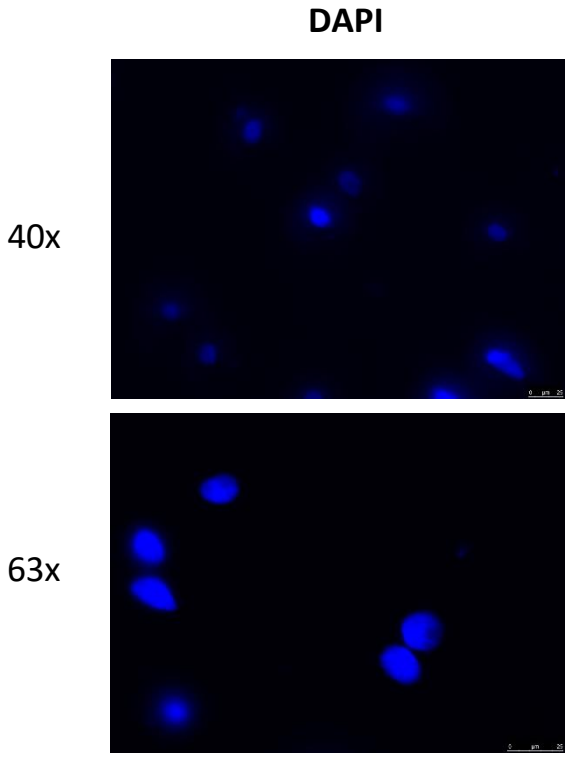

Figure 3.2.23: Subcellular fractionation using a Dounce homogeniser following LMB treatment allows for isolation of intact nuclei from cell lines

COS-7 s10+ cells were treated with 10ng/ml LMB for 6 hours prior to fractionation. A small aliquot of the nuclear fraction from COS-7 cells were stained with DAPI before imaging at 40x and 63x magnifications.

3.2.7 S100P Binding Protein has a mainly nuclear localisation when studied by subcellular fractionation

S100P binding protein (S100PBP) was discovered by Dowen *et al.* (2005) as a novel S100P interactor through co-immunoprecipitation of HEK 293 cell lysates. The same study found that GFP-tagged S100PBP was localised to the nuclei of HeLa cells. Following this work, we sought to assess the localisation of S100PBP by subcellular fractionation.

To this end, JEG-3 and BeWo cells lysates were passed through a Dounce homogeniser, followed by the separation of cellular compartments by differential centrifugation. Following fractionation of cell lines, the cell fractions were subjected to 16% (w/v) SDS-PAGE prior to western blot analysis for S100PBP, nuclear marker lamin A/C and cytoplasmic marker tubulin. Quantification of the band intensity was carried out using Image Studio Lite.

Isolation of the nuclear fraction was confirmed by western blotting for lamin A/C, in which the nuclear fraction of JEG-3 cells contained 97.46% of total cellular lamin A/C. The cytoplasmic fraction of JEG-3 cells contained 72.93% of the total cellular proportion of tubulin, the cytoplasmic marker protein. Analysis of S100PBP within each cell fraction by densitometry found that 73.03% of total cellular S100PBP was detected within the nuclear fraction, with the remainder present in the cytoplasm and membrane fraction.

Correct isolation of nuclei from BeWo cells was confirmed, as the nuclear fraction contained 99.29% of total cellular lamin A/C. The cytoplasm and membrane fraction of BeWo cells contained 79.99% of total cellular tubulin. 57.01% of S100PBP was found in the nuclear fraction of BeWo cells, with the remaining 42.99% detected in the cytoplasm and membrane fraction.

This experiment confirms the predominantly nuclear localisation of S100PBP that was observed through immunofluorescence assays using a biochemical technique.

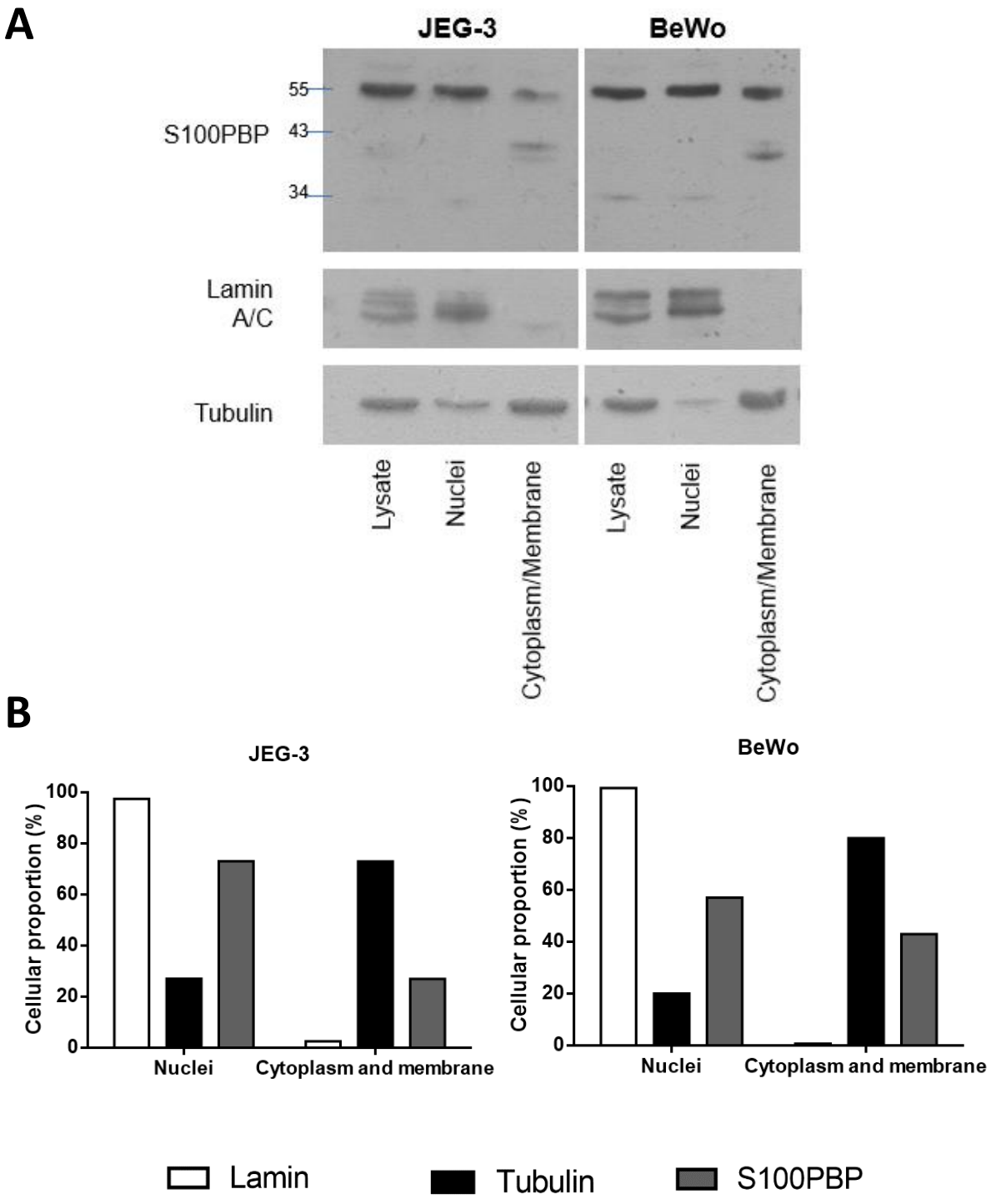

Figure 3.2.24: S100PBP is mainly nuclear when studied by subcellular fractionation

A) Lysed cells (JEG-3 and BeWo) were homogenised using a Dounce homogeniser before differential centrifugation. Samples were run on 16% (w/v) SDS-PAGE followed by western blotting to detect S100PBP, cytoplasmic marker tubulin, and nuclear marker lamin A/C.

B) The cellular proportion of the various proteins were quantified by densitometry using Image Studio Lite.

3.3 Discussion

Expression of S100P has been detected in a number of tissues, with a large focus on its role in malignancies. S100P was first purified from the placenta (Becker *et al.* 1992), but has also been found within the oesophagus and stomach, albeit at very much reduced levels in comparison. Expression of the S100P protein has also been seen at high levels within a multitude of different tumour types (Parkkila *et al.* 2008), and has been demonstrated to affect different cellular behaviours including cell proliferation (Arumugam *et al.* 2004), invasion (Arumugam *et al.* 2005; Tabrizi *et al.* 2018) and migration (Hamada *et al.* 2009; Tabrizi *et al.* 2018). It is however important to note that these cellular behaviours are not only required for tumour development, but also for embryo implantation to occur.

Whilst the majority of reports have linked S100P expression to pathophysiological conditions, much less is known about the physiological role of S100P. Given that S100P has been shown to be expressed in the placenta and mainly trophoblast cells within, we sought to first expand our understanding of the subcellular localisation of this protein within these cells, as well as in better characterised systems such as cancer cells of both breast (MDA-MB-231) and cervical (HeLa) origins. Previous studies have shown S100P localisation in a wide variety of cell and tissue types (see table 3.1.1). In this chapter, it was first demonstrated that cell lines from varying origin express S100P at differential levels. Two of these cell lines, JEG-3 and BeWo, are human choriocarcinoma cell lines that have been widely used as a model system for placental trophoblasts, due to the limited availability of primary trophoblasts. BeWo cells are commonly used as a model to mimic villous trophoblast fusion into syncytiotrophoblast (Orendi *et al.* 2010), therefore assessment of the subcellular localisation of S100P within this cell line would be beneficial. Zhu *et al.* (2015) determined through immunohistochemistry that S100P localisation in syncytiotrophoblasts was both cytoplasmic and nuclear. However, although BeWo cells are used as a syncytiotrophoblast model, they are still choriocarcinoma in origin.

Interestingly, the HTR8/SVneo cell line does not express S100P. The HTR8 cell line are a first trimester extravillous trophoblast cell line, and are therefore used as a model cell line for work involving trophoblasts, including migration, invasion and implantation (Hannan *et al.* 2010; Verma, Pal and Gupta, 2018). However, a study by Abou-Kheir *et al.* (2017) has reported that the HTR8/SVneo cell line contains a mixed population of cells; compared to JEG-3 and JAR cell lines, HTR8 cells showed heterogeneous expression of cytokeratin 7 and HLA-G, markers for trophoblast cells. Cultured HTR8 cells also contained a mixed population of cells expressing vimentin, a marker of mesenchymal cells, and E-cadherin, a marker of epithelial cells. Therefore, while HTR8 cells are used as a model first trimester trophoblast cell line, it is not necessarily surprising that they do not express S100P, since the

typical EVT markers are heterogeneously expressed in this cell line, along with markers of mesenchymal origin that should not be present.

Work within this chapter has also demonstrated the high levels of S100P expression by inducible cell lines COS-7 s10+ and HeLa A3+ following induction with doxycycline over a period of hours or days. The level of S100P in these inducible cell lines is highly regulatable over time. It was therefore thought that there was potential for very high levels of S100P expression to influence its localisation in cells. HeLa A3+ cells demonstrated peak S100P expression at 120-144 hours post initial induction, and COS-7 s10+ cells at 48-72 hours post initial induction. The half-life of doxycycline in cell culture medium is 24 hours (Gomez-Martinez *et al.* 2013), therefore doxycycline was administered to HeLa A3 and COS-7 s10 cells every 48 hours to prevent any reduction in the activity of the inducible system. It is not certain why S100P expression levels in HeLa A3+ and COS-7 s10+ cells decrease somewhat after the peak S100P expression time points previously mentioned, given that doxycycline was continuously administered. Work relating to the activity of the tetracycline-responsive promoter under constant administration of doxycycline could give an insight into biological mechanisms at play behind this decrease in expression.

Immunofluorescent staining of HeLa A3+ cells was undertaken to assess the specific physiological localisation of the S100P protein. The results, demonstrating both a nuclear and cytoplasmic staining, are in line with data published by Du *et al.* (2012) which also shows this pattern of S100P localisation. However, comparative immunofluorescent staining of S100P in JEG-3 and HeLa A3+ cells at different time points following induction of S100P expression do not correlate with western blotting data obtained in this chapter (Figures 3.2.5 and 3.2.6). Western blotting shows an almost 50% decrease in S100P expression in HeLa A3+ cells induced for 24 hours versus HeLa A3+ cells induced for 96 hours. - This is not reflected in the immunofluorescent staining, in which both 24-hour and 96-hour induction time points display the same levels of fluorescence intensity. This data suggests a potential flaw within the detection of S100P by immunofluorescence, which could be due to unspecific binding of the antibody used for immunofluorescence. The S100P antibody is specific to S100P, as HeLa A3- cells do not display any S100P staining, however it seems that using immunofluorescence as a tool for S100P staining is insufficient, as the intensity of S100P staining does not correlate to what is known regarding the level of S100P in the inducible cell line HeLa A3.

To further study this discrepancy, subcellular fractionation was carried out. Subcellular fractionation is a technique that has been utilised to characterise a number of proteins, including smoothelin, a cytoskeletal protein exclusive to smooth muscle cells (Van der Loop *et al.* 1996). Subcellular fractionation has also recently been utilised by Jana *et al.* (2020) in establishing the cellular localisation

of Atox1, a 7.4 kDa protein involved in copper homeostasis in colorectal cancer. Such studies suggest that subcellular fractionation is a valid methodology for characterisation of cellular localisation of proteins, including low molecular weight proteins. Subcellular fractionation by differential centrifugation was performed both in trophoblast cell lines endogenously expressing S100P (JEG-3, BeWo and MDA-MB-231) and in COS-7 s10 and HeLa A3 cells that were engineered to have regulatable levels of S100P expression. In addition, it was possible to assess S100P localisation in HTR8 cells that have been stably transfected with S100P, producing a variety of cell clones that express a different level of S100P.

Fractionation of all cell lines (JEG-3, BeWo, MDA-MB-231, COS-7 s10+, HeLa A3+ and HTR8 clones) into their cellular compartments (a cytoplasm and membrane fraction, and a nuclear fraction) showed undoubtably that S100P is solely localised to the cytoplasm and membrane fraction, with S100P being virtually undetectable in nuclear fractions. This data was confirmed by densitometry analysis with respect to various marker proteins, namely tubulin, lamin A/C and HDAC2. It was interesting to note that HDAC2 present within the nuclear fractions of all cell lines was observed to generate a slightly higher band than in the total cell lysates. This could be due to its phosphorylation state within the nucleus, as previous studies have shown *in vivo* phosphorylation of HDAC2 in HeLa cells (Galasinski *et al.* 2002).

This data concerning S100P localisation is much at odds with many previously published studies (see table 3.1.1), however this is the first time the localisation of S100P has been studied using a biochemical fractionation technique rather than immunohistochemistry or immunofluorescence. One such study is that of Dowen *et al.* (2005), who demonstrated the presence of S100P in the nucleus and cytoplasm of HeLa cells using immunofluorescence, but also showed colocalisation of S100P and S100PBPR (S100P binding protein) within the nucleus. S100PBPR was characterised by Dowen *et al.* (2005) as a novel S100P binding partner, and was shown to be localised solely to the nuclei of HeLa cells transfected with GFP-tagged S100PBPR. A nuclear localisation of S100P would suggest it has a role in the activation of transcription factors to regulate gene expression, however nuclear S100P has not been reported to bind to any nuclear transcription factors as of yet, nor is it believed to actively regulate the expression of genes/proteins in highly overexpressing cell model systems (personal communications with P. Rudland and R. Barraclough, Liverpool University); only extracellular S100P binding to RAGE has been shown to activate NFκB (Arumugam *et al.* 2004).

Assessment of the localisation of S100PBP was also undertaken using subcellular fractionation, in order to observe similarities or differences in localisation between the immunofluorescence data obtained by Dowen *et al.* (2005) and further confirm the specificity of the biochemical assay utilised within these

studies. This work was carried out using trophoblast cell lines JEG-3 and BeWo. The predominantly nuclear localisation of S100PBP reported by Dowen *et al.* (2005) in HeLa cells was also found to be true in both JEG-3 and BeWo cells, although interestingly JEG-3 cells seemed to contain a higher nuclear to cytoplasmic ratio of S100PBP than BeWo cells. Purity of the JEG-3 and BeWo fractions, as assessed by presence of lamin A/C and tubulin within each cell fraction, were similar to each other, suggesting differences in fraction purity may not be the cause for such differences in the nuclear to cytoplasmic ratio of S100PBP between both cell lines.

There are very few papers assessing the localisation of S100PBP, however Clawson *et al.* (2017) assessed its localisation in macrophage-tumour cell fusions isolated from the blood of patients with pancreatic ductal adenocarcinoma, and detected S100PBP in both nuclear and cytoplasmic regions using immunofluorescence. This perhaps suggests a differential localisation of S100PBP dependent on cell or tissue type. Regardless, S100PBP was found to be predominantly nuclear in both JEG-3 and BeWo cells when using a biochemical technique such as subcellular fractionation. The soluble nature of the S100PBP protein suggests that subcellular fractionation is a viable technique for studying protein localisation.

S100P is a protein containing EF hands that bind calcium ions in order to allow S100P to interact with target proteins. The buffer used in Dounce homogeniser-based fractionation assays utilises EDTA and EGTA, which are calcium chelators. It was thought that the presence of these reagents in the fractionation buffer could be preventing S100P from interacting with target proteins. S100P can form dimers in both the presence and absence of calcium ions (Koltzscher and Gerke,2000), however, it is the binding of calcium ions to the loop regions of S100P that allows a conformational change in the protein to take place, exposing residues involved in target protein interaction. Thus far, all characterised target proteins of S100P bind to S100P in a calcium-dependent manner. For example, Clarke *et al.* (2017) found that chelation of calcium using EGTA completely abrogated binding of S100P to tissue plasminogen activator when measured by surface plasmon resonance. Interaction of S100P with its target proteins could be taking place in a variety of cell compartments, and preventing S100P-protein interactions could have an effect on S100P subcellular localisation. In addition, the intracellular concentration of free calcium has been reported as roughly 100nM, however this number can increase to 1-10µM as a consequence of cellular functions, for example nerve impulse transmission and cell membrane stability (Südhof 2012). Therefore, 5µM calcium chloride-containing buffers were used for fractionation experiments to test the hypothesis that protein interactions can facilitate changes to S100P localisation.

There is the possibility of S100P localisation being a dynamic process within trophoblast cells, as translocation of S100P to different cellular locations has been documented by several others in different cell types, for example binding of S100P to ezrin leads to the recruitment of S100P to the cell periphery in epidermoid carcinomas cells (Koltzscher *et al.* 2003). It is also plausible that the localisation of interacting partners of S100P dictates its own subcellular localisation. The presence of binding partners in the cytoplasm, for example, could stimulate the translocation of S100P from other subcellular locations. In addition, there is a possibility that changes in calcium concentration inside the cell can alter the localisation of S100P, as has been seen in other S100 proteins (Mueller *et al.* 1999). For example, Mandinova *et al.* (1998) found that S100A6 was localised to the nucleus and sarcoplasmic reticulum in vascular smooth muscle cells, in contrast to S100A1 and S100A4 which were mainly localised to the cytosol.

In addition to Dounce homogenisation as a tool to allow further separation of cell components, an alternative assay was also employed to ensure that the specific S100P subcellular localisation seen when using a Dounce homogeniser is not an artefact of the assay. NP-40 is a non-ionic and non-denaturing detergent that lyses cell membranes, and has been used to fractionate cells and tissues in other studies (Rosner and Hengstschlager 2008, Holden and Horton 2009). These particular studies have utilised NP-40 at a concentration of 1%, however it was decided that the optimal final concentration of NP-40 should be low (0.5%) to prevent any rupture of nuclear membranes and the release of nuclear proteins into the cytosol. Following either the inclusion of 5µM calcium chloride or NP-40 detergent for cell lysis, it is apparent that S100P is still localised to the cytoplasm and membrane fraction, with only trace levels attributed to contamination present within cell nuclei. In addition, the methodology of fractionation with NP-40 can lead to increased background, as demonstrated by the increased levels of tubulin within the isolated nuclear fraction of HeLa cells fractionated with 0.5% NP-40. This may be due to the fact that a low final concentration of NP-40 may not lyse all cells, leading to whole cells being pelleted along with nuclei. This again is most likely responsible for S100P detected within the nuclear fraction of cells fractionated using this method. Despite the number of sources utilising NP-40 within their fractionation experiments, there is little in the literature about its use in determining the localisation of low molecular weight proteins. However, Kimberly *et al.* (2001) were able to detect a small, 8kDa fragment of the β-amyloid precursor protein (APP) in nuclear extracts using 0.1% NP-40, in addition to detecting a 6kDa fragment of the same protein within a membrane extract using the same methodology. These results suggest using low concentrations of NP-40 for subcellular fractionation assays is sufficient to determine the subcellular localisation of low molecular weight proteins.

In addition to immunofluorescence and immunohistochemical analysis, several studies have demonstrated the localisation of S100P using a GFP-tagged fusion protein. Rehbein *et al.* (2008) stably transfected lung adenocarcinoma cells with S100P that had been tagged with GFP on its N-terminus, as did Koltzscher *et al.* (2003), who transfected epidermoid carcinoma cells with a S100P fusion protein tagged in the same manner. A recently published paper by Du *et al.* (2020) utilises a YFP-S100P (Yellow Fluorescent Protein-S100P) fusion protein within COS-7 cells, in which its clear nuclear and perinuclear localisation can be observed by immunofluorescence.

GFP has long been utilised as a fusion tag to monitor protein localisation (Tsien, 1998), ideally maintaining the localisation and function of the protein of interest. However, it is worth mentioning that GFP, at 26.9kDa, is over twice as large as S100P which is 10.4kDa, and therefore it is conceivable to think that tagging S100P with GFP may alter its subcellular localisation. There is a need to validate if the presence of a GFP tag will alter S100P's subcellular localisation, which can be achieved through a combination of techniques. Results from this chapter suggest that the addition of a fluorescent tag, such as YFP, to the N-terminus of S100P can disturb its subcellular localisation. Tagging of proteins with fluorescent tags generates fusion proteins; these proteins, naturally, are different from their native conformation and could therefore have several effects on the tagged protein, including but not limited to impaired activity or loss of binding partners (Weill *et al.* 2019). In addition, the location of the fluorescent tag on the protein can also affect function and localisation. Disruption of protein localisation due to the addition of fluorescent tags has previously been documented by Cui *et al.* (2016), who show the incorrect localisation of protein EMP12 from *Arabidopsis* due to the addition of a GFP tag. All in all, the data produced in this chapter demonstrates that a fluorescent tag, such as YFP, can alter the localisation of the S100P protein, potentially due to its small size.

With results from this chapter leading to the conclusion that S100P is only present within the cytoplasm and membrane of cell lines JEG-3, BeWo, COS-7 s10+, HeLa A3+ and HTR8, it was deemed necessary to show that S100P is not being exported out of the nucleus during the process of fractionation. Nuclear export receptors known as exportins are required for active transport of molecules across the nuclear envelope into the cytoplasm. The most well-known exportin is exportin 1, otherwise known as CRM1, which recognises leucine-rich NESs on the protein cargo, allowing binding and facilitating nuclear export (Kudo *et al.* 1999).

To assess if S100P is being actively transported out of the nucleus, Leptomycin B (LMB) was utilised as an inhibitor of this type of nuclear transport. LMB is a potent antibiotic produced by *Streptomyces*, whose role in nuclear export was first studied by Wolff, Sanglier and Wang (1997), and was found to block the nuclear export of Rev, a HIV-1 regulatory protein. LMB has been demonstrated to block the

nuclear export of a several of different proteins, including but not limited to CYFIP2 (Jackson *et al.* 2007), IκBα (Castro-Alcaraz *et al.* 2002), and paxillin (Burgess and Gray 2012).

Fornerod *et al.* (1997) showed that LMB directly interacts with CRM1, however the mechanism of action behind this inhibition was not clear until Kudo *et al.* (1999) described a *S. pombe* mutant which showed very high resistance to LMB. This mutant contained a single amino acid change at cysteine residue 529 in CRM1 that is near to CRM1's cargo-binding domain. This mutation allowed the conference of resistance to LMB on the wild type a *S. pombe.* As a consequence, the alteration of this sole amino acid residue at position 529 was found to be solely responsible for the interaction between LMB and CRM1, which has the effect of preventing the association of CRM1 with a NES-containing cargo protein, therefore blocking nuclear export.

As mentioned, active nucleocytoplasmic shuttling of proteins depends on specific localisation sequences within the protein. S100P does not contain a nuclear localisation sequence (NLS) or a nuclear export signal (NES). Most cargoes that bind to CRM1 contain a NES, however there are exceptions; it was found that the 60S ribosomal subunit expressed in yeast instead binds to an adapter protein containing a NES rather than containing its own NES (Hung *et al.* 2008).

Following the prevention of active nucleocytoplasmic shuttling using LMB, cell lines were fractionated and assessed for their presence of S100P in the different cellular compartments. The localisation of paxillin was also determined, as Burgess and Gray (2012) found that following treatment with LMB, paxillin is found at a high level in the nucleus of HeLa cells compared to the untreated counterparts. Paxillin was therefore used as a tool to assess that LMB was working as previously documented.

Densitometry analysis of LMB treated fractions in comparison to their untreated controls allowed for the determination of S100P localisation in different cell lines, and whether S100P as a protein is a target of LMB and therefore has the potential to be actively shuttled out of the nucleus during fractionation assays. Treatment with 10ng/ml LMB was sufficient to see the retention of paxillin in the cell nuclei for all cell lines. This is in line with Burgess and Gray (2012), who found that treating HeLa cells with 5ng/ml LMB was sufficient to prevent nuclear export of paxillin. Regardless of treating cell lines with or without LMB, there was no change in the localisation of S100P.

This work has established that S100P is not exported from the nucleus in a CRM1-dependent manner. LMB has so far only been found to interact with CRM1, and CRM1 is the only export receptor yet to be inhibited, thus experimental identification of receptors involved in nuclear protein export is limited.

Nuclear transport of proteins through the use of nuclear import/export receptors falls under the category of active transport. LMB is capable of blocking active transport through blockade of such

receptors, however there is still potential for S100P to passively diffuse out of the nucleus without the need for a transport receptor. Passive nuclear diffusion, however, is bidirectional in nature (Kumeta *et al.* 2012). If S100P were to passively diffuse out of the nucleus, it would be expected that S100P could also passively diffuse into the nucleus, due to the bidirectionality of passive transport through nuclear pore complexes, and reach a dynamic equilibrium.

In conclusion, the data obtained through this chapter suggests that S100P can be detected in cytoplasmic and membrane fractions in all cell lines, regardless of S100P expression level or through prevention of active nucleocytoplasmic shuttling.

Chapter 4:

The role of S100P and membrane-associated S100P in invasion and motility of trophoblasts

Chapter 4: The role of S100P and membrane-associated S100P in invasion and motility of trophoblasts

Contents

4.1 Introduction

S100P has been shown to promote motility and invasion in a large spectrum of cell types, but principally in disease states (Whiteman *et al.* 2007; Hsu *et al.* 2015, see section 1.1.2.5). However, the molecular mechanisms behind both cellular migration and invasion remain unknown. In the context of cells from a malignant background, prior research has suggested that interaction of S100P with a variety of target proteins is at least in part responsible for these processes, as presented in section 1.1.2.5. For example, Du *et al.* (2012) report that interaction of S100P with nonmuscle myosin IIA (NMIIA) in HeLa cells leads to redistribution of NMIIA and subsequent reduction in the levels of focal adhesion sites formed, leading to increases in cellular motility. Reduction of cellular invasion of pancreatic cancer cell lines has been reported by Arumugam, Ramachandran and Logsdon (2006) through blocking the interaction of S100P with RAGE by use of an anti-allergy drug, cromolyn. We have recently further demonstrated, for the first time, a role for S100P in promoting cellular motility and invasion in a non-pathophysiological background, in that of trophoblasts of the placenta, but little is known about the molecular pathways involved.

Motility and invasion of a subset of cells present within the placenta, extravillous trophoblasts (EVTs), is required for the establishment of the blood supply from mother to foetus through invasion of the primed maternal endometrium, known as decidua. Remodelling and reorganisation of the maternal spiral arteries by EVTs to a reduced resistance state leads to increased blood flow to the foetus, allowing unrestricted growth of the foetus (Ji *et al.* 2013). Absence or obstruction of these processes are believed to lead to pathologies including intrauterine growth restriction (IUGR) and preeclampsia. Zhu *et al.* (2015a) found reduced expression of S100P in first trimester placenta obtained from patients with spontaneous abortion, further suggesting a role for S100P in placental development. We have also shown that S100P is a key regulator of both motility and invasion in trophoblast cells (Tabrizi *et al.* 2018) but the clear mechanisms behind this process are lacking and need further analysis.

The subcellular localisation of S100P within cell lines of both malignant (HeLa, JEG-3, BeWo) and normal physiological backgrounds (COS-7, HTR8) was previously established by utilising a biochemical assay known as subcellular fractionation (Chapter 3). Results established the sole presence of S100P within cytoplasm/membrane fractions of all cell lines studied, regardless of their origin or of alterations to the assay. Much of the literature focuses on either the nuclear or cytoplasmic localisation of the S100P protein, however there is a dearth of literature concerning potential membrane localisation of this protein. One study by Sato and Hitomi (2002) has reported the presence of S100P in the cell membrane and cytoplasm in normal human oesophageal epithelium through the use of immunohistochemistry. As previous fractionation experiments led to isolation of cytoplasm and

membrane cellular compartments in tandem (Chapter 3), it was necessary to fully isolate purified plasma membrane from all cell lines studied to assess its specific localisation in the plasma membrane alone.

In this chapter, we aim to investigate whether S100P is associated with the plasma membrane in a variety of cell lines (either expressing endogenous S100P or stably transfected cell lines) through the use of biochemical isolation by sucrose density gradient and biotinylation studies. We also shed new light on the consequences of S100P localisation at the membrane on cellular motility and invasion, and the molecular mechanisms at play behind these processes. In addition, we aim to explore expression and plasma membrane localisation of S100P in primary first trimester extravillous trophoblasts (EVTs), and establish if elements of the S100P structure suggest how S100P may come to be associated with the plasma membrane.

4.2 Results

4.2.1 S100P is detected within the isolated plasma membrane fractions of cell lines

Many studies have assessed the specific physiological localisation of S100P using a variety of techniques (see Table 3.1.1). However, the presence of S100P within the plasma membrane of various cell types has yet to be fully assessed and has not been discussed within the scientific literature. As previous fractionation experiments led to isolation of cytoplasm and membrane cellular compartments in tandem (Chapter 3), it was necessary to establish a different methodology to fully isolate purified plasma membrane from all cell lines studied to assess its specific localisation.

To achieve this aim, plasma membrane fractions of cells were isolated using nitrogen cavitation and a sucrose cushion, followed by SDS-PAGE western blotting to assess the presence of S100P within these fractions (Figure 4.3.1). In a similar fashion to Chapter 3, it was necessary to utilise marker antibodies to confirm the correct isolation of the plasma membrane with minimal contamination with proteins from other cell compartments. To this end, Caveolin I was used as a marker for the plasma membrane fractions. Caveolin I is a scaffolding protein that is a component of caveolae; these are invaginations of the cell membrane that form in many processes, and are important sites in many cell regulatory processes such as endocytosis (Codrici *et al.* 2018). Tubulin was once again used as a marker for cytoplasmic proteins, in order to detect the presence of any contaminating proteins within the plasma membrane fraction which could lead to the generation of a false signal for S100P (Vanli *et al.* 2017).

Following western blotting of total cell lysates and isolated plasma membrane fractions from JEG-3, BeWo, MDA-MB-231, HTR8 Clone 7, COS-7 s10+ and HeLa A3+ cell lines, caveolin I was found to be significantly enriched in all isolated plasma membrane fractions compared to their relative total cell lysates, confirming the appropriate isolation of plasma membrane (Figure 4.2.1, panel A). In addition, tubulin was detected at very low levels in each isolated plasma membrane fraction compared to their relative cell lysates, demonstrating little to no cytoplasmic contamination of plasma membrane fractions. When studying the levels of S100P detected in these six cell lines, it was observed that the majority of cellular S100P was detected in total cell lysates, comprising of both cytoplasmic and nuclear compartments. However, presence of S100P was also observed in isolated plasma membrane fractions in all cell lines studied, as each of these fractions exhibited a clear band for S100P. Interestingly, S100P detected in the plasma membrane fractions of all cell lines appears to run slightly slower on the gel than S100P detected in total cell lysates.

In a bid to quantify relative S100P levels in isolated plasma membrane fractions, the raw densities of both S100P and tubulin obtained in either total cell lysates or isolated membrane fractions were taken and the ratio of S100P to tubulin in either the total cell lysate or the isolated membrane fractions were calculated. Finally, the fold difference between membrane signal versus total cell lysate signal was calculated (Figure 4.2.1, panel B).

All cell lines demonstrated an increased ratio of S100P to tubulin in the membrane fractions compared to the relative ratio of the two proteins in their respective cell lysates, of which the fold change is reported in Figure 4.2.1, panel B. This data suggests that S100P detected within isolated membrane fractions is due to endogenous S100P localisation, and not contamination of the plasma membrane fraction with cytoplasmic proteins.

A

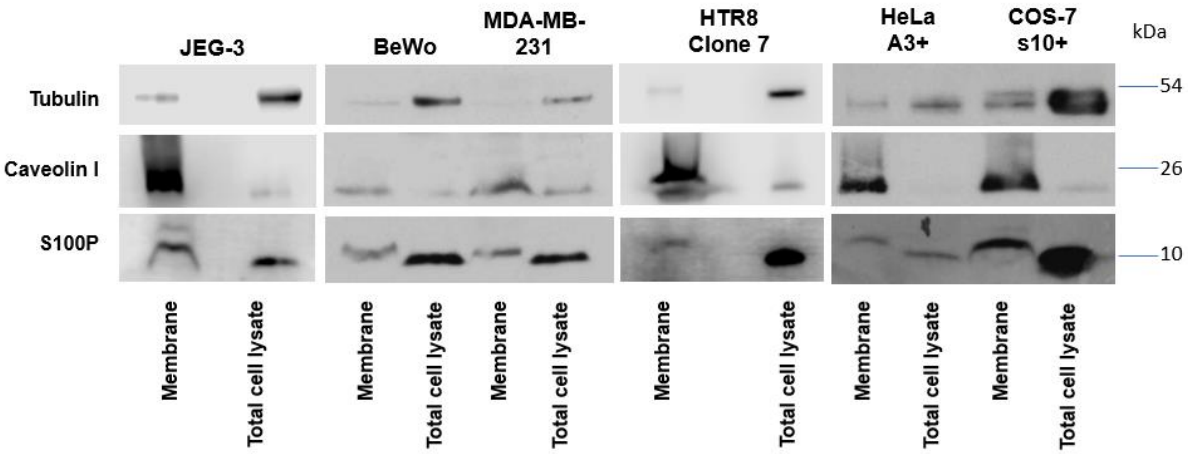

B

Cell line	Ratio of S100P to tubulin in total cell lysate (±SD)	Ratio of S100P to tubulin in membrane (±SD)	Fold increase
JEG-3	1.03	2.97	2.88
BeWo	1.54 (±0.8)	5.57 (±0.02)	3.63
HTR8 Clone 7	4.18 (±1.18)	7.54 (±0.36)	1.80
COS-7 s10+	1.08 (±0.16)	1.54 (±0.08)	1.42
HeLa A3+	0.43	1.13	2.60

Figure 4.2.1: S100P is localised to the plasma membrane fraction of cell lines

A) JEG-3, BeWo, MDA-MB-231, HTR8 Clone 7, HeLa A3+ and COS-7 s10+ cell lines were lysed by nitrogen cavitation, followed by ultracentrifugation to allow separation of the plasma membrane fraction. 10µg and 30µg of total cell lysates and membrane fractions respectively were loaded and run on SDS-PAGE followed by western blotting to detect S100P, plasma membrane marker caveolin I and cytoplasmic marker tubulin within each fraction.

B) Quantification of the ratio of S100P to tubulin in both total cell lysate and membrane samples is presented, in addition to the fold difference between the two ratios calculated. Data represents the mean ±SD from at least 2 independent replicates, apart from JEG-3 and HeLa A3+ where n=1.

Presence of the S100P protein has been demonstrated in various cell lines by western blotting, including those of trophoblast origin. In addition, previous immunohistochemistry studies have illustrated high levels of S100P in first trimester placental tissue, with levels of S100P expression at their highest levels within first trimester placenta and decreasing in expression throughout gestation (Tabrizi *et al.* 2018). Therefore, we wanted to assess the potential membrane presence of S100P within *in vivo* samples. To this end, matched and serial first trimester placental tissue slices were stained for HLA-G and S100P, and images were studied for colocalisation of these two proteins. HLA-G is a protein that is highly expressed in extravillous trophoblast placental membranes (Patel *et al.* 2003), and is therefore an appropriate marker to assess presence of S100P within the plasma membrane of this cell subset of the placenta. This work was carried out by Ms Maral Tabrizi. A representative image of an anchoring villi from stained first trimester placental tissue slices is presented in figure 4.2.2. The presence of HLA-G denotes extravillous trophoblasts.

ImageJ software was utilised to study the colocalisation of HLA-G and S100P at the cell membrane, using the plot profile function. Matched images were taken and a region of interest was drawn across cell membranes for both images. The region of interest for both HLA-G and S100P images was of the same size to allow for correct matching (Figure 4.2.3, panel A). The gray value of the pixels in the selected region of interest was measured for both HLA-G and S100P, and could therefore be plotted versus the length of the region of interest. A higher gray value (on a scale of 0 to 255) designates white pixels, whereas a grey value of 0 pertains to black pixels. Therefore, the lower the gray value, the darker the pixel at the selected region of interest, and therefore the more intense the staining. The midpoint of the region of interest was always selected to be the cell membrane of the cells to allow for quantification, and therefore the mid-point on the graph pertains to the cell membrane (Figure 4.2.3, panel B).

Measurements of multiple regions of interest were taken using at least 3 different matched slices, and at least 30 cells, the totality of which is summarised in figure 4.2.4. Results from this colocalisation analysis using immunostained first trimester placental tissue confirms the presence of HLA-G at the cell membrane in anchoring villi. In addition, the analysis demonstrates the presence of S100P in the cell membrane of EVT cells, colocalising with HLA-G expressed by this cell subset.

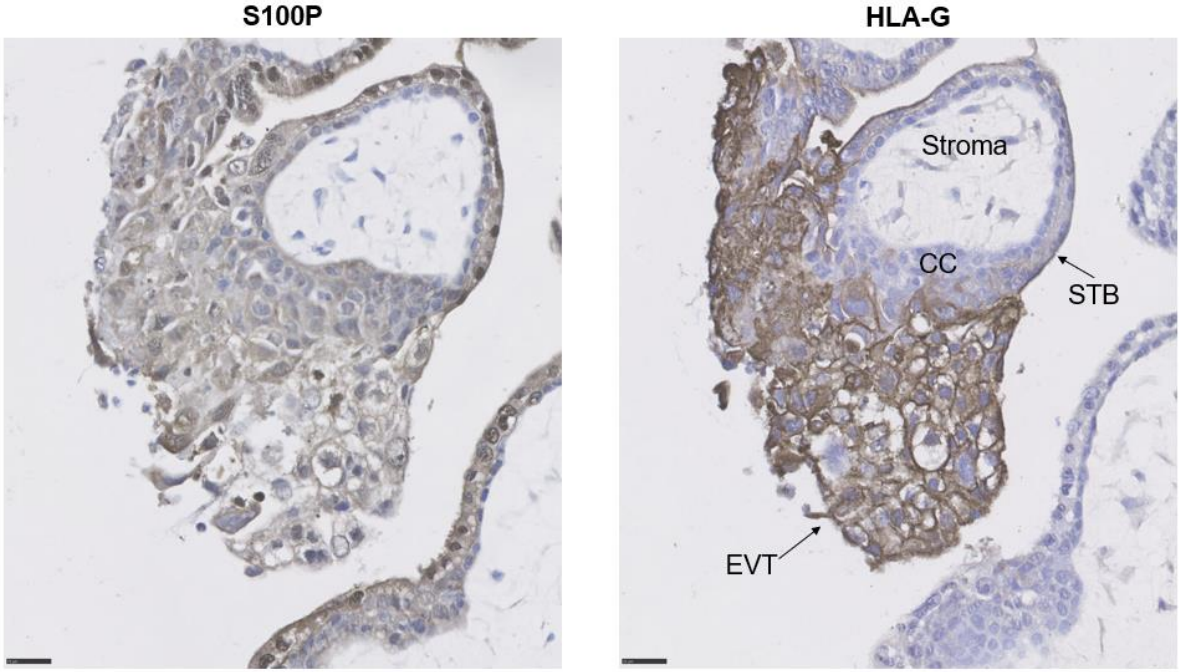

Figure 4.2.2: HLA-G and S100P are expressed by extravillous trophoblasts within first trimester placental tissue

Matched immunohistochemical staining of S100P and HLA-G within first trimester placental tissue.

Scale bar = 25µM. *CC,* cytotrophoblast columns; *EVT,* extravillous trophoblasts; *STB,* syncytiotrophoblasts. This work was carried out by Ms Maral Tabrizi.

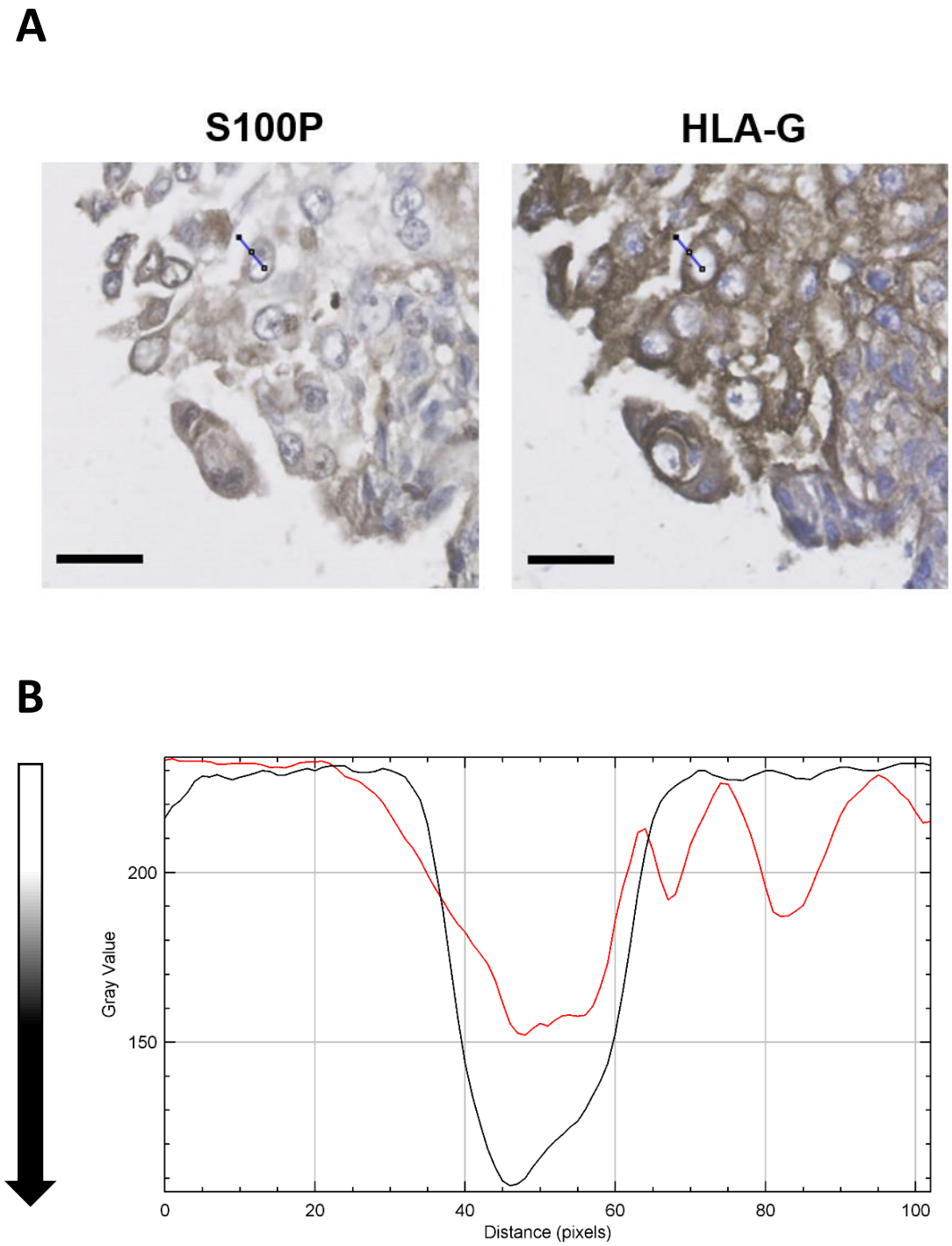

Figure 4.2.3: S100P and HLA-G colocalise at the plasma membrane in placental sections.

A) Matched slices of placental tissue were stained for HLA-G and S100P. Regions of interest were drawn (blue line) to allow for analysis of membrane localisation of S100P, using HLA-G as a marker. Scale = 25µM. This work was carried out by Ms Maral Tabrizi.

B) Representative example of the graphical output from ImageJ of the region of interest, displaying the gray value of the pixels plotted against the length of the region of interest for both HLA-G (black) and S100P (red).

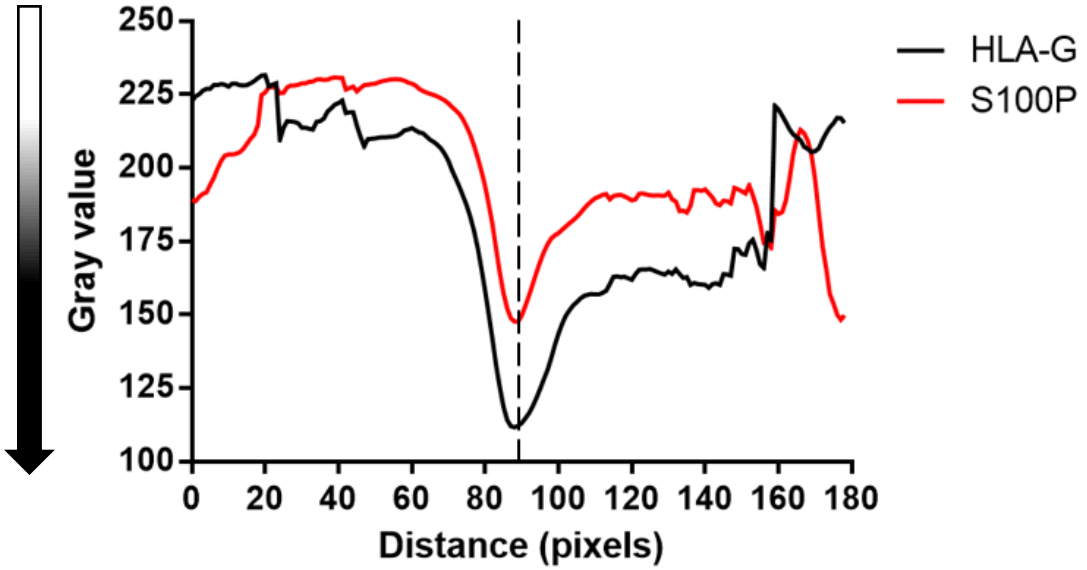

Figure 4.2.4: S100P and HLA-G colocalise at the plasma membrane in placental sections.

A graphical summary of HLA-G (black) and S100P (red) colocalisation at the plasma membrane. Over 30 cells were examined using 3 different matched samples for their membrane localisation of S100P. The midpoint of the graph (at which the region of interest crosses the plasma membrane) is marked by a dotted line.

To further confirm the presence of S100P within the cell surface/plasma membrane, samples containing cell surface proteins were isolated using a commercial kit (Pierce Cell Surface Isolation Kit). This kit contains a form of cell-impermeable, cleavable biotin (Sulfo-NHS-SS-Biotin) which allows for the labelling of molecules present on the cell surface (Jang and Hanash 2003). Cell lines JEG-3, BeWo, HTR8 clone 7, COS-7 s10+ and HeLa A3+ were subjected to biotinylation prior to running alongside total cell lysates on a 16% (w/v) SDS-PAGE and western blotting for S100P.

The resulting western blots for S100P demonstrate the presence of S100P within the biotinylated samples (figure 4.2.5) for all cell lines with the presence of S100P being seen in different forms. Bands were detected at roughly 17kDa in JEG-3 and HeLa A3+ biotinylated samples, and a band at roughly 40kDa was detected in the BeWo biotinylated sample. The COS-7 s10+ cell line, in contrast to every other cell line, exhibited more than two bands for S100P in the biotinylated sample.

To highlight potential differences in cell surface localisation of S100P between cell lines, we sought to compare the density of the S100P band obtained in the biotinylated sample with the S100P band obtained in their respective total cell lysates (Figure 4.2.6). For analysis purposes, densities of the 10kDa bands alone were taken, as these were present in all cell lines.

Interestingly, the JEG-3, BeWo and HTR8 clone 7 trophoblast cell lines demonstrated remarkably similar levels of S100P within their biotinylated membrane extracts when compared to their relative total cell lysates, at a level of over 13-16%.

The densities of the 10kDa S100P band detected in biotinylated samples from HeLa A3+ and COS-7 s10+ cell lines were at 45% and 59%, respectively, of the level of their respective total cell lysates, suggesting a greater presence of cell surface S100P in these cell lines when compared to endogenously expressing trophoblast cells. This is also in line with figure 4.2.1, in which the inducible cell lines seem to demonstrate higher levels of S100P present within their isolated plasma membrane fractions.

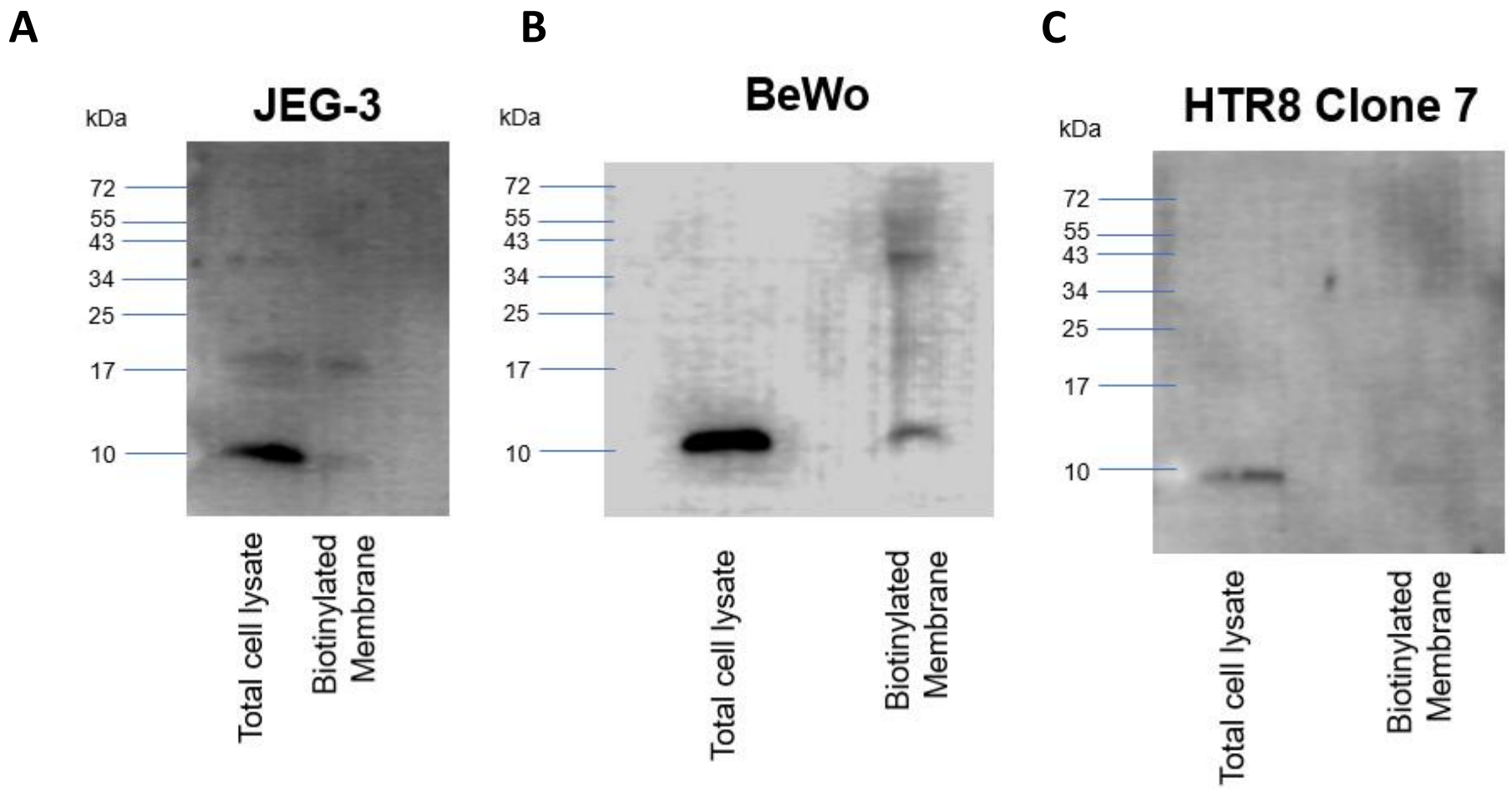
A
JEG-3
kDa
72
55
43
34
25
17
10
Total cell lysate
Biotinylated Membrane
B
BeWo
kDa
72
55
43
34
25
17
10
Total cell lysate
Biotinylated Membrane
C
HTR8 Clone 7
kDa
72
55
43
34
25
17
10
Total cell lysate
Biotinylated Membrane

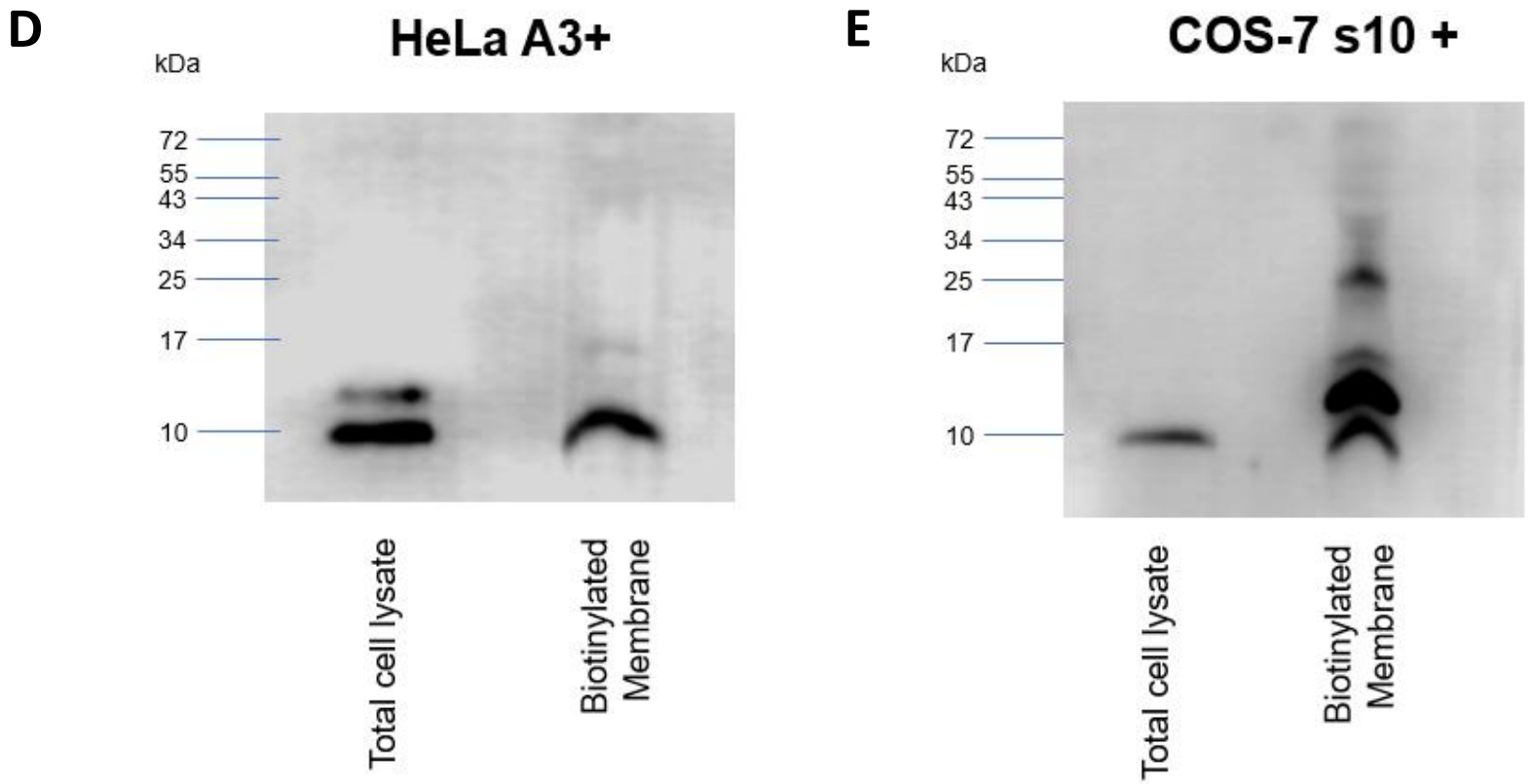

Figure 4.2.5: Biotinylation experiments using the Pierce Cell Surface isolation kit reveal S100P can be detected at the cell surface

JEG-3 (A), BeWo (B), HTR8 Clone 7 (C), HeLa A3+ (D) and COS-7 s10+ (E) cell lines were biotinylated using the Pierce Cell Surface Isolation Kit according to the manufacturer's instructions, and 1/10th of the final eluted volume was loaded and run on 16% (w/v) SDS-PAGE, alongside their respective total cell lysates, followed by western blotting to detect S100P.

A

Cell line	Density of total cell lysate band (% ±SD)	Density of biotinylated membrane band (% ±SD)
JEG-3	100 (±4.78)	15.8 (±4.3)
BeWo	100 (±2.07)	13.54 (±1.18)
HTR8 clone 7	100	15.45
COS-7 s10+	100 (±3.92)	58.93 (±25.24)
HeLa A3+	100 (±5.85)	45.22 (±18.01)

B

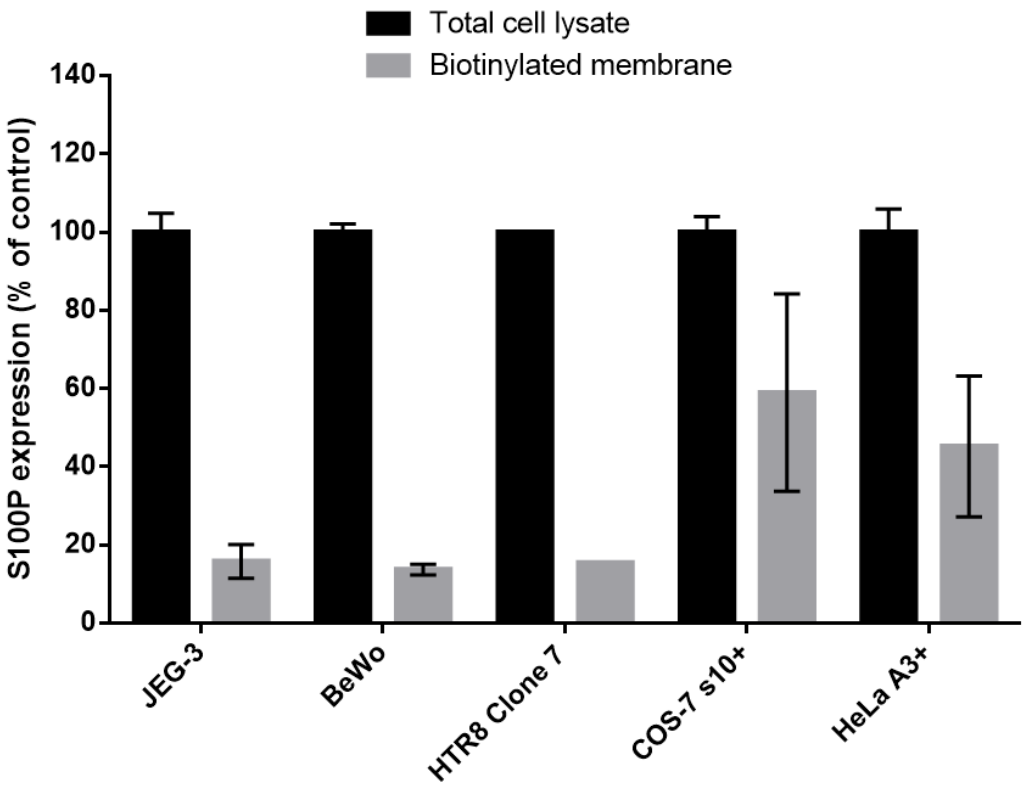

Figure 4.2.6: Comparison of signal densities between total cell lysates and biotinylated membrane samples for multiple cell lines

A) Densities calculated by Image Studio Lite for either total cell lysates or biotinylated membranes from either JEG-3, BeWo, HTR8 clone 7, COS-7 s10+ or HeLa A3+ cell lines were compared to calculate the percentage of signal detected for the biotinylated membranes against their respective total cell lysates. Data represents the mean ±SD from at least 2 independent replicates, apart from HTR8 clone 7 where n=1.

B) Average densities of total cell lysates and biotinylated membranes presented as a percentage of the control (total cell lysate). Data represents the mean ±SD from at least 2 independent replicates, apart from HTR8 clone 7 where n=1.

An alternative method of assessing cell-surface S100P was attempted; flow cytometry. This is due to the fact that flow cytometry only requires a small number of cells to detect a fluorescent signal, whereas nitrogen cavitation requires many millions of cells. Flow cytometry would therefore allow for high throughput analysis of cell surface S100P.

COS-7 s10 and HeLa A3 cells, both induced and non-induced, were incubated with an antibody to S100P prior to being subjected to flow cytometry (Figures 4.2.7 and 4.2.8). Results from these experiments show that there is generally a small increase in the mean fluorescence intensity (MFI) of cells induced to express S100P to high levels, compared to cells not expressing S100P. Induced COS-7 s10 cells demonstrated a 10% increase in MFI compared to non-induced COS-7 s10 cells, whereas induced HeLa A3 cells demonstrated on average a 8.5% increase in MFI compared to their non-induced counterparts. However, the increase seen in the MFI of induced COS-7 s10 and HeLa A3 cells is not reproducible between experiments, and the secondary antibody used creates a large amount of background that hinders true detection of S100P. The differences in MFI between the induced and non-induced samples is not statistically significant enough in either cell line ($p=0.996$) to consider making flow cytometry the primary method for detecting cell surface S100P.

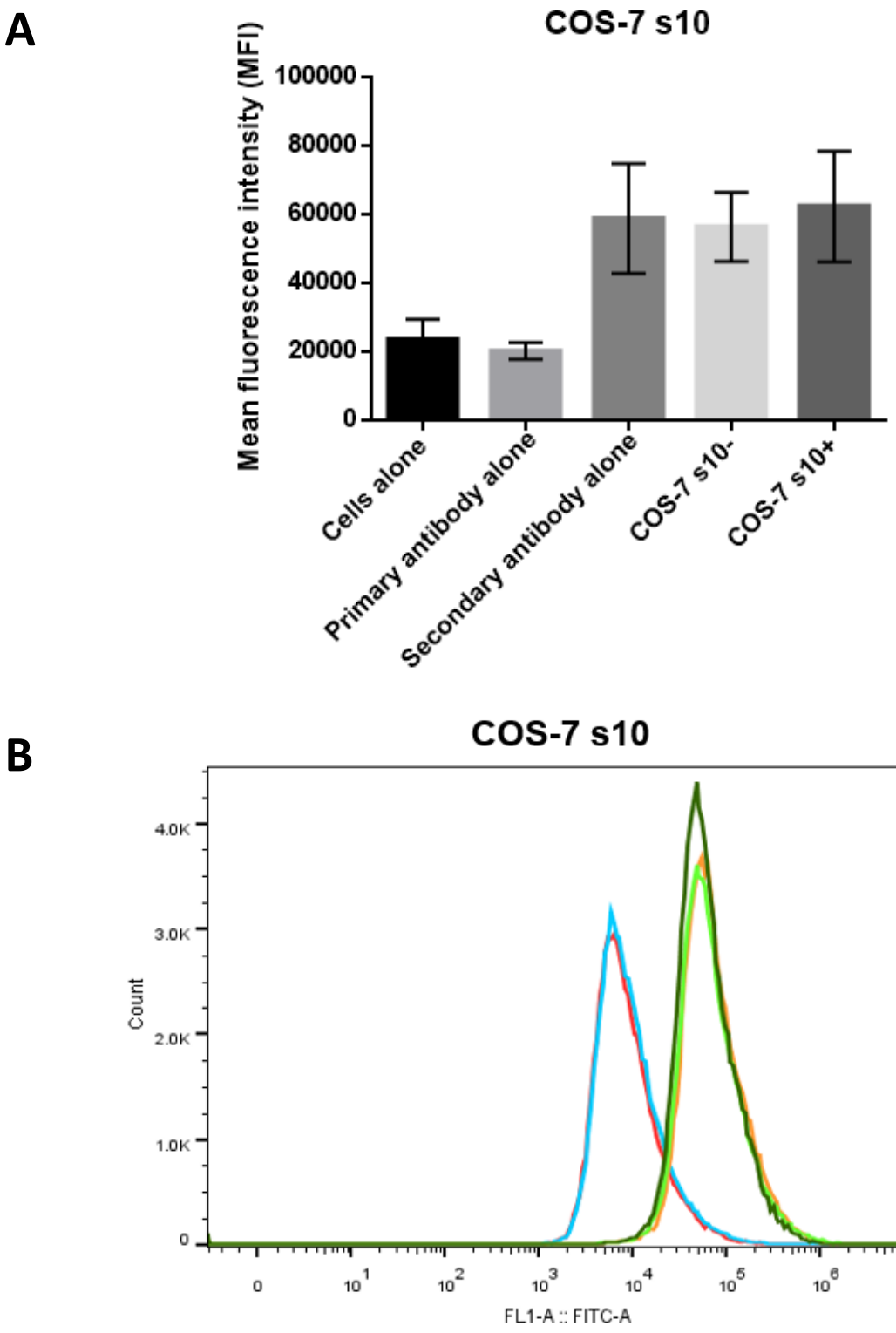

Figure 4.2.7: Cell surface S100P cannot be consistently detected by flow cytometry in COS-7 S10 cells

A) COS-7 s10 cells were subjected to flow cytometry following staining of the cell surface with an antibody to S100P. The mean fluorescence intensity (MFI) was calculated for each condition using FlowJo X software. Data represents ± SEM from 3 independent replicates (one-way ANOVA).

B) Histogram of S100P fluorescence showing cells alone (blue), primary antibody alone (red), secondary antibody alone (orange), non-induced COS-7 s10 cells (dark green) and induced COS-7 s10+ cells (light green).

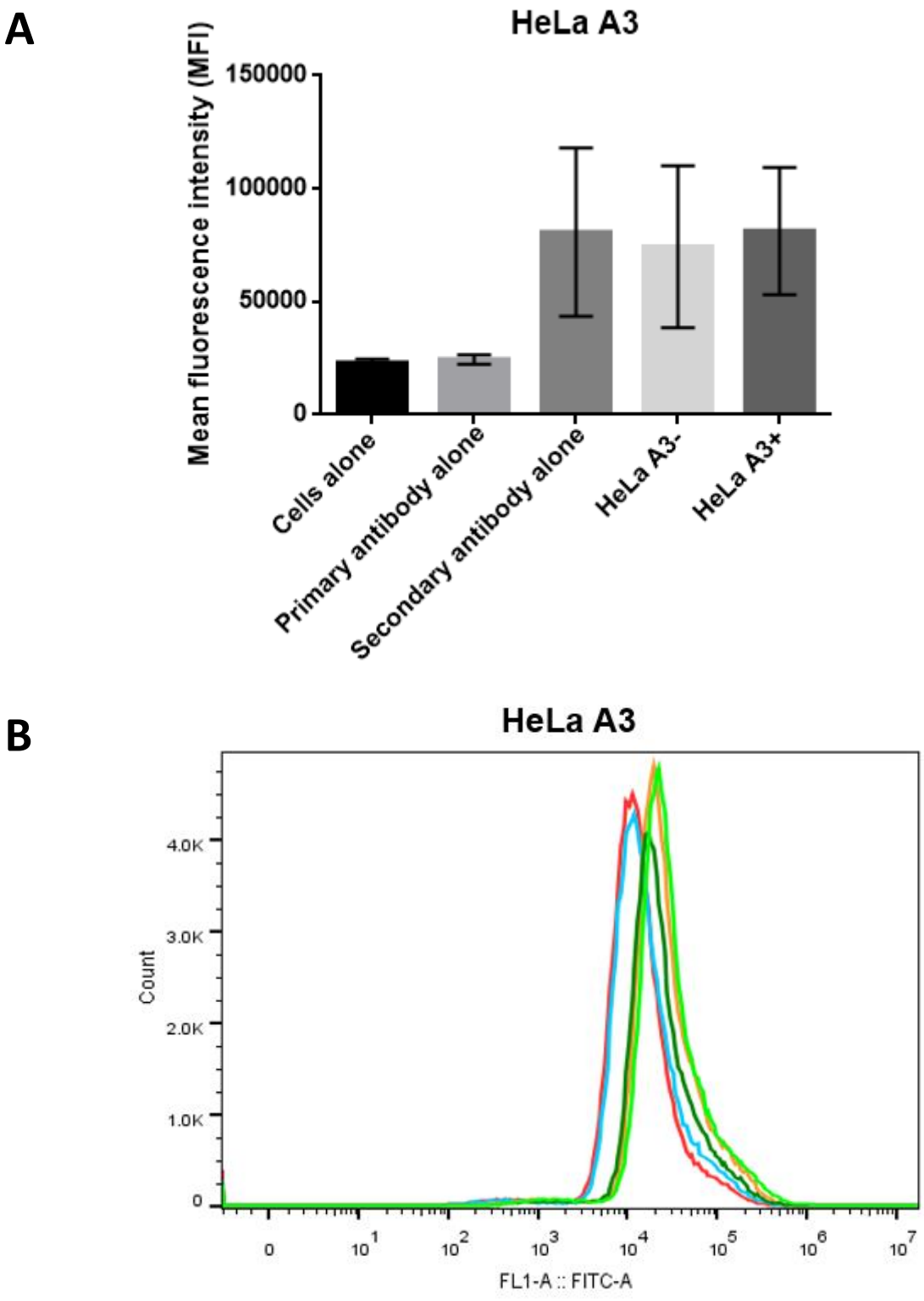

Figure 4.2.8: Cell surface S100P cannot be consistently detected by flow cytometry in HeLa A3 cells

A) HeLa A3 cells were subjected to flow cytometry following staining of the cell surface with an antibody to S100P. The mean fluorescence intensity (MFI) was calculated for each condition using FlowJo X software. Data represents ± SEM from 3 independent replicates (one-way ANOVA).

B) Histogram of S100P fluorescence showing cells alone (blue), primary antibody alone (red), secondary antibody alone (orange), non-induced HeLa A3 cells (dark green) and induced HeLa A3+ cells (light green).

4.2.2 Treatment of JEG-3 cells with an S100P antibody or siRNA technology leads to decreases in migration and invasion

Previously published work has demonstrated that regulation of S100P expression by siRNA treatment significantly reduces both the motility and invasion of trophoblasts (Tabrizi *et al.* 2018). Having shown the presence of S100P at the extracellular membrane surface using a combination of techniques, we wanted to determine if inhibiting cell surface/extracellular S100P had any effect on trophoblast motility or invasion. This work was carried out by Ms Maral Tabrizi.

To this end, JEG-3 cells were subjected to a motility or invasion assay with the addition of the S100P antibody, or an siRNA sequence targeted to S100P to compare levels of motility/invasion inhibition (Figure 4.2.9). Whilst JEG-3 cells treated with goat serum showed no defects in their ability to migrate across a Boyden chamber membrane ($p=0.99$), JEG-3 cells treated with an S100P antibody demonstrated a statistically significant reduction in their migration by 25% ($p=0.0002$). JEG-3 cells treated with an siRNA sequence targeted to S100P, on the other hand, demonstrated an even more significant reduction in their migratory capacity, by almost 65% ($p<0.0001$). In addition, the decrease in migration of JEG-3 cells treated with siRNA was statistically significantly different than migration exhibited by cells treated with the S100P antibody ($p<0.0001$).

A

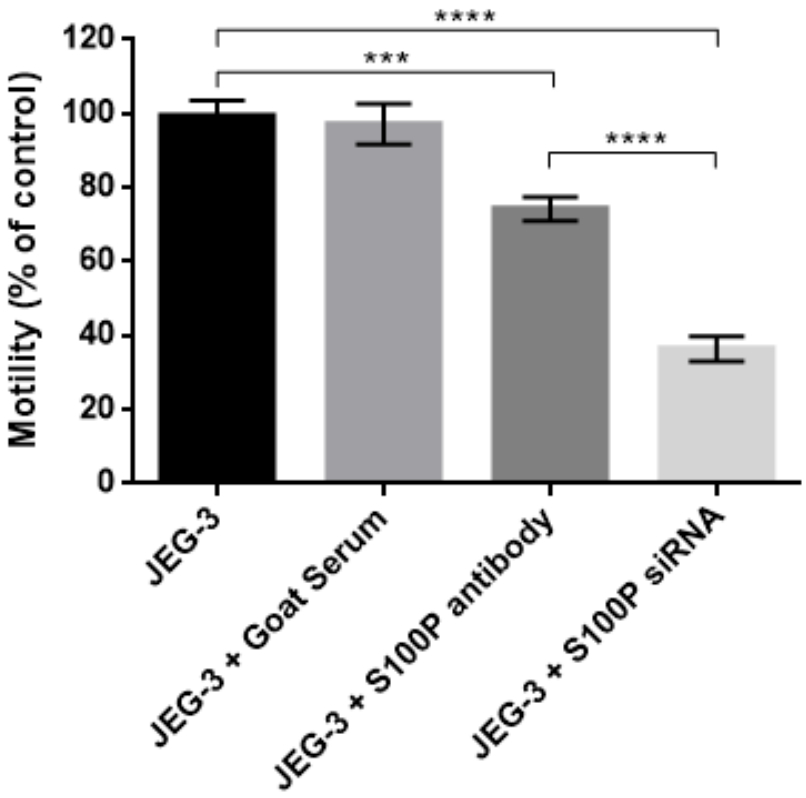

B

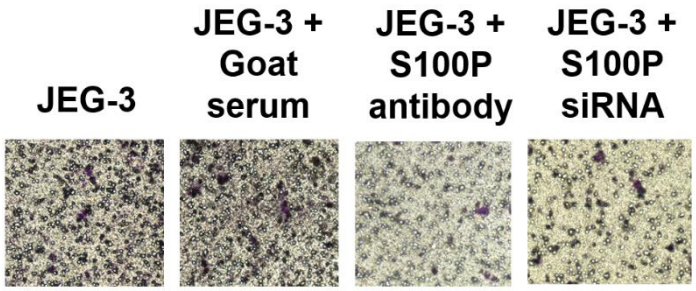

Figure 4.2.9: Treatment with an S100P antibody or siRNA targeted to S100P partially abolishes S100P-dependent migration of JEG-3 cells

A) JEG-3 cells were seeded in triplicate onto Boyden chambers and treated with S100P antibody diluted 1:1000, or with 5nM S100P siRNA. Cells were left to migrate for 24 hours before fixing and staining the transwells. The number of cells migrated per field was counted, for 5 fields per well. Data represents the mean ±SEM from at least 3 independent replicates (one-way ANOVA, **** $p<0.0001$). This work was carried out by Ms Maral Tabrizi.

B) Pictures of one stained transwell per condition were taken at 20x magnification using a Nikon Eclipse TS100 inverted microscope.

The invasive capabilities of JEG-3 cells following S100P antibody or siRNA treatment was also assessed (Figure 4.2.10). Following treatment with a negative control, goat serum, JEG-3 showed no significant changes in their invasion across a Boyden chamber membrane ($p>0.99$). Following treatment with an S100P antibody, JEG-3 cells demonstrated a statistically significant reduction in invasion by 40% ($p<0.0001$). The reduction in JEG-3 invasion was even greater following treatment with siRNA targeted to S100P, in which invasion was reduced by 70% ($p<0.0001$). The difference in migration exhibited between siRNA treated JEG-3 cells and S100P antibody treated JEG-3 cells was statistically significantly different ($p=0.0001$).

A

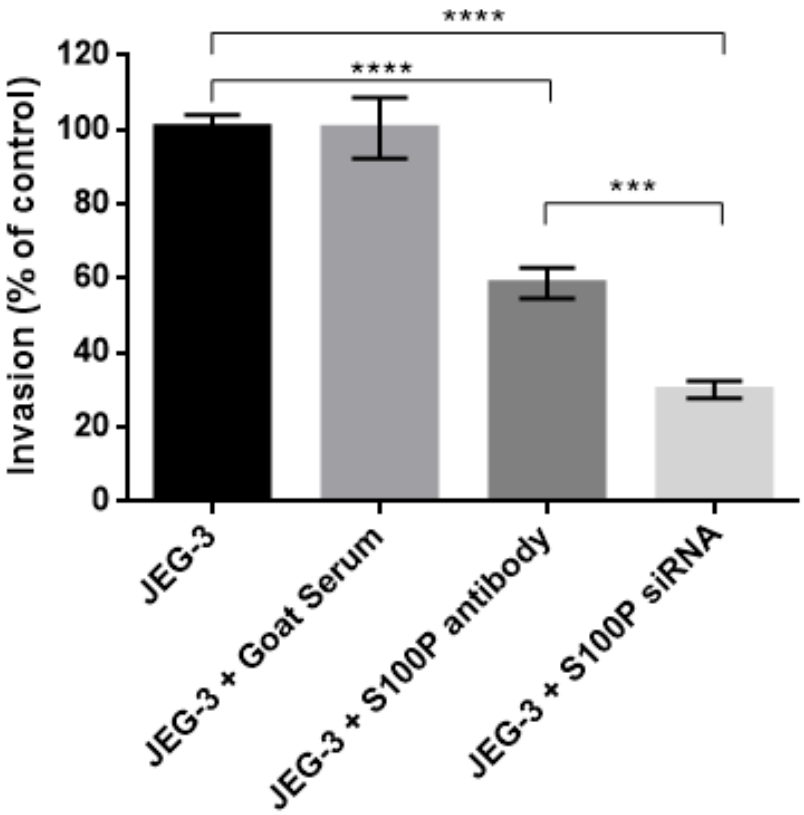

B

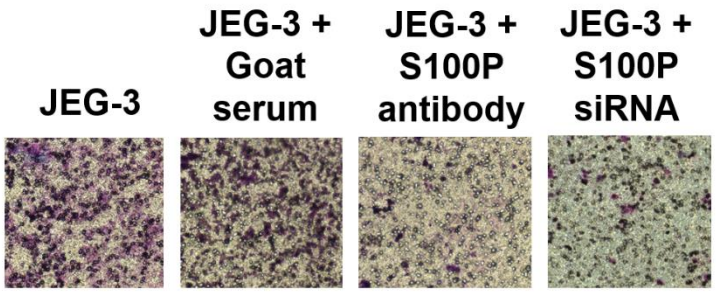

Figure 4.2.10: Treatment with an S100P antibody or siRNA targeted to S100P partially abolishes S100P-dependent invasion of JEG-3 cells

A) JEG-3 cells were seeded in triplicate onto Matrigel-coated Boyden chambers and treated with S100P antibody diluted 1:1000, or with 5nM S100P siRNA. Cells were left to invade for 24 hours before fixing and staining the transwells. The number of cells migrated per field was counted, for 5 fields per well. Data represents the mean ±SEM from at least 3 independent replicates (one-way ANOVA, **** $p<0.0001$). This work was carried out by Ms Maral Tabrizi.

B) Pictures of one stained transwell per condition were taken at 20x magnification using a Nikon Eclipse TS100 inverted microscope.

4.2.3 JEG-3 cells exhibit an increase in focal adhesion formation following treatment with S100P siRNA

Previously published work has demonstrated that regulation of S100P expression by siRNA treatment significantly reduces both the motility and invasion of trophoblasts. Prior to establishing the role of membrane-associated S100P in these processes, it was deemed necessary to explore some of the potential molecular mechanisms behind the reduction seen in motility and invasion. To this end, trophoblast cell line JEG-3 were treated with siRNAs of 2 different sequences that were targeted to S100P (henceforth referred to as siRNA 4 and siRNA 6). Treatment with siRNAs 4 and 6 resulted in a decrease in S100P expression by around 90% in JEG-3 cells (Tabrizi *et al.* 2018) as detected by western blotting for S100P.

Following treatment with siRNA sequences targeted to S100P, cells were fixed and stained with an antibody to paxillin, a marker of focal adhesions, and with rhodamine-phalloidin to visualise F-actin. Focal adhesions are sites at which clusters of membrane-spanning integrins engage with proteins such as fibronectin and vitronectin within the ECM (Turner 2000), providing a structural link to the cytoskeleton. The cytoplasmic tail of integrins can recruit adapter proteins such as paxillin to membrane regions, leading to their phosphorylation by focal adhesion kinase (FAK). Following phosphorylation, paxillin can recruit signalling molecules to activate intracellular pathways involved in restructuration of the actin cytoskeleton, thereby regulating the process of cell migration and attachment (López-Colomé *et al.* 2017). Paxillin can also bind to other adapter proteins, such as vinculin and talin, which upon phosphorylation can bind to F-actin and other components of the cell cytoskeleton.

To quantify the effects of S100P knockdown on focal adhesions, the number of focal adhesions per cell were counted for at least 60 cells for each condition. Control and mock-treated JEG-3 cells were characterised by small, clustered focal adhesions that were mostly localised at the cellular periphery. Upon treating JEG-3 cells with siRNA 4 and 6, cells began to show focal adhesions of an increased size (Figure 4.2.11 panel A). Quantification of the number of focal adhesions present in each cell demonstrated that treatment with either siRNA 4 or 6 generated a significant increase by 77% ($p<0.0001$) and 90% ($p<0.0001$) respectively in the average number of focal adhesions present per cell in comparison to mock-treated or control JEG-3 cells (Figure 4.2.11 panel B). There was no significant difference between the average number of focal adhesions counted per cell between the control and mock conditions ($p=0.37$) or between each of the siRNA treatments ($p=0.49$).

Treatment of JEG-3 cells with siRNA 4 or 6 also resulted in changes to the actin cytoskeleton. Control and mock-treated cells stained with rhodamine phalloidin showed highly motile features, including the presence of a leading edge (otherwise known as lamellipodia). In contrast, cells treated with siRNA 4 or 6 on average did not display these motile features and instead showed the presence of highly organised actin filaments known as stress fibres.

These results establish that reduction of S100P expression by siRNA technology leads to an increase in focal adhesion size and formation by JEG-3 cells, in addition to changes to the actin cytoskeleton suggesting cell motility and migration are inhibited to an extent.

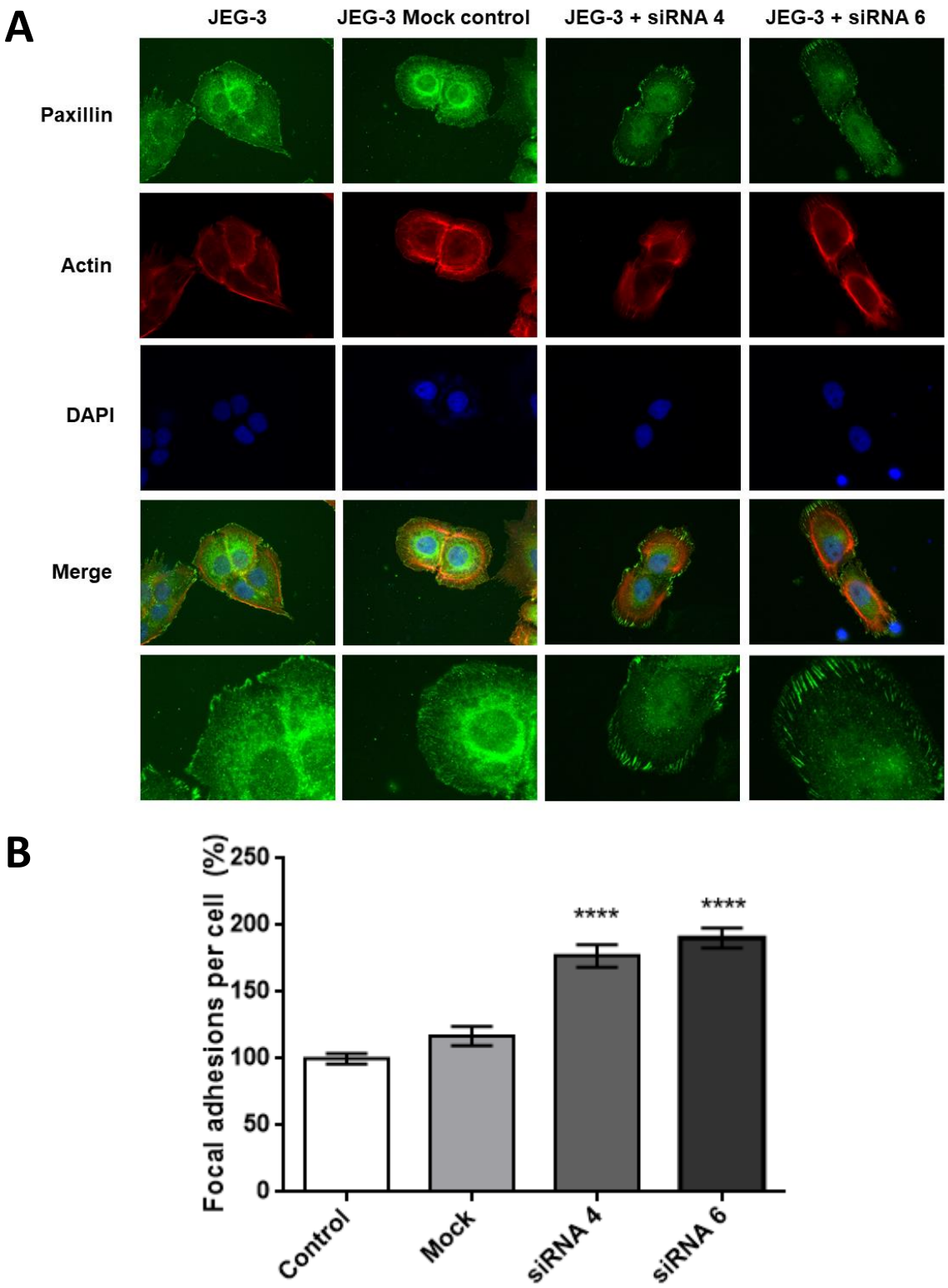

Figure 4.2.11: Knockdown of S100P in JEG-3 cells results in an increased number of focal adhesions per cell

A) JEG-3 cells treated with 5nM siRNA 4 and 6 were grown for 48 hours prior to fixation with 4% (w/v) PFA and permeabilization with 0.1% triton. Cells were stained for focal adhesion marker paxillin and cytoskeletal marker actin, and DAPI to stain nuclei.

B) Average number of focal adhesions containing paxillin per cell, presented as a percentage of the control. Data represents the mean ±SEM from 3 independent replicates (one-way ANOVA, **** $p<0.0001$)

4.2.4 Treatment of EVT-like HTR8/SVneo cells with an S100P antibody partially abolishes S100P-dependent migration and invasion

The results obtained so far demonstrate that S100P can be detected in plasma membrane fractions isolated from six different cell lines (section 4.2.1) and that inhibiting its activity using a specific antibody leads to changes in both cellular motility and invasion in cancer cells, such as choriocarcinoma JEG-3 cells (section 4.2.3) and others (Clarke *et al.* 2017; Ismail *et al.* 2020, submitted). We now wanted to determine if such changes could also be seen in non-cancerous and more EVT-like cell models that we have recently established (Tabrizi *et al.* 2018).

The HTR8/SVneo clones were utilised in the Transwell system for several reasons. Firstly, they are a model first trimester trophoblast cell line, and are therefore considered a physiologically relevant placental cell line. Secondly, and given the absence of S100P expression in the HTR8 cell background acting as a sufficient negative control, they can easily be compared to the S100P expressing clones, i.e. HTR8 clone 7. This allows for the assessment of purely S100P-specific and dependent processes and reduces potential artefacts introduced by utilising physiologically distinct cell lines.

The S100P antibody has the ability to block cell surface and extracellular S100P (Clarke *et al.* 2017), allowing for the determination of the role of this particular cellular pool of S100P in the cellular processes of migration and invasion. It was necessary to first assess if treating HTR8 cells with the S100P antibody causes changes in cell proliferation, as this could potentially influence cell motility and invasion. HTR8 Clones 3 and 7 were treated with the S100P antibody for either 24 or 48 hours before trypsinisation and counting. Figure 4.2.12 displays the effect of the S100P antibody on HTR8 cell proliferation, in which both HTR8 Clones 3 and 7, with and without S100P antibody treatment, show a similar growth pattern over the course of 48 hours, with all conditions showcasing statistically significant growth between 24 and 48 hours ($p<0.0001$). The addition of the S100P antibody did not cause any significant changes in cell proliferation in either Clone 3 or Clone 7 ($p>0.99$). Therefore, it can be said that any changes in motility or invasion that may arise due to treatment with the S100P antibody are not due to changes in cell proliferation, as proliferation of both clones is unaffected by addition of the S100P antibody.

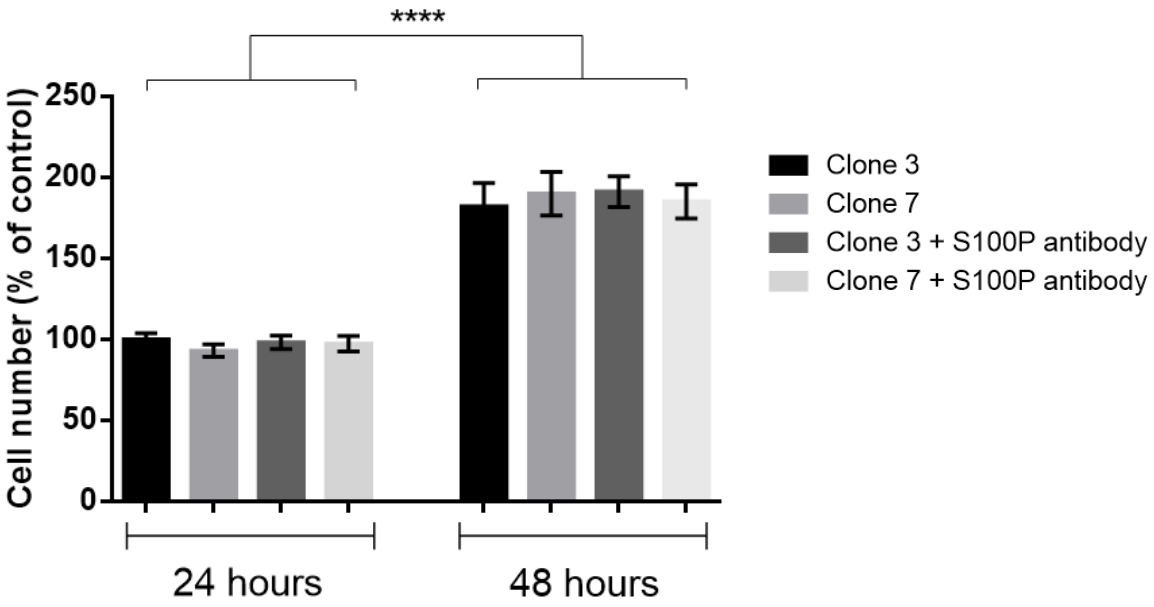

Figure 4.2.12: Treatment with an S100P antibody does not affect cell proliferation of HTR8 clones

HTR8 Clones 3 and 7 were seeded at a density of 20,000 cells per well and left to grow for either 24 or 48 hours prior to trypsinisation and counting. Data represents the mean ±SEM from at least 3 independent replicates (one-way ANOVA, **** $p<0.0001$)

As treatment of HTR8 cell lines with the S100P antibody has no effect on their proliferation, each of the clones were subjected to a motility or invasion assay with the addition of the S100P antibody. Figure 4.2.13 outlines the effect of S100P antibody treatment on the migration of the two HTR8 Clones (control HTR8 Clone 3 and S100P-expressing Clone 7).

In the absence of the S100P antibody, there is a significant, more than 2-fold increase in motility between clone 3 and clone 7 ($p<0.0001$), suggesting that S100P has a role in promoting motility in this cell line. Following treatment with the S100P antibody, the motility of the clone 3 cell line is unaffected when compared to its control ($p=0.63$). In contrast, the motility of the HTR8 clone 7 cell line is significantly reduced by 1.5-fold when compared to its untreated counterpart ($p<0.0001$). The motility of the clone 7 cell line, however, is not reduced to the levels of the control clone 3 cell line, and remains over 80% higher than that of clone 3. This data shows that treatment with the S100P antibody only partially abolishes migration of these cells, and suggests that S100P may be acting via another pathway to influence cellular motility.

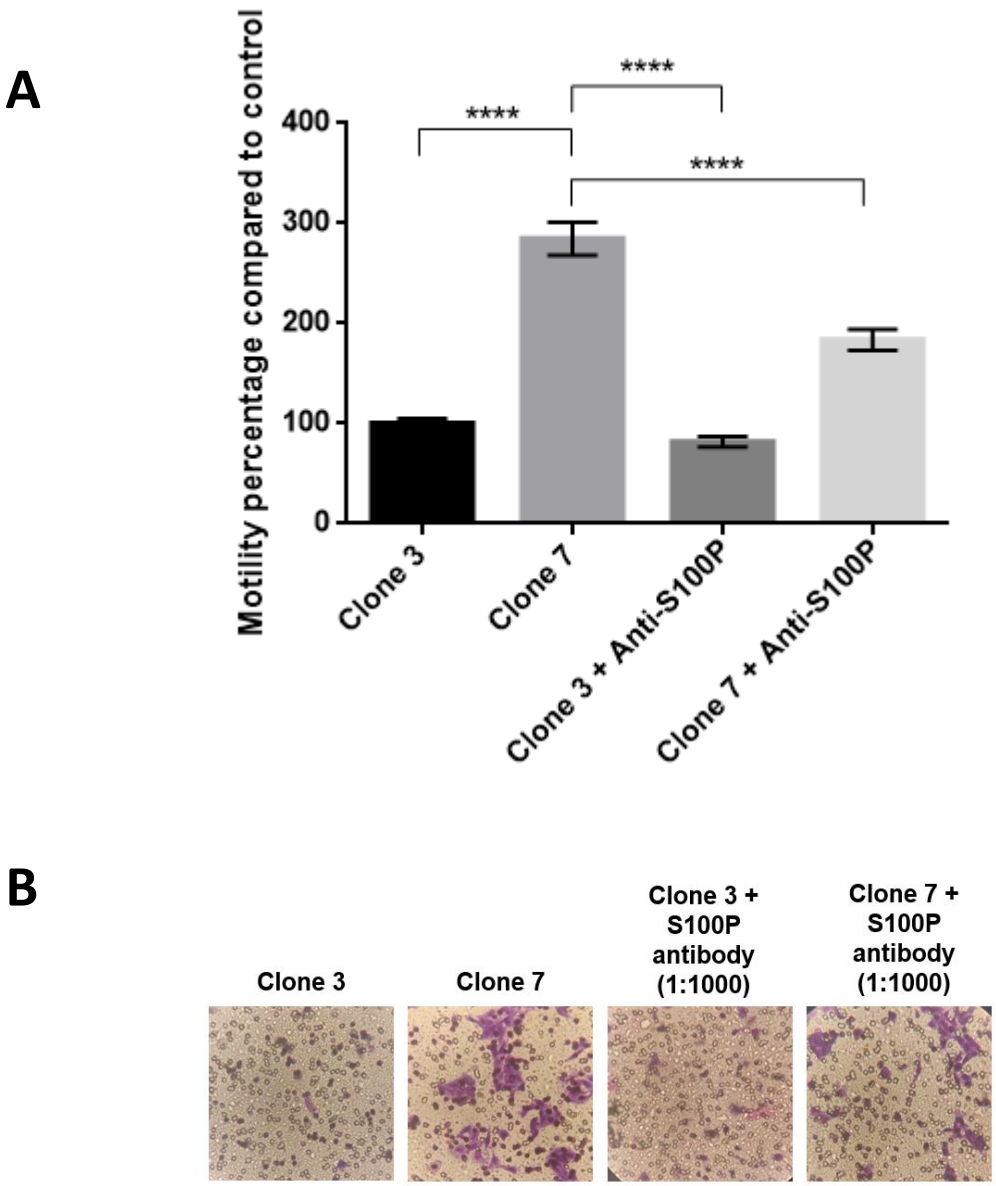

Figure 4.2.13: Treatment with an S100P antibody partially abolishes S100P-dependent migration of S100P-expressing HTR8 cells

A) HTR8 Clones (control Clone 3, and S100P-expressing Clone 7) were seeded in triplicate onto Boyden chambers and treated with S100P antibody diluted 1:1000. Cells were left to migrate for 24 hours before fixing and staining the transwells. The number of cells migrated per field was counted, for 5 fields per well. Data represents the mean ±SEM from at least 3 independent replicates (one-way ANOVA, **** $p<0.0001$)

B) Pictures of one stained transwell per condition were taken at 20x magnification using a Nikon Eclipse TS100 inverted microscope.

The invasive capabilities of HTR8 clones 3 and 7 were also assessed using the Boyden transwell system, both with and without the S100P antibody (Figure 4.2.14). In the absence of the S100P antibody, the clone 7 cell line exhibited an almost 6-fold increase in invasion in comparison to its non-S100P-expressing counterpart, clone 3 ($p<0.0001$). Once again, following antibody treatment, the invasion of clone 3 cells was unchanged when compared to its untreated control ($p=0.99$). On the other hand, treatment of clone 7 cells with the S100P antibody reduced their invasion by 1.5-fold, by almost 40%, compared to their untreated counterpart ($p<0.0001$). Again, as with HTR8 clone 7 cell motility, this is a partial reduction in cell invasion that is not at the level of untreated Clone 3 cell invasion, suggesting that extracellular S100P is only partially responsible for effects on cell invasion.

Together, the data presented in figures 4.2.13 and 4.2.14 demonstrate that S100P has a greater impact on the process of cell invasion than on cell motility in HTR8 cells. However, treatment with the S100P antibody reduced S100P-dependent migration and invasion both by 1.5-fold. The similarity in the fold decrease between motility and invasion following antibody treatment suggests that the S100P antibody is acting in a similar fashion on both motility and invasion, as motility is not reduced more than invasion and vice versa. This data indicates that cell-surface or extracellular S100P has a role in the migration and invasion of trophoblasts, but blockade of extracellular S100P does not fully abolish all of its motility inducting activities.

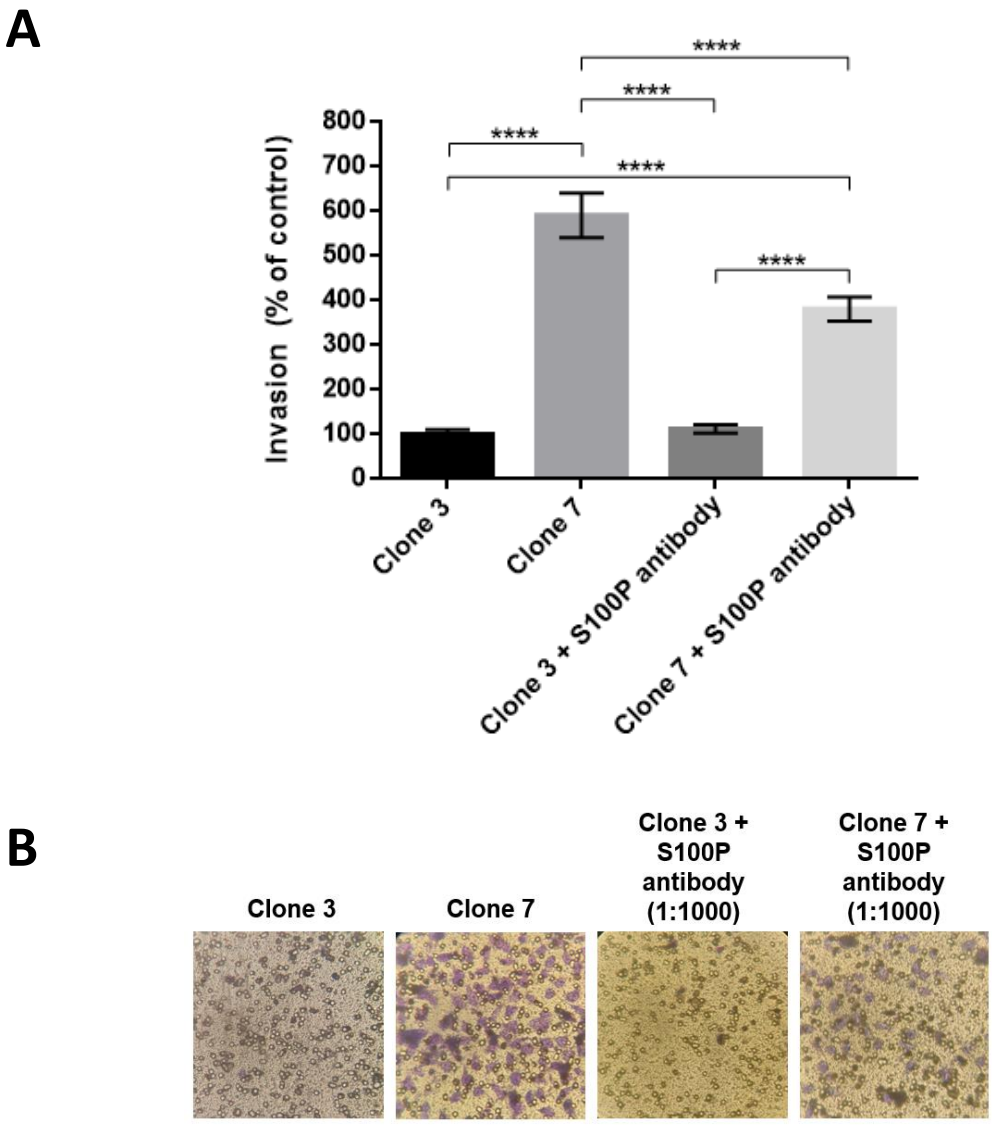

Figure 4.2.14: Treatment with an S100P antibody partially abolishes S100P-dependent invasion of S100P-expressing HTR8 cells

A) HTR8 Clones (control Clone 3, and S100P-expressing Clone 7) were seeded in triplicate onto Matrigel-coated Boyden chambers and treated with S100P antibody diluted 1:1000. Cells were left to invade for 24 hours before fixing and staining the transwells. The number of cells migrated per field was counted, for 5 fields per well. Data represents the mean ±SEM from at least 3 independent replicates (one-way ANOVA, **** $p<0.0001$)

B) Pictures of one stained transwell per condition were taken at 20x magnification using a Nikon Eclipse TS100 inverted microscope.

It has previously been established that knockdown of S100P through the use of siRNA technology in trophoblast cell line JEG-3 leads to an increase in focal adhesion formation, leading to defects in cellular motility and invasion (see figures 4.2.9 to 4.2.11). In order to assess the molecular mechanisms behind cell motility and invasion that may be taking place as a consequence of S100P expression at the membrane, HTR8 Clones 3 and 7 were again treated with S100P antibody for 24 hours prior to being fixed and stained for paxillin. Figure 4.2.15 illustrates the differences in focal adhesion formation between control Clone 3 and Clone 7, both with and without the addition of the S100P antibody. In the absence of the S100P antibody, there is a significant 25% decrease in the number of focal adhesions between Clones 3 and 7, respectively (Figure 4.2.15, panel B, $p=0.006$) demonstrating that S100P has a role in regulating the formation, or disassembly, of focal adhesions.

Changes to the actin cytoskeleton were observed between HTR8 clones 3 and 7. S100P-expressing HTR8 clone 7 cells stained with rhodamine phalloidin, highlighting F-actin structures, showed highly motile features, including the presence of a leading edge (focused regions). In contrast, HTR8 clone 3 cells not expressing S100P did not display these motile features and instead showed the presence of highly organised stress fibres.

Upon treating each clone with an antibody to S100P, there is no change in the average number of focal adhesions counted per cell in either cell line, respective to their controls ($p=0.99$). This suggests that the S100P antibody may be decreasing migration and invasion in HTR8 cells by another mechanistic pathway that is not dependent on the regulation of focal adhesion formation.

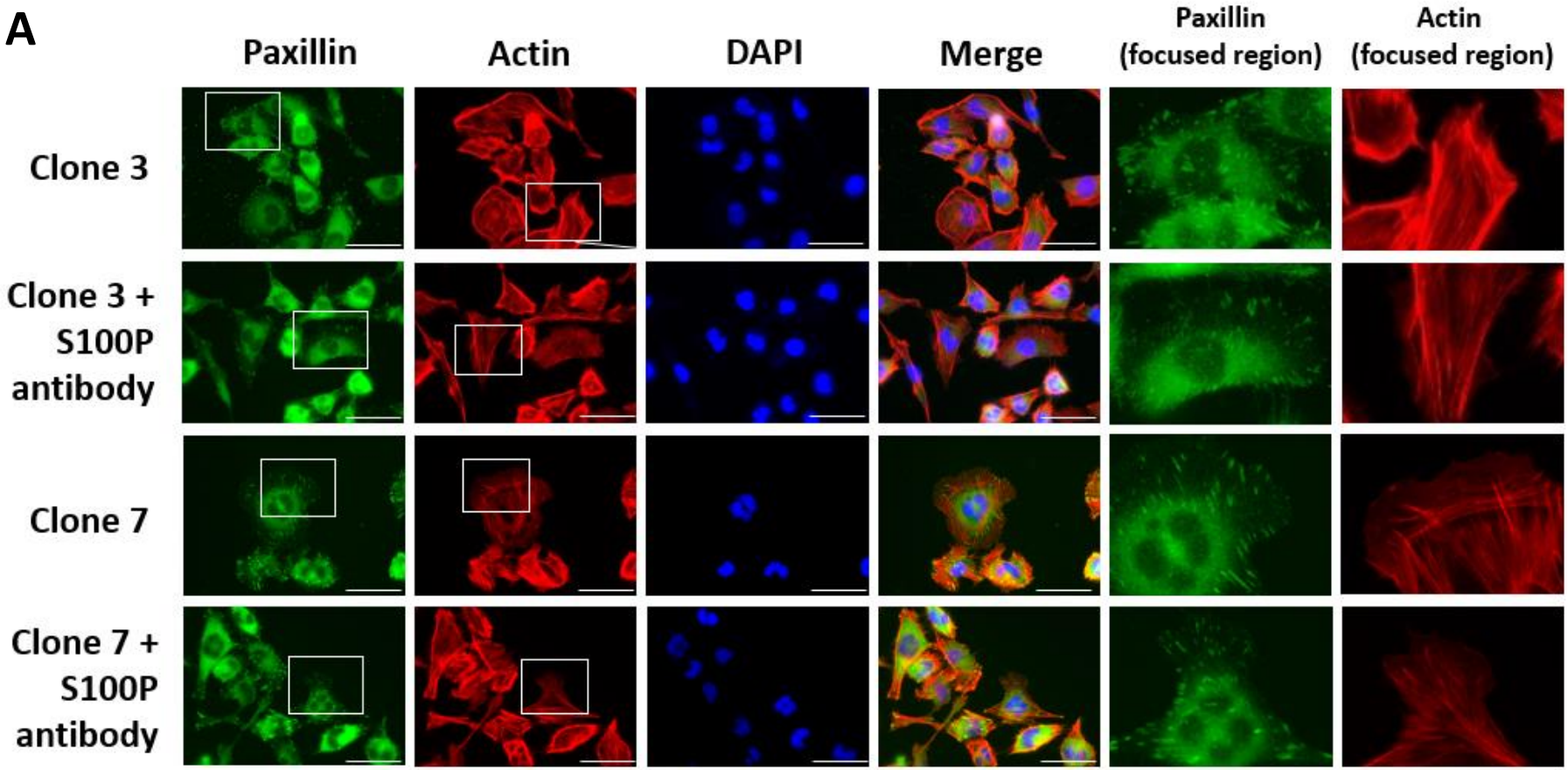
A
Paxillin
Actin
DAPI
Merge
Paxillin (focused region)
Actin (focused region)
Clone 3
Clone 3 + S100P antibody
Clone 7
Clone 7 + S100P antibody

B

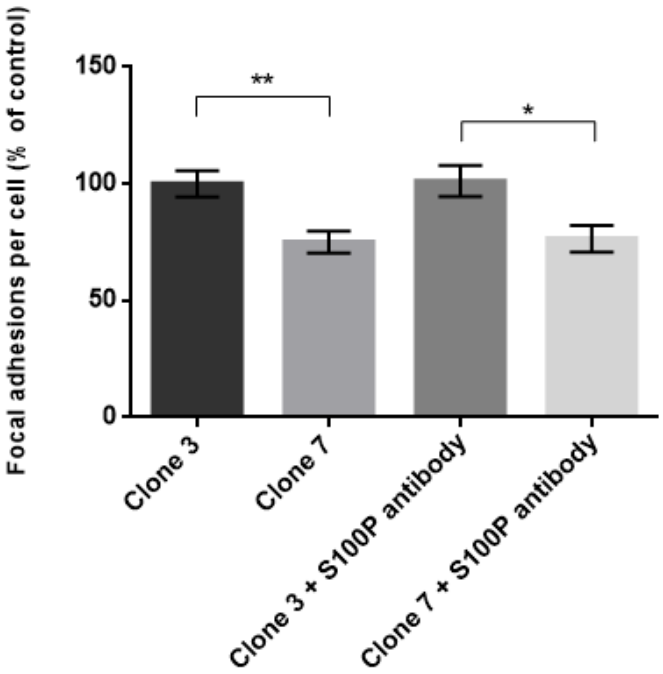

Figure 4.2.15: Treatment with an S100P antibody does not affect the number of focal adhesions formed by HTR8 cells

A) HTR8 Clones (control Clone 3, and S100P-expressing Clone 7) were seeded onto fibronectin-coated coverslips and treated with S100P antibody diluted 1:1000. Cells were incubated for 24 hours before fixing and staining for paxillin (green) and actin (red).

B) Average number of paxillin stained focal adhesions per cell were counted for around 100 cells, with values presented as a percentage of the control Clone 3. Data represents the mean ±SEM from at least 3 independent replicates (one-way ANOVA, * $p<0.05$, ** $p<0.01$)

4.2.5. Cromolyn partially inhibits S100P-dependent migration and invasion

Our earlier work has revealed that an antibody to S100P, added extracellularly in the culture media, reduces the motility and invasion of HTR8 cells. In the context of extracellular interactions of the S100P protein, one such protein that S100P interacts with, RAGE, is a receptor that is present on the cell surface. In order to examine if any of the reported defects in cell motility and invasion are RAGE-dependent, it was decided to treat HTR8 cells with cromolyn. Cromolyn is an anti-allergy drug that is known to have a direct interaction with S100P. Cromolyn binds to S100P dimers at its linker region, helix 4 of one S100P monomer, and helix 1 of another S100P monomer. This is also within the region of the RAGE-S100P binding site, effectively blocking interaction of S100P with RAGE (Penumutchu *et al.* 2014b). Prior to assessing the motility and invasion of HTR8 clones when treated with cromolyn, it was first necessary to see if cromolyn demonstrates any toxicity or has any effect on cell proliferation. Non-S100P expressing HTR8 clone 3 and S100P-expressing HTR8 clone 7 were treated with two different doses of cromolyn (10 and 100µM) over the course of 48 hours prior to trypsinisation and cell counting. These doses were chosen as they are featured prominently in the literature (Arumugam *et al.* 2006).

Figure 4.2.16 shows the effect of cromolyn at different concentrations on HTR8 clone proliferation. HTR8 Clone 3 cells do not demonstrate any differences in proliferation at the 24-hour time point when treated with either 10µM or 100µM cromolyn ($p>0.99$). HTR8 clone 7 cells, on the other hand, seem to show a slight decrease in cell proliferation when treated with 10µM cromolyn, but not 100µM cromolyn, at the 24-hour time point. However, this difference in cell proliferation is not statistically significant ($p>0.18$). After 48 hours of treatment with cromolyn at either 10µM or 100µM dosages, HTR8 clone 3 demonstrate no defects in proliferation ($p>0.99$). Upon treating HTR8 clone 7 with 10µM or 100µM cromolyn, there seems to be a slight decrease in cell proliferation by about 20% on average, however this is not deemed statistically significant ($p>0.2$). When comparing the proliferation of clone 3 to clone 7 at the 48-hour time point, there is no statistically significant difference between their proliferation rates ($p>0.85$). However, there is a statistically significant decrease in proliferation between HTR8 clone 3 and HTR8 clone 7 treated with 10µM cromolyn or 100µM cromolyn respectively at the 48-hour time point ($p<0.001$) by almost 25%.

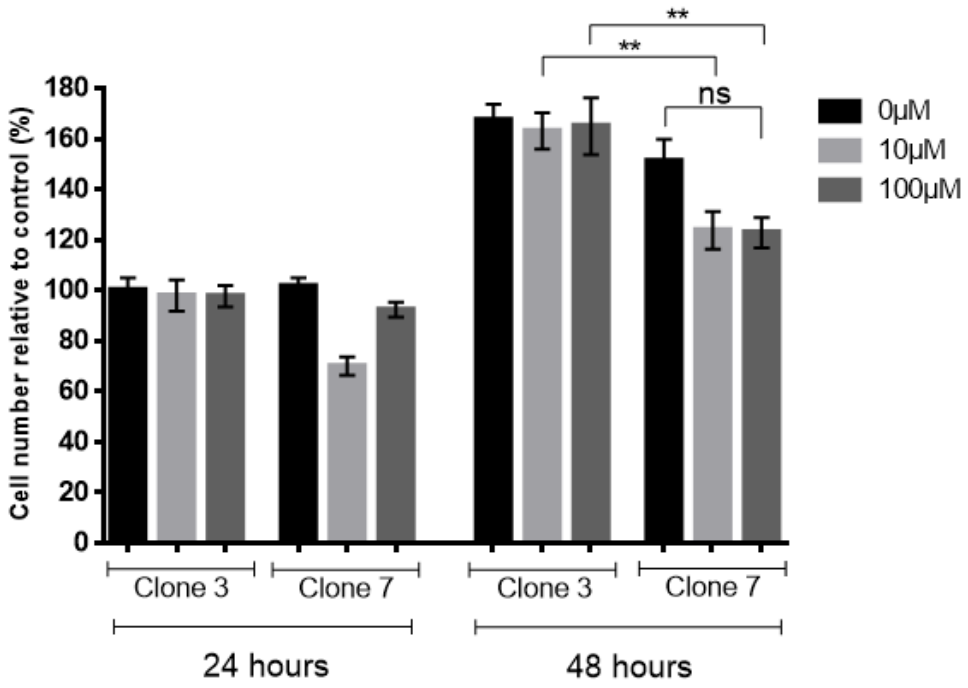

Figure 4.2.16: Treatment with cromolyn does not significantly decrease proliferation of HTR8 cell clones 3 and 7

HTR8 Clones 3 and 7 were seeded at a density of 20,000 cells per well and either left untreated, or treated with 10 or 100μM cromolyn. Cells were trypsinised and counted at either 24 or 48 hours to assess changes in cellular proliferation. Data represents the mean ±SEM from at least 3 independent replicates (one-way ANOVA, ** $p<0.01$)

After confirming the effects of cromolyn on HTR8 clone viability, HTR8 clones 3 and 7 were seeded into transwells for motility or invasion assays, and treated with either 10µm or 100µM cromolyn. Figure 4.2.17 outlines the effect of cromolyn on the migratory capabilities of the two HTR8 Clones.

Results demonstrate a highly significant 2-fold increase in motility between the non-s100P expressing HTR8 Clone 3 and the S100P-expressing HTR8 Clone 7 ($p<0.0001$). This is similar to results previously obtained whilst assessing the effects of the S100P antibody, again suggesting a role for S100P in trophoblast cellular motility as well as previously published data (Tabrizi *et al.* 2018). Treatment of clone 3 cells with either 10µM or 100µM cromolyn does not have a significant effect on motility ($p<0.54$), whereas in contrast, clone 7 cells treated with both 10µM and 100µM cromolyn show a marked decrease in motility by around 1.5-fold when compared to their untreated counterpart ($p<0.0001$). This decrease in motility showcased by Clone 7 cells following cromolyn treatment is shown to be partial, as levels of motility following cromolyn treatment at any dose are not reduced to the levels of motility shown by the non-S100P expressing Clone 3.

The ability of cromolyn to alter the process of invasion was also assessed using transwell assays (Figure 4.2.18). Once again, the invasive capabilities of HTR8 cells expressing S100P were shown to be stronger than motility, as the level of invasion seen in HTR8 clone 7 cells exceeds the level of motility in relation to their controls. There is, on average, an almost 3-fold increase in invasion when comparing Clone 3 to Clone 7 ($p<0.0001$). Treatment of clone 3 cells with cromolyn at both 10µM and 100µM had no significant effect on invasion compared to the untreated control ($p>0.65$). HTR8 clone 7 cells treated with 10µM cromolyn demonstrated an almost 10% decrease in invasion compared to untreated clone 7 cells, however this decrease is not statistically significant ($p=0.55$). Treatment of HTR8 clone 7 with 100µM cromolyn led to a statistically significant decrease in cell invasion of 20% when compared to their untreated counterpart ($p=0.003$).

Previous work demonstrated an equal reduction in cellular motility and invasion upon treatment with an S100P antibody by 1.5-fold when compared to untreated controls. What is interesting to note, is that cromolyn treatment of HTR8 cells at 100µM reduced their motility by 30%, but only decreased their invasion by 20%. This may suggest that cromolyn has greater effect on cellular motility rather than invasion, and that this effect is only partial.

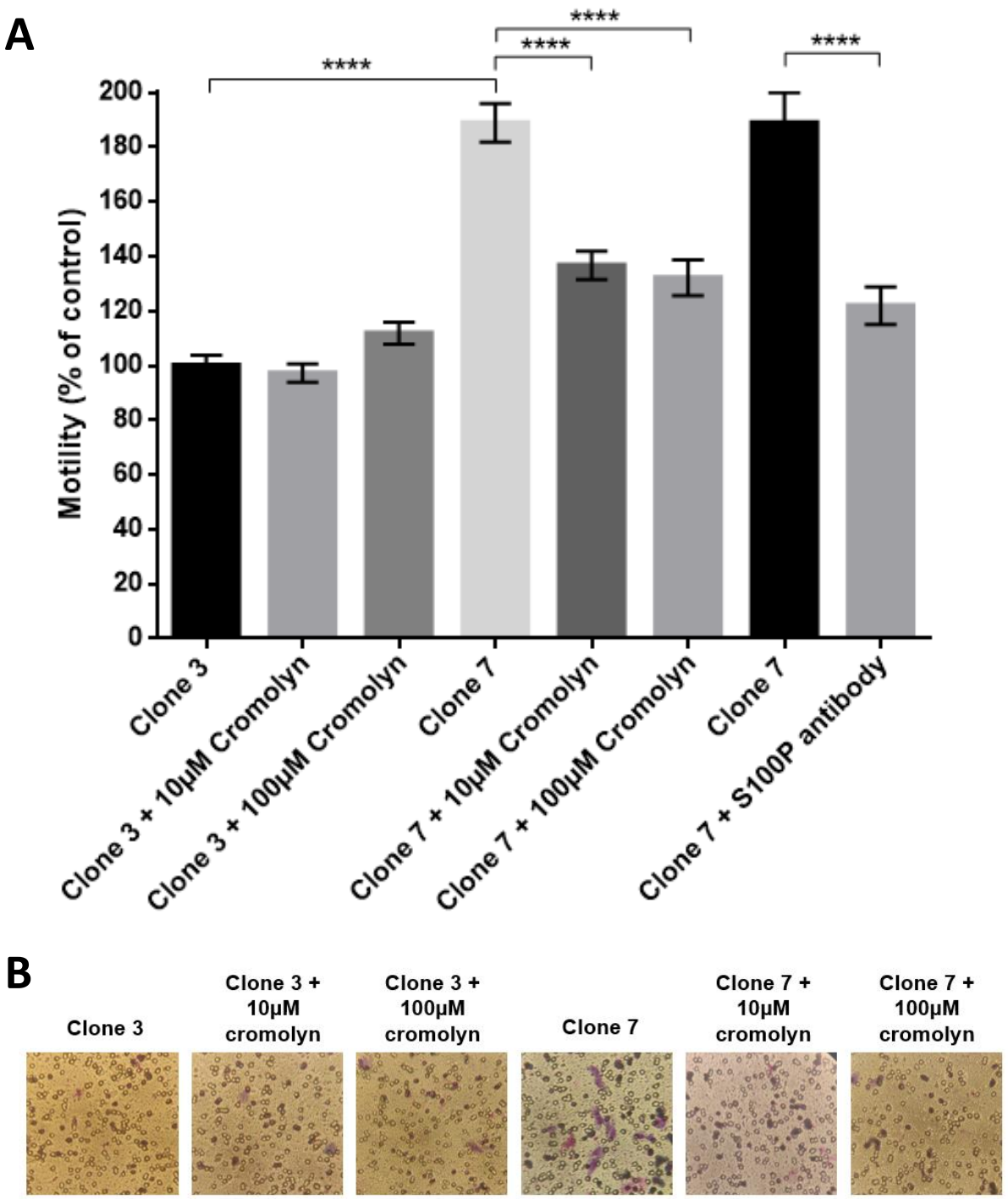

Figure 4.2.17: Treatment with cromolyn partially abolishes S100P-dependent migration of S100P-expressing HTR8 cells

A) HTR8 Clones (control Clone 3, and S100P-expressing Clone 7) were seeded in triplicate onto Matrigel-coated Boyden chambers and treated with cromolyn at concentrations of 10µM and 100µM. Cells were left to migrate for 24 hours before fixing and staining the transwells. The number of cells migrated per field was counted, for 5 fields per well. Data represents the mean ±SEM from at least 3 independent replicates (one-way ANOVA, **** $p<0.0001$)

B) Pictures of one stained transwell per condition were taken at 20x magnification using a Nikon Eclipse TS100 inverted microscope.

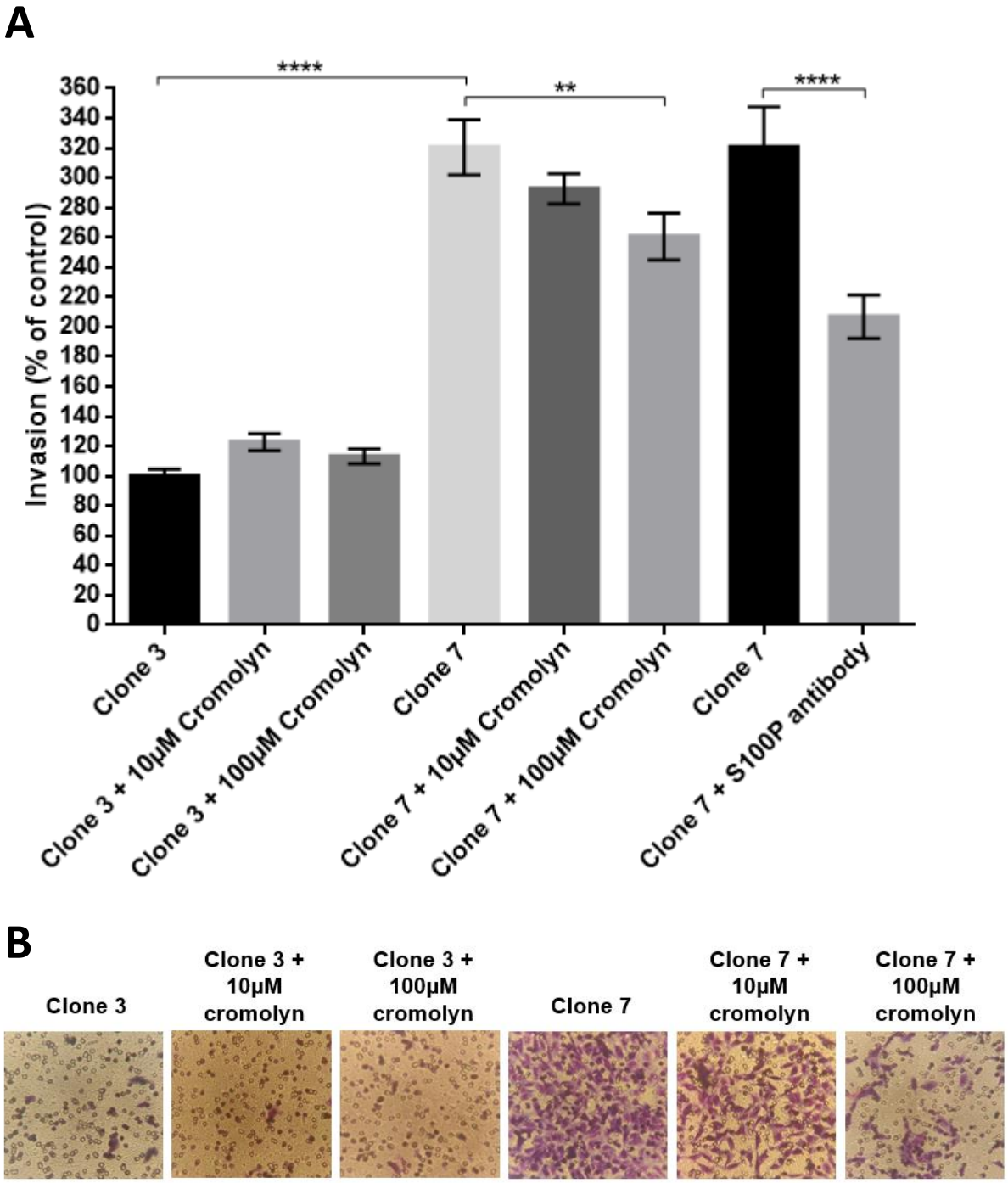

Figure 4.2.18: Treatment with cromolyn has an effect on the invasive capabilities of S100P-expressing HTR8 cells

A) HTR8 Clones (control Clone 3, and S100P-expressing Clone 7) were seeded in triplicate onto Matrigel-coated Boyden chambers and treated with cromolyn at concentrations of 10µM and 100µM. Cells were left to migrate for 24 hours before fixing and staining the transwells. The number of cells migrated per field was counted, for 5 fields per well. Data represents the mean ±SEM from at least 3 independent replicates (one-way ANOVA, ** $p<0.01$, **** $p<0.0001$)

B) Pictures of one stained transwell per condition were taken at 20x magnification using a Nikon Eclipse TS100 inverted microscope.

After establishing the ability of 100μM cromolyn to inhibit both motility and invasion of HTR8 cells expressing S100P, albeit to different degrees, we sought to understand if this drug had any effects on the membrane-association capabilities of S100P. To this end, HTR8 clone 7 cells were grown with and without the presence of 100μM cromolyn prior to isolation of plasma membrane fractions using nitrogen cavitation. Isolated membrane fractions were equally loaded and run on 16% (w/v) SDS-PAGE prior to western blotting for S100P and plasma membrane marker caveolin I (Figure 4.2.19, panel A). Quantification of the band intensity for both S100P and caveolin I was carried out, with S100P band intensity being normalised to caveolin I (Figure 4.2.19, panel B).

The resulting western blot demonstrated a statistically significant difference in the levels of S100P detected by western blot between samples. After normalisation to caveolin I, plasma membranes isolated from cromolyn-treated HTR8 Clone 7 cells demonstrate on average a 30% decrease in detectable S100P ($p=0.03$) when compared to untreated plasma membrane fractions. Interestingly, this decrease is directly proportional to the level of motility defects seen in HTR8 clone 7 following the addition of 100μM cromolyn (see Figure 4.2.17).

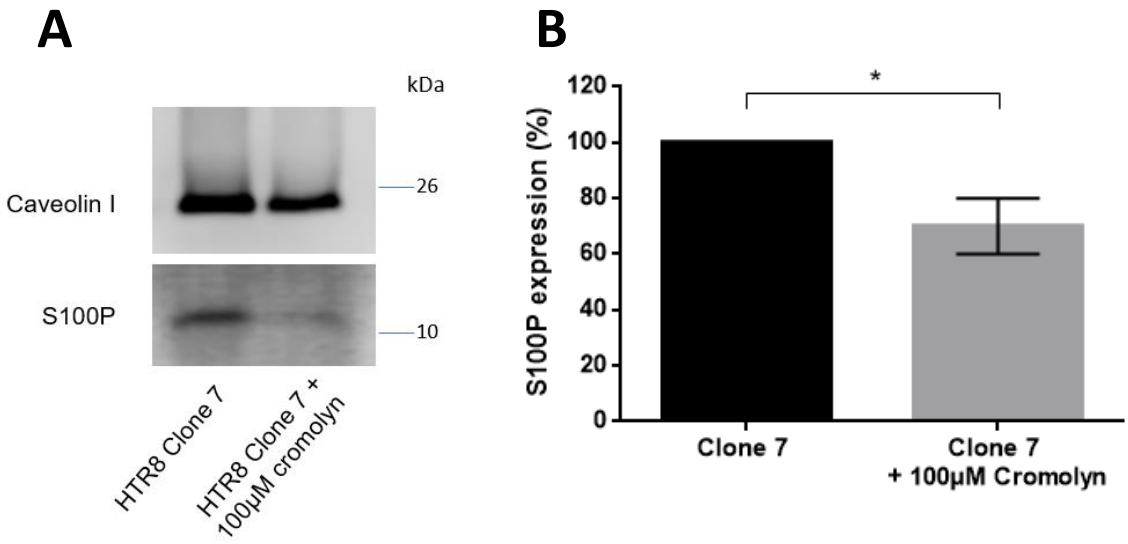

Figure 4.2.19: Treatment of HTR8 Clone 7 with 100µM cromolyn results in reduced detection of S100P in isolated plasma membrane fractions

A) HTR8 Clone 7 cells were grown either with or without 100µM cromolyn for 48 hours prior to plasma membrane isolation using nitrogen cavitation. Isolated plasma membranes were run on a 16% (w/v) SDS-PAGE prior to western blotting for S100P and caveolin I.

B) Levels of S100P within isolated plasma membrane fractions were quantified by densitometry using Image Studio lite, and were normalised to caveolin I. Data represents the mean ±SD from 3 independent replicates (one-way ANOVA, * $p<0.05$).

4.2.6 Residues within S100P may interact with the plasma membrane as predicted by Membrane Optimal Docking Area (MODA)

Protein function can be influenced by subcellular localisation. By controlling access of proteins to different cellular compartments, or by targeting a certain protein to a particular location within the cell, a variety of protein interactions can either take place or be inhibited. As such, proteins can be targeted to membrane regions to facilitate processes including protein trafficking and cytoskeletal reorganisation (Szymanski *et al.* 2015). Many proteins are amphitropic in nature, meaning they bind reversibly to membranes in order to regulate their functionality (Johnson, J. E. and Cornell 1999).

Previous work within this chapter has demonstrated the presence of S100P within the plasma membrane fraction isolated from a variety of cell lines (Figure 4.2.1). It is not possible to assert from these results alone if S100P is an integral part of the membrane, or if S100P is a transient, reversible membrane-binding protein. One way of predicting the potential for membrane interaction of a given protein is the Membrane Optimal Docking Area method (MODA). This method was developed by Kufareva *et al.* (2014) by improving a previously generated method known as the PIER algorithm, and has the ability to detect membrane interactive proteins. MODA does not use homology modelling of known peripheral proteins, but instead uses 3D structural data and protein curvature analysis. MODA alone is not sufficient to fully predict membrane-interacting residues or novel peripheral proteins, and therefore any predictions must be fully validated with experimental studies, such as NMR spectroscopy. Training of the MODA algorithm was achieved by submitting structures of previously validated peripheral membrane proteins in which the residues interacting with the membrane were already established by several methods, including but not limited to surface plasmon resonance (SPR), NMR, or mutagenesis studies. Submission of a protein sequence in PDB format to the MODA server (http://molsoft.com/~eugene/moda/modamain.cgi) generates a list of scores for each residue, usually between 0 and 50, which give the propensity for a particular surface residue to be involved in membrane interaction. Higher values suggest a higher propensity for membrane interaction.

For S100P, the crystal structure PDB file generated by Zhang *et al.* (2003) was utilised, as the structure has a sufficiently high resolution of 2 Å. A list of residues and their scores were given as an output by MODA (Table 4.2.1). Certain residues (46-51, 95) were not present within the PDB file as they were not observed. This stretch of internal residues at positions 46 to 51 are present within the linker region of S100P between helices 2 and 3. This linker region, otherwise known as a hinge region, is known to be highly dynamic when bound to calcium ions (Tutar 2006). Zhang *et al.* (2003) suggest that the linker region may be responsible for interacting with target proteins, as several other S100 proteins are able

to form complexes with targets such as annexins I and II at their relative linker domains, as shown by X-ray and NMR structural studies (Réty *et al.* 1999).

Res	Name	Sel	NonStandard	Counted	plainMODA	curvIndex	curvMODA
1	met	1j55.a/^M1	0	1	0	0.955511	0
2	thr	1j55.a/^T2	0	1	0	0.955511	0
3	glu	1j55.a/^E3	0	1	0	0.955511	0
4	leu	1j55.a/^L4	0	1	47.0802	0.955511	44.9857
5	glu	1j55.a/^E5	0	1	0	0.955511	0
6	thr	1j55.a/^T6	0	1	0	0.919408	0
7	ala	1j55.a/^A7	0	1	0	0.782268	0
8	met	1j55.a/^M8	0	1	294.444	0.703179	207.047
9	gly	1j55.a/^G9	0	1	0	0.651195	0
10	met	1j55.a/^M10	0	1	0	0.612843	0
11	ile	1j55.a/^I11	0	0	0	0.433145	0
12	ile	1j55.a/^I12	0	1	177.364	0.436693	77.4538
13	asp	1j55.a/^D13	0	1	0	0.483244	0
14	val	1j55.a/^V14	0	1	0	0.349849	0
15	phe	1j55.a/^F15	0	0	0	0.276789	0
16	ser	1j55.a/^S16	0	1	0	0.394417	0
17	arg	1j55.a/^R17	0	1	0	0.395656	0
18	tyr	1j55.a/^Y18	0	1	0	0.31316	0
19	ser	1j55.a/^S19	0	1	0	0.343842	0
20	gly	1j55.a/^G20	0	1	0	0.490825	0
21	ser	1j55.a/^S21	0	1	0	0.496672	0
22	glu	1j55.a/^E22	0	1	0	0.522791	0
23	gly	1j55.a/^G23	0	1	0	0.567202	0
24	ser	1j55.a/^S24	0	1	0	0.518284	0
25	thr	1j55.a/^T25	0	1	6.89818	0.5446	3.75675
26	gln	1j55.a/^Q26	0	1	25.3825	0.434977	11.0408
27	thr	1j55.a/^T27	0	1	0	0.376997	0
28	leu	1j55.a/^L28	0	0	0	0.263268	0
29	thr	1j55.a/^T29	0	1	0	0.369117	0
30	lys	1j55.a/^K30	0	1	0	0.339837	0
31	gly	1j55.a/^G31	0	1	0	0.33217	0
32	glu	1j55.a/^E32	0	1	0	0.320752	0
33	leu	1j55.a/^L33	0	0	0	0.265444	0
34	lys	1j55.a/^K34	0	1	0	0.34775	0
35	val	1j55.a/^V35	0	1	0	0.357802	0
36	leu	1j55.a/^L36	0	0	0	0.279353	0
37	met	1j55.a/^M37	0	1	0	0.379091	0
38	glu	1j55.a/^E38	0	1	0	0.487106	0
39	lys	1j55.a/^K39	0	1	9.66757	0.443454	4.28712
40	glu	1j55.a/^E40	0	1	33.5363	0.384567	12.8969
41	leu	1j55.a/^L41	0	1	256.403	0.46325	118.779
42	pro	1j55.a/^P42	0	1	89.7261	0.636076	57.0726
43	gly	1j55.a/^G43	0	1	331.812	0.699377	232.062

44	phe	1j55.a/^F44	0	1	294.713	0.560114	165.073
45	leu	1j55.a/^L45	0	1	146.824	0.542691	79.6802
46	Residue not present in PDB file						
47	Residue not present in PDB file						
48	Residue not present in PDB file						
49	Residue not present in PDB file						
50	Residue not present in PDB file						
51	Residue not present in PDB file						
52	asp	1j55.a/^D52	0	1	0	0.66251	0
53	ala	1j55.a/^A53	0	1	0	0.566379	0
54	val	1j55.a/^V54	0	1	0	0.398489	0
55	asp	1j55.a/^D55	0	1	0	0.465729	0
56	lys	1j55.a/^K56	0	1	0	0.542961	0
57	leu	1j55.a/^L57	0	1	0	0.38589	0
58	leu	1j55.a/^L58	0	1	0	0.349721	0
59	lys	1j55.a/^K59	0	1	0	0.499533	0
60	asp	1j55.a/^D60	0	1	0	0.456767	0
61	leu	1j55.a/^L61	0	1	0	0.336152	0
62	asp	1j55.a/^D62	0	1	0	0.45714	0
63	ala	1j55.a/^A63	0	1	0	0.528976	0
64	asn	1j55.a/^N64	0	1	0	0.615191	0
65	gly	1j55.a/^G65	0	1	0	0.624166	0
66	asp	1j55.a/^D66	0	1	0	0.557337	0
67	ala	1j55.a/^A67	0	1	0	0.481125	0
68	gln	1j55.a/^Q68	0	1	0	0.396957	0
69	val	1j55.a/^V69	0	0	0	0.268973	0
70	asp	1j55.a/^D70	0	1	0	0.355254	0
71	phe	1j55.a/^F71	0	1	337.124	0.288314	97.1974
72	ser	1j55.a/^S72	0	1	220.162	0.361599	79.6104
73	glu	1j55.a/^E73	0	1	0	0.332232	0
74	phe	1j55.a/^F74	0	0	0	0.236306	0
75	ile	1j55.a/^I75	0	1	558.426	0.334884	187.008
76	val	1j55.a/^V76	0	1	232.709	0.391634	91.137
77	phe	1j55.a/^F77	0	1	0	0.332038	0
78	val	1j55.a/^V78	0	0	0	0.389408	0
79	ala	1j55.a/^A79	0	1	74.9814	0.539688	40.4665
80	ala	1j55.a/^A80	0	1	0.994625	0.565276	0.562238
81	ile	1j55.a/^I81	0	1	178.702	0.579071	103.481
82	thr	1j55.a/^T82	0	1	0	0.701509	0
83	ser	1j55.a/^S83	0	1	1.02148	0.823259	0.840942
84	ala	1j55.a/^A84	0	1	55.7153	0.853008	47.5256
85	cys	1j55.a/^C85	0	1	222.573	0.916535	203.996
86	his	1j55.a/^H86	0	1	0	0.955511	0
87	lys	1j55.a/^K87	0	1	2.31926	0.955511	2.21608

88	tyr	1j55.a/^Y88	0	1	1408.26	0.955511	1345.61
89	phe	1j55.a/^F89	0	1	1084.6	0.955511	1036.35
90	glu	1j55.a/^E90	0	1	0	0.955511	0
91	lys	1j55.a/^K91	0	1	192.028	0.955511	183.485
92	ala	1j55.a/^A92	0	1	800.641	0.955511	765.021
93	gly	1j55.a/^G93	0	1	301.54	0.955511	288.125
94	leu	1j55.a/^L94	0	1	425.82	0.955511	406.876
95	Residue not present in PDB file						

Table 4.2.1: List of MODA scores for each amino acid of the 1j55 PDB file suggest membrane-interacting residues

Table listing residues in the PDB file 1j55 (S100P crystal structure) along with their scores generated by the MODA server. Residues not present within the PDB file (46-51, 95) cannot be analysed.
Res, residue; *Name,* residue name; *Sel,* selected residue; *NonStandard,* presence of nonstandard residues; *Counted,* surface residues; *plainMODA,* MODA score; *curvIndex,* curve index of residue; *curvMODA* corrected MODA score where plainMODA/curvIndex = curvMODA.

Regardless of missing residues, the S100P amino acid sequence was plotted against the curvMODA scores obtained from the MODA server in order to visualise the propensity for each amino acid to form a contact interface with the membrane (Figure 4.2.20). Results from the MODA server suggest two potential sites of membrane interaction within the S100P sequence. Residues 41 to 45 demonstrate curvMODA scores over 50, suggesting a potential membrane binding interface is present. In addition, clusters of residues from position 71 onwards have very high curvMODA scores, from the region of 200 to almost 1350. It is important to note that the MODA server does not employ a cut-off value for any score, meaning that there is no particular threshold for which a residue is deemed to definitively interact with membranes. As a consequence, these scores can only be used as a predictor of membrane interaction, with the highest scores representing the residue with the highest likelihood of membrane interaction. The creators of the MODA server have asserted, through empirical evidence, that scores of 40 and above are correlated with membrane interaction.

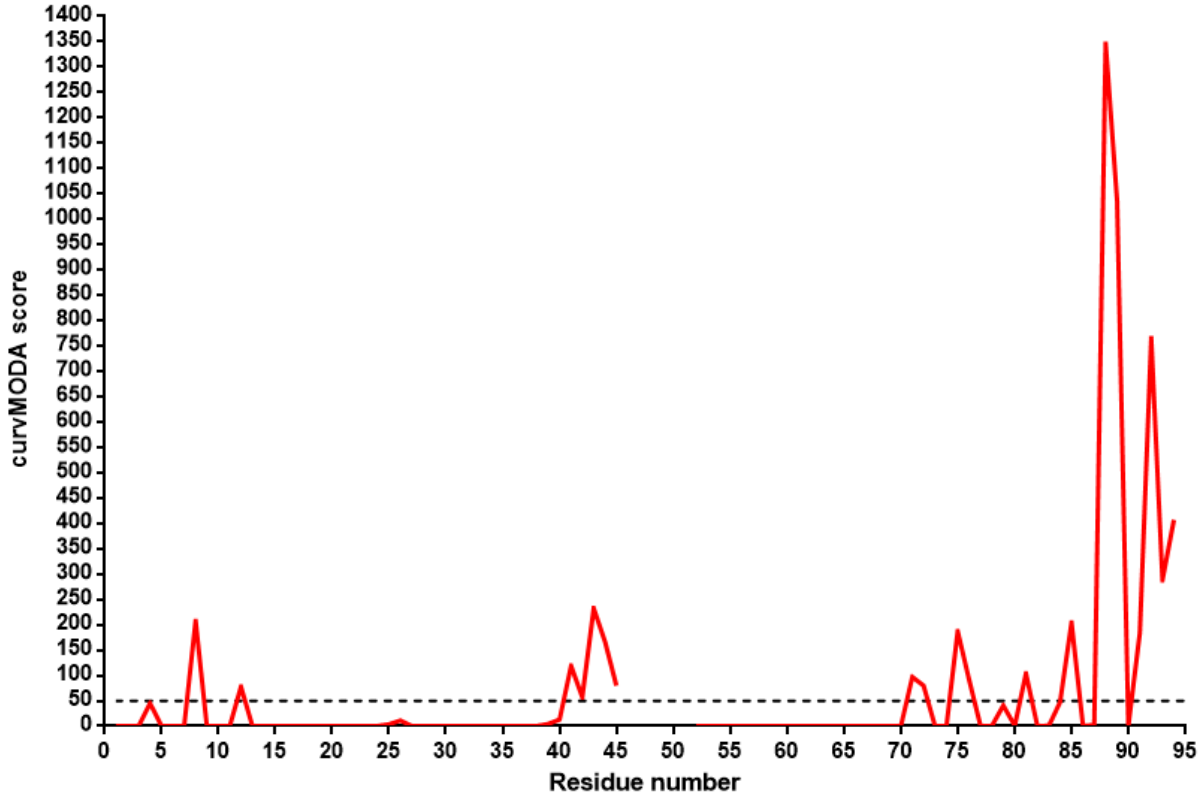

Figure 4.2.20: Graph depicting curvMODA scores for each amino acid of the 1j55 PDB file suggest membrane-interacting residues

The curvMODA score for each amino acid residue present in the S100P PDB file, 1j55, was visualised (red line). Patches of residues with scores above 50 (marked by a black dotted line) are likely to interact with membrane bilayers. Residues 46-51 and 95 are not visualised, due to their absence from the 1j55 PDB file.

Data generated by MODA was exported as an ICB file and visualised using ICM-Browser (figures 4.2.21 and 4.2.22). Visualisation of the S100P protein through the ICM-Browser software highlighted residues suggested by MODA to have a role in membrane interaction; these residues are highlighted in red. The ribbon model of S100P makes apparent a potential membrane-binding interface across one axis of helix 4, involving residues I81, A84, C85, Y88, F89, K91, A92, G93 and L94 (Figure 4.2.21, panel A). Upon visualisation of the space-filling S100P model, it becomes apparent that several residues within the linker region of S100P (L41 to L45) may also be a part of the same binding interface (Figure 4.2.21, panel B). Another set of residues are present on the opposite side of the protein, namely residues L4, M8 and I12 from helix 1, that have been highlighted by MODA as potential membrane-interacting residues (Figure 4.2.22, panel A). The space-filling model also visualises residues F71, S72, I75, V76 and A79 that are spatially opposed to the highlighted residues from helix 1, potentially suggesting the presence of another continuous binding interface for interaction with the membrane (Figure 4.2.22, panel B).

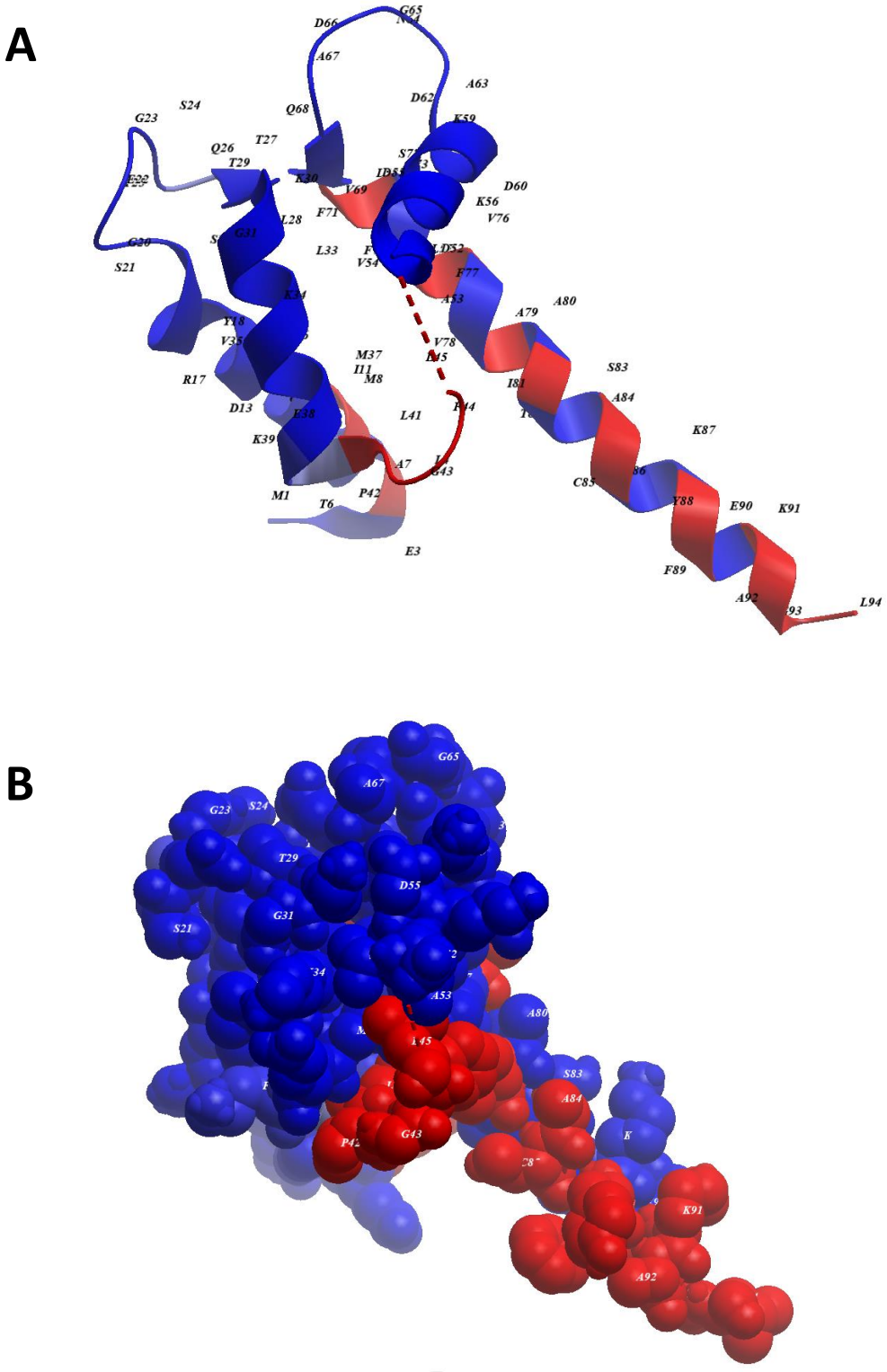

Figure 4.2.21: Models of S100P highlight potential membrane-interacting residues

A) Ribbon model of S100P monomer obtained from PDB file 1j55. Residues predicted to interact with the membrane by MODA are highlighted in red.

B) Space-filling model of S100P monomer obtained from PDB file 1j55. Residues predicted to interact with the membrane by MODA are highlighted in red.

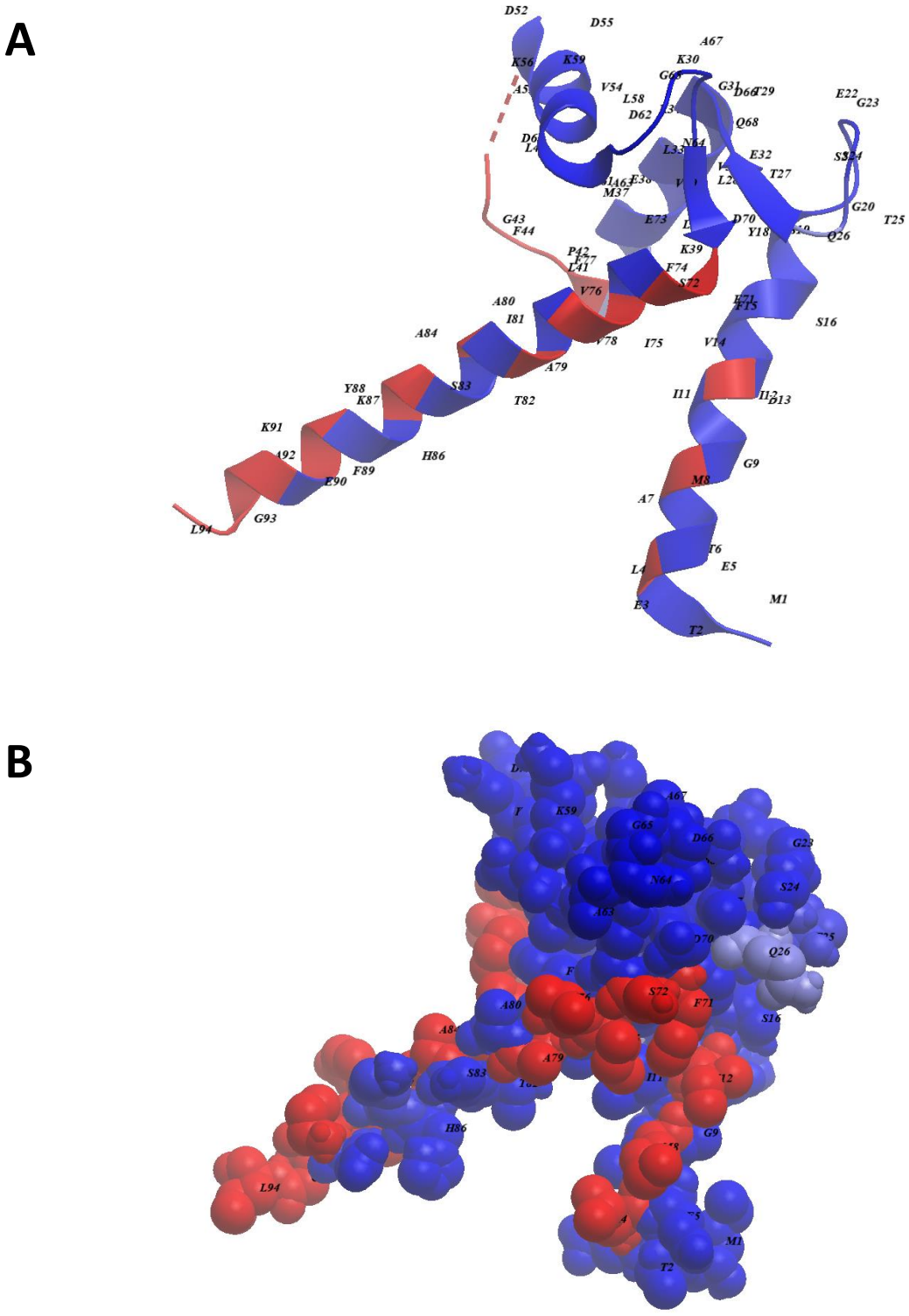

Figure 4.2.22: Models of S100P highlight potential membrane-interacting residues

A) An alternative viewpoint of the ribbon model of S100P monomer obtained from PDB file 1j55. Residues predicted to interact with the membrane by MODA are highlighted in red. Red dotted line indicates missing residues.

B) An alternative viewpoint of the space-filling model of S100P monomer obtained from PDB file 1j55. Residues predicted to interact with the membrane by MODA are highlighted in red.

4.2.7 S100P may undergo lipid modifications, as predicted by Group Prediction Servers

Prior data has demonstrated that S100P detected in plasma membrane fractions of all cell lines runs slower on SDS-PAGE gel than expected in comparison to total cell lysate fractions (Figure 4.2.1) This could either be due to the high lipid content within the plasma membrane fractions, or due to a post-translational modification (PTM).

PTMs are characterised as an alteration of molecules by the covalent attachment of amino acids or functional groups (Zhou *et al.* 2006). There are over 300 different types of post-translational modification that have a key role in a variety of processes, including but not limited to phosphorylation, nitrosylation, glycation, methylation and acetylation. The experimental identification of PTM sites is a laborious process, and therefore utilisation of a prediction server to identify potential PTMs based on sequence data is a viable alternative. Certain types of PTM allow for increased association of a given protein with the plasma membrane, namely lipidation. Lipidation involves the covalent attachment of specific lipid groups to proteins, allowing for interaction with the membrane bilayer and providing an anchor to which the protein can attach to the membrane (Hang and Linder 2011).

In order to ascertain the likelihood of S100P being post-translationally modified, it was necessary to employ group prediction servers. Such prediction servers allow for identification of potential PTM sites based on data sets of proteins that contain known PTMs, along with the sequence information for the protein of interest. Due to the presence of S100P in the plasma membrane fraction of cell lines, there was a focus on prediction servers that assessed the likelihood of PTMs that confer membrane-association of a protein. To this end, GPS-Lipid 1.0 was utilised. This server predicts the presence of lipid modification sites on a protein, including potential sites of palmitoylation, myristoylation, prenylation and geranylgeranylation.

Following the entry of the S100P FASTA sequence into the GPS-Lipid 1.0 server, the server predicted two possible sites of modification (Figure 4.2.23). The first site of potential lipid modification is the 9th residue of S100P, a glycine residue, in which N-myristoylation is predicted. The other site is the sole cysteine residue of S100P at position 85, in which S-farnesylation is predicted. Both of the predictions are based in non-consensus sequences, meaning that the classical motifs for such modifications are not present within S100P, however the server still deemed there to be a likelihood of these modifications taking place within S100P. High thresholding was utilised on the server to make the prediction process more stringent with a lower false positive rate.

A

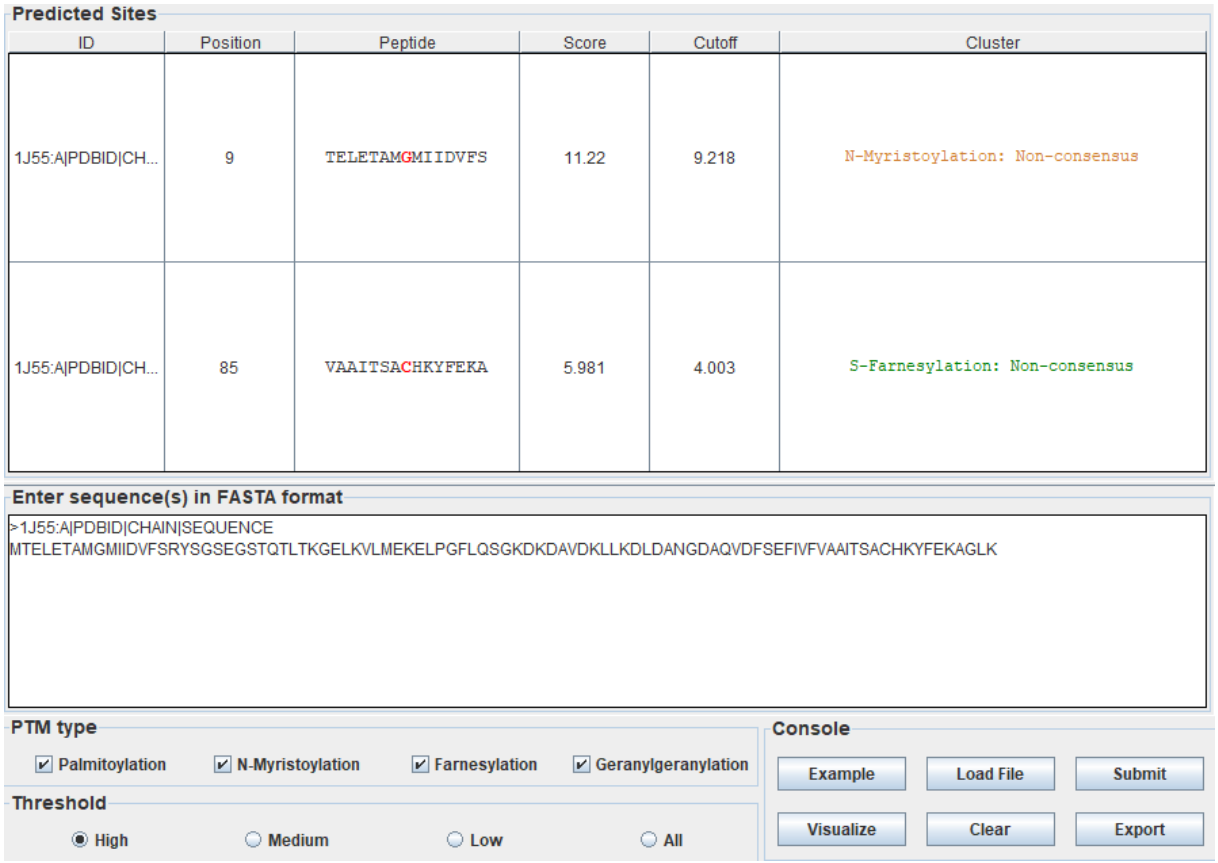

B

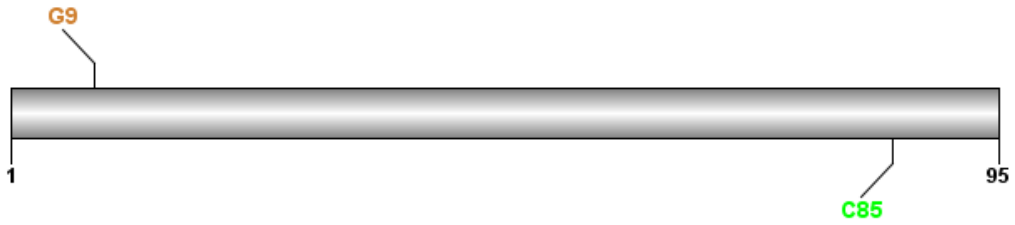

Figure 4.2.23: GPS-Lipid 1.0 predicts N-myristoylation and S-Farnesylation sites within S100P that do not follow a consensus sequence

A) The FASTA sequence of S100P was entered into the GPS-Lipid 1.0 program and assessed for potential lipid modification sites. Both predicted modification sites are displayed.

B) Schematic representation of possible PTM sites in S100P sequence responsible for membrane association.

Literature on the topic of lipid modifications and membrane association of proteins suggests that a lipid modification alone is not sufficient for membrane association. Studies have suggested that along with a lipid anchor, a polybasic domain within the protein is also necessary, as this domain can interact with negatively charged phospholipids at the plasma membrane. This has been seen by Fivaz and Meyer (2005) who found that the KRas protein required a polybasic region along with a palmitoylated residue in order to be targeted to the membrane.

With regards to S100P, a stretch of basic residues were found to be present at the C-terminus of the protein, namely lysine residues (Figure 4.2.24). These lysine residues were also suggested to be involved with membrane interaction when using the MODA server.

A

```
1  MTELETAMGM IIDVFSRYSG SEGSTQTLTK 30
31 GELKVLMEKE LPGFLQSGKD KDAVDKLLKD 60
61 LDANGDAQVD FSEFIVFVAA ITSACHKYFE 90
91 KAGLK
```

S100P

B

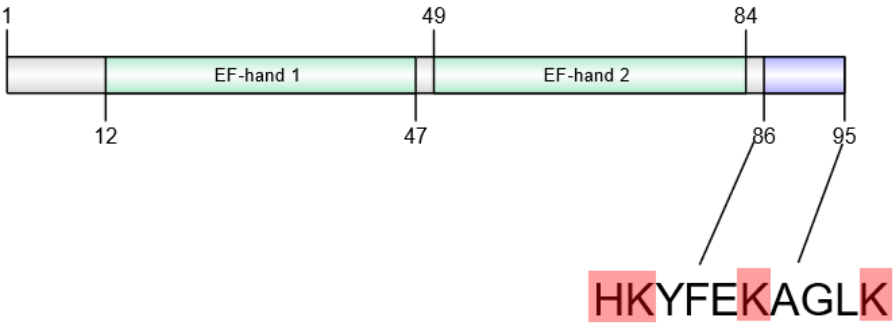

Figure 4.2.24: Schematic representation of the polybasic domain of S100P

A) Amino acid sequence of S100P. Basic residues of interest at the C-terminus are highlighted in red.

B) Full length S100P is presented with both EF hand regions (residues 12 to 47, and residues 49 to 84) and the polybasic domain (residues 86 to 95), which are highlighted in red.

Given that the x-ray structure provided by Zhang *et al.* (2003) is missing several residues, a protein model of dimeric S100P was generated using Robetta, a protein structure prediction server. This server uses comparative modelling to predict the structure of a given protein by treating individual domains as independent folding units, after which each unit can be assembled into a full chain model (Kim, D. E. *et al.* 2004). Following structure prediction, the model was downloaded and imported into PyMol to better visualise the polybasic domain (Figure 4.2.25). The C-terminal lysine residues were highlighted, along with the predicted sites of lipid modification (Figure 4.2.26). Interestingly, the two lysine residues at the C-terminus of S100P (K87 and K91) are aligned together on one face of the protein, with K95 extending outwards, forming a potential binding interface. This latter lysine residue, K95, is most likely highly mobile.

In addition, visualisation of the potentially lipid modified residues G9 and C85 highlights their close proximity to the lysine residues; G9 of one S100P monomer is within close vicinity to the lysine residues of another monomer, again highlighting the potential for the possible involvement of these residues in the membrane-association of S100P.

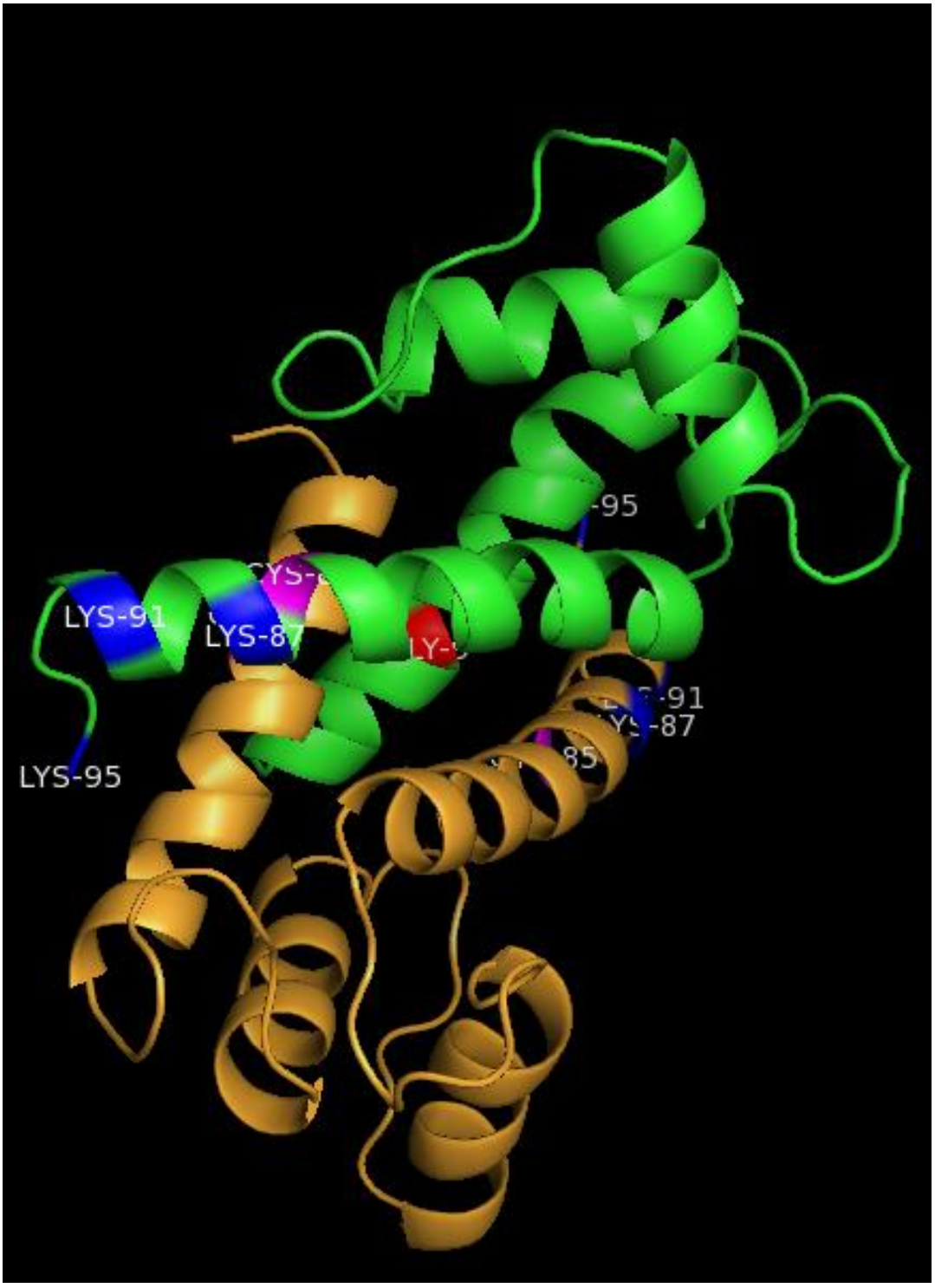

Figure 4.2.25: Modelling of S100P structure highlights a potential binding interface

A full-length structure of the S100P dimer was generated by Robetta and imported into PyMol. Lysine residues at the C-terminus have been highlighted (blue), along with potential lipid modification sites (red for G9, and purple for C85). Each monomer is highlighted in green and orange.

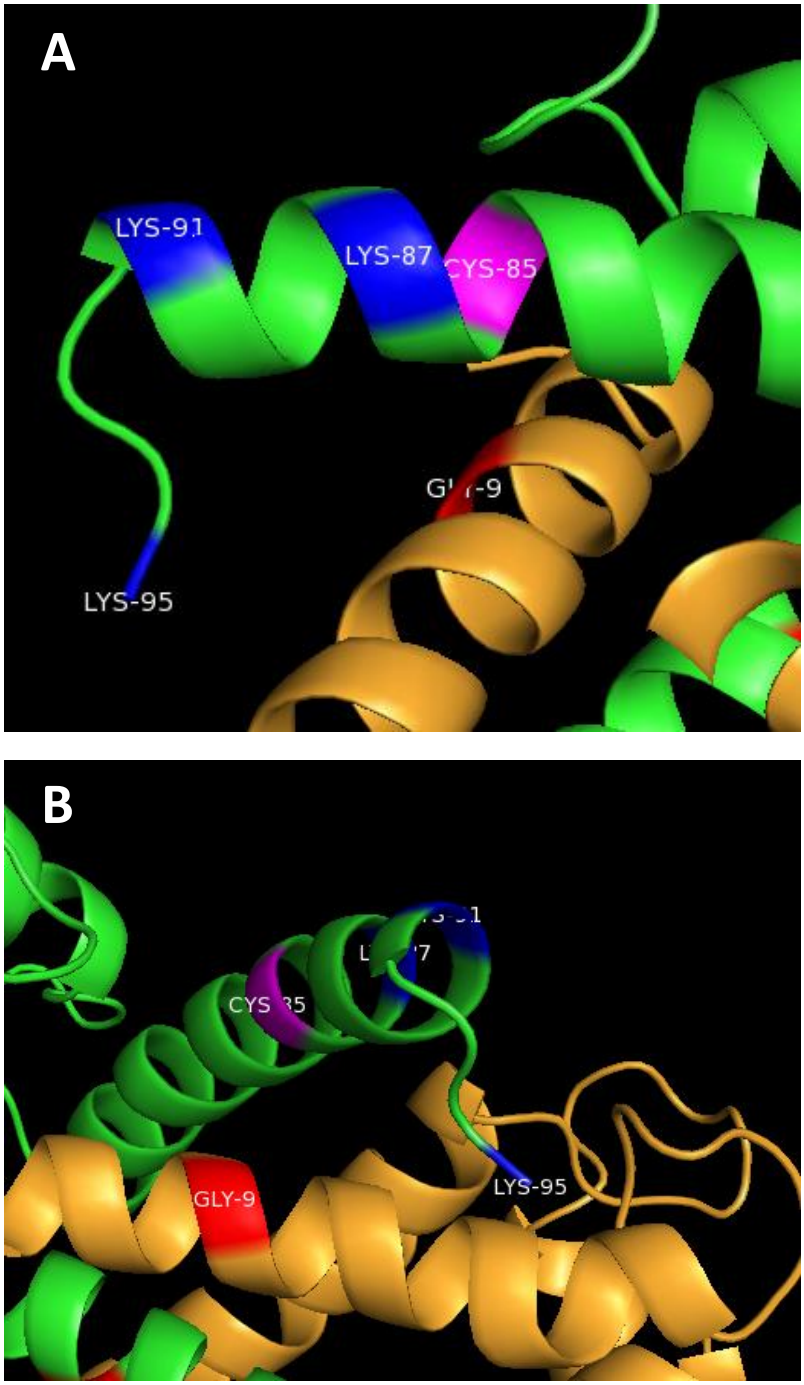

Figure 4.2.26: Modelling of S100P structure highlights a potential binding interface

Images of the C-terminal portion of S100P generated by Robetta and imported into PyMol. Lysine residues at the C-terminus have been highlighted (blue, panel A), along with potential lipid modification sites (red for G9, and purple for C85, panel B). Each monomer is highlighted in green and orange.

4.2.8 Primary first trimester extravillous trophoblasts express high levels of S100P

Previous work within Chapter 3 has shown that expression of S100P can be seen in a variety of cell lines, including those of trophoblastic origin. In order to bring S100P expression into a more physiologically relevant background, we sought to isolate extravillous trophoblasts (EVTs) from first trimester placental tissue and establish its levels of S100P. The isolated EVTs were first examined for expression of HLA-G, a marker that is highly specific to EVTs.

EVTs were seeded onto fibronectin-coated coverslips for 48 hours before completing an immunofluorescent stain for HLA-G (Figure 4.2.27). Pictures were taken at a 10x magnification to allow quantification of the proportion of cells that are expressing HLA-G. Following the counting of over 400 cells, 82.7% were found to express HLA-G, demonstrating the isolation of EVTs was successful. Counterstaining of F-actin using rhodamine phalloidin demonstrated the highly motile nature of these cells, with lamellipodia clearly visible at the edges of the cells in a large majority of the sample.

After confirming that the correct cell type was isolated from placental tissue, we sought to assess the expression level of S100P in EVTs. EVT cells were collected and their corresponding lysates run on SDS-PAGE before western blotting for S100P alongside a positive control, HTR8 clone 7 (Figure 4.2.28). Results from western blotting of EVT cells showed high levels of S100P expression, which was over 17-fold higher than the positive control HTR8 clone 7 after normalisation for tubulin was carried out. These results confirm that S100P is highly expressed in isolated first trimester EVTs.

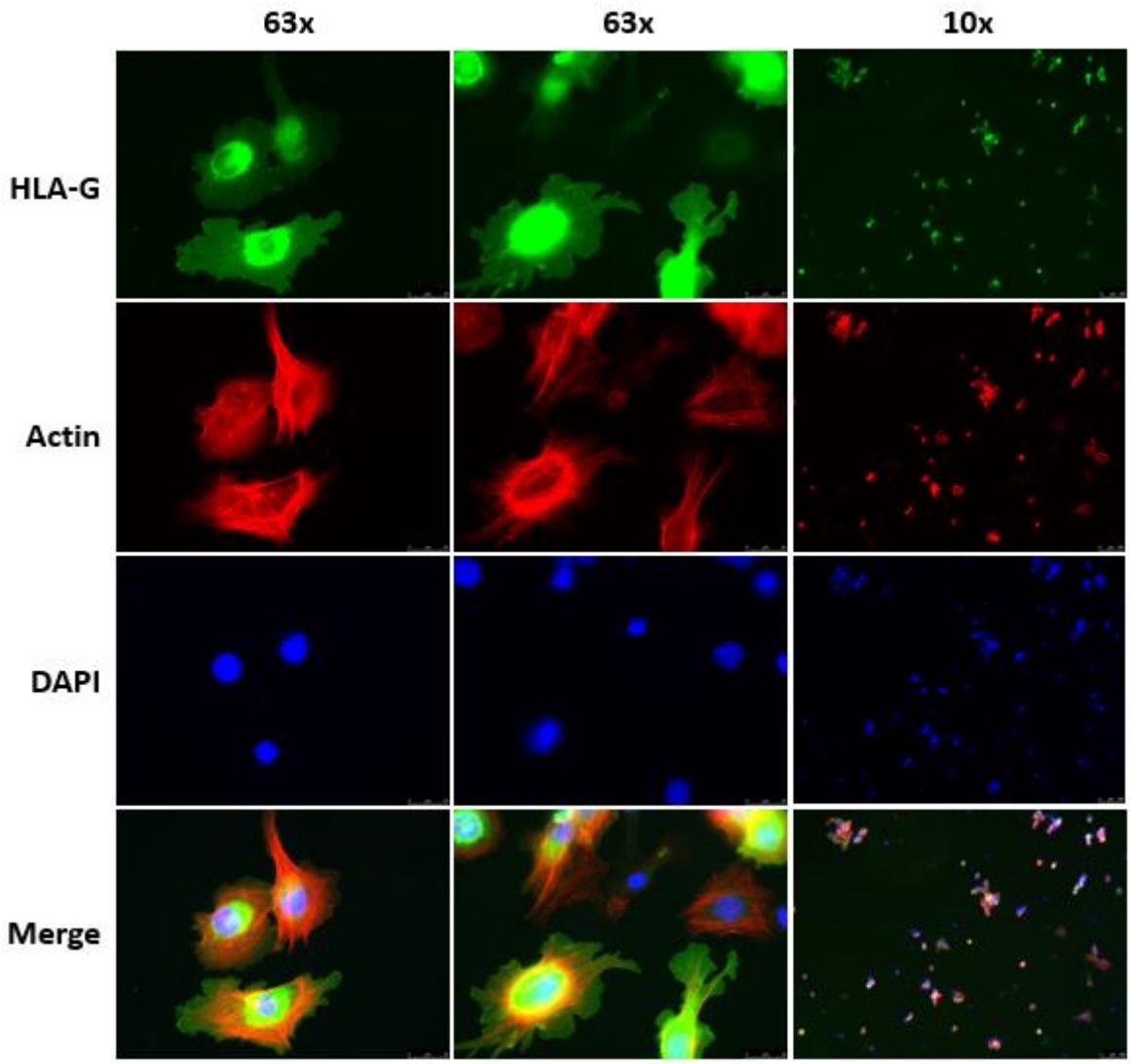

Figure 4.2.27: EVTs isolated from first trimester placental tissue express HLA-G

EVT cells isolated from first trimester placental tissue were seeded at a density of 20,000 cells per well onto fibronectin-coated coverslips and left for 48 hours prior to fixation, permeabilization and staining for HLA-G (green) and F-actin (red). Pictures were taken at 10x and 63x magnification with the Leica DMB4100 microscope.

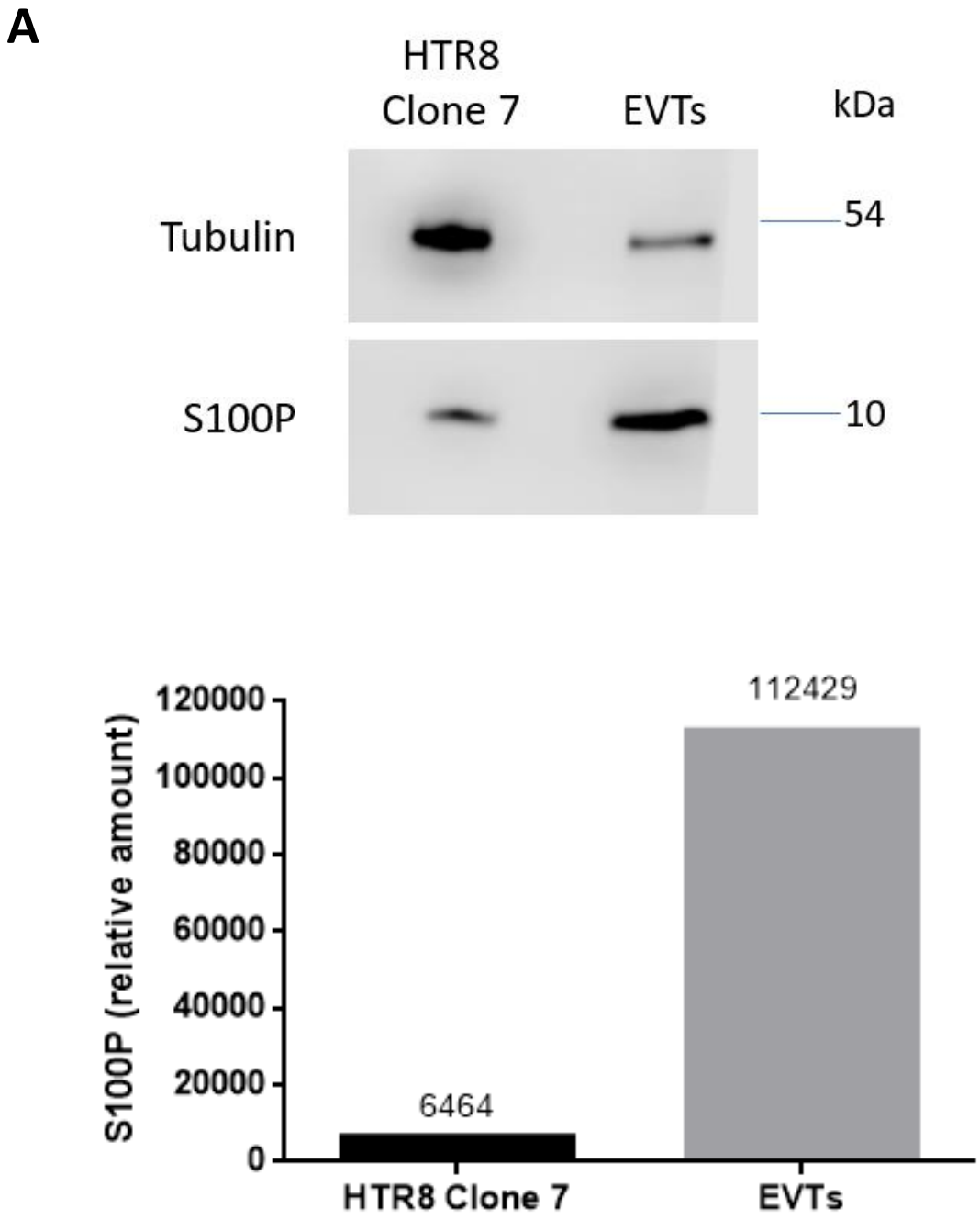

Figure 4.2.28: EVTs isolated from first trimester placental tissue express S100P at very high levels

A) EVT cells isolated from first trimester placental tissue were collected and separated on a 16% (w/v) SDS-PAGE alongside a positive control, HTR8 Clone 7, prior to western blotting for S100P and tubulin.

B) Densitometry analysis of S100P expression by HTR8 Clone 7 and EVTs using Image Studio Lite. S100P levels were normalised to tubulin. Raw density of S100P detected is presented above each bar. Data represents n=1.

4.2.9 S100P is detected at the cell surface of EVTs using biotinylation

Previous work within this chapter demonstrates the presence of S100P with isolated plasma membrane fractions within cell lines. This work was carried out using a variety of methods, namely nitrogen cavitation to isolate plasma membranes, or by using a cell surface protein isolation kit. This kit employs a cell impermeable form of biotin, Sulfo-NHS-SS-Biotin, that allows for isolation of cell surface molecules.

Large numbers of cells are required for plasma membrane isolation by nitrogen cavitation, which makes the isolation of plasma membranes from EVTs unfeasible. This is due to the limited number of EVT cells acquired when working with first trimester placental samples, with 1 to 2 million cells being obtained at the absolute maximum. However, it is possible to assess the presence of S100P on the cell surface using the cell surface protein isolation kit, in which cell surface material is biotinylated and pulldown is achieved using NeutrAvidin agarose slurry. Biotinylated cell surface proteins were eluted from the NeutrAvidin agarose slurry and subjected to separation on a 16% (w/v) SDS-PAGE prior to western blotting for S100P (Figure 4.2.29).

Presence of S100P at the cell surface was clearly demonstrated by western blotting, with bands being detected at around 10kDa and 17kDa. This data suggests that previous observations of S100P's presence at the cell surface within cell lines is conserved in primary cells isolated from first trimester placental tissue.

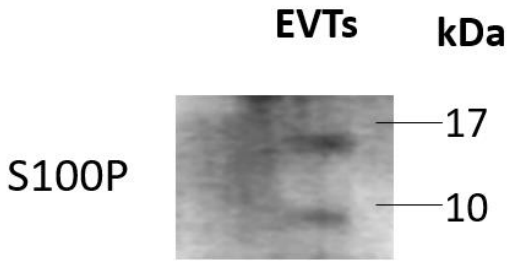

Figure 4.2.29: S100P is detected at the surface of EVT cells using a cell surface protein isolation kit

A) EVT cells isolated from first trimester placenta were seeded onto a 35mm fibronectin-coated dish (20µg/ml) and left to settle for 24 hours prior to biotinylation of cell surface proteins using the Pierce Cell Surface Isolation Kit. The resulting eluate was mixed with bromophenol blue and separated on a 16% (w/v) SDS-PAGE prior to western blotting for S100P.

4.2.10 Treatment of primary EVTs with an S100P antibody reduces their migration and invasion

Prior experiments have confirmed the expression of S100P in EVTs isolated from first trimester placental samples, as well as the presence of S100P at the cell surface. In order to assess if presence of S100P on the outside of EVT cells has an influence on their motility or invasion, isolated EVTs were seeded in a transwell assay system to measure their motility (Figure 4.2.30) and invasion (Figure 4.2.31), both with and without the presence of the S100P antibody. The S100P antibody will block extracellular S100P, allowing for the assessment of the importance of this cellular pool of S100P on motility and invasion.

Treatment of EVTs with an S100P antibody (diluted 1:1000) significantly reduced their motility by almost 35% ($p<0.0001$). Treatment of EVTs with a negative control, goat serum (diluted 1:1000) did not significantly reduce EVT motility ($p=0.13$). This data supports previous results obtained with HTR8 Clone 7, in which motility is also reduced by almost 40% upon treatment with the S100P antibody. These results suggest that extracellular S100P contributes to EVT motility. However, blocking extracellular S100P does not fully abrogate EVT motility, further suggesting the importance of intracellular S100P in the motility process.

In regards to EVT invasion, EVTs treated with the S100P antibody demonstrated a reduced ability to invade; EVT invasion was reduced by 40% ($p<0.0001$) when compared to the untreated control. A small, non-significant 5% decrease in invasion was detected when treating EVTs with goat serum ($p=0.62$). These results are once again very similar to results obtained to reciprocal experiments using HTR8 clone 7, in which invasion was reduced by 40% upon treating the cells with the S100P antibody. These experiments with EVTs confirm the reduction of S100P-dependent motility and invasion following blocking of extracellular S100P, once again suggesting a role for two separate pools of the S100P protein.

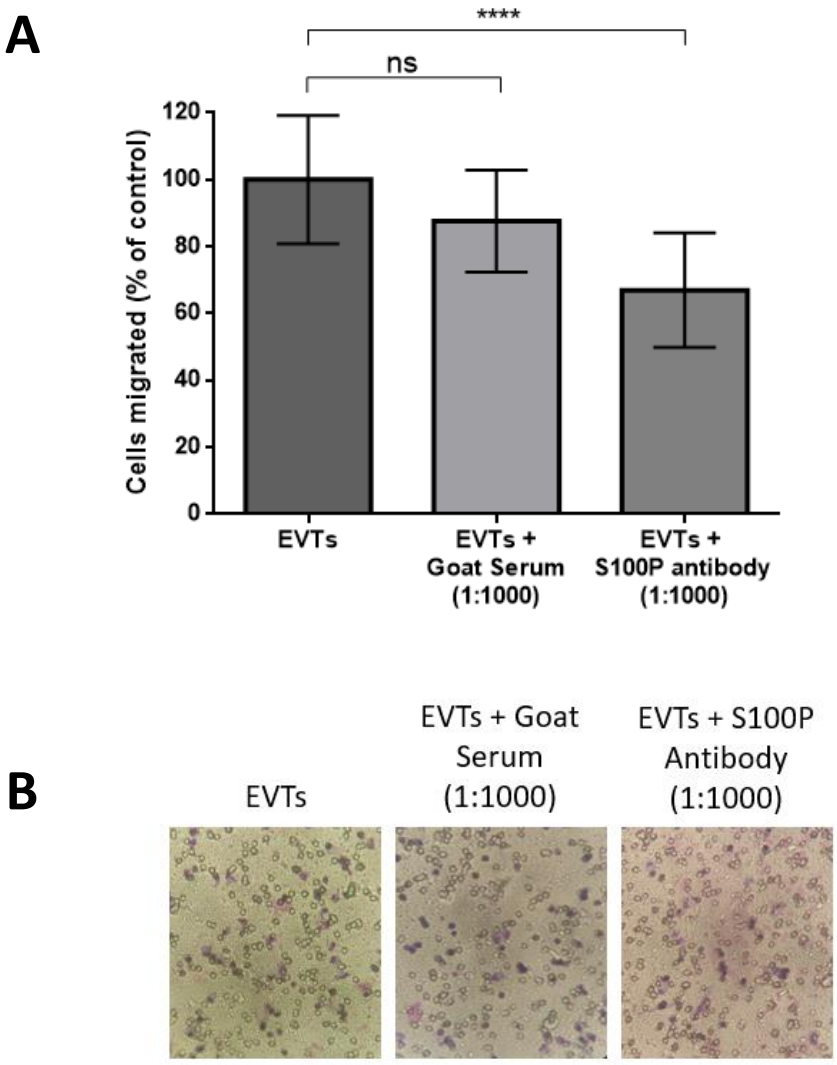

Figure 4.2.30: Treatment of EVTs with an S100P antibody reduces their motility

A) EVT cells isolated from first trimester placenta were seeded in triplicate onto Boyden chambers at a density of 20,000 cells per well, and treated either with goat serum diluted 1:1000 or with S100P antibody diluted 1:1000. Cells were left to invade for 24 hours before fixing and staining the transwell inserts. The number of cells migrated per field was counted, for 5 fields per well. Data represents the mean ±SEM from at least 3 independent replicates.

B) Pictures of one representative stained transwell per condition were taken at 40x magnification using a Nikon Eclipse TS100 inverted microscope.

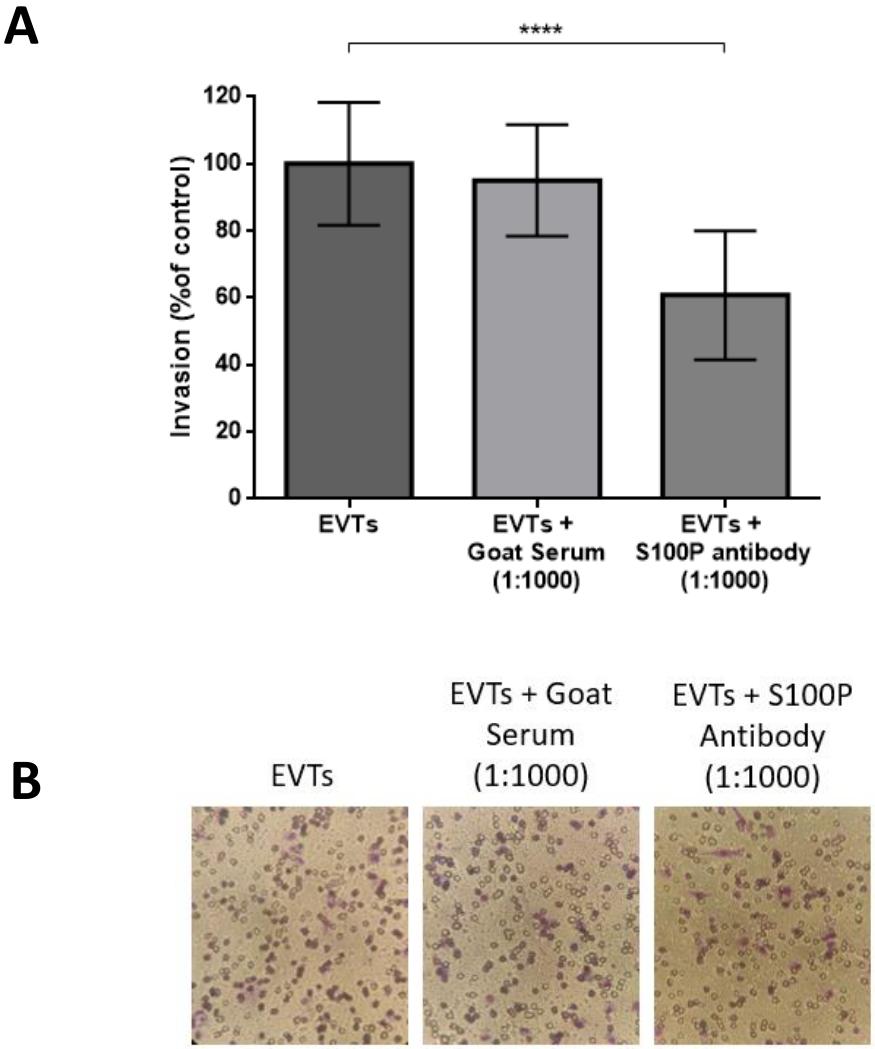

Figure 4.2.31: Treatment of EVTs with S100P antibody reduces their invasion

A) EVT cells isolated from first trimester placenta were seeded in triplicate onto Matrigel-coated Boyden chambers and treated either with goat serum diluted 1:1000 or with S100P antibody diluted 1:1000. Cells were left to invade for 24 hours before fixing the transwells with 4% PFA and staining them with Giemsa. The number of cells migrated per field was counted, for 5 fields per well. Data represents the mean ±SEM from at least 3 independent replicates.

B) Pictures of one stained transwell per condition were taken at 40x magnification using a Nikon Eclipse TS100 inverted microscope.

4.2.11 Treatment of primary EVTs with an S100P antibody does not affect focal adhesion formation

Following treatment of isolated primary EVTs with an S100P antibody for 24 hours, an S100P-dependent decrease in both EVT cell invasion and motility was detected through Boyden chamber assays. In order to assess some of the possible molecular mechanisms behind the decreased motility and invasion taking place as a consequence of blocking extracellular S100P, isolated EVTs were treated with an S100P antibody for 24 hours prior to being fixed and stained for paxillin, a marker for focal adhesions. EVTs were also treated with goat serum as a negative control, as previous experiments showed goat serum had no effect on either the motility or invasion of EVTs (Figures 4.2.30 and 4.2.31). Figure 4.2.32 illustrates the differences in focal adhesion formation between EVTs both prior to and following treatment with the S100P antibody and the negative control, goat serum.

Upon treatment of EVTs with either goat serum or the S100P antibody, there is no significant increase or decrease in the average number of focal adhesions formed by EVTs compared with untreated EVTs ($p>0.92$). This is once again in agreement with data previously obtained using HTR8 clone 7, where no changes in focal adhesion formation/maturation were detected. Staining for F-actin demonstrated no changes in overall actin organisation or structuration.

This data suggests that motility and invasion decreases seen in EVTs upon treatment with the S100P antibody are not reliant on alteration of focal adhesion formation, and perhaps that the S100P antibody alters EVT migration and invasion by another mechanistic route yet to be uncovered.

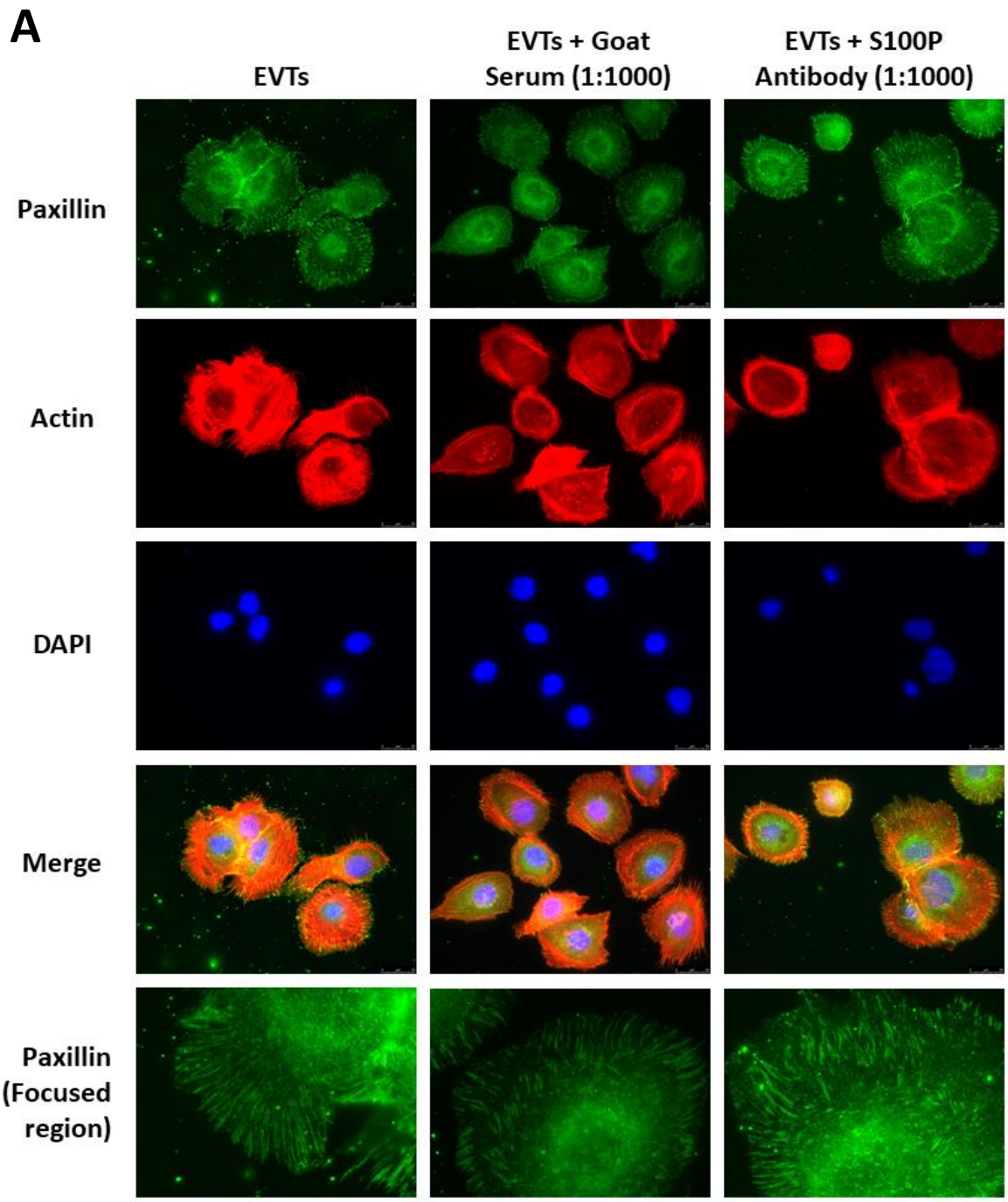
A
EVTs
EVTs + Goat Serum (1:1000)
EVTs + S100P Antibody (1:1000)
Paxillin
Actin
DAPI
Merge
Paxillin (Focused region)

B

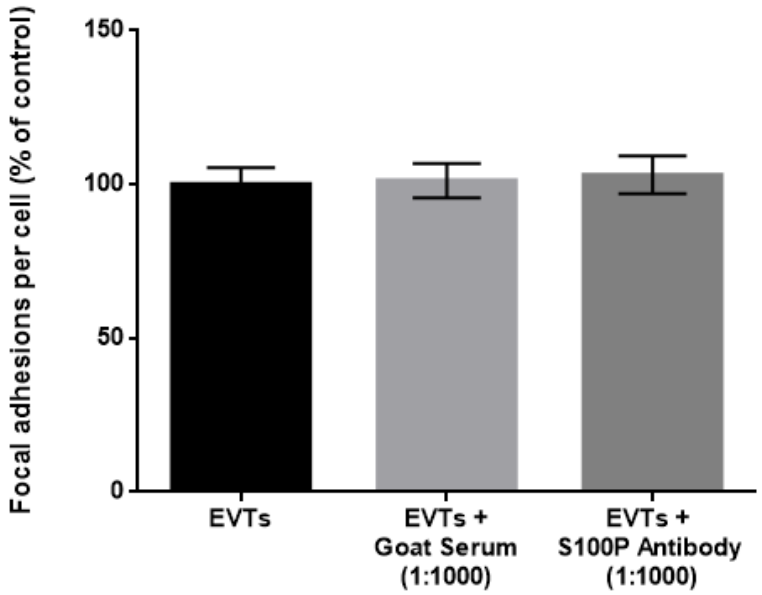

Figure 4.2.32: Treatment with an S100P antibody does not affect the number of focal adhesions formed by first trimester EVT cells

A) Isolated first trimester EVT cells, either untreated, treated with goat serum diluted 1:1000 or with S100P antibody diluted 1:1000, were seeded onto fibronectin-coated coverslips. Cells were incubated for 24 hours before fixing with 4% PFA, permeabilization with 0.1% triton, and staining for paxillin (green) and actin (red).

B) Average number of paxillin stained focal adhesions per EVT cell were counted for around 100 cells, with values presented as a percentage with respect to EVTs. Data represents the mean ±SEM from at least 2 independent replicates.

4.3 Discussion

Previous work within chapter 3 has illustrated the presence of S100P in cytoplasm and membrane fractions isolated from multiple cell lines expressing S100P. Therefore, it was deemed necessary to further dissect cellular compartments into a plasma membrane only fraction to ascertain if S100P is present within the plasma membrane.

Colocalisation of S100P and its target proteins at the internal plasma membrane regions of multiple cell lines has been reported. For example, research by Heil *et al.* (2011) demonstrated colocalisation of IQGAP1 and S100P at membrane ruffles or in close proximity to the plasma membrane of HeLa cells stimulated with EGF. EGF stimulation leads to a signalling cascade resulting in increased intracellular calcium (Bryant *et al.* 2004), therefore suggesting that colocalisation of these two proteins at this specific subcellular location requires calcium. The same could be said for ezrin, which is also found to be colocalised with S100P in or near the internal plasma membrane regions of A431 cells following increases in intracellular calcium (Koltzscher *et al.* 2003). There have not, as of yet, been any reports of S100P being detected, either alone or colocalised with other proteins, within the external plasma membrane of any cells, including trophoblast cells.

Knowing the high levels of expression of S100P within trophoblast cells of first trimester placenta, we sought to assess the localisation of S100P within *in vivo* tissue using first trimester placental tissue previously stained for S100P, along with matched tissue that was stained for HLA-G. HLA-G is a protein primarily expressed by EVT cells of the placenta (Tilburgs *et al.* 2015), and is therefore utilised as a marker of EVT cells within placental sections. The main functionality of HLA-G is thought to involve immune tolerance; membrane-bound HLA-G is an inhibitory ligand for natural killer cells at the maternal-foetal interface, thus preventing natural killer cell-mediated cell death of EVTs and the subsequent rejection of the foetus by the maternal immune system (Mandelboim *et al.* 1997).

The matched nature of the placental sections allowed for analysis of co-localisation of HLA-G and S100P, both confirming the presence of EVT cells and also giving an insight into regional localisation of S100P in EVT cell membranes. Analysis of these stained sections found quite a sufficient overlap of HLA-G and S100P at the plasma membrane of EVT cells within first trimester placental sections. No studies have specifically looked at membrane S100P by immunohistochemistry, however Zhu *et al.* (2015b), who have carried out similar immunohistochemical stainings on first trimester placenta, presented data showing a strong staining for S100P at the syncytiotrophoblast membranes, although this was not commented on by the authors.

Following analysis of *in vivo* human placental samples for membrane localised S100P, we sought to directly analyse the presence of S100P within the plasma membrane of cell lines. This was carried out using nitrogen cavitation and sucrose gradient, using a method that has been used by numerous groups (Chibber and Castle 1983, Noland *et al.* 1983, Zhou, M. and Philips 2017). Nitrogen cavitation of cells involves the dissolution of nitrogen within the cytoplasmic compartment, coupled with high pressure. After exposing cells to atmospheric pressure, nitrogen bubbles form within the cytoplasmic space, breaking open the cells (Simpson, 2010) thereby allowing full separation of plasma membrane fractions following differential centrifugation onto a sucrose cushion. Through the use of nitrogen cavitation to isolate plasma membranes, it is also possible to isolate proteins that are peripherally associated with the membrane (Zhou, M. and Philips 2017). This is as cavitation does not require detergents, which can lead to the presence of membrane proteins within the soluble fraction and loss of detectable protein within isolated plasma membrane fractions.

Following detection of S100P in isolated plasma membrane fractions in multiple cell lines, it was observed that S100P detected within plasma membrane fractions ran slower on the SDS-PAGE gel, and is detected at a higher molecular weight level than the respective cell lysate fractions by western blot. There could be several reasons for this, one of which being the high lipid content within the plasma membrane leading to slower separation of proteins (Rath *et al.* 2009). Given the fact that other marker proteins, tubulin and caveolin I, are not detected at this higher molecular weight level, this scenario was deemed unlikely, as high lipid content should affect the migration of all proteins within the sample, not just S100P. The other possible reason for the shift in molecular weight could therefore be due to a post-translational modification (PTM).

In order to predict potential PTMs of S100P that may be responsible for membrane-association, a group prediction server of lipidation was employed (Xie *et al.* 2016). This computational prediction process offers an alternative to the long process of experimental identification and reduces the amount of experimental testing required to identify a particular PTM. Knowledge of a PTM site can aid the understanding of various biological processes, or even allow for experimental manipulation for a desired biological effect. In order to generate prediction servers, such as the one utilised within this work, data sets of proteins with previously known PTMs are utilised, along with the local sequence information of the protein (Zhao *et al.* 2014; Deng *et al.* 2016). The prediction server GPS-Lipid 1.0 was employed in this study to predict potential sites of lipid modification within the S100P amino acid sequence. Previously, Shen *et al.* (2018) identified a post translationally modified residue within the BRAF protein using the GPS-Lipid 1.0 server, which was then experimentally confirmed by the group.

Lipid modification of proteins, known as lipidation, is the covalent attachment of lipid groups to a protein which can regulate its function and localisation (Hang and Linder 2011). There are several types of lipid that can be covalently attached to proteins. The addition of a 14-carbon saturated fatty acid myristate onto N-terminal glycine residues, known as myristoylation, has been documented in MARCKS, which in combination with its positively charged effector domain leads to its reversible insertion into the plasma membrane (Brudvig and Weimer 2015). The hydrophobicity of the myristoyl group facilitates membrane association due to the negatively charged nature of membrane phospholipids. Mutation of myristoylated residues can prevent association of proteins with cell membranes; for example, a G2A mutation in Lck tyrosine kinase results in a shift from membrane to a cytosolic localisation (Yasuda *et al.* 2000).

Prenylation is another class of lipidation, involving covalent attachment of either 15-carbon (farnesyl) or 20-carbon (geranylgeranyl) isoprenoid lipids to a cysteine residue (Wang and Casey, 2016). Most prenylated proteins contain a CAAX motif at their carboxyl terminus, and modification with a prenyl moiety can, like myristoylation, lead to association of a protein with the plasma membrane (Zhang and Casey, 1996). Such proteins include the Rho family GTPases, which when modified with a prenyl group at the C-terminus leads to their association with the membrane, and as a consequence of this, the activation of their effector proteins (Bishop and Hall, 2000). For proteins that lack membrane-binding capabilities, prenylation is thought to increase protein hydrophobicity and therefore membrane association.

The literature suggests that a single myristoyl or prenyl moiety is not sufficient to permanently anchor a protein to the plasma membrane. Proteins may require an additional lipid modification, or a stretch of polybasic amino acids as found in K-Ras4B (Hancock *et al.* 1990). The positively charged polybasic domain can interact with the inner leaflet of the plasma membrane, which contains acidic phospholipids, such as phosphatidylinositol 4,5-bisphosphate (PI(4,5)P2). Phosphorylation of serine residues in the positively charged effector domain of MARCKS leads to its reduced affinity for the plasma membrane (Kim *et al.* 1994). This mechanism of reversible binding of proteins to the plasma membrane is known as an electrostatic switch (McLaughlin, Stuart and Aderem 1995). Lipidation of proteins can therefore provide a way for their reversible localisation with the plasma membrane, influencing their interaction with other target proteins.

With prediction server GPS-Lipid 1.0 demonstrating sites of potential myristoylation (G9) and farnesylation (C85) in S100P, the combination of one of these modifications with the polybasic domain present at the C-terminus of S100P could lead to its targeting to the plasma membrane in a reversible manner.

Plasma membrane isolation and subsequent western blotting does not confirm if S100P that is present within this isolated fraction is localised to the outer or inner surface of the plasma membrane. To this end, it was possible to isolate cell surface proteins using a biotinylation kit. The biotin reagent, Sulfo-NHS-SS-Biotin, contains a sulfonate group, which is negatively charged and therefore cannot permeate the cell membrane. Sulfo-NHS-SS-Biotin also has high reactivity with primary amine groups, and therefore the longer the amide chain, the higher the chance of isolating a particular protein of interest. S100P as a protein consists of over 10% lysine residues (containing an amide chain), in theory meaning that the isolation of S100P on the cell surface, if it happens to be localised to the outer membrane, should be feasible.

Isolation of cell surface proteins using the aforementioned biotin reagent yielded a signal for S100P in all cell lines. Interestingly, multiple bands were detected in each cell line, with the COS-7 s10+ and HeLa A3+ cell lines demonstrating increased intensity of higher molecular weight S100P bands when compared to trophoblast cell lines. This data together suggests that S100P is present on the outer membrane/extracellularly in cell lines. As the biotin reagent is cell impermeable, there is the potential for it to bind to free amine groups on proteins outside of the cell that were not washed sufficiently, namely proteins that are part of the extracellular matrix (ECM). Several groups have reported the presence of extracellular S100P. Arumugam *et al.* (2005) detected S100P in the culture media of NIH3T3 and Panc-1 cells stably expressing S100P, and also in wild-type cell lines HPAC and BxPC3. The secreted S100P was hypothesised to activate autocrine signalling mechanisms and act as a ligand for RAGE in these cell lines. S100P was also detectable in the plasma of two different xenograft tumour models (Dakhel *et al.* 2014). In addition, prior research by Clarke *et al.* (2017) has demonstrated the ability to detect S100P on the surface of live Rama 37 cells by quantitative ELISA. Such data suggests that S100P is secreted from cells, however, no signal peptide has been predicted to be present within S100P, leading to the question of how S100P is able to be excreted from cells. Further work must be carried out to elucidate the pathway/pathways leading to secretion of S100P.

Through a variety of techniques, we established the presence of a pool of S100P associated with isolated plasma membrane fractions. However, the physiological relevance of membrane S100P, or how S100P came to be associated with the plasma membrane, has yet to be elucidated. It has been demonstrated that S100P expression stimulates the motility and invasion of different cell lines (Arumugam *et al.* 2005), including trophoblast cell lines (Tabrizi *et al.* 2018).

The marked decrease in both motility and invasion of JEG-3 and HTR8 cells following treatment with an S100P antibody suggests a role for S100P in these processes. S100P has been shown to interact with several proteins of an extracellular nature, including RAGE (Arumugam *et al.* 2004), and IL-11 (Kazakov

et al. 2015). Although interaction of IL-11 with S100P has been detected through surface plasmon resonance with purified proteins, no *in vitro* or *in vivo* interaction in cell lines and tissues has been demonstrated as of yet. IL-11 expression has been identified in the decidua, and its receptor, IL11 receptor alpha, has been identified on EVTs *in vivo* (Paiva *et al.* 2009). The authors found that treatment of HTR8 cells and primary EVTs with IL-11 significantly reduced EVT invasion, but not their adhesion, through the STAT3 pathway. It may be that by blocking S100P through use of an antibody, free IL-11 is left to circulate extracellularly, leading to the reported decreases in invasion. Interestingly, IL-11-mediated decreases in invasion were not abrogated through inhibition of MAPK pathways, suggesting a role for several signalling pathways in EVT invasion.

Few papers have characterised the effects of the addition of S100P antibodies on various cells. Dakhel *et al.* (2014) showed that multiple S100P antibodies generated by the group had the ability to neutralise the proliferative effect of recombinant S100P on the BxPC3 cell line, which was both time and dose dependent. Incubation with these antibodies was also able to block the phosphorylation of IκBα that is generated by S100P. Interestingly, the proliferative effect of S100P seen by Dakhel *et al.* (2014) has not been observed within the stably-expressing S100P HTR8 clones or JEG-3 cell line used within our studies. No differences in proliferation were detected between the non-S100P expressing HTR8 clone 3 or the S100P-expressing HTR8 clone 7, either before or after treatment with an S100P antibody (see figure 4.3.10). In contrast to our studies, Dakhel *et al.* (2014) utilised monoclonal antibodies to block the extracellular effects of S100P. It is not certain whether the use of a monoclonal versus a polyclonal antibody to S100P could lead to differences in cellular proliferation, motility or invasion. Clarke *et al.* (2017) further characterised the effect of the addition of an S100P antibody on cell invasion. S100P antibody added to the culture medium of Rama 37 cells expressing S100P reduced their invasion by almost 60% compared to untreated controls. In contrast, cells not expressing S100P, or expressing a C-terminal S100P mutant, showed no significant differences in their invasive capabilities following treatment with the S100P antibody, suggesting that the C-terminal portion of S100P is required for its motility- and invasion-promoting abilities.

We also sought to bring work completed with cell lines into a more physiologically relevant context by isolating EVT cells from first trimester placenta. Isolated EVTs were found to express high levels of S100P, over 17-fold the level expressed by HTR8 clone 7. This is somewhat interesting, given that a model first trimester EVT cell line, HTR8/SVneo, do not express S100P, and S100P is not detectable by either western blotting or qPCR in this cell line (Tabrizi *et al.* 2018). Szklanna *et al.* (2017) completed a comprehensive proteomic analysis of model trophoblast cell lines BeWo and HTR8/SVneo, with S100P being detected only in the BeWo cell line. In contrast, Zhou *et al.* (2016) were able to detect S100P by western blot in HTR8/SVneo. These studies suggest differential detection of S100P in HTR8 cells,

potentially due to the cells being obtained from different sources. In addition to detection of S100P in EVT cell lysates, S100P was also detectable in biotinylated membrane samples. Two bands at roughly 10kDa and 18kDa were detected by western blotting, the latter of which most likely relates to dimer formation. Taken together, this data strongly suggests S100P is present extracellularly, not just in cell lines, but that extracellular S100P localisation is conserved in isolated EVT cells.

Isolated EVTs were treated with an S100P antibody to assess if the response generated by trophoblast cell lines is conserved *ex vivo.* In much the same way as trophoblast cell lines, EVTs that were treated with an S100P antibody exhibited a significant reduction in both motility and invasion. Comparison of the effects on different pools of S100P, intracellular and extracellular, on motility and invasion was achievable through the use of siRNA technology and S100P antibody respectively. The degree of inhibition of both motility and invasion following siRNA treatment in JEG-3 cells is much greater than that seen by blockade of extracellular S100P through use of an S100P antibody, suggesting different pools of S100P have differential effects on motility and invasion, as inhibiting intracellular S100P has a greater effect on motility and invasion than that of extracellular S100P.

We sought to understand the molecular mechanisms at play behind the expression/reduction of S100P and its effects on cellular motility and invasion. Cellular motility and invasion are processes regulated and orchestrated by a wide variety of different proteins. The adhesion of cells to the substratum relies of the formation of focal adhesions, one component of which is paxillin. Our previously published work with choriocarcinoma cell lines JEG-3 and BeWo demonstrates an increase in focal adhesion formation, demonstrated through paxillin staining upon knockdown of S100P using siRNA targeted sequences (Tabrizi *et al.* 2018).

S100P-directed siRNA treatment of JEG-3 cells led to an increase in not only focal adhesion number, but their size. This is in line with the observation that fewer focal adhesions are consistent with migratory cells, as are smaller, less mature focal adhesions. Du *et al.* (2012) have shown a reduction in focal adhesion site disassembly in S100P-expressing HeLa cells following treatment with a FAK phosphorylation inhibitor. In addition, S100P-stimluated cell migration was abolished when HeLa cells were treated with the FAK phosphorylation inhibitor, suggesting S100P-mediated migration requires FAK. FAK redistribution and phosphorylation has been observed in EVTs following treatment with insulin-like growth factor-binding protein (IGFBP-1), mediated through α5β1 integrin binding. The phosphorylation of FAK leads to activation of the MAPK pathway through ERK-1 and ERK-2 phosphorylation (Gleeson *et al.* 2001).

One paper has characterised the interaction between S100P and integrin α7 leading to increased migration of lung cancer cells through activation of FAK and AKT signalling pathways (Hsu *et al.* 2015).

FAK is an important mediator of integrin signalling and has been shown in its activated form to colocalise with integrin α5 and MMP2 in EVT cells (MacPhee *et al.* 2001). Although the work by Hsu *et al.* (2015) concentrated on the interaction of these two proteins in a cancer background, Klaffky *et al.* (2001) have demonstrated expression of integrin α7 in mouse trophectoderm basement membranes and in trophoblast giant cells. In addition, integrin α7 null mice exhibit partial embryonic lethality at the early stages of pregnancy (Welser *et al.* 2007). As integrin α7 is a transmembrane receptor that binds to ECM components, such as laminin, it may be that loss of this receptor potentiates loss of adhesion to the decidual ECM, and therefore leading to poor embryo implantation.

In addition to changes observed in focal adhesions, S100P knockdown also leads to changes in the actin architecture of JEG-3 cells. The remodelling of the actin cytoskeleton is a key process linked to changes in cellular migration. Formation of key structures, including lamellipodia and filopodia at the edge of the cell, promote cellular motility (Blanchoin *et al.* 2014). Untreated JEG-3 cells show clear formation of lamellipodia, suggesting the cells are quite motile. Upon treatment with two different siRNA sequences targeted to S100P, JEG-3 cells demonstrate a lack of lamellipodia and changes in overall actin architecture, which includes the formation of actin stress fibres. Stress fibres are formed from bundles of actin filaments held together by actin crosslinking proteins, with the role of mediating cellular contraction (Pellegrin and Mellor 2007). These stress fibres in siRNA treated JEG-3 cells seem to terminate in focal adhesions, linking the cell to the substratum. An interaction partner of S100P, ezrin, has been shown to enhance tumour cell migration in concert with S100P (Austermann *et al.* 2008). It may be that S100P knockdown prevents activation of ezrin, which in turn inhibits cellular migration, leading to the formation of stress fibres as observed in section 4.3.3.

We aimed to understand the role of extracellular/membrane-associated S100P in focal adhesion formation through the use of an S100P antibody. Interestingly, treatment of both S100P-expressing and non S100P-expressing HTR8 cells, and primary EVT cells, with an S100P antibody led to no changes in focal adhesion number or size. Such observations lead to the suggestion that intracellular S100P and extracellular S100P regulate motility and invasion of cells through different pathways. Previous work by Du *et al.* (2012) has shown that the loss of focal adhesion sites induced by S100P can be reversed through treating cells with a FAK inhibitor, suggesting that S100P-dependent changes in migration require functional FAK. Growth factors such as epidermal growth factor (EGF) can activate FAK through its phosphorylation (Tapia *et al.* 1999). Phosphorylated FAK has been detected in plasma membrane regions of interstitial trophoblasts (differentiated EVTs), and is at its highest levels within the first trimester of pregnancy. Knockdown of FAK led to decreased invasion of CTBs from explanted anchoring villi in culture, as well as decreasing *in vitro* invasion of isolated CTBs (Ilić *et al.* 2001). FAK in complex with Src phosphorylates paxillin, leading to the generation of binding sites for various other adapter

proteins, and consequently the binding and activation of Rho guanine nucleotide exchange factors (Rho-GEFs). Subsequent activation of the Rho family GTPases, including RhoA, Rac and Cdc-42 can lead to activation of further downstream molecules known to regulate the cytoskeleton (Ferretti *et al.* 2007). One such downstream effector of this pathway, p21-activated kinase (PAK) can modulate Rho-associated kinases (ROCKs). Shiokawa *et al.* (2002) have treated isolated CTBs with a specific ROCK inhibitor and noted suppression of migration, suggesting that ROCK signalling is involved in trophoblast migration. Rac and Cdc-42 have been demonstrated to interact with IQGAP1, an interaction partner of S100P (Heil *et al.* 2011). Through interaction with these two GTPases, their GTP-bound forms are maintained which leads to induction of actin polymerisation through interactions with their effector proteins (Noritake *et al.* 2005). Binding of S100P to IQGAP1 has been shown by Heil *et al.* (2011) to have no effect on IQGAP1's interaction with Rac or Cdc-42, suggesting no negative regulation of S100P on cellular motility through its interaction with IQGAP1.

Another interaction partner of S100P, ezrin, directly interacts with FAK through ezrin's N-terminal domain (Poullet *et al.* 2001). In addition, activation of FAK by overexpressed ezrin did not require stimulation by external growth factors. FAK is critical in the turnover of focal adhesions (Ren *et al.* 2000), and interestingly, depletion of ezrin in breast cancer cells leads to an inhibition of focal adhesion turnover, and, in addition, an increase in the number and size of focal adhesions (Hoskin *et al.* 2015). Given that intracellular S100P knockdown leads to an increase in focal adhesions, whereas blockade of extracellular S100P by use of an antibody does not, it is possible that the actions of the extracellular pool of S100P occurs via a different pathway, perhaps without the involvement of FAK.

We sought to understand if the effects of extracellular S100P on motility and invasion are dependent on RAGE, a previously characterised extracellular binding partner of S100P. Penumutchu, Chou and Yu (2014) characterised the interaction between RAGE and S100P, which occurs through RAGE's V domain and S100P's C-terminal hydrophobic patch (Y88, F89, A92, G93) in combination with its linker region (L41, P42, G43, F44) and several residues in helix 1. As one of the only known extracellular binding partners for S100P, we sought to understand if activation of RAGE through S100P plays a part in the reported extracellular actions of S100P in trophoblasts. Cromolyn is an anti-allergy drug that has been documented to block interaction between S100P and RAGE, through direct binding to S100P within its C-terminal hydrophobic patch (Arumugam *et al.* 2006). Binding of other S100 proteins to cromolyn has previously been reported; both S100A12 and S100A13 bound to cromolyn in a calcium dependent manner (Shishibori *et al.* 1999), however the consequences of these interactions have not been fully established; Shishibori *et al.* (1999) hypothesised that cromolyn, through interaction with its binding partners, inhibits IgE-mediated degranulation of basophils and mast cells, although the exact mechanism of cromolyn's actions are not fully understood. Arumugam, Ramachandran and Logsdon

(2006) found that cromolyn treatment of BxPC3 cells led to a dose-dependent inhibition of NFκB activity, with later experiments confirming this inhibition *in vivo.* Namba *et al.* (2009) found that cromolyn did not, however, affect the mRNA expression of S100P in transfected gastric adenocarcinoma cell line AGS.

To understand the role of potential S100P-RAGE interaction in trophoblasts, and to assess if previous defects in motility and invasion following treatment of cells with an S100P antibody is dependent on RAGE, non-S100P expressing HTR8 clone 3 and S100P-expressing HTR8 clone 7 were treated with cromolyn and their proliferation was assessed at 24 and 48 hours following administration. This work demonstrated no significant anti-proliferative effect of cromolyn on HTR8 clones either expressing or not expressing S100P, as growth of both cell lines in the presence of cromolyn were not statistically different from their untreated counterparts. This outcome somewhat contrary to Arumugam, Ramachandran and Logsdon (2006) who found that defects in cell proliferation of pancreatic cancer cells expressing endogenous S100P, but not in pancreatic cells that do not express endogenous S100P. It is possible that the cellular background could contribute to differences observed in proliferation. In addition, this study utilised an MTS reagent which measures differences in cell metabolism, a contrast to our work which uses cell counting with trypan blue exclusion. In addition, significant differences in cell proliferation, as measured by the MTS assay, were only reported at the 72-hour time point following cromolyn treatment. Cell migration and invasion assays on HTR8 clones took place over a 24-hour time period, a point at which no significant differences in cell proliferation between 100μM treated and untreated samples were detected by the group. Whether the effect of cromolyn on cell proliferation is dependent on cell background is not yet known.

Treatment of non-S100P expressing HTR8 clone 3 with cromolyn led to no significant changes in cell migration or invasion. In contrast, S100P-expressing HTR8 clone 7 demonstrated a 30% decrease in motility and a 20% decrease in invasion following treatment with 100μM cromolyn. The level of reduction in S100P-expressing HTR8 motility following cromolyn treatment is at a similar degree to that exhibited by S100P-expressing HTR8 cells treated with S100P antibody, in which a 35% decrease in motility was observed. This suggests the potential for RAGE to be responsible for S100P-dependent motility. However, it is perhaps the case that cromolyn may just be preventing interaction of S100P with its target proteins, as cromolyn's binding site on S100P appears to coincide with binding sites of other S100P target interactors, namely within the C-terminal region of S100P.

The S100P antibody has a greater effect on cell invasion than cromolyn, suggesting the involvement of other S100P target proteins, either characterised or yet to be discovered, in the invasive process. The level of motility and invasion exhibited by S100P-expressing cells following treatment with 100μM

cromolyn was still above basal levels of migration and invasion demonstrated by S100P-negative HTR8 clone 3, suggesting that S100P-RAGE interactions are only partially responsible for S100P-dependent differences in motility and invasion.

There is very little in the literature concerning cromolyn's effects on cellular motility. Skedinger *et al.* (1987) found that treating neutrophils with cromolyn decreased their chemotaxis towards serum. Stimulation of intracellular free calcium by the serum utilised was also inhibited by treating cells with cromolyn. Cromolyn's effects on cell invasion, on the other hand, have been explored by Arumugam, Ramachandran and Logsdon (2006), who treated S100P-expressing BxPC3 cells with cromolyn and reported a significant 60% decrease in cell invasiveness. This effect was S100P dependent, as Panc-1 cells not expressing endogenous S100P did not exhibit the same reduction in cell invasion following cromolyn treatment. Namba *et al.* (2009) treated S100P-expressing AGS cells with cromolyn and found a decrease in their invasion. Reduced invasion was not seen with non S100P-expressing AGS cells, confirming the inhibitory effect of cromolyn on S100P-expressing cell invasion in this cellular background.

These findings may be somewhat limited due to the specificity of cromolyn. Cromolyn could be interacting with other target proteins aside from S100P, evidenced by the fact that cromolyn can also bind to other S100 proteins, such as S100A12 and S100A13 (Shishibori *et al.* 1999). Its use as an anti-allergy and anti-asthmatic drug further implicates cromolyn in other potential target protein interactions.

To assess how cromolyn may interfere with S100P's membrane-association capabilities, HTR8 clone 7 cells were treated with 100µM cromolyn prior to membrane extraction. With results demonstrating a decrease in detectable membrane-associated S100P, it suggests that cromolyn may be interfering with S100P's ability to associate with plasma membranes. Cromolyn binds to residues in helices 1 and 4 within S100P, in addition to S100P's linker region, a region that was predicted to have a high probability of associating with membrane regions (Figure 4.3.19). Given this information, it seems likely that binding of S100P to cromolyn prevents its association with membranes. In addition, binding of several protein targets by S100P is facilitated by residues in the linker region (RAGE) or in helix 4 (ezrin), suggesting that binding of cromolyn to S100P may perturb S100P's interaction with several target proteins.

With the biological implications of extracellular S100P having been investigated, we sought to understand the biochemical and structural nature of S100P that lead to its detection in isolated plasma membrane fractions, and whether S100P detected in these fractions is membrane integral or peripherally linked. Work within this chapter employed the use of MODA, a methodology in which

submission of a protein sequence to an online MODA server leads to the prediction of residues which have the potential to interact with membranes (Kufareva *et al.* 2014). MODA predicted two interfaces of potential membrane-binding residues, one of which is present within the linker region of S100P.

The linker region of S100 proteins, from roughly residues L41 to K51 within S100P, is highly diverse (Zhang *et al.* 2003), and is therefore thought to be involved in potential binding of target proteins. For example, Réty *et al.* (1999) found that interaction between S100A10 and annexin II involves this region. Penumutchu, Chou and Yu, (2014) characterised the binding interface between cromolyn and dimeric S100P, in which G43, F44 (within S100P's linker region), A84, F89 and G93 residues from one monomer and residues within helix 1 from another monomer comprise the binding region. This confirms at least one molecule utilises residues within the linker region of S100P to form a complex.

The other patch of residues within S100P that could be involved in forming a membrane interaction interface involves a spread of residues spanning the entirety of helix 4 at the C-terminus of the protein, from F71 to L94. This region is also said to be part of S100P's dimerisation interface; Koltzscher and Gerke (2000) conducted a detailed study on the residues involved in dimer formation in S100P. Within helix 4, the sole cysteine residue, C85, was replaced with alanine and was found to still interact with wild type S100P. This is similar to the S100A4 protein, in which Tarabykina *et al.* (2000) found that replacing two C-terminal cysteine residues (C76 and C81) with serine residues did once again not prevent homodimerisation, but did prevent interaction of S100A4 with S100A1. Mutation of C84S in S100B leads to an increase in tau phosphorylation, suggesting certain members of the S100 family rely on cysteine residues for S100-target protein interactions (Landar *et al.* 1997). Further studies on S100P dimerization through the use of chemical cross-linking experiments by Austermann *et al.* (2008) showed that residues 88-95 are not necessary for homodimer formation, but are required for calcium-dependent interactions with the N-terminal ERM association domain (N-ERMAD) of ezrin.

These studies raise the question as to whether membrane-associated S100P is in fact monomeric or dimeric. If the C-terminal residues predicted using MODA are in fact dispensable for S100P dimer formation, but are required for target protein interaction, then it is possible that both monomeric and dimeric S100P could be membrane associated. Monomeric activities of S100P have only recently gained attention, as previous literature suggests that dimer formation is obligatory for S100P's functionality (Koltzscher and Gerke, 2000). Kazakov *et al.* (2018) recently characterised the interaction with human serum albumin (HSA) with monomeric S100P, evidenced to be specific due to lack of HSA binding to other S100 proteins. Further research by several of the same authors identified an interaction between monomeric S100P and interferon beta (IFN-β). Cell viability defects in MCF-7 cells

following IFN-β treatment were in fact rescued following treatment with purified S100P (Kazakov *et al.* 2020).

Chapter 5:

S100P interactomes in cytoplasmic, membranous or extracellular compartments

Chapter 5: S100P interactomes in cytoplasmic, membranous, or extracellular compartments

Contents

5.1 Introduction

Work within the previous chapter has demonstrated the presence of S100P primarily in isolated plasma membrane fractions, as well as cytoplasmic, and has established the role of this pool of S100P in promoting both motility and invasion through an alternative pathway to that of intracellular S100P.

As of yet, only few extracellular or membrane-bound interaction partners of S100P have been characterised. Much is known about the implications of RAGE activation by S100P in a cancer background, with S100P binding to RAGE leading to increased proliferation and invasion of pancreatic cancer cell lines (Arumugam *et al.* 2004). Other binding partners of S100P that are localised to the extracellular space include IL-11, whose interaction with S100P is yet to be characterised either in cell lines or *in vivo* (Kazakov *et al.* 2015). More recently, interaction of tPA with S100P was observed by Clarke *et al.* (2017), who established that activation of tPA by S100P is dependent on the presence of C-terminal lysine residues in the S100P structure. In addition, Clarke *et al.* (2017) were able to detect S100P on the outside of S100P-expressing Rama 37 cells by quantitative ELISA, supporting our findings that S100P can be detected in this location.

Our previous work has centred on the role of S100P in trophoblasts (Tabrizi *et al.* 2018), in which both gain and loss of S100P expression led to increases or decreases in migration and invasion respectively. However, the binding partners and pathways regulated that mediate this response in concert with S100P are yet to be elucidated in cells of trophoblastic origin. Given that the above studies were carried out on cells of a cancer background, we sought to identify either previously characterised or novel interactors of the S100P protein solely in trophoblasts.

In this chapter, we wanted to further characterise whether S100P would be integrated into different complexes in cell lysates or cytoplasm/membrane compartments using blue native PAGE (blue native polyacrylamide gel electrophoresis, or BN-PAGE). Proof of the presence of S100P in different complexes would offer further opportunities to establish differences in S100P expressing cells, and would allow us to determine the composition of cytoplasm/membrane fractions of trophoblast cells, previously separated by subcellular fractionation, using mass spectrometric analysis of BN-PAGE gels. Finally, we aimed to assess the effects of S100P expression on changes in protein abundance, with the goal of identifying enriched biological themes within samples and potential regulators/interactors of S100P that may facilitate its interactions either intracellularly or extracellularly in trophoblasts.

5.2 Results

5.2.1 S100P is detected as part of a high molecular weight complex in cell lysates and cytoplasm/membrane fractions by western blotting

Previous work has characterised a new, membrane associated pool of S100P present within multiple cell lines, including EVT cells isolated from primary tissue. We sought to gain further understanding about the S100P interactomes in these cells in an effort to shed new light into the recently characterised role of S100P in cellular migration and invasion of trophoblast cells, be it either in the intracellular or extracellular compartments.

To initiate this process, cell lysates and cell fractions from multiple cell lines, both of cancer and trophoblastic origin, were separated on a blue native PAGE gel, with a gradient of 4-16% (w/v). Blue native PAGE (blue native polyacrylamide gel electrophoresis, or BN-PAGE) allows for separation of proteins under native conditions, without denaturation of protein complexes. Any protein complexes formed within cells will therefore retain their native structure, and allows for assessment of complex sizes and composition within the cell fractions of multiple cell lines (Wittig *et al.* 2006). Furthermore, western blotting of blue native PAGE gels for S100P allows for the determination of S100P-containing complexes present within cell lysates and isolated cell fractions, along with their size.

Cell lysates and cell fractions were collected from cell lines COS-7 s10+, HeLa A3+, JEG-3, BeWo and HTR8 clone 7 prior to separation on a NativePAGE 4-16% (w/v) Bis-Tris gel and western blotting for S100P (figure 5.2.1). In both non-trophoblast cell lines, COS-7 s10+ and HeLa A3+, low molecular-weight bands estimated at 20 to 60kDa were detected by the S100P antibody in both cell lysate and cytoplasm and membrane fractions. These bands are thought to relate to S100P dimer, trimer or tetramer formation. This band is absent in the nuclear fraction of both cell lines. A smear at around 480 to 1000kDa was detected by the S100P antibody in both HeLa A3+ and COS-7 s10+ cell lysates, and was found to be enriched in their respective cytoplasm and membrane fractions.

Low molecular weight complexes, most likely corresponding to S100P dimers, were found in cell lysates and cytoplasm and membrane fractions in trophoblast cell lines JEG-3, BeWo and HTR8 clone 7. A faint band for S100P was detected below 146kDa in the nuclear fraction of the BeWo cell line, however, previous results from fractionation experiments suggest this band is a contaminant from cytoplasmic proteins, or an overspill from neighbouring lanes, and not a true representation of S100P's presence within this fraction. Similar to non-trophoblast cell lines, a smear was detected by the S100P antibody at around 480 to 1000kDa in the cell lysates of JEG-3, BeWo, and HTR8 clone 7 cell lines. As

seen before with both HeLa A3+ and COS-7 s10+ cell lines, this smear is enriched within the cytoplasm and membrane fractions, suggesting this fraction is the source of this high molecular-weight complex containing S100P.

In addition to the high-molecular weight complex that appears to contain S100P at 480 to1000kDa in each of the trophoblast cell lines, S100P was detected at the bottom of each well (arrows). These bands are most prominent within the cell lysate and cytoplasm and membrane fractions, especially in HTR8 clone 7. All in all, these results suggest that S100P is part of a high molecular weight complex within cytoplasm and membrane fractions that appears to somewhat be more enriched within trophoblast cell lines in comparison to inducible cell lines COS-7 s10+ and HeLa A3+.

.

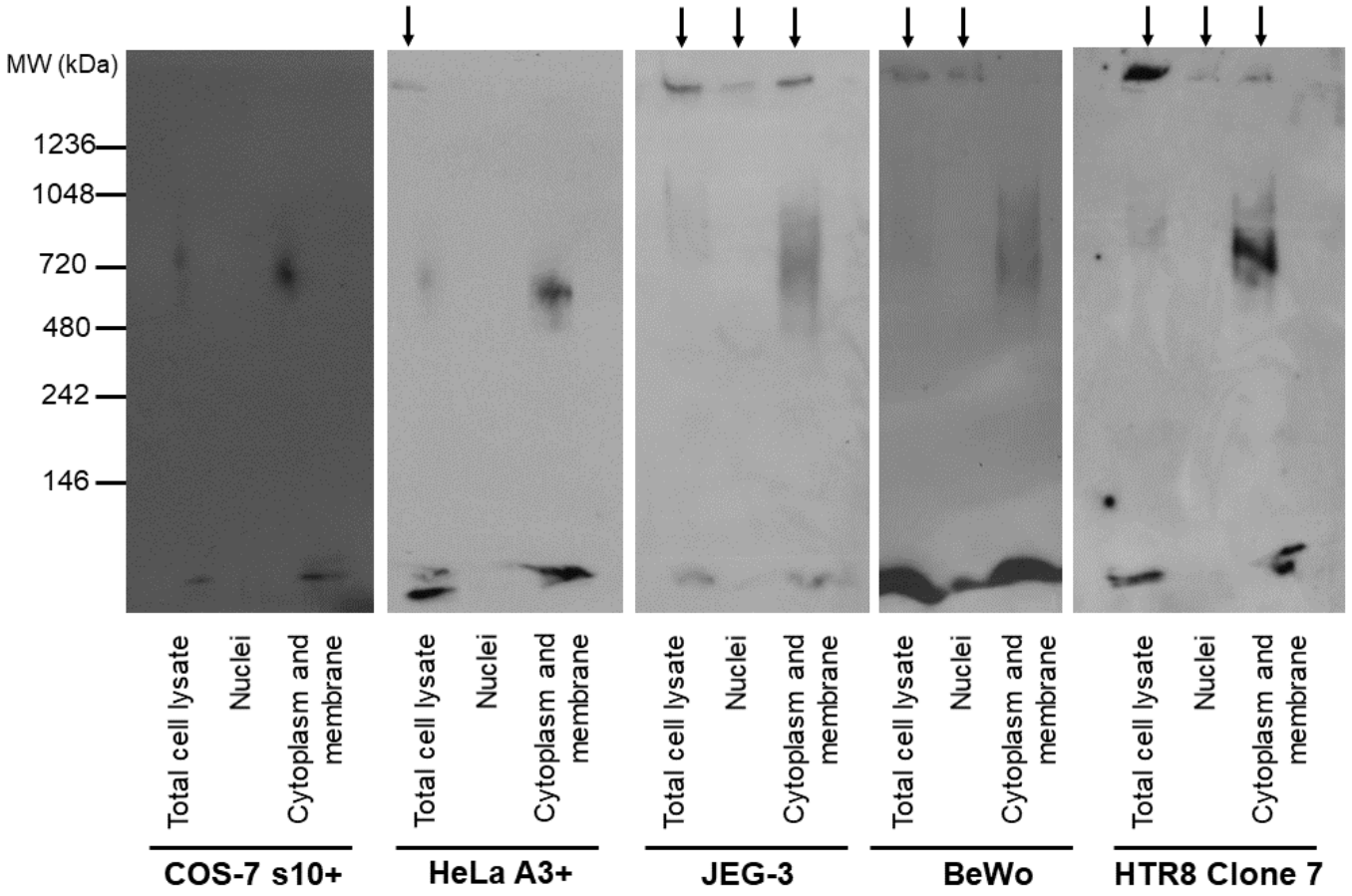

Figure 5.2.1: S100P forms high molecular weight complexes in the cytoplasm and membrane fractions of trophoblast and non-trophoblast cell lines

Cell lysates and cell fractions (nuclei, cytoplasm and membrane) from COS-7 S10+, HeLa A3+, JEG-3, BeWo and HTR8 Clone 7 cell lines were collected and separated on a NativePAGE 4-16% (w/v) Bis-Tris gel prior to western blotting for S100P. Non-migratory S100P was detected (arrows) in multiple cell lines.

5.2.2 S100P expression in trophoblast cell lines leads to significant changes in global protein abundance

As a means to shed more light on the overall protein composition of S100P-expressing cells versus non S100P-expressing cells, cytoplasm and membrane fractions of non-S100P expressing HTR8 SGB16 Clone 3, and S100P-expressing HTR8 SGB217 Clones 5 and 7 were separated on a NativePAGE 4-16% (w/v) Bis-Tris gel in triplicate prior to mass spectrometry analysis. Mass spectrometry was utilised to assess the quantity and natures of all proteins present within these fractions. As the cytoplasm and membrane fractions from each cell line contain many different proteins, it was necessary to cut the gel into four fragments according to their approximate molecular weight (Figure 2.2.6). This allows for filtering of proteins by their presence in each gel fragment, as well as increasing the level of protein digestion by trypsin. Proteins detected only in the lowest molecular weight fraction, fraction 1, were excluded, as these are most likely to contain contaminants and give a greater possibility of false positive results.

Following tryptic digestion of gel fragments from each of the three HTR8 clones, a total of 663 proteins were identified across all samples by mass spectroscopy. The normalised abundance for each protein in the triplicate samples for each of the three cell lines was averaged. At this point, results from HTR8 Clones 5 and 7 were merged to allow for analysis of “S100P negative” (HTR8 SGB16 Clone 3) versus “S100P positive” (HTR8 SGB217 Clones 5 and 7) cell lines, in addition to giving a clearer picture of how abundance of certain proteins may be affected by S100P expression. Normalised abundances from S100P negative and S100P positive samples were input into GraphPad 6.0 for statistical analysis using multiple unpaired T-tests, one T-test per protein detected. Of 663 proteins detected, differences in abundance of 232 proteins between S100P negative and S100P positive samples were detected at a P value below 0.05. These 232 proteins were then analysed for fold changes in abundance between S100P negative and S100P positive samples, and those which were above 1.5-fold difference in abundance between S100P negative and S100P positive samples, a total of 73 proteins, were used for further analysis (Table 5.2.1).

Name	Gene Name	Accession	Fraction	P value	S100P Negative Mean	S100P Positive Mean	Difference	Normalised S100P Negative	Normalised S100P Positive
L-lactate dehydrogenase B chain	LDHB	LDHB_HUMAN	1;2;3	0.000855	5492.89	8279.11	-2786.22	1	1.507241179
Eukaryotic translation initiation factor 2A	EIF2A	EIF2A_HUMAN	4	0.008372	207.617	313.549	-105.931	1	1.510227968
40S ribosomal protein S2	RPS2	RS2_HUMAN	2;3;4	0.000385	1214.94	1856.7	-641.765	1	1.528223616
Small nuclear ribonucleoprotein Sm D3	SNRPD3	SMD3_HUMAN	2	0.001145	8724.82	13365.8	-4640.98	1	1.531928452
Calpain-2 catalytic subunit	CAPN2	CAN2_HUMAN	2	0.017409	206.954	317.32	-110.366	1	1.53328759
Protein phosphatase methylesterase 1	PPME1	PPME1_HUMAN	1;2;3;4	0.000761	2985.24	4605.46	-1620.22	1	1.542743632
Trifunctional purine biosynthetic protein adenosine-3	GART	PUR2_HUMAN	3;4	0.008763	358.817	557.582	-198.766	1	1.553945326
Importin-5	IPO5	IPO5_HUMAN	2;4	0.032778	121.983	189.728	-67.7442	1	1.555364272
Ubiquitin-conjugating enzyme E2 variant 1	UBE2V1	UB2V1_HUMAN	1;4	0.010705	512.987	807.82	-294.833	1	1.574737761
Heterogeneous nuclear ribonucleoprotein Q	SYNCRIP	HNRPQ_HUMAN	2;3;4	0.003218	346.806	570.254	-223.449	1	1.644302578
Moesin	MSN	MOES_HUMAN	2	0.015336	671.878	1106.34	-434.462	1	1.646638229
40S ribosomal protein S4, X isoform	RPS4X	RS4X_HUMAN	1;2;4	0.006731	1019.81	1689.25	-669.442	1	1.656436003
Tubulin-folding cofactor B	TBCB	TBCB_HUMAN	1;2;4	0.015494	576.963	979.541	-402.578	1	1.697753582
Protein RTF2 homolog	RTFDC1	RTF2_HUMAN	1;4	0.000552	154.289	262.995	-108.706	1	1.704560921
Tropomyosin alpha-4 chain	TPM4	TPM4_HUMAN	1;2;3	0.009974	901.84	1592.53	-690.694	1	1.76586756

14-3-3 protein eta	YWHAH	1433F_HUMAN	1;4	< 0.0001	557.065	984.699	-427.634	1	1.76765548
Deoxynucleoside triphosphate triphosphohydrolase SAMHD1	SAMHD1	SAMH1_HUMAN	3	0.006289	26.6896	47.232	-20.5424	1	1.769678077
S-adenosylmethionine synthase isoform type-2	MAT2A	METK2_HUMAN	2	0.000348	444.92	790.059	-345.14	1	1.775732716
60S ribosomal protein L24	RPL24	RL24_HUMAN	3;4	0.007937	66.2423	119.123	-52.8803	1	1.798292028
DNA-(apurinic or apyrimidinic site) lyase	APEX1	APEX1_HUMAN	1;4	0.013116	126.197	232.926	-106.729	1	1.845733258
Exosome RNA helicase MTR4	MTREX	MTREX_HUMAN	2;3;4	0.018437	470.192	897.052	-426.86	1	1.907841903
Proteasome activator complex subunit 3	PSM	PSME3_HUMAN	1;4	0.006825	424.231	817.813	-393.582	1	1.927753983
Structural maintenance of chromosomes protein 4	SMC4	SMC4_HUMAN	3;4	0.014771	155.792	303.938	-148.146	1	1.950921742
Dynamin-1	DNM1	DYN1_HUMAN	4	0.010563	128.034	253.066	-125.032	1	1.976553103
Heat shock 70 kDa protein 1A	HSPA1A	HS71A_HUMAN	2;3;4	0.005755	795.736	1584.78	-789.04	1	1.991590176
Eukaryotic initiation factor 4A-I	EIF4A1	IF4A1_HUMAN	1;2;3;4	0.008175	1019.72	2051.24	-1031.52	1	2.011571804
Tropomyosin alpha-1 chain	TPM1	TPM1_HUMAN	1;2	0.021547	226.728	459.413	-232.685	1	2.026273773
High mobility group protein B1	HMGB1	HMGB1_HUMAN	1;2	0.008281	2404.9	4879.07	-2474.17	1	2.028803692
40S ribosomal protein S17	RPS17	RS17_HUMAN	1;4	0.000272	228.609	487.704	-259.095	1	2.13335433
Copine-1	CPNE1	CPNE1_HUMAN	2	< 0.0001	473.668	1049.23	-575.558	1	2.215116917
Purine nucleoside phosphorylase	PNP	PNPH_HUMAN	2	0.008218	204.542	459.423	-254.881	1	2.246105934
Glycine--tRNA ligase	GARS1	GARS_HUMAN	2	0.029892	117.989	267.252	-149.263	1	2.265058607
60S ribosomal protein L18a	RPL18A	RL18A_HUMAN	3;4	0.046122	180.963	411.043	-230.08	1	2.271420125
High mobility group protein B2	HMGB2	HMGB2_HUMAN	1;2	0.003837	747.219	1727.25	-980.026	1	2.311571306

Heat shock protein beta-1	HSPB1	HSPB1_HUMAN	1;2;3;4	0.020571	293.303	680.996	-387.693	1	2.32181737
Histone H2B type 1-B	HIST1H2BB	H2B1B_HUMAN	1;2	0.038916	53.3656	129.224	-75.8587	1	2.421485002
60S ribosomal protein L10	RPL10	RL10_HUMAN	4	0.039013	71.7055	176.813	-105.107	1	2.465822008
Hsc70-interacting protein	ST13	F10A1_HUMAN	2	0.005894	275.609	699.77	-424.161	1	2.538995461
RNA-binding protein 8A	RBM8A	RBM8A_HUMAN	1;2	< 0.0001	91.8645	244.848	-152.983	1	2.665316853
Far upstream element-binding protein 2	KHSRP	FUBP2_HUMAN	1;2	0.021134	99.2664	278.644	-179.378	1	2.80703239
60S ribosomal protein L10a	RPL10A	RL10A_HUMAN	4	0.005901	321.053	907.043	-585.99	1	2.82521266
Ribonuclease inhibitor	RNH1	RINI_HUMAN	1;4	0.046374	41.894	119.048	-77.1539	1	2.841647969
Ribonucleoside-diphosphate reductase large subunit	RRM1	RIR1_HUMAN	2	0.000353	46.1987	136.644	-90.4457	1	2.957745564
Eukaryotic peptide chain release factor subunit 1	ETF1	ERF1_HUMAN	2;4	0.021393	183.13	548.224	-365.094	1	2.993632938
Ubiquitin carboxyl-terminal hydrolase 14	USP14	UBP14_HUMAN	1;2;4	< 0.0001	95.3841	308.088	-212.704	1	3.229972291
Annexin A6	ANXA6	ANXA6_HUMAN	2;3	0.001288	696.281	2514.13	-1817.85	1	3.610797939
Eukaryotic translation initiation factor 3 subunit F	EIF3F	EIF3F_HUMAN	4	0.049199	11.8955	46.7365	-34.841	1	3.928922702
Heterogeneous nuclear ribonucleoprotein F	HNRNPF	HNRPF_HUMAN	2	0.007531	56.8723	236.654	-179.782	1	4.161146991
26S proteasome regulatory subunit 6A	PSMC3	PRS6A_HUMAN	4	0.026945	17.2391	73.638	-56.3989	1	4.271568701
Xaa-Pro dipeptidase	PEPD	PEPD_HUMAN	2	0.0026	47.675	212.465	-164.79	1	4.456528579

Basic leucine zipper and W2 domain-containing protein 1	BZW1	BZW1_HUMAN	4	0.031188	8.60153	39.1805	-30.579	1	4.555061716
Multidrug resistance-associated protein 6	ABCC6	MRP6_HUMAN	4	0.007995	16.6521	84.8963	-68.2442	1	5.098233856
Peptidyl-prolyl cis-trans isomerase FKBP4	FKBP4	FKBP4_HUMAN	2	0.03322	24.0511	125.636	-101.585	1	5.223711182
Heat shock protein 105 kDa	HSPH1	HS105_HUMAN	2;3	0.000776	191.952	1257.83	-1065.88	1	6.552836126
Phosphoribosylformylglycinamidine synthase	PFAS	PUR4_HUMAN	2	0.008212	89.0063	623.704	-534.698	1	7.007414082
UV excision repair protein RAD23 homolog A	RAD23A	RD23A_HUMAN	2	0.049831	18.9983	137.558	-118.559	1	7.240542575
Protein SET	SET	SET_HUMAN	2	0.022668	12.6042	102.891	-90.2865	1	8.163231304
Ubiquitin-conjugating enzyme E2 Z	UBE2Z	UBE2Z_HUMAN	4	0.007609	4.5762	37.4343	-32.8582	1	8.180215026
Acetyl-CoA carboxylase 1	ACACA	ACACA_HUMAN	4	0.020754	6.26821	52.9685	-46.7002	1	8.450339092
Tryptophan--tRNA ligase, cytoplasmic	WARS	SYWC_HUMAN	2	0.003399	20.5259	179.499	-158.973	1	8.745000219
ATP synthase subunit beta, mitochondrial	ATP5B	ATPB_HUMAN	2;3;4	0.010755	27.1124	271.115	-244.003	1	9.999668049
Nascent polypeptide-associated complex subunit alpha, muscle-specific form	NACA	NACAM_HUMAN	2	0.000242	56.9245	587.191	-530.267	1	10.31525969
Nicotinamide phosphoribosyltransferase	NAMPT	NAMPT_HUMAN	2	0.024536	19.5602	208.854	-189.294	1	10.67749819
S-formylglutathione hydrolase	ESD	ESTD_HUMAN	2	< 0.0001	22.5858	304.272	-281.686	1	13.47182743

2-hydroxyacylsphingosine 1-beta-galactosyltransferase	UGT8	CGT_HUMAN	2	0.003951	18.8423	287.511	-268.669	1	15.25880598
Obg-like ATPase 1	OLA1	OLA1_HUMAN	2;4	0.023053	8.34395	150.395	-142.052	1	18.02443687
Quinone oxidoreductase PIG3	TP53I3	QORX_HUMAN	2	0.02953	3.15014	58.6406	-55.4904	1	18.61523615
60S acidic ribosomal protein P0-like	RPLP0P6	RLA0L_HUMAN	4	0.005725	7.50906	195.549	-188.04	1	26.04174158
Acetyl-CoA acetyltransferase, cytosolic	ACAT2	THIC_HUMAN	2	0.003368	2.84204	92.2642	-89.4221	1	32.4640751
Vitronectin	VTN	VTNC_HUMAN	2	0.003236	4.53595	153.562	-149.026	1	33.85442961
ATP-dependent RNA helicase DDX39A	DDX39A	DX39A_HUMAN	4	0.048158	0.290679	19.5081	-19.2174	1	67.11217529
Cyclin-C	CCNC	CCNC_HUMAN	2;3	0.002269	1.10937	113.431	-112.321	1	102.2481228
Activating molecule in BECN1-regulated autophagy protein 1	AMBRA1	AMRA1_HUMAN	2	0.002378	0.320286	193.781	-193.461	1	605.024884
Golgi resident protein GCP60	ACBD3	GCP60_HUMAN	2;4	0.024299	0	89.0982	-89.0982	N/A	N/A
Cytoplasmic dynein 1 intermediate chain 2	DYNC1I2	DC1I2_HUMAN	2	0.029646	0	20.4781	-20.4781	N/A	N/A
Nicotinamide phosphoribosyltransferase	RCC2	RCC2_HUMAN	2	0.02449	0	46.4637	-46.4637	N/A	N/A

Table 5.2.1: List of proteins detected by mass spectrometry that demonstrate at least a 1.5-fold increase in normalised abundance between S100P negative (HTR8 SGB16 Clone 3) and S100P positive (HTR8 SGB217 Clones 5 and 7) cytoplasm and membrane fractions. Raw normalised means and calculated fold changes are shown.

Each of the 73 proteins with a fold change of over 1.5 between S100P negative and S100P positive samples were submitted to DAVID. DAVID (The Database for Annotation, Visualization and Integrated Discovery) contains a set of web-based tools that allow for the understanding of biological meaning behind gene sets. To this end, DAVID was utilised to identify enriched biological themes based on the submitted proteins and by consequence their associated genes. These biological themes are explored in GO (Gene Ontology) terms, which describe various biological functions, molecular pathways and cellular locations where certain genes and proteins come into play. Upon submission of the 73 gene names to DAVID, a functional annotation chart was generated, displaying a number of enriched terms associated with the submitted set of genes (Table 5.2.2). The chart displays the database from which terms originate from (either GO or Uniprot), the number of genes associated with each term, and the percentage of involved genes out of the total genes submitted.

A large range of cellular components, processes and molecular functions were associated with the 73 submitted proteins, suggesting the wide variety of processes these proteins are involved in. For example, 85% of the submitted genes were associated with the "phosphoprotein" key word, and 78% were associated with the "acetylation" key word. This does not necessarily mean the detected proteins have undergone these processes, rather that the proteins submitted can be found in phosphorylated/acetylated forms or associated with these processes. These enriched terms were generated alongside p values, and another value called Benjamini. This parameter is a multiple testing correction technique that allows for global correction of enrichment values to control the rate of false discovery (Huang, D. W. *et al.* 2009). All p values generated from the enriched terms by DAVID were deemed statistically significant, however after applying the Benjamini correction, 11 of the 39 terms were deemed below the 0.05 threshold. These terms include both cellular components and keywords such as "nucleus", "mitochondrion", and "hydrolase", among others.

Category	Term	Count	%	P value	Benjamini
UP_KEYWORDS	Phosphoprotein	63	85.1	3.00E-15	2.50E-13
GOTERM_MF_DIRECT	protein binding	61	82.4	2.60E-08	3.00E-06
UP_KEYWORDS	Acetylation	58	78.4	8.10E-31	1.30E-28
GOTERM_CC_DIRECT	cytoplasm	47	63.5	1.00E-09	6.10E-08
UP_KEYWORDS	Cytoplasm	45	60.8	1.70E-11	9.10E-10
GOTERM_CC_DIRECT	cytosol	41	55.5	2.20E-12	3.90E-10
GOTERM_CC_DIRECT	extracellular exosome	37	50.0	1.10E-11	1.00E-09
GOTERM_CC_DIRECT	nucleus	33	44.6	7.20E-03	8.70E-02
GOTERM_CC_DIRECT	nucleoplasm	28	37.8	4.50E-06	1.30E-04
UP_KEYWORDS	Nucleus	27	36.5	3.50E-02	2.10E-01
GOTERM_CC_DIRECT	membrane	25	33.8	2.50E-06	1.10E-04
GOTERM_MF_DIRECT	poly(A) RNA binding	24	32.4	1.30E-10	2.90E-08
UP_KEYWORDS	Ubl conjugation	18	24.3	7.50E-05	1.80E-03
UP_KEYWORDS	Isopeptide bond	17	23.0	1.70E-06	5.60E-05
UP_KEYWORDS	Nucleotide-binding	17	23.0	4.40E-04	6.60E-03
GOTERM_MF_DIRECT	ATP binding	17	23.0	4.60E-04	2.10E-02
UP_KEYWORDS	ATP-binding	16	21.6	9.10E-05	1.70E-03
UP_KEYWORDS	Hydrolase	13	17.6	1.40E-02	1.10E-01
UP_SEQ_FEATURE	mutagenesis site	13	17.6	8.90E-02	9.80E-01
UP_KEYWORDS	Ribonucleoprotein	11	14.9	9.10E-08	3.70E-06
GOTERM_MF_DIRECT	RNA binding	11	14.9	1.00E-04	5.90E-03
UP_KEYWORDS	Methylation	11	14.9	2.70E-03	2.80E-02
GOTERM_CC_DIRECT	mitochondrion	11	14.9	3.90E-02	2.90E-01
GOTERM_BP_DIRECT	translational initiation	10	13.5	7.70E-09	4.30E-06
GOTERM_CC_DIRECT	focal adhesion	10	13.5	2.50E-05	6.40E-04
GOTERM_MF_DIRECT	identical protein binding	10	13.5	4.40E-03	1.20E-01
UP_KEYWORDS	Cytoskeleton	10	13.5	1.90E-02	1.30E-01
GOTERM_BP_DIRECT	nuclear-transcribed mRNA catabolic process, nonsense-mediated decay	9	12.2	4.60E-08	1.30E-05
GOTERM_BP_DIRECT	translation	9	12.2	1.40E-05	1.30E-03
UP_KEYWORDS	RNA-binding	9	12.2	2.40E-03	2.60E-02

GOTERM_CC_DIRECT	nucleolus	9	12.2	2.10E-02	1.90E-01
UP_SEQ_FEATURE	nucleotide phosphate-binding region:ATP	9	12.2	2.60E-02	9.30E-01
UP_KEYWORDS	Ribosomal protein	8	10.8	4.20E-06	1.10E-04
GOTERM_CC_DIRECT	ribosome	8	10.8	4.50E-06	1.60E-04
GOTERM_MF_DIRECT	structural constituent of ribosome	8	10.8	4.40E-05	3.30E-03
GOTERM_BP_DIRECT	viral process	8	10.8	3.20E-04	2.50E-02
UP_KEYWORDS	Host-virus interaction	8	10.8	4.30E-04	7.00E-03
GOTERM_CC_DIRECT	perinuclear region of cytoplasm	8	10.8	1.20E-02	1.20E-01
INTERPRO	P-loop containing nucleoside triphosphate hydrolase	8	10.8	5.70E-02	8.60E-01

Table 5.2.2: List of statistically significantly enriched terms associated with the list of 74 proteins submitted to DAVID.

Analysis includes the number of genes involved in each term (Count) and the percentage of involved genes out of the total genes submitted (%). Only enriched terms which contained over 10% of the total submitted list of genes were included. Benjamini represents corrected P value.

CC, Cellular Component; *MF,* Molecular Function; *BP,* Biological Process; *UP*, Uniprot

5.2.3 Identification of enriched terms following mass spectrometric analysis of trophoblast cell lines

Previous results in this chapter suggest that presence of S100P at the plasma membrane may be, at least in part, responsible for changes in both motility and invasion that are seen upon treating cells with an S100P antibody. To this end, three enriched terms generated by DAVID associated with these cellular compartments, or processes related to cellular motility or invasion, were further analysed; extracellular exosome, focal adhesion, and membrane (Table 5.2.3). These terms were found to be enriched at a statistically significant level after correction of false discovery rate.

Genes associated with these three terms, containing a select number of the 73 proteins submitted to DAVID, are listen in Tables 5.2.4, 5.2.5 and 5.2.6, in addition to their fold change in protein abundance detected by mass spectrometry. These three tables list a wide variety of proteins detected by mass spectrometry analysis of S100P negative and S100P positive cells that are linked by three terms; extracellular exosome, focal adhesion, and membrane. The proteins in these tables, although while associated with the terms listed above, are also involved in many other cellular processes and functions, for example chaperone-mediated processes and translational initiation (Modelska *et al.* 2015).

Category	Enriched terms	% involved genes	P value	Benjamini
GOTERM_CC_DIRECT	Extracellular exosome	50	1.1E-11	1.0E-9
GOTERM_CC_DIRECT	Focal adhesion	13.5	2.5E-5	6.4E-4
GOTERM_CC_DIRECT	Membrane	33.8	2.5E-6	1.1E-4

Table 5.2.3: Selected enriched terms of interest from the DAVID functional annotation chart (Table 5.2.2) generated by submission of 73 proteins to DAVID.

GOTERM_CC_DIRECT Extracellular exosome		
UNIPROT_ID	**PROTEIN NAME**	**Fold change in abundance (S100P negative to S100P positive)**
ATPB_HUMAN	ATP synthase, H+ transporting, mitochondrial F1 complex, beta polypeptide (ATP5B)	9.999668049
FKBP4_HUMAN	FK506 binding protein 4(FKBP4)	5.223711182
OLA1_HUMAN	Obg like ATPase 1(OLA1)	18.02443687
UB2V1_HUMAN	Ubiquitin-conjugating enzyme E2 variant 1	1.574737761
THIC_HUMAN	acetyl-CoA acetyltransferase 2(ACAT2)	32.4640751
ACACA_HUMAN	acetyl-CoA carboxylase alpha (ACACA)	8.450339092
ANXA6_HUMAN	annexin A6(ANXA6)	3.610797939
CAN2_HUMAN	calpain 2(CAPN2)	1.53328759
CPNE1_HUMAN	copine 1(CPNE1)	2.215116917
DYN1_HUMAN	dynamin 1(DNM1)	1.976553103
ESTD_HUMAN	S-formylglutathione hydrolase	13.47182743
IF4A1_HUMAN	eukaryotic translation initiation factor 4A1(EIF4A1)	2.011571804
HSPB1_HUMAN	heat shock protein family B (small) member 1(HSPB1)	2.32181737
HS105_HUMAN	heat shock protein family H (Hsp110) member 1(HSPH1)	6.552836126
LDHB_HUMAN	lactate dehydrogenase B(LDHB)	1.507241179
MOES_HUMAN	Moesin (MSN)	1.646638229
NACAM_HUMAN	nascent polypeptide-associated complex alpha subunit (NACA)	10.31525969
NAMPT_HUMAN	nicotinamide phosphoribosyltransferase (NAMPT)	10.67749819
PEPD_HUMAN	peptidase D(PEPD)	4.456528579
PUR4_HUMAN	phosphoribosylformylglycinamidine synthase(PFAS)	7.007414082
PUR2_HUMAN	Trifunctional purine biosynthetic protein adenosine-3	1.553945326
PNPH_HUMAN	purine nucleoside phosphorylase(PNP)	2.246105934
RINI_HUMAN	ribonuclease/angiogenin inhibitor 1(RNH1)	2.841647969

RIR1_HUMAN	ribonucleotide reductase catalytic subunit M1(RRM1)	2.957745564
RL10A_HUMAN	ribosomal protein L10a(RPL10A)	2.82521266
RL24_HUMAN	ribosomal protein L24(RPL24)	1.798292028
RS17_HUMAN	ribosomal protein S17(RPS17)	2.13335433
RS2_HUMAN	ribosomal protein S2(RPS2)	1.528223616
RS4X_HUMAN	ribosomal protein S4, X-linked (RPS4X)	1.656436003
SMD3_HUMAN	small nuclear ribonucleoprotein D3 polypeptide (SNRPD3)	1.531928452
F10A1_HUMAN	suppression of tumorigenicity 13 (colon carcinoma) (Hsp70 interacting protein) (ST13)	2.538995461
TPM4_HUMAN	tropomyosin 4(TPM4)	1.76586756
SYWC_HUMAN	tryptophanyl-tRNA synthetase (WARS)	8.745000219
QORX_HUMAN	tumor protein p53 inducible protein 3(TP53I3)	18.61523615
1433F_HUMAN	tyrosine 3-monooxygenase/tryptophan 5-monooxygenase activation protein eta (YWHAH)	1.76765548
UBP14_HUMAN	ubiquitin specific peptidase 14(USP14)	3.229972291
VTNC_HUMAN	Vitronectin (VTN)	33.85442961

Table 5.2.4: List of proteins under the GOTERM_CC_DIRECT Extracellular exosome identifier out of 73 submitted proteins. List generated by DAVID.

GOTERM_CC_DIRECT Focal adhesion		
UNIPROT_ID	**GENE NAME**	**Fold change in abundance (S100P negative to S100P positive)**
ANXA6_HUMAN	annexin A6(ANXA6)	3.610797939
CAN2_HUMAN	calpain 2(CAPN2)	1.53328759
HS71A_HUMAN	heat shock protein family A (Hsp70) member 1A(HSPA1A)	1.991590176
HSPB1_HUMAN	heat shock protein family B (small) member 1(HSPB1)	2.32181737
MOES_HUMAN	moesin(MSN)	1.646638229
RL10A_HUMAN	ribosomal protein L10a(RPL10A)	2.82521266
RS17_HUMAN	ribosomal protein S17(RPS17)	2.13335433
RS2_HUMAN	ribosomal protein S2(RPS2)	1.528223616
RS4X_HUMAN	ribosomal protein S4, X-linked(RPS4X)	1.656436003
TPM4_HUMAN	tropomyosin 4(TPM4)	1.76586756

Table 5.2.5: List of proteins under the GOTERM_CC_DIRECT Focal adhesion identifier out of 73 submitted proteins. List generated by DAVID.

GOTERM_CC_DIRECT Membrane		
UNIPROT_ID	**GENE NAME**	**Fold change in abundance (S100P negative to S100P positive)**
ATPB_HUMAN	ATP synthase, H+ transporting, mitochondrial F1 complex, beta polypeptide (ATP5B)	9.999668049
DX39A_HUMAN	DExD-box helicase 39A(DDX39A)	67.11217529
FUBP2_HUMAN	KH-type splicing regulatory protein (KHSRP)	2.80703239
OLA1_HUMAN	Obg like ATPase 1(OLA1)	18.02443687
ANXA6_HUMAN	annexin A6(ANXA6)	3.610797939
BZW1_HUMAN	basic leucine zipper and W2 domains 1(BZW1)	4.555061716
CPNE1_HUMAN	copine 1 (CPNE1)	2.215116917
EIF3F_HUMAN	eukaryotic translation initiation factor 3 subunit F(EIF3F)	3.928922702
IF4A1_HUMAN	eukaryotic translation initiation factor 4A1(EIF4A1)	2.011571804
HNRPF_HUMAN	heterogeneous nuclear ribonucleoprotein F(HNRNPF)	4.161146991
IPO5_HUMAN	importin 5(IPO5)	1.555364272
LDHB_HUMAN	lactate dehydrogenase B(LDHB)	1.507241179
PRS6A_HUMAN	proteasome 26S subunit, ATPase 3(PSMC3)	4.271568701
PSME3_HUMAN	proteasome activator subunit 3(PSME3)	1.927753983
RL10_HUMAN	ribosomal protein L10(RPL10)	2.465822008
RL10A_HUMAN	ribosomal protein L10a(RPL10A)	2.82521266
RL18A_HUMAN	ribosomal protein L18a(RPL18A)	2.271420125
RL24_HUMAN	ribosomal protein L24(RPL24)	1.798292028
RS17_HUMAN	ribosomal protein S17(RPS17)	2.13335433
RS2_HUMAN	ribosomal protein S2(RPS2)	1.528223616
RS4X_HUMAN	ribosomal protein S4, X-linked (RPS4X)	1.656436003
TPM4_HUMAN	tropomyosin 4(TPM4)	1.76586756

Table 5.2.6: List of proteins under the GOTERM_CC_DIRECT Membrane identifier out of 73 submitted proteins. List generated by DAVID.

5.2.4 Identification of Annexin A6 and its potential involvement in S100P-dependent processes

Upon assessment of the three enriched term tables generated by DAVID, one protein in particular stood out as a potential target for involvement in S100P-dependent processes for a variety of reasons; annexin A6. Abundance of the annexin A6 protein was found to be increased by over 3.6-fold in S100P positive samples when compared to S100P negative samples, and was identified in gel fragments 2 and 3, suggesting that annexin A6 has potential to be a part of the high molecular weight complex containing S100P. In addition, annexin A6 was listed in each of the three enriched term tables, solidifying its presence and role in the compartments of interest.

To determine whether annexin A6 expression differs between S100P-expressing and non S100P-expressing cells, as observed using mass spectrometry, cell lysates from S100P negative HTR8 Clone 3 and S100P positive HTR8 clones 5 and 7 were separated on a 16% (w/v) SDS-PAGE gel prior to western blotting for annexin A6, S100P and tubulin (Figure 5.2.2, panel A). Quantification of band intensity for annexin A6, S100P and tubulin was carried out on each sample, and band intensity of annexin A6 and S100P in each cell line were normalised to tubulin (Figure 5.2.2, panels B and C)

The resulting western blot for S100P once again confirmed the variance in S100P expression seen in the transfected HTR8 clones; S100P expression by HTR8 clone 7 was significantly increased in comparison to non-S100P expressing HTR8 Clone 3, which demonstrated no S100P expression ($p<0.029$). Western blotting of cell lysates for annexin A6 demonstrated a 56% increase in annexin A6 expression between HTR8 clone 7 and S100P negative HTR8 clone 3. However, this increase in expression was not deemed statistically significant ($p=0.067$). Moreover, the increase in annexin A6 expression seen between clones 7 and 3 is not in line with data obtained using the mass-spectrometry based approach, and is in fact 7-fold lower than the expected 3.6-fold (360%) increase in expression in annexin A6 between S100P-negative and S100P-positive cell lines. Western blot data therefore suggests that annexin A6 may not likely be a target for regulation by S100P, at least in this cell background.

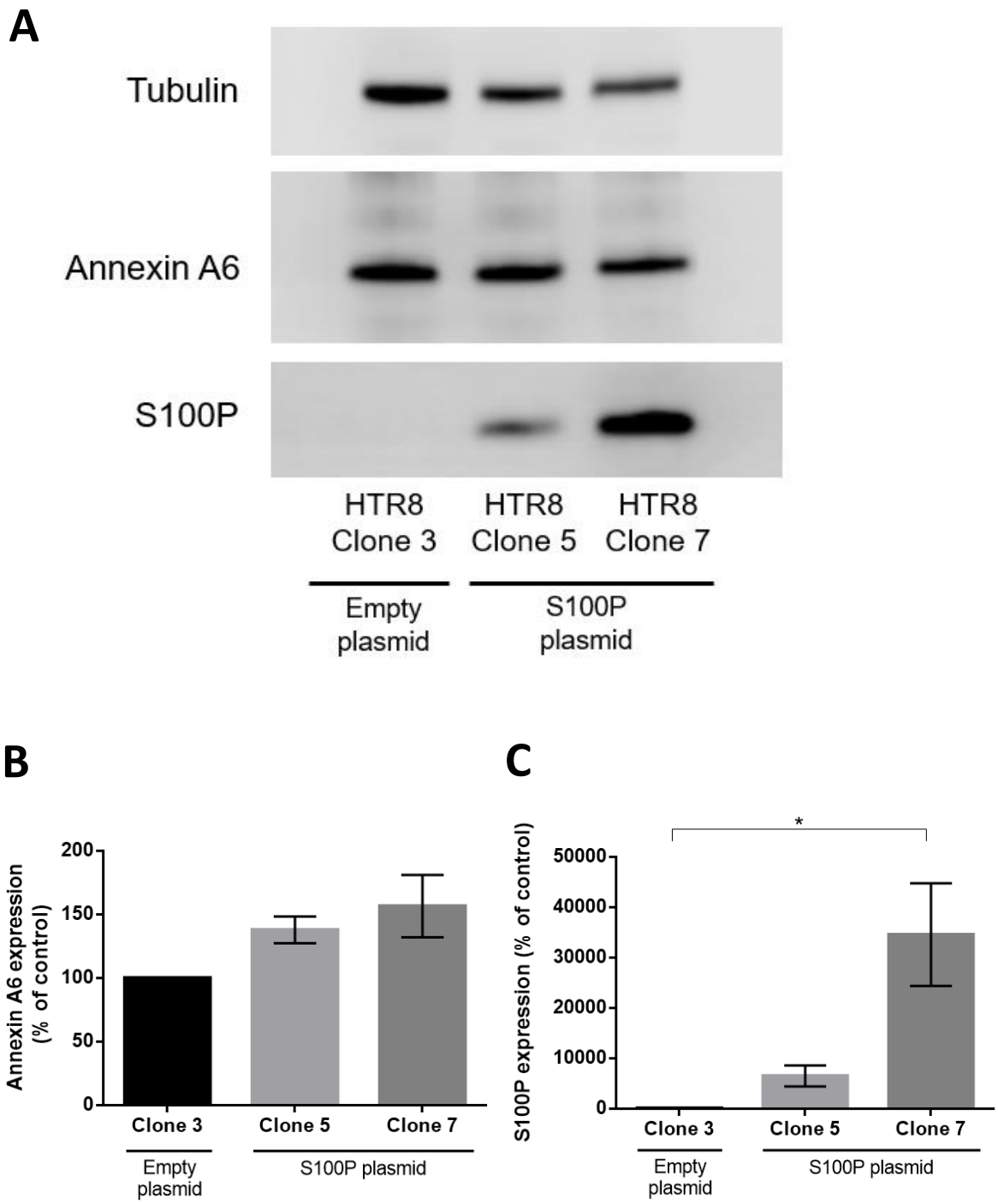

Figure 5.2.2: Expression of Annexin A6 in HTR8 clones 5 and 7 stably expressing S100P is not significantly different from S100P-negative HTR8 SGB16 Clone 3

A) Cell lysates from S100P-negative HTR8 Clone 3 and S100P-positive HTR8 Clones 5 and 7 were collected and run on 16% (w/v) SDS-PAGE before western blotting for annexin A6, S100P and tubulin.

B) Levels of annexin A6 present within cell lysates was quantified by densitometry using Image Studio Lite, normalised to tubulin. Data represents the mean ±SEM from 4 independent replicates.

C) Levels of S100P present within cell lysates was quantified by densitometry using Image Studio Lite, normalised to tubulin. Data represents the mean ±SEM from 3 independent replicates (one-way ANOVA, * p=0.029)

5.3 Discussion

We have previously characterised the role of S100P in trophoblast cell motility and invasion (Tabrizi *et al.* 2018). Following the detection of a novel pool of S100P in isolated plasma membranes of trophoblasts, and its role in promoting motility and invasion, we sought to understand the target proteins through which S100P exerts its effects, either those previously characterised or novel interactors.

To this end, we utilised BN-PAGE, a technique that allows for separation of complexes (Swamy *et al.* 2006). BN-PAGE is well suited for complex analysis, as the absence of SDS prevents the denaturation of protein complexes that would otherwise be denatured when running samples on SDS-PAGE (Jha *et al.* 2017). The anionic dye Coomassie Brilliant Blue G250 (CBB G250) was added to samples, and binding of CBB G250 to proteins leads to a charge shift, causing proteins to migrate. As the BN-PAGE gel is a gradient gel, from 4-16% acrylamide concentration, proteins are not separated by charge to mass ratio but by their size, as the size of the pores formed by the acrylamide prevent proteins within complexes from migrating due to particle size (Wittig *et al.* 2006). BN-PAGE has been used by Jha, Wang and Auwerx, (2017) to isolate supercomplexes from mitrochondrial membranes, as well as complexes from both Gram-positive and Gram-negative bacteria (Dresler *et al.* 2011).

Western blotting of cell lysates and cell fractions from multiple cell lines, either those engineered to express S100P by means of an inducible system (COS-7 s10+, HeLa A3+) or those endogenously expressing S100P (JEG-3 and BeWo) led to the detection of low molecular weight S100P complexes in all cell lines. It is assumed that these complexes are primarily dimers or higher order oligomers of S100P, as S100P must form dimers to interact with target proteins (Santamaria-Kisiel *et al.* 2006). Gribenko and Makhatadze (1998) have shown that the oligomerization state of S100P can vary depending on calcium concentration, leading to the formation of higher order oligomers, namely trimers or tetramers.

To observe the localisation of these high molecular weight complexes containing S100P, western blotting of cytoplasm/membrane fractions and nuclear fractions, isolated by subcellular fractionation with a Dounce homogeniser, was undertaken alongside their respective cell lysates. Detection of S100P in HeLa A3+ and COS-7 s10+ cell lysates showed the formation of both high and low molecular weight complexes, with the former exhibiting a more intense signal in the cytoplasm/membrane fraction when compared to its respective cell lysate, signifying enrichment of the S100P-containing complex in this fraction. Interestingly, two low molecular weight bands were detected in the COS-7 s10+ cytoplasm/membrane fractions, potentially relating to the higher order oligomers mentioned above.

Western blotting for S100P also led to the detection of a high molecular weight complex (between 480-1000kDa) in the cytoplasm and membrane fraction of trophoblast cell lines JEG-3 and BeWo, in addition to the stably-transfected S100P-expressing HTR8 clone 7 cell line. Interestingly, the intensity and definition of the band obtained in the cytoplasm and membrane fraction of HTR8 clone 7 is much stronger than those obtained in JEG-3 and BeWo cytoplasm/membrane fractions, and is also of a much stronger intensity than their respective lower molecular weight (predicted) oligomers. The implications of this could be that more S100P within the HTR8 clone 7 cell line could be involved in high molecular weight complexes compared to the choriocarcinoma cell lines JEG-3 and BeWo. Proteins including vimentin 3 and N-cadherin, for example, were found to be present in HTR8/SVneo cells but absent in BeWo cells (Szklanna *et al.* 2017). It may be that differences in the proteome profiles of certain trophoblast cell lines lead to differences in complex formation involving S100P.

COS-7 s10 cells do not express non-muscle myosin IIA (NMIIA) (Bao *et al.* 2005), a target protein of S100P. NMMIIA is formed of two heavy chains, two essential light chains and two regulatory light chains, forming a hexamer of roughly 450kDa (Althaus and Greinacher 2009). The lack of defined high molecular weight bands containing S100P in COS-7 s10+ cells in comparison to other cell lines could potentially therefore be as a result of differences in target protein expression such as NMIIA. It is thought that S100 proteins can form dimers to allow their interaction with two either homologous or heterologous proteins, with the each binding surface on opposite regions of the dimer (Donato, Rosario 2001). If S100P could form this type of interaction, with multiple different target proteins in one multiprotein complex, this might further explain differences seen in S100P-containing complexes in each cell line. In addition to the high molecular weight complex containing S100P detected in trophoblast cell lines, another band was detected at the top of the gel, mainly in cell lysates or cytoplasm/membrane fractions. This suggests the presence of S100P in a non-soluble environment, given that this material has not migrated out of the well in which it was placed.

This non-soluble environment could be lipid material present in plasma membranes. However, the presence of CBB G250 coats proteins in a negative charge, suggesting negatively charged proteins within the sample will repel each other. This leads to decreased aggregation of membrane proteins, allowing for their migration into the gel due to their increased solubility (Wittig *et al.* 2006). The addition of aminocaproic acid into the sample buffer maintains the solubility of protein complexes (Schägger and von Jagow 1991), however proteins can precipitate in the gel pocket with CBB G250, leading to samples not entering the gel. In addition, salt concentration in samples can interfere with protein migration through BN-PAGE (Wittig *et al.* 2006), meaning that efforts to dialyse protein samples prior to running on BN-PAGE may alleviate this issue. Several groups have included the use of weak, non-ionic detergents to solubilise membrane complexes, including dodecylmaltoside and

digitonin (Krause, F. 2006). Addition of a mild detergent prior to running samples on BN-PAGE may also aid the sample to enter the gel, although the exact detergent to use and the concentration required to extract lipids from membranes, without denaturing protein complexes, would require extensive optimisation.

In order to gain an understanding of proteins involved in this high molecular weight complex formed in each cell line, and to assess global protein differences between S100P-positive and S100P-negative cells, we sought to separate both S100P-positive (HTR8 clones 5 and 7) and S100P-negative (HTR8 clone 3) samples by BN-PAGE prior to mass spectrometric analysis in triplicate to detect increases in normalised abundances. 633 proteins were detected between each of the three cell lines, of which 232 were detected at statistically significant increased abundances between S100P-negative and S100P-positive cells. This is quite a large number of proteins, representing over one third of total proteins detected by mass spectrometry. To narrow down this list and to enable characterisation of only the most significant changes in protein abundance, only those proteins which demonstrated at least a 1.5-fold increase in S100P-positive samples compared to their negative counterparts were analysed. This led to a total of 73 proteins being submitted to DAVID to glean enriched terms that are associated with this subset of proteins.

Given that S100P has been detected in solely in the cytoplasm and in isolated membrane fractions, we specifically targeted further analysis towards terms associated with these cellular compartments to further narrow down proteins that may potentially play a role in S100P-mediated processes of motility and invasion. Three terms were selected for further analysis; “extracellular exosome”, “membrane” and “focal adhesion”. A wide variety of proteins comprised these three terms, including but not limited to proteins involved in protein transport, ribosomal proteins, and several heat shock proteins. After a careful analysis of these proteins, their roles, and their potential for mediating S100P-dependent processes, one protein was selected for analysis; annexin A6.

Annexin A6 is a 68kDa member of the annexin family, with many documented roles including membrane repair, endocytic transport and calcium homeostasis (Bandorowicz-Pikula and Seliga 2018). The annexin family of proteins are highly conserved and bind to membrane phospholipids through their conserved annexin cores in a calcium-dependent manner (Gerke, Volker and Moss, S. E. 2002). Each annexin protein contains modular domains to enable their interaction with a variety of proteins or lipids (Gerke, Volker *et al.* 2005). Upon binding calcium, annexins can translocate from the cytosol to membrane structures in a reversible manner dependent on calcium. Annexin A6 is highly expressed in many tissues, including smooth muscle, liver and breast, and has been implicated in either suppression or promotion of cancer metastasis through MAPK/PI3K signalling pathways (Qi *et al.*

2015). Its expression in breast carcinoma cells was found to enhance both their invasion and motility, with elongation of vinculin-containing focal adhesions observed following annexin A6 depletion (Sakwe *et al.* 2011). This suggests that annexin A6 promotes the loss of cell-ECM contacts which in turn increases cellular motility.

Interactions of S100 proteins with members of the annexin family have been studied by various groups. For example, the interaction of S100A10 with annexin A2, which does not require calcium, leads to the formation of an annexin A2-S100A10 heterotetramer (AIIt). AIIt is present on the cell surface, where binding of S100A10's C-terminal lysine residues to tPA results in production of plasmin from plasminogen (Kassam *et al.* 1998a). The interaction between S100A10 dimers and annexin A2 is facilitated by S100A10's linker region in addition to helix 4 (Réty *et al.* 1999). Annexin A6 has also been documented to interact with other members of the S100 family, namely S100A1 and S100B (Garbuglia *et al.* 1998), however the structure of this complex, or the binding sites on these S100 proteins for annexin A6 have not been identified (Miwa *et al.* 2008). Interestingly, binding of the S100A8/A9 heterodimer to annexin A6 has been documented by Bode *et al.* (2008) through affinity chromatography, with their colocalisation observed in membrane structures of the SKBR3 breast cancer cell line. The authors speculated that upon influx of calcium, SKBR3 cells demonstrated exposition of the membrane-associated S100A8/A9 complex on the cell surface, from the inner leaflet to the outer leaflet of the plasma membrane, however the authors did not investigate the molecular mechanisms behind the membrane-association of this complex.

Rambotti, Spreca and Donato (1993) have documented the expression and localisation of annexin A6 in trophoblasts by immunohistochemistry, and found that STBs seem to contain the highest levels of annexin A6. Annexin A6 was found associated with multiple cellular membranes, such as the Golgi membrane, endoplasmic reticulum, and plasma membrane, as well as dispersed throughout the cytoplasm in these cells. The authors suggest a role for annexin A6 in modulating trophoblast membrane processes in a calcium-dependent manner. However, Riquelme *et al.* (2004) have detailed the specific localisation in annexin A6 in the apical membrane of STBs, and demonstrated its presence at the membrane is both dependent and independent of calcium. The group suggested a role for annexin A6 in modulating ion transport across apical STB membranes, specifically through the Maxi-chloride channel. Another group identified a number of proteins that are associated with microvillus membranes of human STBs through mass spectrometry-based methods, including annexin A6, further highlighting its presence in this cell subset (Paradela *et al.* 2005).

Proteomic analysis of S100P-positive versus S100P-negative cells highlighted differences in annexin A6 global abundance between these conditions, suggesting the potential for this protein's involvement in

S100P-dependent processes. In addition, its presence in gel fragments 2 and 3 suggest it may be part of a high molecular weight complex. Western blotting of HTR8 clones provided somewhat less statistically significant differences in annexin A6 abundance in comparison to global abundance analysis. It is unknown why this may be, as multiple samples, including those used for mass spectrometry analysis, were analysed by western blot, and therefore it would be hoped that the results obtained by two different methodologies would be similar. Perhaps it is that the annexin A6 primary antibody used for western blotting did not recognise the target epitope, leading to incorrect detection of expression levels. Bode *et al.* (2008) have noted proteolytic digestion of annexin A6 in granulocyte lysates, however the annexin A6 antibody used was able to recognise a 55kDa band that was assumed to be a degradation product of annexin A6. Use of a variety of protease inhibitors by the authors did not prevent this phenomenon.

Regardless, it may be that S100P could in fact bind to the annexin A6 protein without affecting its levels of expression. Rather, their interaction could facilitate the exposure of S100P on the cell surface much like the S100A8/A9 heterodimer. Similarities also exist between S100P and S100A10, as the C-terminal lysine residues of S100A10 are required for extracellular tPA activation as part of the AIIt. Deletion of S100A10's C-terminal lysine residues as part of the AIIt complex results in a large loss of tPA-dependent plasminogen activation compared to its WT counterpart (Kassam *et al.* 1998b). In addition, the formation of this complex enhanced tPA activation when compared to S100A10 alone (Kassam *et al.* 1998a). S100P also contains a C-terminal lysine residue, which, when mutated, can no longer activate tPA as effectively as its WT counterpart (Clarke *et al.* 2017). However, no interaction between annexin A2 and S100P has been demonstrated *in vitro* as of yet, suggesting a role for other S100P target proteins to facilitate membrane-association of S100P.

Chapter 6:

General Discussion

The S100 proteins are a diverse family of calcium-binding proteins with high levels of structural homology. Each member is characterised by a pair of EF-hand calcium-binding motifs, connected by a hinge region, with differing affinities for calcium (Donato, R 1999). Upon binding of calcium ions, S100 protein dimers undergo a conformational change in their C-terminal helix, facilitating their interaction with either intracellular or extracellular target proteins (Donato, Rosario 2003). Although the presence of several S100 proteins in the extracellular environment have been detected, S100 proteins do not contain canonical secretion sequences (Donato *et al.* 2013), suggesting their secretion occurs via a yet uncharacterised non-canonical pathway.

Several different proteins have been documented to associate with S100P, mainly in cancer cell lines and tissues, including ezrin (Austermann *et al.* 2008), IQGAP1 (Heil *et al.* 2011), NMIIA (Du *et al.* 2012) and S100PBP (Dowen *et al.* 2005). Regardless of the large body of work concerning the role of S100P in promoting cellular migration and invasion in cancers of varying origins, little research has been conducted on the role of S100P in normal physiologically relevant tissues, such as the placenta, or on the target proteins in the placenta through which S100P exerts its effects. S100P expression is at its highest in the placenta (Parkkila *et al.* 2008), namely within trophoblasts, a subset of cells that are required to migrate and invade in order to aid in nutrient uptake and establish a blood supply, via maternal arterial remodelling, to the growing foetus (Zhu *et al.* 2015a) Furthermore, there is a somewhat striking similarity in the migratory and invasive capacity of trophoblasts and of cancer cells (Ferretti *et al.* 2007). Given this link, it seems imperative to understand the role of S100P in trophoblasts of the placenta, which could aid in the prevention of certain pregnancy-related disorders; insufficient or deregulated invasion and migration of trophoblasts are thought to contribute to pregnancy-related disorders including preeclampsia and IUGR (Burton and Jauniaux, 2018; Ridder *et al.* 2019). In addition, Zhu *et al.* (2015b) documented the dramatic and significant downregulation of S100P in isolated placental villi obtained from spontaneous abortion.

We have recently established a role for S100P in promoting both migration and invasion in trophoblast cell lines, through both gain and loss of function studies (Tabrizi *et al.* 2018). The work presented in this thesis firstly examined the localisation of S100P in a variety of cell backgrounds, with a particular focus on trophoblast cells of the placenta, using a biochemical technique known as subcellular fractionation. Knowledge of a protein's subcellular localisation is vital, as it underpins potential protein functionality. Depending on the localisation of a particular protein, interactions with their target partners can either take place or be inhibited, which has consequences on overall biological outcome (Hung, M. C. and Link 2011). Several works have observed the localisation of the S100P protein, mainly through the use of indirect techniques, including immunohistochemistry and immunofluorescence (see section 3.1).

Initial work in this study demonstrated discrepancies between detection of S100P through immunofluorescence and western blotting, with limited sensitivity of immunofluorescence at detecting differences in S100P expression levels. Western blotting, comparatively, offered a more sensitive approach to characterising expression levels of S100P in a variety of cell lines, both those induced to express variable levels of S100P under the actions of an inducible system or through stable transfection, and those of trophoblast origin that endogenously express S100P.

Analysis of S100P localisation through biochemical fractionation of multiple cell lines of differing origins led to the detection of S100P in cytoplasm/membrane fractions, with barely detectable traces of S100P in the nuclear fractions of all cell lines examined. The data therefore suggests that S100P is undoubtably localised to the cytoplasm/membrane, regardless of S100P expression level. This observation is at somewhat at odds with much of the previous work regarding S100P, in which nuclear localisation has been observed. For example, Rehbein *et al.* (2008) conducted immunofluorescence analysis on H358 lung cancer cells that had been stably transfected with GFP-S100P and observed both its nuclear and cytoplasmic localisation. Differential fractionation methods were utilised, including addition of excess calcium and a non-ionic detergent for cell lysis. These strategies yielded almost identical results to the original work, further corroborating the reliability of the assay and in addition demonstrating that S100P expression level does not influence its subcellular localisation in cells of either a cancer background or of trophoblast origin.

Given the extensive use of fluorescent protein tags in assessing protein localisation (Rehbein *et al.* 2008; Koltzscher *et al.* 2003) we aimed to understand if an N-terminal YFP tag can influence S100P subcellular localisation. Densitometric analysis confirmed that a percentage of YFP-S100P was present within isolated nuclear fractions, suggesting that addition of a fluorescent tag to S100P can alter its localisation. Depending on the positioning of the fluorescent tag, signal peptides or motifs required for the specific subcellular localisation of a protein could be masked, leading to changes in protein localisation. For example, Weill *et al.* (2019) found a large subset of yeast proteins were differentially localised when tagged at either the N or C-terminus with GFP. It is therefore understandable to think that prior research utilising a fluorescent tag system for S100P, a 10kDa protein that is almost three times smaller than YFP, may not yield reliable results.

Further experiments to block active nuclear export by the use of LMB also did not alter S100P localisation. LMB binds to and inhibits CRM1, a protein required for active transport of proteins out of the nucleus (Fornerod *et al.* 1997). Most cargoes that bind to CRM1 contain an NES. S100P itself does not contain an NLS or NES, however there are some proteins that instead bind to adapter proteins that contain a NES, facilitating their exit from the nucleus (Trotta *et al.* 2003). IQGAP1, an interaction

partner of S100P, has been shown localise to the nucleus in a CRM1-dependent manner; significant increases in nuclear IQGAP1 were observed following overnight LMB treatment (Johnson *et al.* 2011). It may be that S100P binding to a protein containing an NLS, such as IQGAP1, could facilitate a nuclear localisation, however the size of such a complex could not passively diffuse out from the nucleus.

The presence of other S100 proteins in the nucleus has been investigated previously. S100A11, for example, is a cytosolic protein in human pulmonary artery smooth muscle cells (HPASMCs). However, upon stimulation of these cells with hypoxia-induced mitogenic factor (HIMF), S100A11 translocates from the cytosol to plasma membrane structures and the nucleus, suggesting it may in fact regulate gene transcription (Fan *et al.* 2011). High levels of extracellular calcium have also shown to induce S100A11 nuclear translocation in keratinocytes (HaCaT cells), whereas a S100A11 mutant without calcium-binding abilities was not translocated to the nucleus (Sakaguchi *et al.* 2003). IL-1β-stimulated translocation of S100A4 to the nucleus has also been observed in human articular chondrocytes, however this translocation was dependent on sumoylated lysine residues (Miranda *et al.* 2010). In addition, association of S100A4 with the promoter region of MMP-13 suggests that nuclear S100A4 plays a role in regulating expression of MMP-13, although the authors suggest this interaction is indirect as S100 proteins do not contain DNA-binding motifs.

Passive nuclear diffusion, in contrast to active transport, does not require transport receptors such as CRM1 to transport proteins through nuclear pore complexes. It is thought that passive diffusion of proteins beyond 60kDa into the nucleus does not occur; for example, 70kDa dextran molecules cannot diffuse through HeLa nuclear membranes (Samudram *et al.* 2016). Such transport is also thought to occur in seconds and minutes. Timney *et al.* (2016) found that GFP, at 27kDa, could equilibrate between the nucleus and the cytosol in 15 seconds, in contrast to 67kDa GFP-6PrA, which took roughly 6-8 minutes. If a molecule such as S100P can passively diffuse out of the nucleus, its presence in the cytoplasmic and nuclear compartments would reach an equilibrium, as such passive transport is bidirectional (Kumeta *et al.* 2012). The small size of S100P suggests its equilibration between these cellular locations would occur in seconds.

Prior research has uncovered several S100P interaction partners, mainly those of an intracellular nature. Interestingly, only one of the characterised target proteins of S100P, S100PBP, has been shown to be predominantly nuclear in nature (Dowen *et al.* 2005). The authors suggested that interaction of S100PBP with S100P possibly occurs in the nucleus. Our studies highlighted the presence of S100PBP in both nuclear and cytoplasmic compartments of trophoblast cell lines, suggesting the potential for S100P and S100PBP to interact in the cytosol, although the biological outcome of such an interaction is not yet clear. Although IQGAP1 has been found to localise to the nucleus (Johnson *et al.* 2011),

interaction of IQGAP1 and ezrin with S100P were both shown in plasma membrane protrusions of HeLa cells (Austermann *et al.* 2008; Heil *et al.* 2011). However, the colocalisation of S100P with these proteins, as well as S100PBP, have not been observed in trophoblast cells.

Further dissection of cellular compartments into a plasma membrane only fraction enabled the detection of S100P in this localisation in all cell lines examined, including trophoblasts. In addition, analysis of *in vivo* first trimester placental tissue further suggested the presence of S100P within this location through colocalisation analysis with HLA-G, a protein exclusively expressed by invasive EVTs (Tilburgs *et al.* 2015). Observation of S100P at this location *in vivo* in close proximity to HLA-G at the cell surface has not been reported previously. It is not yet known how S100P is localised to this cellular location, although interaction partners of S100P, including IQGAP1 (Heil *et al.* 2011) and ezrin (Austermann *et al.* 2008) have been shown to be localised to these areas, albeit at the intracellular side of the membrane.

Ezrin, specifically, has been found to colocalise with S100P within protrusions of the plasma membrane (Austermann *et al.* 2008). Ezrin's role to provide a linkage between F-actin and the plasma membrane, or to membrane proteins, is essential for several processes including cell motility and signal transduction (Bretscher *et al.* 2002). Clustering of PI(4,5)P2 within the plasma membrane recruits ezrin, in close proximity to Rho kinases (ROCKs). Phosphorylation of T567 in ezrin by ROCKs leads to its activation and subsequent recruitment of its target proteins. Prag *et al.* (2007) reported that activated ezrin *in vitro* can bind to Dbl, a guanine nucleotide exchange factor, and lead to recruitment and activation of the Rho GTPase Cdc42 at lipid domains. Cdc42 activation is required for the formation of actin protrusions, with its inhibition leading to the prevention of cell polarisation and directional migration (Ridley 2015).

Cell polarisation requires reorganisation of the actin cytoskeleton in a coordinated manner (Raman *et al.* 2018). The GTP-bound form of Cdc42 is a known interactor of IQGAP1, a cytoskeletal regulator that can bind to S100P, F-actin, ERK2 and E-cadherin among others (Noritake *et al.* 2005). Its direct binding to F-actin at the leading edge of cells undergoing directional migration facilitates F-actin crosslinking (Fukata *et al.* 1997). IQGAP1 can also bind to and capture microtubules through interaction with CLIP-170, a protein that accumulates at the plus ends of microtubules (Fukata *et al.* 2002). This interaction at the leading edge leads to stabilisation of microtubules which are required for the stability of the cell's actin meshwork. Inhibition of IQGAP1 expression by use of siRNA technology in MDCKII cells was found to lead to reduced accumulation of F-actin and E-cadherin associated with β-catenin at cell-cell contact sites, suggesting the necessity of IQGAP1 in cell-cell adhesion (Noritake *et al.* 2004). IQGAP1 is

seen as a scaffolding protein due to the presence of multiple protein-binding domains and its consequent ability to in involved in multiprotein complexes.

S100P's calcium-dependent interaction with IQGAP1 is somewhat novel, as the binding site in S100P was mapped to its N-terminal EF-hand (Heil *et al.* 2011). No other known S100P interactors have been shown to bind to S100P in this manner, with all known targets instead binding to its C-terminal portion. Heil *et al.* (2011) also found that interaction of S100P with IQGAP1 did not affect interactions of IQGAP1 with Rac1 and Cdc42, but did prevent the phosphorylation of IQGAP1 and subsequent activation of MEK, to a lesser extent, triggered by EGF stimulation in HeLa cells. This indicates that interaction of S100P with IQGAP1 prevents activation of the MAPK pathway. S100P binding to IQGAP1 is mediated by IQGAP1's IQ domain, a domain which is essential for MEK binding (Roy *et al.* 2005). Transient transfection of WT IQGAP1 in HEK-293H cells significantly lessened the ability of EGF to activate MEK, whereas IQGAP1 without its IQ domain did not. Binding of MEK to the IQ domain of IQGAP1 is therefore thought to regulate MEK's activation by EGF. Ultimately, binding and activation of components of the MAPK signalling cascade leads to activation of transcription factors involved in the expression of genes required in processes including cell proliferation, migration and differentiation (Knight and Irving 2014). EGF stimulation was found by Heil *et al.* (2011) to lead to IQGAP1 accumulation in plasma membrane regions, in contrast to its diffuse cytoplasmic localisation observed without EGF stimulation. As S100P binding to IQGAP1, occurring in plasma membrane protrusions, was not found to affect interaction of IQGAP1 with Cdc42 and Rac 1, Heil *et al.* (2011) suggests that Cdc42-dependent actin reorganisation is therefore not mediated through S100P-IQGAP1 interactions.

Biotinylation of cell surface proteins using a cell-impermeable form of biotin led to detection of S100P in both trophoblast and non-trophoblast cell lines (see section 4.3.1). Given that biotinylation is utilised for pulldown of cell surface proteins and related extracellular proteins, it is possible that S100P that was detected could be present either on the extracellular membrane surface, or in the ECM. Secretion of S100P in cancer cells has been shown by Arumugam *et al.* (2004, 2005), however there is no evidence as of yet for this process to occur in trophoblasts. In addition, S100P does not contain a signal peptide for secretion, and therefore the pathways regulating this secretion are unknown. Secretion of S100A8/A9 was found to take place in an energy-dependent process involving activated PKC and an intact microtubule network (Rammes *et al.* 1997). S100A8/A9 was localised to tubulin filament networks, with tubulin filament depolymerisation leading to altered localisation of S100A8/A9. Given that the direct interaction of S100P with tubulin was recently demonstrated (Du *et al.* 2020), it may be that S100P is secreted through a similar, non-canonical pathway.

Expression of S100 proteins have been detected on the cell surface, including the S100A8/A9 heterodimer in breast cancer cells (Bode *et al.* 2008). Following knockdown of annexin A6, S100A8/A9 was no longer detected in this location, suggesting annexin A6 is required for their presence on the cell surface. S100A10 binds to annexin A2 through its C-terminal extension and forms a complex present on membrane surfaces, with S100A10 influencing the affinity of annexin A2 with phosphatidylserine-containing liposomes (Powell and Glenney 1987).

Work by Kathir *et al.* (2007) hypothesised the extracellular release of fibroblast growth factor 1 (FGF-1) occurred through its interaction with the S100A13 homodimer, which forms a multiprotein complex with p65 synaptotagmin at the plasma membrane. S100A13, like other S100 proteins, lacks a classical signal sequence but has been shown to be released from NIH3T3 cells in a spontaneous manner (Landriscina *et al.* 2001). It was theorized by Kathir *et al.* (2007) that interaction of S100A13 with phospholipids, alongside membrane-bound annexins, anchors the multiprotein complex, with the "flip-flop" action of annexins facilitating the localisation of S100A13 and FGF-1 in the extracellular space. In addition, mutant S100A13 lacking its C-terminal extension could not facilitate the extracellular export of FGF-1, suggesting the potential for this domain to be involved in this process.

A study by Deora *et al.* (2004) showed that annexin A2 in particular was found to translocate to the extracellular membrane following temperature-induced stress. In addition, this translocation did not require the canonical secretion pathway from the ER to the Golgi apparatus. Further work by Stewart *et al.* (2018) demonstrated the need for lipid scramblases and transbilayer movement of phospholipids to enable translocation of both annexins A2 and A5 across the cell membrane. It may be that binding of S100P to membrane proteins, such as annexins, facilitates its release into the extracellular space through a non-canonical secretion pathway.

Given that S100P has been shown to enhance the migration and invasion of trophoblasts (Tabrizi *et al.* 2018), we aimed to characterise the role of the extracellular/membrane-associated pool of S100P in these processes (see section 4.3.4). A S100P-directed antibody was able to significantly reduce both the motility and invasion of JEG-3 and EVT-like HTR8 cells, suggesting that this pool of S100P promotes these processes. Recent work has shown the ability of extracellular S100P to promote motility and invasion in rat mammary cells (Clarke *et al.* 2017; Ismail *et al.* 2020 submitted), but this has not yet been reported specifically in trophoblasts. Exogenous addition of S100P has been shown to activate the NFκB pathway in BxPC3 cells, leading to increased secretion of MMP-9, which may facilitate ECM degradation (Dakhel *et al.* 2014). Activation of this pathway was reduced following the addition of several different monoclonal S100P antibodies.

Interestingly, reduction of motility and invasion in JEG-3 cells following S100P antibody treatment was not as pronounced as the effect of S100P-directed siRNA, suggesting that different pools of S100P require two separate pathways to promote these processes to different degrees. This was further supported by quantification of focal adhesions; knockdown of presumably intracellular S100P using S100P siRNA in JEG-3 cells demonstrated a marked reduction in focal adhesion size and number, in contrast to S100P antibody-treated HTR8 cells which no changes in focal adhesion number were observed. Given that Du *et al.* (2012) observed a reversal of loss of focal adhesion sites in S100P-expressing HeLa cells following treatment with a FAK inhibitor, it seems likely that this pathway involving loss of focal adhesions in trophoblasts may also be regulated by FAK. High levels of phosphorylated, active FAK have been observed in EVTs within the first trimester of pregnancy (Ilić *et al.* 2001), a time in which cell motility and invasion is required to invade maternal spiral arteries and enhance placental perfusion (Knöfler and Pollheimer 2013). FAK has also been shown to directly bind to ezrin (Poullet *et al.* 2001), with overexpression of ezrin promoting activation of FAK without growth factor stimulation. Mao *et al.* (2019) have found that downregulation of ezrin, mediated by increased the expression of mir-96-5p following titanium dioxide treatment, led to the disruption of the cytoskeleton in human trophoblasts. Consequently, human trophoblast invasion was decreased suggesting the importance of ezrin in the invasion of trophoblasts. Downregulation of ezrin was found to significantly increase the number and size of focal adhesion complexes and FAK in MDA-MB-231 cells, in addition to a reduction in focal adhesion turnover (Hoskin *et al.* 2015). Taken together, it is therefore suggested that interaction of intracellular S100P with ezrin, and perhaps other yet uncharacterised proteins, may lead to the enhanced motility and invasion of trophoblasts through FAK.

In regards to the extracellular S100P pathway that regulates motility and invasion in EVTs, there are several known extracellular interactors of S100P that may facilitate these processes. Several groups have shown the activation of RAGE following the addition of exogenous S100P to pancreatic and colon cancer cells, with outcomes of increased migration and invasion (Arumugam *et al.* 2004; Fuentes *et al.* 2007). Our work found a reduction in both EVT motility and invasion following treatment with cromolyn, an inhibitor of RAGE-S100P interactions, to a similar degree seen by treatment with an S100P antibody. This suggests RAGE-S100P interactions could be responsible for promoting EVT motility and invasion through an extracellular pathway, however cromolyn has also been observed to interact with other S100 proteins (Shishibori *et al.* 1999). In addition, cromolyn binding to S100P occurs in S100P's hinge region, as well as helices 1 and 4. These sites are crucial for interaction of S100P with various other proteins, including ezrin (Austermann *et al.* 2008) and S100A1 (Wang *et al.* 2004). It therefore could be that cromolyn is not just preventing interaction of S100P with RAGE, but also with other extracellular target proteins that bind to S100P in this manner. However, binding interfaces for

S100P's extracellular interactions with tPA and IL-11 have not yet been characterised. Further work, which found a decrease in S100P associated with isolated plasma membrane fractions following cromolyn treatment, suggests that cromolyn may bind to and sequester S100P, preventing its association with membrane structures or proteins associated with membrane structures.

S100P's association with the intracellular side of the plasma membrane could be facilitated by several stretches of residues, namely in helices 1 and 4, in addition to S100P's linker region. The residues involved in the interaction between S100P and cromolyn has been characterised by Penumutchu, Chou and Yu (2014), who found these same regions are also responsible for cromolyn's interaction with S100P, suggesting the above explanation for reduced detection of S100P following cromolyn treatment to be plausible. The data generated by MODA should be interpreted with caution, as such data is a prediction and must be fully validated with experimental studies. The data can, however, be used to inform mutagenesis studies to ascertain if the suspected residues are in fact involved in a membrane-binding interface.

We explored the possibility of a PTM within S100P that could facilitate its interaction with the plasma membrane, as S100P from isolated plasma membrane fractions was seen to migrate slower on SDS-PAGE than S100P obtained from cell lysates (see section 4.3.7). Given the extensive time required to identify PTM sites experimentally, we utilised a prediction server for lipid modifications which are likely to facilitate protein-membrane bilayer interactions (Xie *et al.* 2016). Lipid modifications, such as myristoylation and prenylation, can confer increased affinity for membranes in a reversible manner (McLaughlin and Aderem, 1995; Welman, Burger and Hagmann, 2000; Resh, 2013) in combination with a polybasic motif as seen in p21ras (Hancock *et al.* 1990) and $G\gamma_2$ (Noguera-Salvà *et al.* 2017). The GPS-Lipid predicted that residues G9 and C85 may undergo N-myristoylation and S-farnesylation, respectively.

The enzyme that catalyses the process of farnesylation, farnesyltransferase, has been previously purified from the placenta (Ray and Lopez-Belmonte 1992) and found to be expressed in trophoblasts (Rozovski *et al.* 2007), demonstrating the potential for this process to take place in trophoblast cells. Whilst there are no studies that specifically identify expression of N-myristoyltransferase, the catalyst for N-myristoylation, in the placenta, one study has found decreases in N-myristoyltransferase expression by RT-PCR in endometrial stromal cells following co-culture with trophoblasts (Popovici *et al.* 2006). These lipid modifications alone, however, would likely not be sufficient to strongly anchor S100P to the plasma membrane. Given that S100P was isolated from the plasma membrane fraction following ultracentrifugation and a sucrose cushion, it seems unlikely that its association with the

plasma membrane fraction is a result of transient interactions with receptors, and suggests that it is instead a stable interaction due to its ability to withstand the ultracentrifugation process.

The presence of a polybasic domain has been shown to enhance membrane-binding capabilities of several proteins (Fivaz and Meyer 2005, Hancock *et al.* 1990). Several lysine residues at the C-terminus of S100P (K87, K91, K95) could provide a sufficient positive charge to enable binding to negatively-charged phospholipids in the plasma membrane, along with the aforementioned lipid modifications, to create an anchor. In addition, these lysine residues are predicted by the MODA server to have a high probability of membrane-association, further strengthening the likelihood of this scenario. However, further mutagenesis studies, involving mutation of potentially lipid-modified residues or the C-terminal lysine residues of S100P, followed by both detection of S100P in isolated plasma membrane fractions and characterisation of the role of the mutants in migration and invasion, would help to confirm the contribution of lipidation to S100P's membrane association.

In the final chapter, we aimed to characterise if S100P would be integrated into different complexes in different cellular compartments. After finding presence of S100P in high molecular weight complexes within trophoblast cytoplasm/membrane fractions, we detected many proteins with an increased global abundance in S100P-expressing cells in comparison to S100P-negative cells, which were further sorted through DAVID to identify enriched themes, including biological functions and cellular locations. With a focus on membrane-associated proteins that could mediate S100P's effects on cellular motility and invasion, we identified annexin A6 as a protein with a statistically significant increased abundance in S100P-expressing cells. Given that an interaction between S100 proteins and annexins at the cell surface has been well documented (Semov *et al.* 2005; Bode *et al.* 2008; O'Connell *et al.* 2010), as well as the fact that annexin A6 is expressed in trophoblast membranes (Rambotti, Spreca and Donato, 1993; Paradela *et al.* 2005), we sought to further confirm this finding.

Increased abundance of annexin A6 in EVT-like HTR8 cells was not detectable by western blotting at a statistically significant level, although this does not rule out a direct interaction between S100P and annexin A6. Both S100A10 and S100P have the ability to activate tPA through their C-terminal lysine residues (Kassam *et al.* 1998; Clarke *et al.* 2017), however S100A10 mediates this effect as part of the S100A10-annexin A2 heterotetramer. Further analysis of S100P interactions, either through co-immunoprecipitation or surface plasmon resonance studies with annexin A6 specifically would enable characterisation of S100P interaction partners in trophoblasts.

S100P's ability to enhance cell motility and invasion has been extensively characterised in cancer cell lines. This work shows for the first time that different pools of S100P, either intracellular or membrane-associated, promote trophoblast motility and invasion through two independent pathways. Studies of

S100P's requirements for membrane association, through the generation of mutants that do not have membrane binding capacity, and subsequent analysis of cellular migration and invasion would further confirm the role of membrane-associated S100P in these processes. Co-immunoprecipitation of purified membranes could also shed light into S100P's interaction partners in trophoblasts. A combination of these approaches may provide insight into the molecular mechanisms behind motility and invasion in a physiological process, placental implantation.

References

Abd El-Aleem, S.A. and Dekker, L. V. (2018) 'Assessment of the Cellular Localisation of the Annexin A2/S100A10 Complex in Human Placenta'. *Journal of Molecular Histology* [online] 49 (5), 531–543. available from <http://dx.doi.org/10.1007/s10735-018-9791-2>

Abou-Kheir, W., Barrak, J., Hadadeh, O., and Daoud, G. (2017) 'HTR-8/SVneo Cell Line Contains a Mixed Population of Cells'. *Placenta* [online] 50, 1–7. available from <http://dx.doi.org/10.1016/j.placenta.2016.12.007>

Akoumianaki, T., Kardassis, D., Polioudaki, H., Georgattos, S.D., and Theodoropoulos, P.A. (2009) 'Nucleocytoplasmic Shuttling of Soluble Tubulin in Mammalian Cells'. *Journal of Cell Science* 122 (8), 1111–1118

Al-Lamki, R.S., Skepper, J.N., and Burton, G. J. (1999) 'Are Human Placental Bed Giant Cells Merely Aggregates of Small Mononuclear Trophoblast Cells? An Ultrastructural and Immunocytochemical Study'. *Human Reproduction* 14 (2), 496–504

Althaus, K. and Greinacher, A. (2009) 'MYH9-Related Platelet Disorders'. *Seminars in Thrombosis and Hemostasis* 35 (2), 189–203

Apps, R., Sharkey, A., Gardner, L., Male, V., Trotter, M., Miller, N., North, R., Founds, S., and Moffett, A. (2011) 'Genome-Wide Expression Profile of First Trimester Villous and Extravillous Human Trophoblast Cells'. *Placenta* [online] 32 (1), 33–43. available from <http://dx.doi.org/10.1016/j.placenta.2010.10.010>

Arumugam, T. and Logsdon, C.D. (2011) 'S100P: A Novel Therapeutic Target for Cancer'. *Amino Acids* 41 (4), 893–899

Arumugam, T., Ramachandran, V., and Logsdon, C.D. (2006) 'Effect of Cromolyn on S100P Interactions with RAGE and Pancreatic Cancer Growth and Invasion in Mouse Models'. *Journal of the National Cancer Institute* 98 (24), 1806–1818

Arumugam, T., Simeone, D.M., Van Golen, K., and Logsdon, C.D. (2005) 'S100P Promotes Pancreatic Cancer Growth, Survival, and Invasion'. *Clinical Cancer Research* 11 (15), 5356–5364

Arumugam, T., Simeone, D.M., Schmidt, A.M., and Logsdon, C.D. (2004) 'S100P Stimulates Cell Proliferation and Survival via Receptor for Activated Glycation End Products (RAGE)'. *Journal of Biological Chemistry* 279 (7), 5059–5065

Austermann, J., Nazmi, A.R., Müller-Tidow, C., and Gerke, Volker (2008) 'Characterization of the Ca2+-Regulated Ezrin-S100P Interaction and Its Role in Tumor Cell Migration'. *Journal of Biological Chemistry* 283 (43), 29331–29340

Bagur, R. and Hajnóczky, G. (2017) 'Intracellular Ca2+ Sensing: Its Role in Calcium Homeostasis and Signaling'. in *Molecular Cell*. vol. 66 (6). Cell Press, 780–788

Bandorowicz-Pikula, J. and Seliga, A.K. (2018) 'Annexin A6 as a Cholesterol and Nucleotide Binding Protein Involved in Membrane Repair and in Controlling Membrane Transport during Endo- and Exocytosis'. *Postępy Biochemii* 64 (3), 190–195

Bao, J., Jana, S.S., and Adelstein, R.S. (2005) 'Vertebrate Nonmuscle Myosin II Isoforms Rescue Small Interfering RNA-Induced Defects in COS-7 Cell Cytokinesis'. *Journal of Biological Chemistry* 280 (20), 19594–19599

Barbetti, V., Morandi, A., Tusa, I., Digiacomo, G., Riverso, M., Marzi, I., Cipolleschi, M.G., Bessi, S., Giannini, A., Di Leo, A., Dello Sbarba, P., and Rovida, E. (2014) 'Chromatin-Associated CSF-1R Binds to the Promoter of Proliferation-Related Genes in Breast Cancer Cells'. *Oncogene* 33 (34), 4359–4364

Barger, S.W., Wolchok, S.R., and Van Eldik, L.J. (1992) 'Disulfide-Linked S100β Dimers and Signal Transduction'. *Biochimica et Biophysica Acta (BBA)/Protein Structure and Molecular* 1160 (1), 105–112

Barry, S., Chelala, C., Lines, K., Sunamura, M., Wang, A., Marelli-Berg, F.M., Brennan, C., Lemoine, Nicholas R., and Crnogorac-Jurcevic, T. (2013) 'S100P Is a Metastasis-Associated Gene That Facilitates Transendothelial Migration of Pancreatic Cancer Cells'. *Clinical and Experimental Metastasis* 30 (3), 251–264

Becker, T., Gerke, V., Kube, E., and Weber, K. (1992) 'S100P, a Novel Ca2+-Binding Protein from Human Placenta. CDNA Cloning, Recombinant Protein Expression and Ca2+ Binding Properties'. *European Journal of Biochemistry* 207 (2), 541–547

Bigelow, R.L.H., Williams, B.J., Carroll, J.L., Daves, L.K., and Cardelli, J.A. (2009) 'TIMP-1 Overexpression Promotes Tumorigenesis of MDA-MB-231 Breast Cancer Cells and Alters Expression of a Subset of Cancer Promoting Genes in Vivo Distinct from Those Observed in Vitro'. *Breast Cancer Research and Treatment* 117 (1), 31–44

Bishop, A.L. and Hall, A. (2000) 'Rho GTPases and Their Effector Proteins.' *The Biochemical journal* [online] 348 Pt 2, 241–55. available from

<http://www.pubmedcentral.nih.gov/articlerender.fcgi?artid=1221060&tool=pmcentrez&rendertype=abstract>

Bissonnette, L., Drissennek, L., Antoine, Y., Tiers, L., Hirtz, C., Lehmann, S., Perrochia, H., Bissonnette, F., Kadoch, I.J., Haouzi, D., and Hamamah, S. (2016) 'Human S100A10 Plays a Crucial Role in the Acquisition of the Endometrial Receptivity Phenotype'. *Cell Adhesion and Migration* 10 (3), 282–298

Blanchoin, L., Boujemaa-Paterski, R., Sykes, C., and Plastino, J. (2014) 'Actin Dynamics, Architecture, and Mechanics in Cell Motility'. *Physiological Reviews* 94 (1), 235–263

Bode, G., Lüken, A., Kerkhoff, C., Roth, J., Ludwig, S., and Nacken, W. (2008) 'Interaction between S100A8/A9 and Annexin A6 Is Involved in the Calcium-Induced Cell Surface Exposition of S100A8/A9'. *Journal of Biological Chemistry* 283 (46), 31776–31784

Bresnick, A.R., Weber, David J., and Zimmer, D.B. (2015) 'S100 Proteins in Cancer'. *Nature Reviews Cancer* [online] 15 (2), 96–109. available from <http://dx.doi.org/10.1038/nrc3893>

Bretscher, A., Edwards, K., and Fehon, R.G. (2002) 'ERM Proteins and Merlin: Integrators at the Cell Cortex'. *Nature Reviews Molecular Cell Biology* 3 (8), 586–599

Brudvig, J.J. and Weimer, J.M. (2015) 'X MARCKS the Spot: Myristoylated Alanine-Rich C Kinase Substrate in Neuronal Function and Disease'. *Frontiers in Cellular Neuroscience* 9 (407), 1–10

Bryant, J.A., Finn, R.S., Slamon, D.J., Cloughesy, T.F., and Charles, A.C. (2004) 'EGF Activates Intracellular and Intercellular Calcium Signaling by Distinct Pathways in Tumor Cells'. *Cancer Biology and Therapy* 3 (12), 1243–1249

Bucciarelli, L.G., Kaneko, M., Ananthakrishnan, R., Harja, E., Lee, L.K., Hwang, Y.C., Lerner, S., Bakr, S., Li, Q., Lu, Y., Song, F., Qu, W., Gomez, T., Yu, S.Z., Shi, F.Y., Schmidt, A.M., and Ramasamy, R. (2006) 'Receptor for Advanced-Glycation End Products: Key Modulator of Myocardial Ischemic Injury'. *Circulation* 113 (9), 1226–1234

Burgess, H.M. and Gray, N.K. (2012) 'An Integrated Model for the Nucleo-Cytoplasmic Transport of Cytoplasmic Poly(A)-Binding Proteins'. *Communicative and Integrative Biology* 5 (3), 243–247

Burton, Graham J. and Jauniaux, E. (2017) 'The Cytotrophoblastic Shell and Complications of Pregnancy'. *Placenta* [online] 60, 134–139. available from <https://doi.org/10.1016/j.placenta.2017.06.007>

Burton, Graham J. and Jauniaux, E. (2018) 'Pathophysiology of Placental-Derived Fetal Growth

Restriction'. *American Journal of Obstetrics and Gynecology* [online] 218 (2), S745–S761. available from <https://doi.org/10.1016/j.ajog.2017.11.577>

Cai, X.Y., Lu, L., Wang, Y.N., Jin, C., Zhang, R.Y., Zhang, Qi, Chen, Q.J., and Shen, W.F. (2011) 'Association of Increased S100B, S100A6 and S100P in Serum Levels with Acute Coronary Syndrome and Also with the Severity of Myocardial Infarction in Cardiac Tissue of Rat Models with Ischemia-Reperfusion Injury'. *Atherosclerosis* [online] 217 (2), 536–542. available from <http://dx.doi.org/10.1016/j.atherosclerosis.2011.05.023>

Capozzi, F., Casadei, F., and Luchinat, C. (2006) 'EF-Hand Protein Dynamics and Evolution of Calcium Signal Transduction: An NMR View'. *Journal of Biological Inorganic Chemistry* 11 (8), 949–962

Carter, A.M. (2007) 'Animal Models of Human Placentation - A Review'. *Placenta* [online] 2 (Supplement A), S41–S47. available from <http://dx.doi.org/10.1016/j.placenta.2006.11.002>

Castro-Alcaraz, S., Miskolci, V., Kalasapudi, B., Davidson, D., and Vancurova, I. (2002) 'NF-KB Regulation in Human Neutrophils by Nuclear IκBα: Correlation to Apoptosis'. *The Journal of Immunology* 169 (7), 3947–3953

Chang, W.L., Liu, Y.W., Dang, Y.L., Jiang, X.X., Xu, Honglin, Huang, X., Wang, Y.L., Wang, Haibin, Zhu, C., Xue, L.Q., Lin, H.Y., Meng, W., and Wang, Hongmei (2018) 'PLAC8, a New Marker for Human Interstitial Extravillous Trophoblast Cells, Promotes Their Invasion and Migration'. *Development (Cambridge)* 145 (2)

Chen, Hongyan, Yuan, Y., Zhang, C., Luo, A., Ding, F., Ma, J., Yang, S., Tian, Y., Tong, T., Zhan, Q., and Liu, Zhihua (2012) 'Involvement of S100A14 Protein in Cell Invasion by Affecting Expression and Function of Matrix Metalloproteinase (MMP)-2 via P53-Dependent Transcriptional Regulation'. *Journal of Biological Chemistry* 287 (21), 17109–17119

Chen, P.S., Wang, M.Y., Wu, S.N., Su, J.L., Hong, C.C., Chuang, S.E., Chen, M.W., Hua, K.T., Wu, Y.L., Cha, S.T., Babu, M.S., Chen, C.N., Lee, P.H., Chang, K.J., and Kuo, M.L. (2007) 'CTGF Enhances the Motility of Breast Cancer Cells via an Integrin-Avβ3-ERK1/2-Dependent S100A4-Upregulated Pathway'. *Journal of Cell Science* 120 (12), 2053–2065

Chiang, J.M., Tan, R., Wang, J.Y., Chen, J.S., Lee, Y.S., Hsieh, P.S., Changchien, C.R., and Chen, J.R. (2015) 'S100p, a Calcium-Binding Protein, Is Preferentially Associated with the Growth of Polypoid Tumors in Colorectal Cancer'. *International Journal of Molecular Medicine* 35 (3), 675–683

Chibber, R. and Castle, A.G. (1983) 'Subcellular Fractionation of Porcine Neutrophils by Nitrogen

Cavitation and Sucrose-density-gradient Centrifugation'. *European Journal of Biochemistry* 136 (2), 383–389

Choi, K.-S., Fogg, D.K., Yoon, C.-S., and Waisman, D.M. (2003) 'P11 Regulates Extracellular Plasmin Production and Invasiveness of HT1080 Fibrosarcoma Cells.' *FASEB journal : official publication of the Federation of American Societies for Experimental Biology* [online] 17 (2), 235–46. available from <http://www.ncbi.nlm.nih.gov/pubmed/12554702> [25 October 2019]

Clarke, C.J., Gross, S.R., Ismail, T.M., Rudland, Philip S, Al-Medhtiy, M., Santangeli, M., and Barraclough, Roger (2017) 'Activation of Tissue Plasminogen Activator by Metastasis-Inducing S100P Protein'. *Biochemical Journal* [online] 474 (19), 3227–3240. available from <http://biochemj.org/lookup/doi/10.1042/BCJ20170578>

Clawson, G.A., Matters, G.L., Xin, P., McGovern, C., Wafula, E., DePamphilis, C., Meckley, M., Wong, J., Stewart, L., D'Jamoos, C., Altman, N., Kawasawa, Y.I., Du, Z., Honaas, L., and Abraham, T. (2017) *'Stealth Dissemination' of Macrophage-Tumor Cell Fusions Cultured from Blood of Patients with Pancreatic Ductal Adenocarcinoma*. vol. 12

Codrici, E., Albulescu, L., Popescu, I.D., Mihai, S., Enciu, A.M., Albulescu, R., Tanase, C., and Hinescu, M.E. (2018) 'Caveolin-1-Knockout Mouse as a Model of Inflammatory Diseases'. *Journal of Immunology Research* 2018

Cui, Y., Gao, C., Zhao, Qiong, and Jiang, L. (2016) 'Using Fluorescent Protein Fusions to Study Protein Subcellular Localization and Dynamics in Plant Cells'. in *Methods in Molecular Biology*. vol. 1474. Humana Press Inc., 113–123

Dakhel, S., Padilla, L., Adan, J., Masa, M., Martinez, J.M., Roque, L., Coll, T., Hervas, R., Calvis, C., Messeguer, R., Mitjans, F., and Hernández, J.L. (2014) 'S100P Antibody-Mediated Therapy as a New Promising Strategy for the Treatment of Pancreatic Cancer.' *Oncogenesis* [online] 3 (February), e92. available from <http://www.pubmedcentral.nih.gov/articlerender.fcgi?artid=4038391&tool=pmcentrez&rendertype=abstract>

Damsky, C. H., Fitzgerald, M.L., and Fisher, S. J. (1992) 'Distribution Patterns of Extracellular Matrix Components and Adhesion Receptors Are Intricately Modulated during First Trimester Cytotrophoblast Differentiation along the Invasive Pathway, in Vivo'. *Journal of Clinical Investigation* 89 (1), 210–222

Dasilva-Arnold, S., James, J.L., Al-Khan, A., Zamudio, S., and Illsley, N.P. (2015) 'Differentiation of First

Trimester Cytotrophoblast to Extravillous Trophoblast Involves an Epithelial-Mesenchymal Transition'. *Placenta*

Davies, J., Pollheimer, J., Yong, H.E.J., Kokkinos, M.I., Kalionis, B., Knöfler, M., and Murthi, P. (2016) 'Epithelial-Mesenchymal Transition during Extravillous Trophoblast Differentiation'. *Cell Adhesion and Migration* 10 (3), 310–321

Deng, W., Wang, C., Zhang, Y., Xu, Yang, Zhang, Shuang, Liu, Zexian, and Xue, Y. (2016) 'GPS-PAIL: Prediction of Lysine Acetyltransferase-Specific Modification Sites from Protein Sequences'. *Scientific Reports* [online] 6 (December), 1–10. available from <http://dx.doi.org/10.1038/srep39787>

Deora, A.B., Kreitzer, G., Jacovina, A.T., and Hajjar, K.A. (2004) 'An Annexin 2 Phosphorylation Switch Mediates P11-Dependent Translocation of Annexin 2 to the Cell Surface'. *Journal of Biological Chemistry* 279 (42), 43411–43418

Detzen, L., Cheng, B., Chen, C.Y., Papapanou, P.N., and Lalla, E. (2019) 'Soluble Forms of the Receptor for Advanced Glycation Endproducts (RAGE) in Periodontitis'. *Scientific Reports* [online] 9 (1), 1–8. available from <http://dx.doi.org/10.1038/s41598-019-44608-2>

Donato, R (1999) 'Functional Roles of S100 Proteins, Calcium-Binding Proteins of the EF- Hand Type'. *Biochim Biophys Acta* [online] 1450 (3), 191–231. available from <http://www.ncbi.nlm.nih.gov/cgi-bin/Entrez/referer?http://www.elsevier.com:80/cgi-bin/cas/tree/store/bbamcr/cas_sub/browse/browse.cgi?year=1999&volume=1450&issue=3&aid=14486>

Donato, Rosario (1986) 'S-100 Proteins'. *Cell Calcium* 7 (3), 123–145

Donato, Rosario (1988) 'Calcium-Independent , PH-Regulated Effects of S- 100 Proteins on Assembly-Disassembly of Brain Microtubule Protein in Vitro'. *The Journal of Biological Chemistry* 263 (1), 106–110

Donato, Rosario (2001) 'S100: A Multigenic Family of Calcium-Modulated Proteins of the EF-Hand Type with Intracellular and Extracellular Functional Roles'. *International Journal of Biochemistry and Cell Biology* 33 (7), 637–668

Donato, Rosario (2003) 'Intracellular and Extracellular Roles of S100 Proteins'. *Microscopy Research and Technique* 60 (6), 540–551

Donato, Rosario, Cannon, B.R., Sorci, G., Riuzzi, F., Hsu, K., Weber, D.J., and Geczy, C.L. (2013) 'Functions of S100 Proteins'. *Curr Mol Med* 13 (1), 24–57

Donato, Rosario, Sorci, G., Riuzzi, F., Arcuri, C., Bianchi, R., Brozzi, F., Tubaro, C., and Giambanco, I. (2009) 'S100B's Double Life: Intracellular Regulator and Extracellular Signal'. *Biochimica et Biophysica Acta - Molecular Cell Research* [online] 1793 (6), 1008–1022. available from <http://dx.doi.org/10.1016/j.bbamcr.2008.11.009>

Dowen, S.E., Crnogorac-Jurcevic, T., Gangeswaran, R., Hansen, M., Eloranta, J.J., Bhakta, V., Brentnall, T.A., Lüttges, J., Klöppel, G., and Lemoine, Nick R (2005) 'Expression of S100P and Its Novel Binding Partner S100PBPR in Early Pancreatic Cancer.' *The American journal of pathology* [online] 166 (1), 81–92. available from <http://www.pubmedcentral.nih.gov/articlerender.fcgi?artid=1602285&tool=pmcentrez&rendertype=abstract>

Dresler, J., Klimentova, J., and Stulik, J. (2011) 'Bacterial Protein Complexes Investigation Using Blue Native PAGE'. *Microbiological Research* [online] 166 (1), 47–62. available from <http://dx.doi.org/10.1016/j.micres.2010.01.005>

Du, M., Wang, G., Barsukov, I.L., Gross, S.R., Smith, R., and Rudland, Philip S (2020) 'Direct Interaction of Metastasis-Inducing S100P Protein with Tubulin Causes Enhanced Cell Migration without Changes in Cell Adhesion'. *Biochemical Journal* BCJ2019064

Du, M., Wang, G., Ismail, T.M., Gross, S., Fernig, D.G., Barraclough, Roger, and Rudland, Philip S. (2012) 'S100P Dissociates Myosin IIA Filaments and Focal Adhesion Sites to Reduce Cell Adhesion and Enhance Cell Migration'. *Journal of Biological Chemistry* 287 (19), 15330–15344

Duarte-Costa, S., Castro-Ferreira, R., Neves, J.S., and Leite-Moreira, A.F. (2014) 'S100A1: A Major Player in Cardiovascular Performance'. *Physiological Research* 63 (6), 669–681

Dunn, C.L., Kelly, R.W., and Critchley, H.O. (2003) 'Decidualization of the Human Endometrial Stromal Cell: An Enigmatic Transformation'. *Reproductive BioMedicine Online* [online] 7 (2), 151–161. available from <http://linkinghub.elsevier.com/retrieve/pii/S1472648310617452>

Even-Ram, S., Doyle, A.D., Conti, M.A., Matsumoto, K., Adelstein, R.S., and Yamada, K.M. (2007) 'Myosin IIA Regulates Cell Motility and Actomyosin – Microtubule Crosstalk'. *Nature Cell Biology* 9 (3), 299–309

Fan, C., Fu, Z., Su, Q., Angelini, D.J., Van Eyk, J., and Johns, R.A. (2011) 'S100A11 Mediates Hypoxia-Induced Mitogenic Factor (HIMF)-Induced Smooth Muscle Cell Migration, Vesicular Exocytosis, and Nuclear Activation'. *Molecular and Cellular Proteomics* 10 (3), 1–7

Ferretti, C., Bruni, L., Dangles-Marie, V., Pecking, A.P., and Bellet, D. (2007) 'Molecular Circuits Shared

by Placental and Cancer Cells, and Their Implications in the Proliferative, Invasive and Migratory Capacities of Trophoblasts'. *Human Reproduction Update* 13 (2), 121–141

Filipek, A., Jastrzebska, B., Nowotny, M., and Kuznicki, J. (2002) 'CacyBP/SIP, a Calcyclin and Siah-1-Interacting Protein, Binds EF-Hand Proteins of the S100 Family.' *The Journal of biological chemistry* 277 (32), 28848–28852

Fisher, S. J., Cui, T., Zhang, L., Hartman, L., Grahl, K., Guo-Yang, Z., Tarpey, J., and Damsky, C. H. (1989) 'Adhesive and Degradative Properties of Human Placental Cytotrophoblast Cells in Vitro'. *Journal of Cell Biology* 109 (2), 891–902

Fivaz, M. and Meyer, T. (2005) 'Reversible Intracellular Translocation of KRas but Not HRas in Hippocampal Neurons Regulated by Ca2+/Calmodulin'. *Journal of Cell Biology* 170 (3), 429–441

Flather, D., Nguyen, J.H.C., Semler, B.L., and Gershon, P.D. (2018) 'Exploitation of Nuclear Functions by Human Rhinovirus, a Cytoplasmic RNA Virus'. *PLoS Pathogens* 14 (8)

Fluhr, H., Bischof-Islami, D., Krenzer, S., Licht, P., Bischof, P., and Zygmunt, M. (2008) 'Human Chorionic Gonadotropin Stimulates Matrix Metalloproteinases-2 and -9 in Cytotrophoblastic Cells and Decreases Tissue Inhibitor of Metalloproteinases-1, -2, and -3 in Decidualized Endometrial Stromal Cells'. *Fertility and Sterility* 90 (Suppl 2), 1390–1395

Foell, D., Wittkowski, H., Kessel, C., Lüken, A., Weinhage, T., Varga, G., Vogl, T., Wirth, T., Viemann, D., Björk, P., Van Zoelen, M.A.D., Gohar, F., Srikrishna, G., Kraft, M., and Roth, J. (2013) 'Proinflammatory S100A12 Can Activate Human Monocytes via Toll-like Receptor 4'. *American Journal of Respiratory and Critical Care Medicine* 187 (12), 1324–1334

Fornerod, M., Ohno, M., Yoshida, Minoru, and Mattaj, I.W. (1997) 'CRM1 Is an Export Receptor for Leucine-Rich Nuclear Export Signals'. *Cell* 90 (6), 1051–1060

Fuchs, R. and Ellinger, I. (2004) 'Endocytic and Transcytotic Processes in Villous Syncytiotrophoblast: Role in Nutrient Transport to the Human Fetus'. *Traffic* 5 (10), 725–738

Fuentes, M.K., Nigavekar, S.S., Arumugam, T., Logsdon, C.D., Schmidt, A.M., Park, J.C., and Huang, E.H. (2007) 'RAGE Activation by S100P in Colon Cancer Stimulates Growth, Migration, and Cell Signaling Pathways'. *Diseases of the Colon and Rectum* 50 (8), 1230–1240

Fukata, M., Kuroda, S., Fujii, K., Nakamura, T., Shoji, I., Matsuura, Y., Okawa, K., Iwamatsu, A., Kikuchi, A., and Kaibuchi, K. (1997) 'Regulation of Cross-Linking of Actin Filament by IQGAP1, a Target for Cdc42'. *Journal of Biological Chemistry* 272 (47), 29579–29583

Fukata, M., Watanabe, T., Noritake, J., Nakagawa, M., Yamaga, M., Kuroda, S., Matsuura, Y., Iwamatsu, A., Perez, F., and Kaibuchi, K. (2002) 'Rac1 and Cdc42 Capture Microtubules through IQGAP1 and CLIP-170'. *Cell* 109 (7), 873–885

Galasinski, S.C., Resing, K.A., Goodrich, J.A., and Ahn, N.G. (2002) 'Phosphatase Inhibition Leads to Histone Deacetylases 1 and 2 Phosphorylation and Disruption of Corepressor Interactions'. *Journal of Biological Chemistry* 277 (22), 19618–19626

Gamage, T.K.J.B., Chamley, L.W., and James, J.L. (2016) 'Stem Cell Insights into Human Trophoblast Lineage Differentiation'. *Human Reproduction Update* 23 (1), 77–103

Garbuglia, M., Verzini, M., and Donato, Rosario (1998) 'Annexin VI Binds S100A1 and S100B and Blocks the Ability of S100A1 and S100B to Inhibit Desmin and GFAP Assemblies into Intermediate Filaments'. *Cell Calcium* 24 (3), 177–191

Gerke, Volker, Creutz, C.E., and Moss, S.E. (2005) 'Annexins: Linking Ca2+ Signalling to Membrane Dynamics'. *Nature Reviews Molecular Cell Biology* 6 (6), 449–461

Gerke, Volker and Moss, S.E. (2002) 'Annexins: From Structure to Function'. *Physiological Reviews* 82, 331–371

Gialeli, C., Theocharis, A.D., and Karamanos, N.K. (2011) 'Roles of Matrix Metalloproteinases in Cancer Progression and Their Pharmacological Targeting'. *FEBS Journal* 278 (1), 16–27

Gilston, B.A., Skaar, E.P., and Chazin, W.J. (2016) 'Binding of Transition Metals to S100 Proteins'. *Science China Life Sciences* 59 (8), 792–801

Gleeson, L.M., Chakraborty, C., Mckinnon, T., and Lala, P.K. (2001) 'Insulin-like Growth Factor-Binding Protein 1 Stimulates Human Trophoblast Migration by Signaling through A5β1 Integrin via Mitogen-Activated Protein Kinase Pathway'. *Journal of Clinical Endocrinology and Metabolism* 86 (6), 2484–2493

Gomez-Martinez, M., Schmitz, D., and Hergovich, A. (2013) 'Generation of Stable Human Cell Lines with Tetracycline-Inducible (Tet-on) ShRNA or CDNA Expression'. *Journal of Visualized Experiments* (73), 1–7

Grevers, L.C., De Vries, T.J., Vogl, T., Abdollahi-Roodsaz, S., Sloetjes, A.W., Leenen, P.J.M., Roth, J., Everts, V., Van Den Berg, W.B., and Van Lent, P.L.E.M. (2011) 'S100A8 Enhances Osteoclastic Bone Resorption in Vitro through Activation of Toll-like Receptor 4: Implications for Bone Destruction in Murine Antigen-Induced Arthritis'. *Arthritis and Rheumatism* 63 (5), 1365–1375

Gribenko, A. V and Makhatadze, G.I. (1998) 'Oligomerization and Divalent Ion Binding Properties of the S100P Protein: A Ca2+/Mg2+-Switch Model.' *Journal of molecular biology* [online] 283 (3), 679–94. available from <http://www.ncbi.nlm.nih.gov/pubmed/9784376>

Gross, S.R., Sin, C.G.T., Barraclough, Roger, and Rudland, Philip S. (2014) 'Joining S100 Proteins and Migration: For Better or for Worse, in Sickness and in Health'. *Cellular and Molecular Life Sciences* 71 (9), 1551–1579

Gude, N.M., Roberts, C.T., Kalionis, B., and King, R.G. (2004) 'Growth and Function of the Normal Human Placenta'. *Thrombosis Research* 114 (5-6 SPEC. ISS.), 397–407

Gulmann, C., Paner, G.P., Parakh, R.S., Hansel, D.E., Shen, S.S., Ro, J.Y., Annaiah, C., Lopez-Beltran, A., Rao, P., Arora, K., Cho, Y., Herrera-Hernandez, L., Alsabeh, R., and Amin, M.B. (2013) 'Immunohistochemical Profile to Distinguish Urothelial from Squamous Differentiation in Carcinomas of Urothelial Tract'. *Human Pathology* [online] 44 (2), 164–172. available from <http://dx.doi.org/10.1016/j.humpath.2012.05.018>

Guo, L., Chen, S., Jiang, H., Huang, J., Jin, W., and Yao, S. (2014) 'The Expression of S100P Increases and Promotes Cellular Proliferation by Increasing Nuclear Translocation of β-Catenin in Endometrial Cancer'. *International Journal of Clinical and Experimental Pathology* 7 (5), 2102–2112

Güttler, T. and Görlich, D. (2011) 'Ran-Dependent Nuclear Export Mediators: A Structural Perspective'. *EMBO Journal* 30 (17), 3457–3474

Györffy, Balazs, Surowiak, Paweł, Kiesslich, O., Denkert, C., Schäfer, R., Dietel, Manfred, and Lage, Hermann (2006) 'Gene Expression Profiling of 30 Cancer Cell Lines Predicts Resistance towards 11 Anticancer Drugs at Clinically Achieved Concentrations'. *International Journal of Cancer* 118 (7), 1699–1712

Hamada, S., Satoh, K., Hirota, M., Fujibuchi, W., Kanno, A., Umino, J., Ito, H., Satoh, A., Kikuta, K., Kume, K., Masamune, A., and Shimosegawa, T. (2009) 'Expression of the Calcium-Binding Protein S100P Is Regulated by Bone Morphogenetic Protein in Pancreatic Duct Epithelial Cell Lines'. *Cancer Science* 100 (1), 103–110

Hamamoto, T., Gunji, S., Tsuji, H., and Beppu, T. (1983) 'Leptomycins A and B, New Antifungal Antibiotics. I. Taxonomy of the Producing Strain and Their Fermentation, Purification and Characterization.' *The Journal of antibiotics* [online] 36 (6), 639–45. available from <http://www.ncbi.nlm.nih.gov/pubmed/6874585> [7 October 2019]

Hancock, J.F., Paterson, H., and Marshall, C.J. (1990) 'A Polybasic Domain or Palmitoylation Is Required in Addition to the CAAX Motif to Localize P21ras to the Plasma Membrane'. *Cell* 63 (1), 133–139

Handschuh, K., Guibourdenche, J., Tsatsaris, V., Guesnon, M., Laurendeau, I., Evain-Brion, D., and Fournier, T. (2007) 'Human Chorionic Gonadotropin Produced by the Invasive Trophoblast but Not the Villous Trophoblast Promotes Cell Invasion and Is Down-Regulated by Peroxisome Proliferator-Activated Receptor-γ'. *Endocrinology* 148 (10), 5011–5019

Hang, H.C. and Linder, M.E. (2011) 'Exploring Protein Lipidation with Chemical Biology'. *Chem Rev* 111 (10), 6341–6358

Hannan, N.J., Paiva, P., Dimitriadis, E., and Salamonsen, L.A. (2010) 'Models for Study of Human Embryo Implantation: Choice of Cell Lines?' *Biology of Reproduction* 82 (2), 235–245

Heil, A., Nazmi, A.R., Koltzscher, M., Poeter, M., Austermann, J., Assard, N., Baudier, J., Kaibuchi, K., and Gerke, Volker (2011) 'S100P Is a Novel Interaction Partner and Regulator of IQGAP1'. *Journal of Biological Chemistry* 286 (9), 7227–7238

Heizmann, Claus W. (2002) 'The Multifunctional S100 Protein Family.' *Methods in Molecular Biology* 172 (Calcium-Binding Protein Protocols, Vol. 1), 69–80

Hermani, A., Hess, J., De Servi, B., Medunjanin, S., Grobholz, R., Trojan, L., Angel, P., and Mayer, D. (2005) 'Calcium-Binding Proteins S100A8 and S100A9 as Novel Diagnostic Markers in Human Prostate Cancer'. *Clinical Cancer Research* 11 (14), 5146–5152

Hessner, F., Dlugos, C.P., Chehab, T., Schaefer, C., Homey, B., Gerke, V., Weide, T., Pavenstädt, H., and Rescher, U. (2016) 'CC Chemokine Receptor 10 Cell Surface Presentation in Melanocytes Is Regulated by the Novel Interaction Partner S100A10'. *Scientific Reports* [online] 6 (March). available from <http://dx.doi.org/10.1038/srep22649>

Hofmann, G., Glatstein, I., Schatz, F., Heller, D., and Deligdisch, L. (1994) 'Immunohistochemical Localization of Urokinase-Type Plasminogen Activator and the Plasminogen Activator Inhibitors 1 and 2 in Early Human Implantation Sites'. *Am J Obstet Gynecol.* 170 (2), 671–676

Hofmann, M.A., Drury, S., Fu, C., Qu, W., Taguchi, A., Lu, Y., Avila, C., Kambham, N., Bierhaus, A., Nawroth, P., Neurath, M.F., Slattery, T., Beach, D., Mcclary, J., Nagashima, M., Morser, J., Stern, D., and Schmidt, A.M. (1999) 'RAGE Mediates a Novel Proinflammatory Axis : A Central Cell Surface Receptor for S100 / Calgranulin Polypeptides'. *Cell* 97, 889–901

Holden, P. and Horton, W.A. (2009) *Crude Subcellular Fractionation of Cultured Mammalian Cell*

Lines. 10

Holtan, S.G., Creedon, D.J., Haluska, P., and Markovic, S.N. (2009) 'Cancer and Pregnancy: Parallels in Growth, Invasion, and Immune Modulation and Implications for Cancer Therapeutic Agents'. *Mayo Clinic Proceedings* [online] 84 (11), 985–1000. available from <http://linkinghub.elsevier.com/retrieve/pii/S0025619611606691>

Hoskin, V., Szeto, A., Ghaffari, A., Greer, P.A., CÃtéc, G.P., and Elliott, B.E. (2015) 'Ezrin Regulates Focal Adhesion and Invadopodia Dynamics by Altering Calpain Activity to Promote Breast Cancer Cell Invasion'. *Molecular Biology of the Cell* 26 (19), 3464–3479

Hsu, Y.-L., Hung, J.-Y., Liang, Y.-Y., Lin, Y.-S., Tsai, M.-J., Chou, S.-H., Lu, C.-Y., and Kuo, P.-L. (2015) *S100P Interacts with Integrin A7 and Increases Cancer Cell Migration and Invasion in Lung Cancer* [online] vol. 6. available from <www.impactjournals.com/oncotarget/> [23 October 2019]

Huang, D.W., Sherman, B.T., and Lempicki, R.A. (2009) 'Systematic and Integrative Analysis of Large Gene Lists Using DAVID Bioinformatics Resources'. *Nature Protocols* 4 (1), 44–57

Huang, D.W., Sherman, B.T., Tan, Q., Collins, J.R., Alvord, W.G., Roayaei, J., Stephens, R., Baseler, M.W., Lane, H.C., and Lempicki, R.A. (2007) 'The DAVID Gene Functional Classification Tool: A Novel Biological Module-Centric Algorithm to Functionally Analyze Large Gene Lists'. *Genome Biology* 8 (9)

Hung, M.C. and Link, W. (2011) 'Protein Localization in Disease and Therapy'. *Journal of Cell Science* 124 (20), 3381–3392

Hung, N.-J., Lo, K.-Y., Patel, S.S., Helmke, K., and Johnson, A.W. (2008) 'Arx1 Is a Nuclear Export Receptor for the 60S Ribosomal Subunit in Yeast'. *Molecular Biology of the Cell* [online] 19, 735–744. available from <http://www.molbiolcell.org/cgi/doi/10.1091/mbc.E07-09> [7 October 2019]

Huppertz, B. (2008) 'Placental Origins of Preeclampsia'. *Hypertension* 51, 970–975

Huttunen, H.J., Fages, C., and Rauvala, H. (1999) 'Receptor for Advanced Glycation End Products (RAGE)-Mediated Neurite Outgrowth and Activation of NF-KB Require the Cytoplasmic Domain of the Receptor but Different Downstream Signaling Pathways'. *Journal of Biological Chemistry* 274 (28), 19919–19924

Huttunen, H.J., Kuja-Panula, J., Sorci, G., Agneletti, A.L., Donato, Rosario, and Rauvala, H. (2000) 'Coregulation of Neurite Outgrowth and Cell Survival by Amphoterin and S100 Proteins through

Receptor for Advanced Glycation End Products (RAGE) Activation'. *Journal of Biological Chemistry* 275 (51), 40096–40105

Ilić, D., Genbačev, O., Jin, Fang, Caceres, E., Almeida, E.A.C., Bellingard-Dubouchaud, V., Schaefer, E.M., Damsky, Caroline H., and Fisher, Susan J. (2001) 'Plasma Membrane-Associated PY397FAK Is a Marker of Cytotrophoblast Invasion in Vivo and in Vitro'. *American Journal of Pathology* 159 (1), 93–108

Jackson, R.S., Cho, Y.J., Stein, S., and Liang, P. (2007) 'CYFIP2, a Direct P53 Target, Is Leptomycin-B Sensitive'. *Cell Cycle* 6 (1), 95–103

Jaiswal, J.K., Lauritzen, S.P., Scheffer, L., Sakaguchi, M., Bunkenborg, J., Simon, S.M., Kallunki, T., Jäättelä, M., and Nylandsted, J. (2014) 'S100A11 Is Required for Efficient Plasma Membrane Repair and Survival of Invasive Cancer Cells'. *Nature Communications* 5 (3795)

Jana, A., Das, A., Krett, N.L., Guzman, G., Thomas, A., Mancinelli, G., Bauer, J., Ushio-Fukai, M., Fukai, T., and Jung, B. (2020) *Nuclear Translocation of Atox1 Potentiates Activin A-Induced Cell Migration and Colony Formation in Colon Cancer*. 15 (1), 1–16

Jang, J.H. and Hanash, S. (2003) 'Profiling of the Cell Surface Proteome'. *Proteomics* 3 (10), 1947–1954

Jenkinson, S.R., Barraclough, R., West, C.R., and Rudland, P. S. (2004) 'S100A4 Regulates Cell Motility and Invasion in an in Vitro Model for Breast Cancer Metastasis'. *British Journal of Cancer* 90 (1), 253–262

Jha, P., Wang, Xu, and Auwerx, J. (2017) 'Analysis of Mitochondrial Respiratory Chain Supercomplexes Using Blue Native Polyacrylamide Gel Electrophoresis (BN-PAGE)'. *Curr Protoc Mouse Biol.* 6 (1), 1–14

Ji, L., Brkić, J., Liu, Ming, Fu, G., Peng, Chun, and Wang, Y.L. (2013) 'Placental Trophoblast Cell Differentiation: Physiological Regulation and Pathological Relevance to Preeclampsia'. *Molecular Aspects of Medicine* 34 (5), 981–1023

Johnson, C.W. (1999) 'Issues in Immunohistochemistry'. *Toxicologic Pathology* 27 (2), 246–248

Johnson, J.E. and Cornell, R.B. (1999) 'Amphitropic Proteins: Regulation by Reversible Membrane Interactions'. *Molecular Membrane Biology* 16 (3), 217–235

Johnson, M., Sharma, M., Brocardo, M.G., and Henderson, B.R. (2011) 'IQGAP1 Translocates to the Nucleus in Early S-Phase and Contributes to Cell Cycle Progression after DNA Replication Arrest'.

International Journal of Biochemistry and Cell Biology [online] 43 (1), 65–73. available from <http://dx.doi.org/10.1016/j.biocel.2010.09.014>

Justus, C.R., Leffler, N., Ruiz-Echevarria, M., and Yang, L. V. (2014) 'In Vitro Cell Migration and Invasion Assays'. *Journal of Visualized Experiments* (88), 1–8

Kaczan-Bourgois, D., Salles, J.P., Hullin, F., Fauvel, J., Moisand, A., Duga-Neulat, I., Berrebi, A., Campistron, G., and Chap, H. (1996) 'Increased Content of Annexin II (P36) and P11 in Human Placenta Brush-Border Membrane Vesicles during Syncytiotrophoblast Maturation and Differentiation'. *Placenta* 17 (8), 669–676

Kang, R., Tang, D., Loze, M.T., and Zeh, H.J. (2017) 'Apoptosis to Autophagy Switch Triggered by the MHC Class III-Encoded Receptor for Advanced Glycation Endproducts (RAGE)'. *Autophagy* 7 (1), 91–93

Kaoutzani, P., Parkos, C.A., Delp-Archer, C., and Madara, J.L. (1993) 'Isolation of Plasma Membrane Fractions from the Intestinal Epithelial Model T84'. *American Journal of Physiology - Cell Physiology* 264 (5 33-5)

Kassam, G., Choi, K.S., Ghuman, J., Kang, H.M., Fitzpatrick, S.L., Zackson, T., Zackson, S., Toba, M., Shinomiya, A., and Waisman, D.M. (1998a) 'Role of Annexin II Tetramer in Plasminogen Activation'. *The Journal of Biological Chemistry* 273 (8), 4790–4799

Kassam, G., Le, B.H., Choi, K.S., Kang, H.M., Fitzpatrick, S.L., Louie, P., and Waisman, D.M. (1998b) 'The P11 Subunit of the Annexin II Tetramer Plays a Key Role in the Stimulation of T-PA-Dependent Plasminogen Activation'. *Biochemistry* 37 (48), 16958–16966

Kathir, K.M., Ibrahim, K., Rajalingam, D., Prudovsky, I., Yu, C., and Kumar, T.K.S. (2007) 'S100A13-Lipid Interactions-Role in the Non-Classical Release of the Acidic Fibroblast Growth Factor'. *Biochimica et Biophysica Acta - Biomembranes* 1768 (12), 3080–3089

Kaufmann, P., Black, S., and Huppertz, B. (2003) 'Endovascular Trophoblast Invasion: Implications for the Pathogenesis of Intrauterine Growth Retardation and Preeclampsia'. *Biology of Reproduction* 69 (1), 1–7

Kazakov, Alexei S., Shevelyova, M.P., Ismailov, R.G., Permyakova, M.E., Litus, E.A., Permyakov, E.A., and Permyakov, S.E. (2018) 'Calcium-Dependent Interaction of Monomeric S100P Protein with Serum Albumin'. *International Journal of Biological Macromolecules* [online] 108, 143–148. available from <http://dx.doi.org/10.1016/j.ijbiomac.2017.11.134>

Kazakov, Alexei S., Sokolov, A.S., Rastrygina, V.A., Solovyev, V. V., Ismailov, R.G., Mikhailov, R. V.,

Ulitin, A.B., Yakovenko, A.R., Mirzabekov, T.A., Permyakov, E.A., and Permyakov, S.E. (2015) 'High-Affinity Interaction between Interleukin-11 and S100P Protein'. *Biochemical and Biophysical Research Communications* [online] 468 (4), 733–738. available from <http://dx.doi.org/10.1016/j.bbrc.2015.11.024>

Kazakov, Alexey S., Mayorov, S.A., Deryusheva, E.I., Avkhacheva, N. V., Denessiouk, K.A., Denesyuk, A.I., Rastrygina, V.A., Permyakov, E.A., and Permyakov, S.E. (2020) 'Highly Specific Interaction of Monomeric S100P Protein with Interferon Beta'. *International Journal of Biological Macromolecules* [online] 143, 633–639. available from <https://doi.org/10.1016/j.ijbiomac.2019.12.039>

Kerkhoff, C., Klempt, M., and Sorg, C. (1998) 'Novel Insights into Structure and Function of MRP8 (S100A8) and MRP14 (S100A9)'. *Biochimica et Biophysica Acta - Molecular Cell Research* 1448 (2), 200–211

Kim, B., Lee, H.J., Choi, H.Y., Shin, Y., Nam, S., Seo, G., Son, D.-S., Jo, J., Kim, J., Lee, J., Kim, J., Kim, K., and Lee, S. (2007) 'Clinical Validity of the Lung Cancer Biomarkers Identified by Bioinformatics Analysis of Public Expression Data'. *Cancer Research* [online] 67 (15), 7431–7438. available from <http://cancerres.aacrjournals.org/cgi/doi/10.1158/0008-5472.CAN-07-0003>

Kim, D.E., Chivian, D., and Baker, D. (2004) 'Protein Structure Prediction and Analysis Using the Robetta Server'. *Nucleic Acids Research* 32 (WEB SERVER ISSUE), 526–531

Kim, E.J. and Helfman, D.M. (2003) 'Characterization of the Metastasis-Associated Protein, S100A4: Roles of Calcium Binding and Dimerization in Cellular Localization and Interaction with Myosin'. *Journal of Biological Chemistry* 278 (32), 30063–30073

Kim, H., Lee, Y.D., Kim, M.K., Kwon, J.O., Song, M.K., Lee, Z.H., and Kim, H.H. (2017) 'Extracellular S100A4 Negatively Regulates Osteoblast Function by Activating the NF-KB Pathway'. *BMB Reports* 50 (2), 97–102

Kim, J., Blackshear, P.J., Johnson, J.D., and McLaughlin, S. (1994) 'Phosphorylation Reverses the Membrane Association of Peptides That Correspond to the Basic Domains of MARCKS and Neuromodulin'. *Biophysical Journal* 67 (1), 227–237

Kim, Jiyoon, Gee, H.Y., and Lee, M.G. (2018) 'Unconventional Protein Secretion – New Insights into the Pathogenesis and Therapeutic Targets of Human Diseases'. *Journal of Cell Science* 131 (12), jcs213686

Kim, S.-W., Roh, J., and Park, C.-S. (2016) *Immunohistochemistry for Pathologists: Protocols, Pitfalls,*

and Tips. [online] 50, 411–418. available from <https://doi.org/10.4132/jptm.2016.08.08> [11 November 2019]

Kimberly, W.T., Zheng, J.B., Guénette, S.Y., and Selkoe, D.J. (2001) 'The Intracellular Domain of the β-Amyloid Precursor Protein Is Stabilized by Fe65 and Translocates to the Nucleus in a Notch-like Manner'. *Journal of Biological Chemistry* 276 (43), 40288–40292

Klaffky, E., Williams, R., Yao, C.C., Ziober, B., Kramer, R., and Sutherland, A. (2001) 'Trophoblast-Specific Expression and Function of the Integrin A7 Subunit in the Peri-Implantation Mouse Embryo'. *Developmental Biology* 239 (1), 161–175

Knight, T. and Irving, J.A.E. (2014) 'Ras/Raf/MEK/ERK Pathway Activation in Childhood Acute Lymphoblastic Leukemia and Its Therapeutic Targeting'. *Frontiers in Oncology* 4 JUN (June), 1–12

Knöfler, M., Haider, S., Saleh, L., Pollheimer, J., Gamage, T.K.J.B., and James, J. (2019) 'Human Placenta and Trophoblast Development: Key Molecular Mechanisms and Model Systems'. *Cellular and Molecular Life Sciences* [online] 76 (18), 3479–3496. available from <https://doi.org/10.1007/s00018-019-03104-6>

Knöfler, M. and Pollheimer, J. (2013) 'Human Placental Trophoblast Invasion and Differentiation: A Particular Focus on Wnt Signaling'. *Frontiers in Genetics* 4 (SEP), 1–14

Kobayashi, M., Nagashio, R., Saito, K., Aguilar-Bonavides, C., Ryuge, S., Katono, K., Igawa, S., Tsuchiya, B., Jiang, S.X., Ichinoe, M., Murakumo, Y., Saegusa, M., Satoh, Y., and Sato, Y. (2018) 'Prognostic Significance of S100A16 Subcellular Localization in Lung Adenocarcinoma'. *Human Pathology* [online] 74, 148–155. available from <https://doi.org/10.1016/j.humpath.2018.01.001>

Koltzscher, M. and Gerke, Volker (2000) 'Identification of Hydrophobic Amino Acid Residues Involved in the Formation Of'. *Biochemistry* 39, 9533–9539

Krause, F. (2006) 'Detection and Analysis of Protein-Protein Interactions in Organellar and Prokaryotic Proteomes by Native Gel Electrophoresis: (Membrane) Protein Complexes and Supercomplexes'. *Electrophoresis* 27 (13), 2759–2781

Kristoffersen, E.K. and Matre, R. (1996) 'Surface Annexin II on Placental Membranes of the Fetomaternal Interface'. *American Journal of Reproductive Immunology* 36 (3), 141–149

Kudo, N., Matsumori, N., Taoka, H., Fujiwara, D., Schreiner, E., Wolff, B, Yoshida, M, and Horinouchi, S. (1999) 'Leptomycin B Inactivates CRM1 Exportin 1 by Covalent Modification at a Cysteine Residue in the Central Conserved Region'. *Proc Natl Acad Sci USA* 96 (16), 9112–9117

Kufareva, I., Lenoir, M., Dancea, F., Sridhar, P., Raush, E., Bissig, C., Gruenberg, J., Abagyan, R., and Overduin, M. (2014) 'Discovery of Novel Membrane Binding Structures and Functions'. *Biochemistry and Cell Biology* 92 (6), 555–563

Kumeta, M., Yoshimura, S.H., Hejna, J., and Takeyasu, K. (2012) 'Nucleocytoplasmic Shuttling of Cytoskeletal Proteins: Molecular Mechanism and Biological Significance'. *International Journal of Cell Biology* 2012

Landar, A., Hall, T.L., Cornwall, E.H., Correia, J.J., Drohat, A.C., Weber, David J., and Zimmer, D.B. (1997) 'The Role of Cysteine Residues in S100B Dimerization and Regulation of Target Protein Activity'. *Biochimica et Biophysica Acta - Protein Structure and Molecular Enzymology* 1343 (1), 117–129

Lander, H.M., Tauras, J.M., Ogiste, J.S., Hori, O., Moss, R.A., and Schmidt, A.M. (1997) 'Activation of the Receptor for Advanced Glycation End Products Triggers a P21(Ras)-Dependent Mitogen-Activated Protein Kinase Pathway Regulated by Oxidant Stress'. *Journal of Biological Chemistry* 272 (28), 17810–17814

Landriscina, M., Bagalá, C., Mandinova, Anna, Soldi, R., Micucci, I., Bellum, S., Prudovsky, I., and Maciag, T. (2001) 'Copper Induces the Assembly of a Multiprotein Aggregate Implicated in the Release of Fibroblast Growth Factor 1 in Response to Stress'. *Journal of Biological Chemistry* 276 (27), 25549–25557

Leclerc, E., Fritz, Günter, Vetter, S.W., and Heizmann, Claus W. (2009) 'Binding of S100 Proteins to RAGE: An Update'. *Biochimica et Biophysica Acta - Molecular Cell Research* [online] 1793 (6), 993–1007. available from <http://dx.doi.org/10.1016/j.bbamcr.2008.11.016>

Leclerc, E., Fritz, Günter, Weibel, M., Heizmann, Claus W., and Galichet, A. (2007) 'S100B and S100A6 Differentially Modulate Cell Survival by Interacting with Distinct RAGE (Receptor for Advanced Glycation End Products) Immunoglobulin Domains'. *Journal of Biological Chemistry* 282 (43), 31317–31331

Li, Z.H., Spektor, A., Varlamova, O., and Bresnick, A.R. (2003) 'Mts1 Regulates the Assembly of Nonmuscle Myosin-IIA'. *Biochemistry* 42 (48), 14258–14266

Li, Zhuosi, Kurosawa, O., and Iwata, H. (2019) 'Establishment of Human Trophoblast Stem Cells from Human Induced Pluripotent Stem Cell-Derived Cystic Cells under Micromesh Culture'. *Stem Cell Research and Therapy* 10 (245), 1–14

Lines, K.E., Chelala, C., Dmitrovic, B., Wijesuriya, N., Kocher, H.M., Marshall, J.F., and Crnogorac-

jurcevic, T. (2012) ‘S100P-Binding Protein , S100PBP , Mediates Adhesion through Regulation of Cathepsin Z in Pancreatic Cancer Cells’. *AJPA* [online] 180 (4), 1485–1494. available from <http://dx.doi.org/10.1016/j.ajpath.2011.12.031>

Liu, A.-X., Jin, Fan, Zhang, W.-W., Zhou, T.-H., Zhou, C.-Y., Yao, W.-M., Qian, Y.-L., and Huang, H.-F. (2006) ‘Proteomic Analysis on the Alteration of Protein Expression in the Placental Villous Tissue of Early Pregnancy Loss’. *Biology of Reproduction* 75 (3), 414–420

Liu, X.M., Ding, G.L., Jiang, Y., Pan, H.J., Zhang, D., Wang, T.T., Zhang, R.J., Shu, J., Sheng, J.Z., and Huang, H.F. (2012) ‘Down-Regulation of S100A11, a Calcium-Binding Protein, in Human Endometrium May Cause Reproductive Failure’. *Journal of Clinical Endocrinology and Metabolism* 97 (10), 3672–3683

Van der Loop, F.T.L., Schaart, G., Timmer, E.D.J., Ramaekers, F.C.S., and Van Eys, G.J.J.M. (1996) ‘Smoothelin, a Novel Cytoskeletal Protein Specific for Smooth Muscle Cells’. *The Journal of Cell Biology* 134 (2), 401–411

López-Colomé, A.M., Lee-Rivera, I., Benavides-Hidalgo, R., and López, E. (2017) ‘Paxillin: A Crossroad in Pathological Cell Migration’. *Journal of Hematology and Oncology* 10 (1), 1–15

Lou, Y., Han, M., Liu, H., Niu, Y., Liang, Y., Guo, J., Zhang, Wen, and Wang, Hui (2019) ‘Essential Roles of S100A10 in Toll-like Receptor Signaling and Immunity to Infection’. *Cellular and Molecular Immunology* [online] (August). available from <http://dx.doi.org/10.1038/s41423-019-0278-1>

Lowry, O.H., Rosebrough, N.J., Farr, A.L., and Randall, R.J. (1951) ‘Protein Measurement with the Folin Phenol Reagent’. *J Biol Chem* 193 (1), 265–275

Lv, Y., Niu, Z., Guo, X., Yuan, F., and Liu, Y. (2018) ‘Serum S100 Calcium Binding Protein A4 (S100A4, Metatasin) as a Diagnostic and Prognostic Biomarker in Epithelial Ovarian Cancer’. *British Journal of Biomedical Science* 75 (2), 88–91

Maciejczyk, Adam, Łacko, A., Ekiert, M., Jagoda, E., Wysocka, T., Matkowski, R., Hałoń, A., Györffy, Balázs, Lage, Hermann, and Surowiak, Pawel (2013) ‘Elevated Nuclear S100P Expression Is Associated with Poor Survival in Early Breast Cancer Patients’. *Histology and Histopathology* 28, 513–524

MacPhee, D.J., Mostachfi, H.H., Han, R., Lye, S.J., Post, M., and Caniggia, I. (2001) ‘Focal Adhesion Kinase Is a Key Mediator of Human Trophoblast Development’. *Laboratory Investigation* 81 (11), 1469–1483

Mandelboim, O., Pazmany, L., Davis, D.M., Valés-Gómez, M., Reyburn, H.T., Rybalov, B., and

Strominger, J. L. (1997) ‘Multiple Receptors for HLA-G on Human Natural Killer Cells’. *Proceedings of the National Academy of Sciences of the United States of America* 94 (26), 14666–14670

Mandinova, A, Atar, D., Schäfer, B W, Spiess, M., Aebi, U., and Heizmann, C W (1998) ‘Distinct Subcellular Localization of Calcium Binding S100 Proteins in Human Smooth Muscle Cells and Their Relocation in Response to Rises in Intracellular Calcium.’ *Journal of cell science* [online] 111 (Pt 1, 2043–2054. available from <http://www.ncbi.nlm.nih.gov/pubmed/9645951>

Mao, Z., Guan, Y., Li, T., Zhang, Lina, Liu, Menglu, Xing, B., Yao, M., and Chen, M. (2019) ‘Up Regulation of MiR-96-5p Is Responsible for TiO2 NPs Induced Invasion Dysfunction of Human Trophoblastic Cells via Disturbing Ezrin Mediated Cytoskeletons Arrangement’. *Biomedicine and Pharmacotherapy* [online] 117 (June), 109125. available from <https://doi.org/10.1016/j.biopha.2019.109125>

Marcado-Pimentel, M.E., Onyeagucha, B.C., Li, Q., Pimentel, A.C., Jandova, J., and Nelson, M.A. (2015) *The S100P/RAGE Signalling Pathway Regulates Expression of MicroRNA-21 in Colon Cancer Cells*. 589 (18), 2388–2393

Marenholz, I., Heizmann, C.W., and Fritz, G. (2004) ‘S100 Proteins in Mouse and Man: From Evolution to Function and Pathology (Including an Update of the Nomenclature)’. *Biochemical and Biophysical Research Communications* 322, 1111–1122

McLaughlin, Stuart and Aderem, A. (1995) ‘The Myristoyl-Electrostatic Switch: A Modulator of Reversible Protein-Membrane Interactions’. *Trends in Biochemical Sciences* 20 (7), 272–276

Miranda, K.J., Loeser, R.F., and Yammani, R.R. (2010) ‘Sumoylation and Nuclear Translocation of S100A4 Regulate IL-1β-Mediated Production of Matrix Metalloproteinase-13’. *Journal of Biological Chemistry* 285 (41), 31517–31524

Miwa, N., Uebi, T., and Kawamura, S. (2008) ‘S100-Annexin Complexes - Biology of Conditional Association’. *FEBS Journal* 275 (20), 4945–4955

Modelska, A., Turro, E., Russell, R., Beaton, J., Sbarrato, T., Spriggs, K., Miller, J., Gräf, S., Provenzano, E., Blows, F., Pharoah, P., Caldas, C., and Le Quesne, J. (2015) ‘The Malignant Phenotype in Breast Cancer Is Driven by EIf4A1-Mediated Changes in the Translational Landscape’. *Cell Death and Disease* 6 (1), 1–12

Mohr, D., Frey, S., Fischer, T., Gü Ttler, T., and Gö Rlich, D. (2009) ‘Characterisation of the Passive Permeability Barrier of Nuclear Pore Complexes’. *The EMBO Journal* [online] 28, 2541–2553.

available from <www.embojournal.org> [2 October 2019]

Moore, B.W. (1965) 'A Soluble Protein Characteristic of the Nervous System'. *Biochemical and Biophysical Research Communications* 19 (6), 739–744

Moroz, O. V., Antson, A.A., Dodson, E.J., Burrell, H.J., Grist, S.J., Lloyd, R.M., Maitland, N.J., Dodson, G. G., Wilson, K. S., Lukanidin, E., and Bronstein, I. B. (2002) 'The Structure of S100A12 in a Hexameric Form and Its Proposed Role in Receptor Signalling'. *Acta Crystallographica Section D: Biological Crystallography* 58 (3), 407–413

Moroz, Olga V., Blagova, E. V., Wilkinson, A.J., Wilson, Keith S., and Bronstein, Igor B. (2009) 'The Crystal Structures of Human S100A12 in Apo Form and in Complex with Zinc: New Insights into S100A12 Oligomerisation'. *Journal of Molecular Biology* [online] 391 (3), 536–551. available from <http://dx.doi.org/10.1016/j.jmb.2009.06.004>

Mueller, A., Bächi, T., Höchli, M., Schäfer, Beat W., and Heizmann, Claus W. (1999) 'Subcellular Distribution of S100 Proteins in Tumor Cells and Their Relocation in Response to Calcium Activation'. *Histochemistry and Cell Biology* 111 (6), 453–459

Murata, S., Minami, Y., Minami, M., Chiba, T., and Tanaka, K. (2001) 'CHIP Is a Chaperone-Dependent E3 Ligase That Ubiquitylates Unfolded Protein'. *EMBO Reports* 2 (12), 1133–1138

Nair, R.R., Khanna, A., and Singh, K. (2013) 'Role of Inflammatory Proteins S100A8 and S100A9 in Pathophysiology of Recurrent Early Pregnancy Loss'. *Placenta* [online] 34 (9), 824–827. available from <http://dx.doi.org/10.1016/j.placenta.2013.06.307>

Namba, T., Homan, T., Nishimura, T., Mima, S., Hoshino, T., and Mizushima, T. (2009) 'Up-Regulation of S100P Expression by Non-Steroidal Anti-Inflammatory Drugs and Its Role in Anti-Tumorigenic Effects'. *Journal of Biological Chemistry* 284 (7), 4158–4167

Nedjadi, T., Kitteringham, N., Campbell, F., Jenkins, R.E., Park, B.K., Navarro, P., Ashcroft, F., Tepikin, A., Neoptolemos, J.P., and Costello, E. (2009) 'S100A6 Binds to Annexin 2 in Pancreatic Cancer Cells and Promotes Pancreatic Cancer Cell Motility'. *British Journal of Cancer* [online] 101 (7), 1145–1154. available from <http://dx.doi.org/10.1038/sj.bjc.6605289>

Neisch, A.L. and Fehon, R.G. (2011) 'Ezrin, Radixin and Moesin: Key Regulators of Membrane-Cortex Interactions and Signaling'. *Current Opinion in Cell Biology* [online] 23 (4), 37–382. available from <https://www.ncbi.nlm.nih.gov/pmc/articles/PMC3624763/pdf/nihms412728.pdf>

Noguera-Salvà, M.A., Guardiola-Serrano, F., Martin, M.L., Marcilla-Etxenike, A., Bergo, M.O., Busquets, X., and Escribá, P. V. (2017) 'Role of the C-Terminal Basic Amino Acids and the Lipid

Anchor of the Gγ2 Protein in Membrane Interactions and Cell Localization'. *Biochimica et Biophysica Acta - Biomembranes* [online] 1859 (9), 1536–1547. available from <http://dx.doi.org/10.1016/j.bbamem.2017.02.012>

Noland, T.D., Olson, G.E., and Garbers, D.L. (1983) 'Purification and Partial Characterization of Plasma Membranes from Bovine Spermatozoa'. *Biology of Reproduction* 29 (4), 987–998

Noritake, J., Fukata, M., Sato, K., Nakagawa, M., Watanabe, T., Izumi, N., Wang, S., Fukata, Y., and Kaibuchi, K. (2004) 'Positive Role of IQGAP1, an Effector of Rac1, in Actin-Meshwork Formation at Sites of Cell-Cell Contact'. *Molecular Biology of the Cell* 15 (March), 1065–1076

Noritake, J., Watanabe, T., Sato, K., Wang, S., and Kaibuchi, K. (2005) 'IQGAP1: A Key Regulator of Adhesion and Migration.' *Journal of cell science* [online] 118 (Pt 10), 2085–92. available from <http://www.ncbi.nlm.nih.gov/pubmed/15890984>

O'Connell, P.A., Surette, A.P., Liwski, R.S., Svenningsson, P., and Waisman, D.M. (2010) 'S100A10 Regulates Plasminogen-Dependent Macrophage Invasion'. *Blood* 116 (7), 1136–1146

Orczyk, K. and Smolewska, E. (2018) 'A Granulocyte-Specific Protein S100A12 as a Potential Prognostic Factor Affecting Aggressiveness of Therapy in Patients with Juvenile Idiopathic Arthritis'. *Journal of Immunology Research* 2018 (1)

Orendi, K., Gauster, M., Moser, G., Meiri, H., and Huppertz, B. (2010) 'The Choriocarcinoma Cell Line BeWo: Syncytial Fusion and Expression of Syncytium-Specific Proteins'. *Reproduction* 140 (5), 759–766

Orre, L.M., Pernemalm, M., Lengqvist, J., Lewensohn, R., and Lehtiö, J. (2007) 'Up-Regulation, Modification, and Translocation of S100A6 Induced by Exposure to Ionizing Radiation Revealed by Proteomics Profiling'. *Molecular and Cellular Proteomics* 6 (12), 2122–2131

Ostendorp, T., Leclerc, E., Galichet, A., Koch, M., Demling, N., Weigle, B., Heizmann, Claus W., Kroneck, P.M.H., and Fritz, Günter (2007) 'Structural and Functional Insights into RAGE Activation by Multimeric S100B'. *EMBO Journal* 26 (16), 3868–3878

Paiva, P., Salamonsen, L.A., Manuelpillai, U., and Dimitriadis, E. (2009) 'Interleukin 11 Inhibits Human Trophoblast Invasion Indicating a Likely Role in the Decidual Restraint of Trophoblast Invasion During Placentation1'. *Biology of Reproduction* 80 (2), 302–310

Pallett, R., Leslie, L.J., Lambert, P.A., Milic, I., Devitt, A., and Marshall, L.J. (2019) 'Anaerobiosis Influences Virulence Properties of Pseudomonas Aeruginosa Cystic Fibrosis Isolates and the Interaction with Staphylococcus Aureus'. *Scientific Reports* 9 (1), 1–18

Paradela, A., Bravo, S.B., Henrquez, M., Gavilanes, F., Gonzlez-ros, J.M., Albar, J.P., Henrı, M., Riquelme, G., and Gonza, M. (2005) 'Proteomic Analysis of Apical Microvillous Membranes of Syncytiotrophoblast Cells Reveals A High Degree of Similarity with Lipid Rafts Proteomic Analysis of Apical Microvillous Membranes of Syncytiotrophoblast Cells Reveals A High Degree of Similarity With'. *Journal of Proteome Research*

Parkkila, S., Pan, P.-W., Ward, A., Gibadulinova, A., Oveckova, I., Pastorekova, S., Pastorek, J., Martinez, A.R., Helin, H.O., and Isola, J. (2008) 'The Calcium-Binding Protein S100P in Normal and Malignant Human Tissues.' *BMC Clinical Pathology* 8 (2)

Patel, R.N., Quack, K.C., Hill, J.A., and Schust, D.J. (2003) 'Expression of Membrane-Bound HLA-G at the Maternal-Fetal Interface Is Not Associated with Pregnancy Maintenance among Patients with Idiopathic Recurrent Prenancy Loss'. *Molecular Human Reproduction* 9 (9), 551–557

Pellegrin, S. and Mellor, H. (2007) 'Actin Stress Fibers'. *Journal of Cell Science* 120 (20), 3491–3499

Peng, Cike, Chen, Hongda, Wallwiener, M., Modugno, C., Cuk, K., Madhavan, D., Trumpp, A., Heil, J., Marmé, F., Nees, J., Riethdorf, S., Schott, S., Sohn, C., Pantel, K., Schneeweiss, A., Yang, R., and Burwinkel, B. (2016) 'Plasma S100P Level as a Novel Prognostic Marker of Metastatic Breast Cancer'. *Breast Cancer Research and Treatment* 157 (2), 329–338

Penumutchu, S.R., Chou, R.H., and Yu, C. (2014a) 'Interaction between S100P and the Anti-Allergy Drug Cromolyn'. *Biochemical and Biophysical Research Communications* [online] 454 (3), 404–409. available from <http://dx.doi.org/10.1016/j.bbrc.2014.10.048>

Penumutchu, S.R., Chou, R.H., and Yu, C. (2014b) 'Structural Insights into Calcium-Bound S100P and the V Domain of the RAGE Complex'. *PLoS ONE* 9 (8)

Plaisier, M. (2011) 'Decidualisation and Angiogenesis'. *Best Practice and Research: Clinical Obstetrics and Gynaecology* 25 (3), 259–271

Popovici, R.M., Betzler, N.K., Krause, M.S., Luo, M., Jauckus, J., Germeyer, A., Bloethner, S., Schlotterer, A., Kumar, R., Strowitzki, T., and Von Wolff, M. (2006) 'Gene Expression Profiling of Human Endometrial-Trophoblast Interaction in a Coculture Model'. *Endocrinology* 147 (12), 5662–5675

Potts, B.C.M., Carlstrom, G., Okazaki, K., Hidaka, H., and Chazin, W.J. (1996) '1H NMR Assignments of Apo Calcyclin and Comparative Structural Analysis with Calbindin D9k and S100B'. *Protein Science* 5, 2162–2174

Poullet, P., Gautreau, A., Kadaré, G., Girault, J.A., Louvard, D., and Arpin, M. (2001) 'Ezrin Interacts

with Focal Adhesion Kinase and Induces Its Activation Independently of Cell-Matrix Adhesion'. *Journal of Biological Chemistry* 276 (40), 37686–37691

Powell, M.A. and Glenney, J.R. (1987) 'Regulation of Calpactin I Phospholipid Binding by Calpactin I Light-Chain Binding and Phosphorylation by P60(v-Src)'. *Biochemical Journal* 247 (2), 321–328

Prag, S., Parsons, M., Keppler, M.D., Ameer-Beg, S.M., Barber, P., Hunt, James, Beavil, A.J., Calvert, R., Arpin, M., Vojnovic, B., and Ng, T. (2007) 'Activated Ezrin Promotes Cell Migration through Recruitment of the GEF Dbl to Lipid Rafts and Preferential Downstream Activation of Cdc42'. *Molecular Biology of the Cell* 18 (March), 2935–2948

Prica, F., Radon, T., Cheng, Y., and Crnogorac-Jurcevic, T. (2016) 'The Life and Works of S100P - from Conception to Cancer'. *American Journal of Cancer Research* 6 (2), 562–576

Pruenster, M., Vogl, T., Roth, J., and Sperandio, M. (2016) 'S100A8/A9: From Basic Science to Clinical Application.' *Pharmacology & therapeutics* [online] 167, 120–131. available from <http://www.ncbi.nlm.nih.gov/pubmed/27492899>

Qi, Houbao, Liu, S., Guo, C., Wang, J., Greenaway, F.T., and Sun, M.Z. (2015) 'Role of Annexin A6 in Cancer (Review)'. *Oncology Letters* 10 (4), 1947–1952

Raman, R., Pinto, C.S., and Sonawane, M. (2018) 'Polarized Organization of the Cytoskeleton: Regulation by Cell Polarity Proteins'. *Journal of Molecular Biology* [online] 430 (19), 3565–3584. available from <https://doi.org/10.1016/j.jmb.2018.06.028>

Rambotti, M.G., Spreca, A., and Donato, R. (1993) *Immunocytochemical Localization of Annexins V and VI in Human Placentae of Different Gestational Ages*. 39 (6), 579–589

Rammes, A., Roth, J., Goebeler, M., Klempt, M., Hartmann, M., and Sorg, C. (1997) 'Myeloid-Related Protein (MRP) 8 and MRP14, Calcium-Binding Proteins of the S100 Family, Are Secreted by Activated Monocytes via a Novel, Tubulin- Dependent Pathway'. *Journal of Biological Chemistry* 272 (14), 9496–9502

Rath, A., Glibowicka, M., Nadeau, V.G., Chen, G., and Deber, C.M. (2009) 'Detergent Binding Explains Anomalous SDS-PAGE Migration of Membrane Proteins'. *Proceedings of the National Academy of Sciences of the United States of America* 106 (6), 1760–1765

Ray, K.P. and Lopez-Belmonte, J. (1992) 'Partial Characterization of P21(Ras) Farnesyltransferase Present in Human Placental Tissue'. *Biochemical Society Transactions* 20 (2), 494–497

Rayet, Â. and Gelinas, Â. (1999) 'Aberrant Rel / Nfkb Genes and Activity in Human Cancer'. *Oncogene*

18, 6938–6947

Rehbein, G., Simm, A., Hofmann, H.-S., Silber, R.-E., and Bartling, B. (2008) 'Molecular Regulation of S100P in Human Lung Adenocarcinomas.' *International journal of molecular medicine* 22 (1), 69–77

Ren, X.D., Kiosses, W.B., Sieg, D.J., Otey, C.A., Schlaepfer, D.D., and Schwartz, M.A. (2000) 'Focal Adhesion Kinase Suppresses Rho Activity to Promote Focal Adhesion'. *Journal of Cell Science* 113 (20), 3673–3678

Resh, M.D. (2013) 'Covalent Lipid Modifications of Proteins'. *Curr Biol.* 23 (10), 431–435

Réty, S., Osterloh, D., Arié, J.P., Tabaries, S., Seeman, J., Russo-Marie, F., Gerke, Volker, and Lewit-Bentley, A. (2000) 'Structural Basis of the Ca2+-Dependent Association between S100C (S100A11) and Its Target, the N-Terminal Part of Annexin I'. *Structure* 8 (2), 175–184

Réty, S., Sopkova, J., Renouard, M., Osterloh, D., Gerke, Volker, Tabaries, S., Russo-Marie, F., and Lewit-Bentley, A. (1999) 'The Crystal Structure of a Complex of P11 with the Annexin II N-Terminal Peptide'. *Nature Structural Biology* 6 (1), 89–95

Ridder, A., Giorgione, V., Khalil, A., and Thilaganathan, B. (2019) 'Preeclampsia: The Relationship between Uterine Artery Blood Flow and Trophoblast Function'. *International Journal of Molecular Sciences* 20 (13)

Ridley, A.J. (2015) 'Rho GTPase Signalling in Cell Migration'. *Current Opinion in Cell Biology* [online] 36, 103–112. available from <http://dx.doi.org/10.1016/j.ceb.2015.08.005>

Rintala-Dempsey, A.C., Santamaria-Kisiel, L., Liao, Y., Lajoie, G., and Shaw, G.S. (2006) 'Insights into S100 Target Specificity Examined by a New Interaction between S100A11 and Annexin A2'. *Biochemistry* 45 (49), 14695–14705

Riquelme, G., Llanos, P., Tischner, E., Neil, J., and Campos, B. (2004) 'Annexin 6 Modulates the Maxi-Chloride Channel of the Apical Membrane of Syncytiotrophoblast Isolated from Human Placenta'. *Journal of Biological Chemistry* 279 (48), 50601–50608

Roche, J. (2018) 'The Epithelial-to-Mesenchymal Transition in Cancer'. *Cancers* 10 (2), 10–13

Rosner, M. and Hengstschlager, M. (2008) *Cytoplasmic and Nuclear Distribution of the Protein Complexes MTORC1 and MTORC2 : Rapamycin Triggers Dephosphorylation and Delocalization of the MTORC2 Components Rictor and Sin1*. 17 (19), 2934–2948

Roy, M., Li, Z., and Sacks, D.B. (2005) 'IQGAP1 Is a Scaffold for Mitogen-Activated Protein Kinase

Signaling'. *Molecular and Cellular Biology* 25 (18), 7940–7952

Rozovski, U., Jonish-Grossman, A., Bar-Shira, A., Ochshorn, Y., Goldstein, M., and Yaron, Y. (2007) 'Genome-Wide Expression Analysis of Cultured Trophoblast with Trisomy 21 Karyotype'. *Human Reproduction* 22 (9), 2538–2545

Russo, J. and Russo, I.H. (2004) *Molecular Basis of Breast Cancer* [online] vol. 1. available from <http://link.springer.com/10.1007/978-3-642-18736-0>

Sakaguchi, M., Miyazaki, M., Takaishi, M., Sakaguchi, Y., Makino, E., Kataoka, N., Yamada, H., Namba, M., and Huh, N.H. (2003) 'S100C/A11 Is a Key Mediator of Ca2+-Induced Growth Inhibition of Human Epidermal Keratinocytes'. *Journal of Cell Biology* 163 (4), 825–835

Sakwe, A.M., Koumangoye, R., Guillory, B., and Ochieng, J. (2011) 'Annexin A6 Contributes to the Invasiveness of Breast Carcinoma Cells by Influencing the Organization and Localization of Functional Focal Adhesions Amos'. *Exp Cell Res.* 317 (6), 823–937

Samudram, A., Bijeesh, M.M., Kowshik, M., Nandakumar, P., and Varier, G.K. (2016) 'Passive Permeability and Effective Pore Size of HeLa Cell Nuclear Membranes'. *Cell Biology International* 40 (9), 991–998

Santamaria-Kisiel, L., Rintala-Dempsey, A.C., and Shaw, G.S. (2006) 'Calcium-Dependent and -Independent Interactions of the S100 Protein Family.' *The Biochemical journal* 396 (2), 201–214

Sato, N. and Hitomi, J. (2002) 'S100P Expression in Human Esophageal Epithelial Cells: Human Esophageal Epithelial Cells Sequentially Produce Different S100 Proteins in the Process of Differentiation'. *Anatomical Record* 267 (1), 60–69

Schägger, H. and von Jagow, G. (1991) 'Blue Native Electrophoresis for Isolation of Membrane Protein Complexes in Enzymatically Active Form'. *Analytical Biochemistry* 199 (2), 223–231

Schmidt, A.M. (2015) 'Soluble RAGEs – Prospects for Treating & Tracking Metabolic and Inflammatory Disease'. *Vascul. Pharmacol.* 72, 1–8

Schol, P.B.B., Güzel, C., Steegers, E.A.P., De Krijger, R.R., and Luider, T.M. (2014) 'Trophoblast Calcyclin Is Elevated in Placental Tissue from Patients with Early Pre-Eclampsia'. *Pregnancy Hypertension* [online] 4 (1), 7–10. available from <http://dx.doi.org/10.1016/j.preghy.2013.11.003>

Schor, A.P.T., Carvalho, F.M., Kemp, C., Silva, I.D.C.G., and Russo, J. (2006) 'S100P Calcium-Binding Protein Expression Is Associated with High-Risk Proliferative Lesions of the Breast'. *Oncology*

Reports 15 (1), 3–6

Schwanhüusser, B., Busse, D., Li, N., Dittmar, G., Schuchhardt, J., Wolf, J., Chen, W., and Selbach, M. (2011) 'Global Quantification of Mammalian Gene Expression Control'. *Nature* 473 (7347), 337–342

Semov, A., Moreno, M.J., Onichtchenko, A., Abulrob, A., Ball, M., Ekiel, I., Pietrzynski, G., Stanimirovic, D., and Alakhov, V. (2005) 'Metastasis-Associated Protein S100A4 Induces Angiogenesis through Interaction with Annexin II and Accelerated Plasmin Formation'. *Journal of Biological Chemistry* 280 (21), 20833–20841

Shang, X., Cheng, H., and Zhou, R. (2008) 'Chromosomal Mapping, Differential Origin and Evolution of the S100 Gene Family'. *Genetics, selection, evolution: GSE* 40, 449–464

Shen, J., Zhao, Qiong, Wang, Xiangfeng, Gao, C., Zhu, Y., Zeng, Y., and Jiang, L. (2018) 'A Plant Bro1 Domain Protein BRAF Regulates Multivesicular Body Biogenesis and Membrane Protein Homeostasis'. *Nature Communications* [online] 9 (1). available from <https://doi.org/10.1038/s41467-018-05913-y>

Shevchenko, A., Tomas, H., Havliš, J., Olsen, J. V., and Mann, M. (2007) 'In-Gel Digestion for Mass Spectrometric Characterization of Proteins and Proteomes'. *Nature Protocols* 1 (6), 2856–2860

Shimamoto, S., Kubota, Y., Yamaguchi, F., Tokumitsu, H., and Kobayashi, R. (2013) 'Ca2+/S100 Proteins Act as Upstream Regulators of the Chaperone-Associated Ubiquitin Ligase Chip (c Terminus of Hsc70-Interacting Protein)'. *Journal of Biological Chemistry* 288 (10), 7158–7168

Shiokawa, S., Iwashita, M., Akimoto, Y., Nagamatsu, S., Sakai, K., Hanashi, H., Kabir-Salmani, M., Nakamura, Y., Uehata, M., and Yoshimura, Y. (2002) 'Small Guanosine Triphospatase RhoA and Rho-Associated Kinase as Regulators of Trophoblast Migration'. *Journal of Clinical Endocrinology and Metabolism* 87 (12), 5808–5816

Shiota, M., Tsunoda, T., Song, Y., Yokomizo, A., Tada, Y., Oda, Y., and Naito, S. (2011) 'Enhanced S100 Calcium-Binding Protein P Expression Sensitizes Human Bladder Cancer Cells to Cisplatin'. *BJU International* 107 (7), 1148–1153

Shishibori, T., Oyama, Y., Matsushita, O., Yamashita, K., Furuichi, H., Okabe, A., Maeta, H., Hata, Y., and Kobayashi, R. (1999) 'Three Distinct Anti-Allergic Drugs, Amlexanox, Cromolyn and Tranilast, Bind to S100A12 and S100A13 of the S100 Protein Family'. *Biochemical Journal* 338 (3), 583–589

Simpson, R.J. (2010) 'Disruption of Cultured Cells by Nitrogen Cavitation'. *Cold Spring Harbor*

Protocols 5 (11)

Skedinger, M.C., Augustine, N.H., Morris, E.Z., Nielson, D.W., Zimmerman, G.A., and Hill, H.R. (1987) 'Effect of Disodium Cromoglycate on Neutrophil Movement and Intracellular Calcium Mobilization'. *The Journal of Allergy and Clinical Immunology* 80 (4), 573–577

Spratt, D.E., Barber, K.R., Marlatt, N.M., Ngo, V., Macklin, J.A., Xiao, Y., Konermann, L., Duennwald, M.L., and Shaw, G.S. (2019) 'A Subset of Calcium-Binding S100 Proteins Show Preferential Heterodimerization'. *FEBS Journal* 286 (10), 1859–1876

Springer, J.M., Monach, P., Cuthbertson, D., Carette, S., Khalidi, N.A., McAlear, C.A., Pagnoux, C., Seo, P., Warrington, K.J., Ytterberg, S.R., Hoffman, G., Langford, C., Hamilton, T., Foell, D., Vogl, T., Holzinger, D., Merkel, P.A., Roth, J., and Hajj-Ali, R.A. (2018) 'Serum S100 Proteins as a Marker of Disease Activity in Large Vessel Vasculitis'. *Journal of Clinical Rheumatology* 24 (7), 393–395

Staun-Ram, E., Goldman, S., Gabarin, D., and Shalev, E. (2004) 'Expression and Importance of Matrix Metalloproteinase 2 and 9 (MMP-2 and -9) in Human Trophoblast Invasion.' *Reproductive biology and endocrinology* [online] 2, 59. available from <http://www.pubmedcentral.nih.gov/articlerender.fcgi?artid=516041&tool=pmcentrez&rendertype=abstract>

Stewart, S.E., Ashkenazi, A., Williamson, A., Rubinsztein, D.C., and Moreau, K. (2018) 'Transbilayer Phospholipid Movement Facilitates the Translocation of Annexin across Membranes'. *Journal of Cell Science* 131 (14)

Südhof, T.C. (2012) 'Calcium Control of Neurotransmitter Release'. *Cold Spring Harbor Perspectives in Biology* 4 (1)

Surowiak, P., Maciejczyk, A., Materna, V., Drag-Zalesińska, M., Wojnar, A., Pudelko, M., Kędzia, W., Spaczyński, M., Dietel, M., Zabel, M., and Lage, H. (2007) 'Unfavourable Prognostic Significance of S100P Expression in Ovarian Cancers'. *Histopathology* 51 (1), 125–128

Swamy, M., Siegers, G.M., Minguet, S., Wollscheid, B., and Schamel, W.W.A. (2006) 'Blue Native Polyacrylamide Gel Electrophoresis (BN-PAGE) for the Identification and Analysis of Multiprotein Complexes.' *Science's STKE : signal transduction knowledge environment* 2006 (345), 1–18

Szklanna, P.B., Wynne, K., Nolan, M., Egan, K., Áinle, F.N., and Maguire, P.B. (2017) 'Comparative Proteomic Analysis of Trophoblast Cell Models Reveals Their Differential Phenotypes, Potential Uses, and Limitations'. *Proteomics* 17 (10), 6–11

Szymanski, W.G., Zauber, H., Erban, A., Gorka, M., Wu, X.N., and Schulze, W.X. (2015) 'Cytoskeletal Components Define Protein Location to Membrane Microdomains'. *Molecular and Cellular Proteomics* 14 (9), 2493–2509

Tabrizi, M.E.A., Lancaster, T.L., Ismail, T.M., Georgiadou, A., Ganguly, A., Mistry, J.J., Wang, K., Rudland, Philip S, Ahmad, S., and Gross, S.R. (2018) *S100P Enhances the Motility and Invasion of Human Trophoblast Cell Lines*. 1–18

Taguchi, A., Blood, D.C., del Toro, G., Canet, A., Lee, D.C., Wu, Q., Tanji, N., Lu, Y., Lalla, E., Fu, C., Hofmann, M.A., Kislinger, T., Ingram, M., Lu, A., Tanaka, H., Hori, O., Ogawa, S., Stern, D.M., and Schmidt, A.M. (2000) 'Blockade of RAGE-Amphoterin Signalling Suppresses Tumour Growth and Metastases'. *Nature* 405 (May), 354–360

Tapia, J.A., Camello, C., Jensen, R.T., and García, L.J. (1999) 'EGF Stimulates Tyrosine Phosphorylation of Focal Adhesion Kinase (P125(FAK)) and Paxillin in Rat Pancreatic Acini by a Phospholipase C-Independent Process That Depends on Phosphatidylinositol 3-Kinase, the Small GTP-Binding Protein, P21(Rho), and the Inte'. *Biochimica et Biophysica Acta - Molecular Cell Research* 1448 (3), 486–499

Tarabykina, S., Kriajevska, M., Scott, D.J., Hill, T.J., Lafitte, D., Derrick, P.J., Dodson, Guy G., Lukanidin, Eugene, and Bronstein, I. (2000) 'Heterocomplex Formation between Metastasis-Related Protein S100A4 (Mts1) and S100A1 as Revealed by the Yeast Two-Hybrid System'. *FEBS Letters* 475 (3), 187–191

Tilburgs, T., Crespo, Â.C., Van Der Zwan, A., Rybalov, Basya, Raj, T., Stranger, B., Gardner, Lucy, Moffett, Ashley, and Strominger, Jack L. (2015) 'Human HLA-G+ Extravillous Trophoblasts: Immune-Activating Cells That Interact with Decidual Leukocytes'. *Proceedings of the National Academy of Sciences of the United States of America* 112 (23), 7219–7224

Timney, B.L., Raveh, B., Mironska, R., Trivedi, J.M., Kim, S.J., Russel, D., Wente, S.R., Sali, A., and Rout, M.P. (2016) 'Simple Rules for Passive Diffusion through the Nuclear Pore Complex'. *Journal of Cell Biology* 215 (1), 57–76

Tong, X.M., Lin, X.N., Song, T., Liu, L., and Zhang, S.Y. (2010) 'Calcium-Binding Protein S100P Is Highly Expressed during the Implantation Window in Human Endometrium'. *Fertility and Sterility* [online] 94 (4), 1510–1518. available from <http://dx.doi.org/10.1016/j.fertnstert.2009.07.1667>

Trotta, C.R., Lund, E., Kahan, L., Johnson, A.W., and Dahlberg, J.E. (2003) 'Coordinated Nuclear Export

of 60s Ribosomal Subunits and NMD3 in Vertebrates'. *EMBO Journal* 22 (11), 2841–2851

Tsien, R.Y. (1998) 'The Green Fluorescent Protein'. *Annual Review Biochemistry* [online] 67, 509–544. available from <http://www.tsienlab.ucsd.edu/Publications/Tsien 1998 Annu. Rev. Biochem - GFP.pdf>

Turco, M.Y. and Moffett, Ashley (2019) 'Development of the Human Placenta'. *Development (Cambridge)* 146 (22), 1–14

Turner, C.E. (2000) 'Paxillin and Focal Adhesion Signalling'. *Nature Cell Biology* 2 (12), 231–236

Tutar, Y. (2006) *Target Peptide Recognition by S100P Protein and Role of Central Linker Region and Dimer Interface*. 307–311

Vanli, G., Cuesta-Marban, A., and Widmann, C. (2017) 'Evaluation and Validation of Commercial Antibodies for the Detection of Shb'. *PLoS ONE* 12 (12)

Verma, S., Pal, R., and Gupta, S.K. (2018) 'Decrease in Invasion of HTR-8/SVneo Trophoblastic Cells by Interferon Gamma Involves Cross-Communication of STAT1 and BATF2 That Regulates the Expression of JUN'. *Cell Adhesion and Migration* 12 (5), 432–446

Vogl, T., Ludwig, S., Goebeler, M., Strey, A., Thorey, I.S., Reichelt, R., Foell, D., Gerke, Volker, Manitz, M.P., Nacken, W., Werner, S., Sorg, C., and Roth, J. (2004) 'MRP8 and MRP14 Control Microtubule Reorganization during Transendothelial Migration of Phagocytes'. *Blood* 104 (13), 4260–4268

Wang, G., Platt-Higgins, A., Carroll, J., De Silva Rudland, S., Winstanley, J., Barraclough, Roger, and Rudland, Philip S. (2006) 'Induction of Metastasis by S100P in a Rat Mammary Model and Its Association with Poor Survival of Breast Cancer Patients'. *Cancer Research* 66 (2), 1199–1207

Wang, G., Zhang, Shu, Fernig, D.G., Spiller, D., Martin-Fernandez, M., Zhang, H., Ding, Y., Rao, Z., Rudland, Philip S, and Barraclough, Roger (2004) 'Heterodimeric Interaction and Interfaces of S100A1 and S100P.' *The Biochemical journal* [online] 382 (Pt 1), 375–83. available from <http://www.pubmedcentral.nih.gov/articlerender.fcgi?artid=1133950&tool=pmcentrez&rendertype=abstract>

Wang, M. and Casey, Patrick J. (2016) 'Protein Prenylation: Unique Fats Make Their Mark on Biology'. *Nature Reviews Molecular Cell Biology* [online] 17 (2), 110–122. available from <http://dx.doi.org/10.1038/nrm.2015.11>

Wang, Q., Zhang, Y.N., Lin, G. Le, Qiu, H.Z., Wu, B., Wu, H.Y., Zhao, Yu, Chen, Y.J., and Lu, C.M. (2012)

'S100P, a Potential Novel Prognostic Marker in Colorectal Cancer'. *Oncology Reports* 28 (1), 303–310

Warner-Schmidt, J.L., Flajolet, M., Maller, A., Chen, E.Y., Qi, Hongshi, Svenningsson, P., and Greengard, P. (2009) 'Role of P11 in Cellular and Behavioral Effects of 5-HT4 Receptor Stimulation'. *Journal of Neuroscience* 29 (6), 1937–1946

Weill, U., Krieger, G., Avihou, Z., Milo, R., Schuldiner, M., and Davidi, D. (2019) 'Assessment of GFP Tag Position on Protein Localization and Growth Fitness in Yeast'. *Journal of Molecular Biology*

Welser, J. V., Lange, N.D., Flintoff-Dye, N., Burkin, H.R., and Burkin, D.J. (2007) 'Placental Defects in A7 Integrin Null Mice'. *Placenta* 28 (11–12), 1219–1228

West, R.C., Bouma, G.J., and Winger, Q.A. (2018) 'Shifting Perspectives from "Oncogenic" to Oncofetal Proteins; How These Factors Drive Placental Development'. *Reproductive Biology and Endocrinology* 16 (1), 1–12

White, Colin D., Erdemir, Huseyin H., Sacks, D.B. (2013) 'IQGAP1 and Its Binding Proteins Control Diverse Biological Functions'. *Cell Signal* 24 (4), 826–834

Whiteman, H.J., Weeks, M.E., Dowen, S.E., Barry, S., Timms, J.F., Lemoine, Nicholas R., and Crnogorac-Jurcevic, T. (2007) 'The Role of S100P in the Invasion of Pancreatic Cancer Cells Is Mediated through Cytoskeletal Changes and Regulation of Cathepsin D'. *Cancer Research* 67 (18), 8633–8642

Wittig, I., Braun, H.P., and Schägger, H. (2006) 'Blue Native PAGE'. *Nature Protocols* 1 (1), 418–428

Wolff, Barbara, Sanglier, J.J., and Wang, Y. (1997) 'Leptomycin B Is an Inhibitor of Nuclear Export: Inhibition of Nucleo-Cytoplasmic Translocation of the Human Immunodeficiency Virus Type 1 (HIV-1) Rev Protein and Rev-Dependent MRNA'. *Chemistry and Biology*

Wu, Z., Boonmars, T., Nagano, I., Boonjaraspinyo, S., Srinontong, P., Ratasuwan, P., Narong, K., Nielsen, P.S., and Maekawa, Y. (2016) 'Significance of S100P as a Biomarker in Diagnosis, Prognosis and Therapy of Opisthorchiasis-Associated Cholangiocarcinoma'. *International Journal of Cancer* 138 (2), 396–408

Xie, Y., Zheng, Y., Li, H., Luo, X., He, Z., Cao, S., Shi, Y., Zhao, Qi, Xue, Y., Zuo, Z., and Ren, J. (2016) 'GPS-Lipid: A Robust Tool for the Prediction of Multiple Lipid Modification Sites'. *Scientific Reports* 6 (June), 1–9

Xu, Han, Li, M., Zhou, Y., Wang, F., Li, X., Wang, L., and Fan, Q. (2016) 'S100A4 Participates in

Epithelial-Mesenchymal Transition in Breast Cancer via Targeting MMP2'. *Tumor Biology* 37 (3), 2925–2932

Yammani, R.R. (2012) 'S100 Proteins in Cartilage: Role in Arthritis'. *Biochim Biophys Acta* 1822 (4), 600–606

Yan, S.F., Ramasamy, R., and Schmidt, A.M. (2010) 'Soluble RAGE: Therapy and Biomarker in Unraveling the RAGE Axis in Chronic Disease and Aging'. *Biochemical Pharmacology* 79 (10), 1379–1386

Yang, Z., Yan, W.X., Cai, H., Tedla, N., Armishaw, C., Di Girolamo, N., Wang, H.W., Hampartzoumian, T., Simpson, J.L., Gibson, P.G., Hunt, John, Hart, P., Hughes, J.M., Perry, M.A., Alewood, P.F., and Geczy, C.L. (2007) 'S100A12 Provokes Mast Cell Activation: A Potential Amplification Pathway in Asthma and Innate Immunity'. *Journal of Allergy and Clinical Immunology* 119 (1), 106–114

Yasuda, K., Kosugi, A., Hayashi, F., Saitoh, S., Nagafuku, M., Mori, Y., Ogata, M., and Hamaoka, T. (2000) 'Serine 6 of Lck Tyrosine Kinase: A Critical Site for Lck Myristoylation, Membrane Localization, and Function in T Lymphocytes'. *The Journal of Immunology* 165 (6), 3226–3231

Zhang, D., Ma, C., Sun, X., Xia, H., and Zhang, Wei (2012) 'S100P Expression in Response to Sex Steroids during the Implantation Window in Human Endometrium.' *Reproductive biology and endocrinology : RB&E* [online] 10 (1), 106. available from <http://www.pubmedcentral.nih.gov/articlerender.fcgi?artid=3551790&tool=pmcentrez&rendertype=abstract>

Zhang, F.L. and Casey, P J (1996) 'Protein Prenylation: Molecular Mechanisms and Functional Consequences.' *Annual review of biochemistry* 65, 241–269

Zhang, H., Wang, G., Ding, Y., Wang, Z., Barraclough, Roger, Rudland, Philip S., Fernig, D.G., and Rao, Z. (2003) 'The Crystal Structure at 2 Å Resolution of the Ca2+-Binding Protein S100P'. *Journal of Molecular Biology* 325 (4), 785–794

Zhang, Libo, Fogg, D.K., and Waisman, D.M. (2004) 'RNA Interference-Mediated Silencing of the S100A10 Gene Attenuates Plasmin Generation and Invasiveness of Colo 222 Colorectal Cancer Cells'. *Journal of Biological Chemistry* 279 (3), 2053–2062

Zhang, Qingying, Zhou, T., Xu, X., Guo, Y., Zhao, Z., Zhu, M., Li, W., Yi, D., and Huo, X. (2011) 'Downregulation of Placental S100P Is Associated with Cadmium Exposure in Guiyu, an e-Waste Recycling Town in China'. *Science of the Total Environment* [online] 410–411, 53–58. available from <http://dx.doi.org/10.1016/j.scitotenv.2011.09.032>

Zhao, Qi, Xie, Y., Zheng, Y., Jiang, S., Liu, W., Mu, W., Liu, Zexian, Zhao, Yong, Xue, Y., and Ren, J. (2014) 'GPS-SUMO: A Tool for the Prediction of Sumoylation Sites and SUMO-Interaction Motifs'. *Nucleic Acids Research* 42 (W1), 325–330

Zhou, F., Xue, Y., Yao, X., and Xu, Ying (2006) *PROTOCOL A General User Interface for Prediction Servers of Proteins ' Post-Translational Modification Sites*. 1–4

Zhou, M. and Philips, M.R. (2017) 'Nitrogen Cavitation and Differential Centrifugation Allows for Monitoring the Distribution of Peripheral Membrane Proteins in Cultured Cells'. *Journal of visualized experiments : JoVE* (126)

Zhou, T., Wang, Haiying, Zhang, Shen, Jiang, X., and Wei, X. (2016) 'S100P Is a Potential Molecular Target of Cadmium-Induced Inhibition of Human Placental Trophoblast Cell Proliferation'. *Experimental and Toxicologic Pathology* [online] 68 (10), 565–570. available from <http://dx.doi.org/10.1016/j.etp.2016.09.002>

Zhu, H.Y., Tong, X.M., Lin, X.N., Jiang, L.Y., Wang, J.X., and Zhang, S.Y. (2015a) 'Expression and Distribution of Calcium-Binding Protein S100p in Human Placenta during Pregnancy'. *International Journal of Fertility and Sterility* 8 (4), 445–452

Zhu, H.Y., Wang, J.X., Tong, X.M., Xue, Y.M., and Zhang, S.Y. (2015b) 'S100P Regulates Trophoblast-like Cell Proliferation via P38 MAPK Pathway'. *Gynecological Endocrinology* [online] 31 (10), 796–800. available from <http://dx.doi.org/10.3109/09513590.2015.1069268>

Zhu, J.-Y., Pang, Z.-J., and Yu, Y.-H. (2012) 'Regulation of Trophoblast Invasion: The Role of Matrix Metalloproteinases.' *Reviews in obstetrics & gynecology* [online] 5 (3–4), e137-43. available from <http://www.ncbi.nlm.nih.gov/pubmed/23483768%5Cnhttp://www.pubmedcentral.nih.gov/articlerender.fcgi?artid=PMC3594863>

Zimmer, D.B., Wright Sadosky, P., and Weber, David J. (2003) 'Molecular Mechanisms of S100-Target Protein Interactions.' *Microscopy research and technique* 60 (6), 552–559